NMR Characterization of Intrinsically Disordered α-Synuclein: implication for aggregation in Parkinson's Disease

By

KUEN-PHON WU

A Dissertation submitted to the

Graduate School-New Brunswick

Rutgers, The State University of New Jersey

in partial fulfillment of the requirements

for the degree of

Doctor of Philosophy

Graduate Program in Chemistry and Chemical Biology

written under the direction of

Dr. Jean Baum

and approved by

Jean Baum

Ronald M. Levy

New Brunswick, New Jersey
January, 2010

ABSTRACT OF THE DISSERTATION

NMR Characterization of Intrinsically Disordered α-Synuclein:

Implication for Aggregation in Parkinson's Disease

by KUEN-PHON WU

Dissertation Director:

Jean Baum Ph. D.

A broad range of human diseases arise from the loss of the native function of a specific peptide or protein. The pathological conditions of these diseases are generally referred to as protein misfolding and aggregation problem. An increasing number of misfolded proteins are associated with the deposition of protein aggregation in the brain cells resulting in neurodegenerative diseases, for example, the aggregated α-synuclein (αSyn) in sporadic Parkinson's disease.

αSyn is an intrinsically disordered protein and the aggregation kinetics are sensitive to the changes of amino acids and chemical environments. The structural conversion of αSyn from an unfolded monomeric ensemble to a well-ordered fibril remains unclear. In this work, nuclear magnetic resonance (NMR) was applied to characterize the aggregation-prone species including homologous mouse αSyn and human αSyn at low pH. Comparison of human and mouse αSyn at pH 7.4 and at supercooled aqueous solution presents a less compact mouse αSyn ensemble with

transient inter-chain interactions at the N-terminal region. Characterization of αSyn conformational ensembles at both neutral and low pH shows that the altered charge distribution at low pH changes the structural properties of these ensembles and leads to rapid aggregation. Paramagnetic relaxation enhancement (PRE) experiments using mixed isotope (^{15}N) and spin labeled αSyn further illustrate different intermolecular contacts of low-populated transient complex at neutral and low pH. A head-to-tail αSyn complex transiently stabilized by the electrostatic interactions at neutral pH is observed while a tail-to-tail αSyn complex via hydrophobic interactions at low pH is seen. This work provides novel structural insight into the molecular conversion of αSyn at the very early nucleation state.

In addition to understanding the aggregation mechanism of αSyn, an approach that deconvolutes the strong modulation of fast hydrogen exchange (HX) rates on the transverse relaxation rate (R_2) of disordered proteins is also presented. This work shows an HX-free R_2 profile of αSyn at pH 7.4 and provides an opportunity to understand NMR relaxation of disordered proteins or unstructured loop regions in folded proteins at fast HX conditions such as high pH or high temperature.

Acknowledgement

At the beginning point, I would like to express my deepest and sincere gratitude to my advisor, Dr. Jean Baum, for giving me this fascinating, rewarding, and challenging research topic and for her guidance, patience, encouragement and outstanding expertise throughout my research career.

I am so grateful to Dr. Ronald Levy and Dr. David Talaga for their advices and opinions in conducting and completing the research projects.

I also want to express my appreciation to Dr. John Taylor and Dr. Vikas Nanda for serving on the committee of thesis proposal and thesis defense, respectively.

Many people are involved in the research projects at different points. Without their contributions the results would not be carried out in such wealthy and fruitful shape. I thank Dr. Seho Kim in the Chemistry Department for his NMR expertise in theory, and pulse sequence and for his help of data acquisition, data analysis and discussions. Many thanks to the present and past members in the Baum laboratory, especially Yu-Jen Chen and Dr. Yingjie Li, for their skillful assistances of protein purification and NMR operation, respectively. Members in the Levy laboratory including Chitra Narayanan, Dr. Daniel Weinstock and Dr. Michael Andrec and members in the Talaga laboratory including Jeremy Pronchik and Dr. Jason Guirleo are helpful in sample preparation, design of experiments and discussions.

I owe a lot of debts to my friends who share me their scientific knowledge and the philosophy of life. I am so grateful to have “long-range” and “long-term” scientific consults and discussions with Dr. Shang-Te Danny Hsu, Dr. Yuan-Chou Lou, Dr. Meng-

Ru Ho, Dr. Iren Wang, Dr. Chih-Hong Lin, Dr. Shih-Hsin Kan, and Dr. Chia-en Chang in Europe, Taiwan and California. I feel very fortunate to have close friendship and enjoy every great moment with Tim, Lisa, Jin, Yu-Ming, RK and Rita at Rutgers.

I also want to thank the departmental staffs including Melissa Grunwerg, Kevin Abbey, Katherine Lam and Janice Pawlo for every of their helps.

Finally, I am very much obliged to my parents for their endless love, their efforts in every stage of my education, and their unlimited, warm and sweet supports for this dissertation.

Kuen-Phon Wu
November, 2009

Table of content

Abstract ii
Acknowledgement iv
Table of content vi
List of figures ix
List of tables xii
Abbreviations xiii
Chapter 1 . Introduction 1
1.1 Protein folding, misfolding and amyloid disease 1
1.2 α-Synuclein, its variants and Parkinson's disease 5
1.3 NMR spectroscopy and intrinsically disordered protein (IDP) 9
1.4 Objectives 11
1.4.1. Characterization of sequence- and pH-dependent conformational ensembles of αSyn using NMR spectroscopy and implication for aggregation. 11
1.4.2 Determination of interactions in early aggregation events 13
Chapter 2 . Methods, materials and experimental procedures 15
2.1 Expression of αSyn and variants 15
2.2 Purification of αSyn and variants 17
2.3 Strategy of backbone assignment 21
2.3.1 ^{13}C-^{13}C connections 21
2.3.2 ^{15}N-^{15}N connections 22
2.4 Analysis of NMR relaxation data. 24
2.4.1 General information 24
2.4.2 Fitting relaxation data 25
2.4.3 Calculation of steady-state heteronuclear NOE 26
2.4.4 Calculation of R_{ex} 26
2.5 MTSL spin label reaction and PRE measurement 29
2.5.1 Spin label reaction 29
2.5.2 PRE measurement 31
2.5.3 Calculation of theoretical PRE intensity ratios of fully extended protein 33
2.6 Residual dipolar coupling experiments 34
2.6.1 Medium preparation 34
2.6.2 NMR measurement of D_{NH} 36
2.7 Translational diffusion coefficient 37
Chapter 3 . NMR Characterization of Intrinsically Disordered Human and Mouse α-Synuclein: implication for protein aggregation 41
3.1 Introduction 41
3.2 Material and methods 44
3.2.1 Chemicals 44
3.2.2 Protein preparation 45
3.2.3 NMR experiments 45
3.2.4 SDSL and PRE experiments 49
3.3 Results 51
3.3.1 NMR assignment and characterization of human and mouse αSyn at 15 °C ... 51

3.3.2 Assignments and secondary structural propensities of human and mouse αSyn at low temperature. 57
3.3.3 Backbone dynamics of human and mouse αSyn at 263K 59
3.3.4 Long-range interactions from the C-terminal to the N-terminal and hydrophobic NAC region are eliminated in mouse αSyn. 64
3.4 Discussion 67
3.4.1 Correlation of transient long-range tertiary contacts and restricted mobility in human αSyn 68
3.4.2 Loss of long-range contacts in mouse αSyn relative to human αSyn 71
3.4.3 Implications for aggregation 73
Chapter 4 . Structural Reorganization of Acid-induced α-Synuclein Characterized by NMR Spectroscopy 75
4.1 Introduction 75
4.2 Material and methods 80
4.2.1 Sample preparation 80
4.2.2 NMR experiments for assignment 81
4.2.3 Translational diffusion coefficients and hydrodynamic radii 81
4.2.4 ^{15}N backbone relaxation experiments 83
4.2.5 Site-directed spin label 83
4.2.6 RDC measurements 84
4.3 Results 84
4.3.1 Acid-induced changes in structure and dynamics probed by NMR 84
4.3.2 The C-terminus is structurally collapsed at pH 2.5 88
4.4 Discussion 92
Chapter 5 . Detection of transient intermolecular contacts of α-synuclein using paramagnetic NMR spectroscopy 101
5.1 Introduction 101
5.2 Material and Methods 102
5.2.1 Preparation of mixed labeled samples 102
5.2.2 Macromolecular crowding solution and highly viscous solution 104
5.3 Results 105
5.3.1 Theory of ^{1}H R_2 and its application for PRE measurement 105
5.3.2 Transient intermolecular contacts at pH 2.5 109
5.3.3 Transient intermolecular contacts at pH 6.0 111
5.3.4 Concentration-dependent PRE and PRE-derived local structural conformation 113
5.3.5 Macromolecular crowding effect enhances the transient intermolecular interactions 115
5.3.6 Viscosity effect on the transient intermolecular interactions 119
5.4 Conclusion and discussion 123
Chapter 6 . Fast Hydrogen Exchange Reaction Modulates ^{15}N Backbone Transverse Relaxation in Intrinsically Disordered Protein 129
6.1 Introduction 129
6.2 Materials and methods 130
6.2.1 αSyn preparation and NMR data acquisition 130
6.2.2 indole-^{15}N-labeled tryptophan preparation and NMR data collection 131

6.3 Results 132
6.4 Conclusion and discussion 145
Chapter 7 . Conclusion 149
7.1 Aggregation-prone αSyn ensemble 149
7.2 Transient inter-molecular contacts of αSyn 150
7.3 Future consideration 151
Reference 153
Appendix 167
A.1 Backbone assignment of human α-synuclein at 15 °C and pH 7.4 167
A.2 Backbone assignment of mouse α-synuclein at 15 °C and pH 7.4 171
A.3 Backbone assignment of human α-synuclein at -10 °C and pH 7.4 175
A.4 Backbone assignment of mouse α-synuclein at -10 °C and pH 7.4 179
A.5 Backbone assignment of human α-synuclein at 15 °C and pH 2.5 183
A.6 HSQC spectral assignment of human α-synuclein at -10 °C and pH 2.5 187
A.7 Backbone assignment of human α-synuclein in 2 M glucose at 15 °C and pH 7.4 188
A.8 RDC values of human and mouse α-synuclein at pH 7.4 or 2.5 and at 15 °C 192
A.9 Shell script of SALSA 196
Curriculum Vita 199

List of figures

Figure 1.1 Schematic of folding energy landscape. 2

Figure 1.2 Model of protein misfolding, degradation and fibrilization in cells.....4

Figure 1.3 Primary amino acid sequences of human αSyn and variants. 6

Figure 2.1 FPLC profile and SDS-PAGE of purified αSyn.....21

Figure 2.2 Examples of ^{13}C-^{13}C and ^{15}N-^{15}N connections for assignment.....23

Figure 2.3 Example fitting data of the different relaxation parameters 26

Figure 2.4 R_2^{HE} versus η_{xy} plot and correlation of η_{xy} from two pulse sequences.....28

Figure 2.5 FPLC desalting process of αSyn cysteine variants for spin labeling. 30

Figure 2.6 Chemical equation of spin label reaction.....31

Figure 2.7 Schematic PRE application for IDP 32

Figure 2.8 Measurement of quadrupolar deuterium splitting constant.....35

Figure 2.9 Illustrated spectra showing the measurement of D_{NH}.....37

Figure 2.10 Examples of data fitting of 1D PFG-NMR spectra 39

Figure 3.1 Sequence alignment of human and mouse αSyn.....43

Figure 3.2 Examples of sequential strips of human and mouse αSyn at 15 °C 52

Figure 3.3 ^{1}H-^{15}N HSQC spectra of human and mouse αSyn at 15 °C.....53

Figure 3.4 $^{13}C^{\alpha}$ CSD and D_{NH} RDC values of human and mouse αSyn. 54

Figure 3.5 ^{15}N backbone dynamic profiles of human and mouse αSyn at 15 °C. 56

Figure 3.6 ^{1}H-^{15}N HSQC spectra of human and mouse αSyn at 263K. 57

Figure 3.7 Secondary structure propensity of human and mouse αSyn at 263K.....59

Figure 3.8 ^{15}N Relaxation parameters of human and mouse αSyn at 263K. 62

Figure 3.9 PRE profiles of amide protons in human and mouse αSyn 65

Figure 3.10 Model representations of structural clusters and long-range contacts of human and mouse αSyn 70

Figure 4.1 Distribution of charged residues of αSyn and the pH-dependency. 77

Figure 4.2 PFG-NMR data fitting of dioxane and αSyn. 82

Figure 4.3 ^{1}H-^{15}N HSQC spectrum of αSyn dissolved in phosphate buffet at pH 2.5..... 87

Figure 4.4 NMR parameters for αSyn at pH 7.4 and 2.5..... 88

Figure 4.5 PRE profiles of spin-labeled αSyn at neutral and low pH 90

Figure 4.6 Hydrodynamic radii of αSyn at pH 7.4 and 2.5 from 5 to 50 °C. 92

Figure 4.7 Selected representative simulated conformation of αSyn ensemble. 95

Figure 4.8 Hydrophobcity profiles and charge-hydrophobicity correlation of αSyn..... 96

Figure 5.1 Schematic of intermolecular PRE measurement using mixed samples..... 103

Figure 5.2 ^{1}H R_2 pulse sequence 108

Figure 5.3 Correlation of reduction in intensity and enhancement in R_2 at pH 6.0. 108

Figure 5.4 Intermolecular PRE profiles and possible dimeric contacts at pH 2.5. 111

Figure 5.5 Intermolecular PRE profiles and possible dimeric contacts at pH 6.0. 113

Figure 5.6 Concentration-dependent PRE profiles and detailed local C-terminal conformation at pH 2.5 115

Figure 5.7 ^{1}H and ^{15}N R_2 profiles and HSQC spectrum of αSyn in crowded PEG solution. 117

Figure 5.8 Intermolecular PRE profiles of αSyn in PEG crowded solution. 118

Figure 5.9 NMR spectral assignment and SSP scores of αSyn in 2 M glucose..... 120

Figure 5.10 Comparison of ^{15}N R_2 of αSyn in 2 M glucose and at -10 °C and diamagnetic ^{1}H R_2 of αSyn in 2 M glucose. 122

Figure 5.11 Intermolecular PRE profiles of αSyn in viscous glucose solution. 123

Figure 5.12 Plot of charge density and mean hydrophobicity and schematic of αSyn aggregation. 126

Figure 6.1 Distinct patterns of measured R_2^{CPMG} values of αSyn at two neutral pHs..... 132

Figure 6.2 ^{1}H-^{15}N HSQC spectra at different pH and temperature..... 134

Figure 6.3 pH-dependent R_{1zz} and R_2^{CPMG} of indole-^{15}N-labeled tryptophan 141

Figure 6.4 k_{HX} values and corrected R_2^{CPMG} at pH 6.1 and 7.4 143

Figure 6.5 Example fitting and correction curves and fitting errors. 145

Figure 7.1 Schematic of αSyn aggregation..... 151

List of tables

Table 2.1. List of used NMR relaxation experiments 25

Table 3.1. The local clusters defined by R_2 profiles of human and mouse αSyn 60

Table 4.1. Distribution of charges in the sequence of αSyn 79

Abbreviations

^{1}H-^{15}N NOE	Steady-state heteronuclear NOE
Γ_2	Paramagnetic transverse relaxation enhancement
αSyn	α-synuclein
βSyn	β-synuclein
γSyn	γ-synuclein
η_{xy}	CSA/dipole-dipole cross-correlation rate
Aβ	Amyloid β peptide
AD	Alzheimer's disease
AFM	Atomic force microscopy
C8E5	Pentaethylene glycol monooctyl ether
CD	Circular dichroism
CNS	Central nervous system
CPMG	Carr-Purcell-Meiboom-Gill
CSD	Chemical shift deviation
D_{NH}	N-H bond residual dipolar coupling constant
DOSY	Diffusion order spectroscopy
DTT	Dithiothreitol
E. coli	*Escherichia coli*
EPR	Electronic paramagnetic resonance
FID	Free induction decay
FT-IR	Fourier transform infrared resonance

HSQC	Heteronuclear single quantum coherence spectroscopy
HX	Hydrogen-hydrogen exchange
IDP	Intrinsically disordered protein
INEPT	Insensitive nuclei enhanced by polarization transfer
IPAP	In-phase-anti-phase
IPTG	Isopropyl-β-D-thiogalactopyranoside
k_{HX}	Hydrogen-hydrogen exchange rate
LB	Lewy body
LB	Luria broth
LOESS	Locally weighted scatterplot smoothing method
MES	2-(N-morpholino)ethanesulfonic acid
μs	Microseconds
MTSL	(1-oxy-2,2,5,5-tetramethyl-D-pyrroline-3-methyl)- methanethiosulfonate
NAC	Non-Aβ component of Alzheimer's disease amyloid plaques
NMR	Nuclear magnetic resonance
NOE	Nuclear Overhauser effect
ns	Nanoseconds
PBS	Phosphate buffer saline
PD	Parkinson's disease
PEG	Polyethylene glycol
PFG-NMR	Pulse field gradient nuclear magnetic resonance
PMSF	Phenylmethanesulphonylfluoride
ppm	Parts per million

PRE	Paramagnetic relaxation enhancement
ps	Picoseconds
R_1	Longitudinal (spin-lattice) relaxation rate
R_2	Transverse (spin-spin) relaxation rate
R_{ex}	Chemical exchange rate
R_g	Radius of gyration
R_h	Hydrodynamic radius
R_2^{CPMG}	Transverse relaxation using CPMG pulse cycle
R_2^{HE}	Transverse relaxation using Hanh-echo pulse cycle
RDC	Residual dipolar coupling
REMD	Replica exchange molecular dynamics
SASA	Solvent accessible surface areas
SAXS	Small angle x-ray scattering
SDS-PAGE	Sodium dodecyl sulfate polyacrylamide gel electrophoresis
SSP	Secondary structural propensity
ThT	Thioflavin T
wt	Wild type

Chapter 1 . Introduction

1.1 Protein folding, misfolding and amyloid disease

Proteins are one of the most important and perhaps the most complex classes of biological molecules in nature. After the synthesis on the ribosome, a released protein must fold to be functional. The folding of proteins into their compact three-dimensional structures is the most fundamental and universal example of biological mechanism. The folding problem was first addressed by Levinthal stating that a protein folding through an unbiased search of conformations would, due to the enormous number of possibilities, take longer than the age of the universe to finish the folding process, and hence defined pathways must exist (Levinthal 1968; Karplus 1997). It has been about four decades since Anfinsen's elegant demonstration on the spontaneous folding *in vitro* and the information that the folded structure is fully encoded in the primary amino acid sequence (Anfinsen 1973). Despite enormous efforts in the past 40 years, protein folding mechanisms remain unclear. A new view of protein folding pathways termed "folding landscapes" based on the concept of statistical mechanics was proposed to explain the complicated multi-state folding theory (Dinner et al. 2000). The global folding landscape topography is determined by the evolution of protein conformation on a rough energy scale. Starting as an unfolded protein, collapsed chain reactions lead the protein to fold correctly to its native functional structure. In addition, several long-lived native-like intermediate structures trapped in the funnel-like free-energy landscape also explain some dramatically different folding features of experimental data of two very similar sequences (Onuchic and Wolynes 2004).

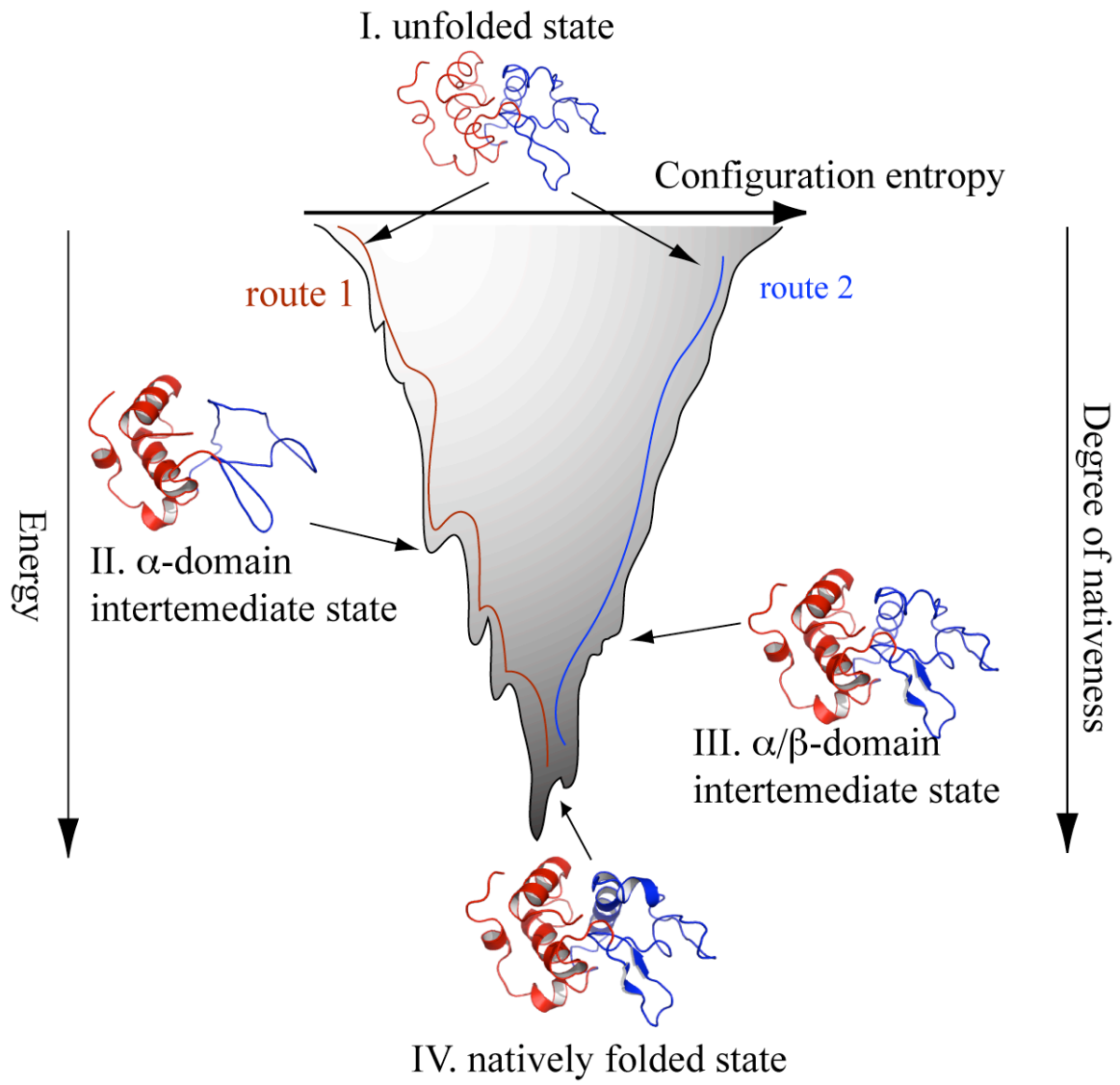

Figure 1.1 Schematic of folding energy landscape.

A funnel like version of the free-energy surface landscape of lysozyme is shown to present two folding trajectories (red and blue) toward the natively folded state. The red trajectory illustrates a slow track folding in which the β domain folds following the folded α domain with a long-lived intermediate (state II). Blue trajectory presents the fast track folding that α and β domains concurrently fold and the intermediate is short-lived (state III). This figure was created based on the figures from (Dinner et al. 2000) and (Onuchic and Wolynes 2004), respectively. Solution structure of hen lysozyme (PDB: 1E8L) is used to display the 3D conformation.

However proteins in the living cells, especially in eukaryotic cells, do not always fold to the correct three-dimensional conformation and are not fully functional as an enzyme, a transporter or other important biological roles. Many details of *in vivo* protein folding depend on the environmental or molecular factors such as chaperones, ionic strength, pH states, and macromolecular crowding conditions. Molecular chaperones are a special factor that assist the partially folded proteins to their correct folding and in remaining folded (Pearl and Prodromou 2006). Once the protein incorrectly or incompletely folds, the misfolded proteins no longer execute their biological functions correctly. Proteasome or lysosome machinery in the cytoplasm is in charge of degrading the misfolded cellular proteins as quality-control mechanism to remove unneeded proteins (Dobson 2003). The folding of cellular proteins sensitively relies on the physiochemical conditions and the misfolded proteins are unstable or denatured while existing under improper cellular conditions. They have a tendency to aggregate and precipitate in the cytoplasm before the degradation process. Amorphous insoluble aggregates of proteins are often found in cells as the product of precipitation of a cellular pathway that prevents misfolded proteins from interfering with cellular functions. In contrast to amorphous aggregates, an ordered and well-structured aggregate also known as amyloid fibrils have been identified in cells and have been correlated to many diseases (Chiti and Dobson 2006; Tycko 2006).

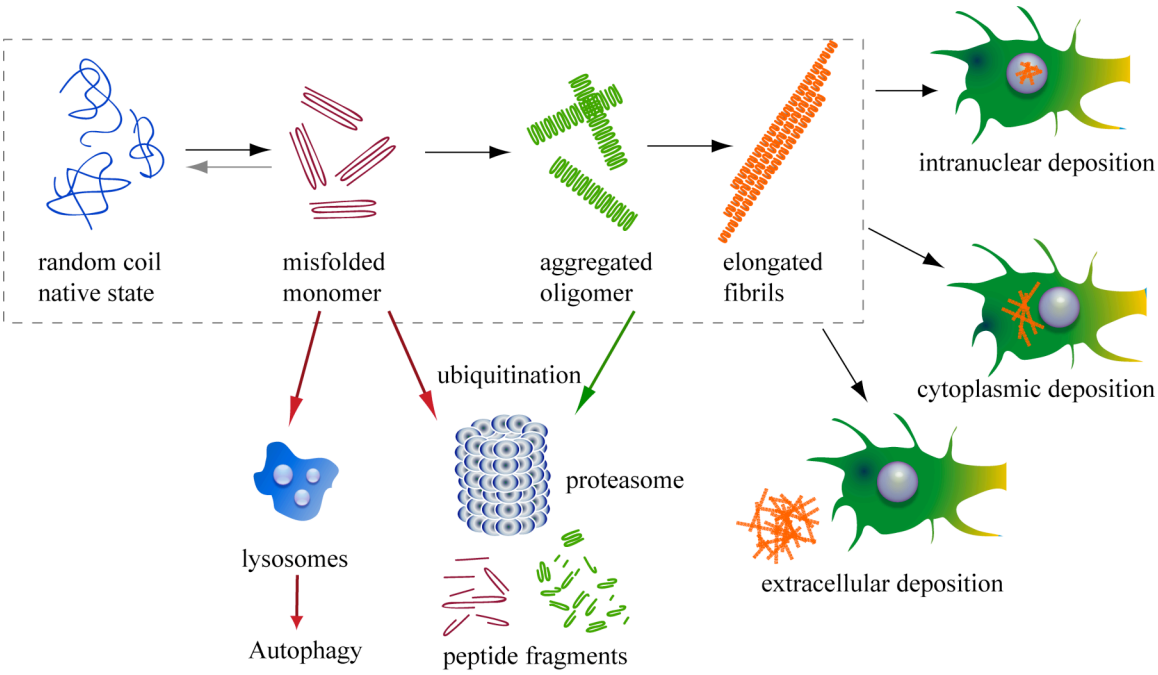

Figure 1.2 Model of protein misfolding, degradation and fibrilization in cells.

During the *in vivo* protein folding process, the random coil-like native protein can remain folded as normal structure and function by molecular chaperones. The misfolded form tends to aggregate leading the deposition of filamentous polymers inside or outside cells. A quality-control system delivers unnecessary misfolded proteins to ubiquitin-proteasome or lysosome for degradation to limit the accumulative amount of unneeded proteins in the cytoplasm. This figure is created based on the concept from reference (Forman et al. 2004)).

Many human diseases are associated with proteins that convert from their normally soluble form to misfolded aggregates that accumulate in the affected organs. The final forms of the aggregates include fibrillar plaques known as amyloid. This disease class includes neurodegenerative diseases such as Alzheimer's disease (AD), Parkinson's disease (PD) and Creutzfeldt-Jakob disease (CJD) and non-neuropathic system amyloidose such as Huntington's disease, Lysozyme amyloidosis and type II diabetes

(Dobson 1999; Perutz 1999; Dobson 2001; Goedert 2001; Siderowf and Stern 2003; Forman et al. 2004; Chiti and Dobson 2006). A common mechanism is that misfolded proteins relevant to neurodegenerative diseases are aggregated and deposited in brain neuronal cells leading to progressive central nervous system (CNS) amyloidosis. A proposed cellular pathway of amyloid formation illustrated in figure 1.2 shows that the aggregation process is gradually converted from misfolded soluble form into nucleated oligomers to elongated insoluble filamentous polymer. The filamentous polymers can be deposited in various places including the cytoplasm, nucleus or extracellular space (senile plaques). Solid state NMR and EPR studies have characterized the common molecular constitution of well-structured fibrils (longer than 40 aa) as is in-register and parallel cross-β pleated sheet (Tycko 2006; Margittai and Langen 2008).

1.2 α-Synuclein, its variants and Parkinson's disease

Parkinson's disease is the second most prevalent neurodegenerative disease and the sufferers often have impaired motor skills, speech, or other moving functions. Amyloid deposition in the brain neuronal cells, also known as Lewy body (LB) and Lewy neurite, is the pathological hallmark of PD. α-Synuclein (αSyn) has been characterized as the main structural component of Lewy body (Spillantini et al. 1997). αSyn is an intrinsically disordered 14.5 kDa protein with an unclear function though it is particularly expressed in the presynatpic brain neuronal cells (Rochet and Lansbury 2000). In contrast to the disordered conformation in the cytoplasm, αSyn also adopts α helical conformation upon binding to membranes and the membrane-bound conformation has been implicated for recruitment of neuron transmitters such as dopamine and calcium (Yavich et al. 2004).

Primary sequence analysis of αSyn shows that the 140-aa protein is composed of three distinct regions (figure 1.3): amphipathic N-terminal region (residues 1-60), central hydrophobic non-Amyloid β component (NAC) region (residues 61-95) (El-Agnaf et al. 1998), and an acidic C-terminal region (residues 96-140). Six 11-residues repeats encoding with KTKE/QGV imperfect motifs in the N-terminal and NAC regions have shown transient helical propensity in solution and highly helical conformation while associating with biological membrane or membrane like environment (Jo et al. 2000; Eliezer et al. 2001; Bussell and Eliezer 2003; 2004; Bussell et al. 2005).

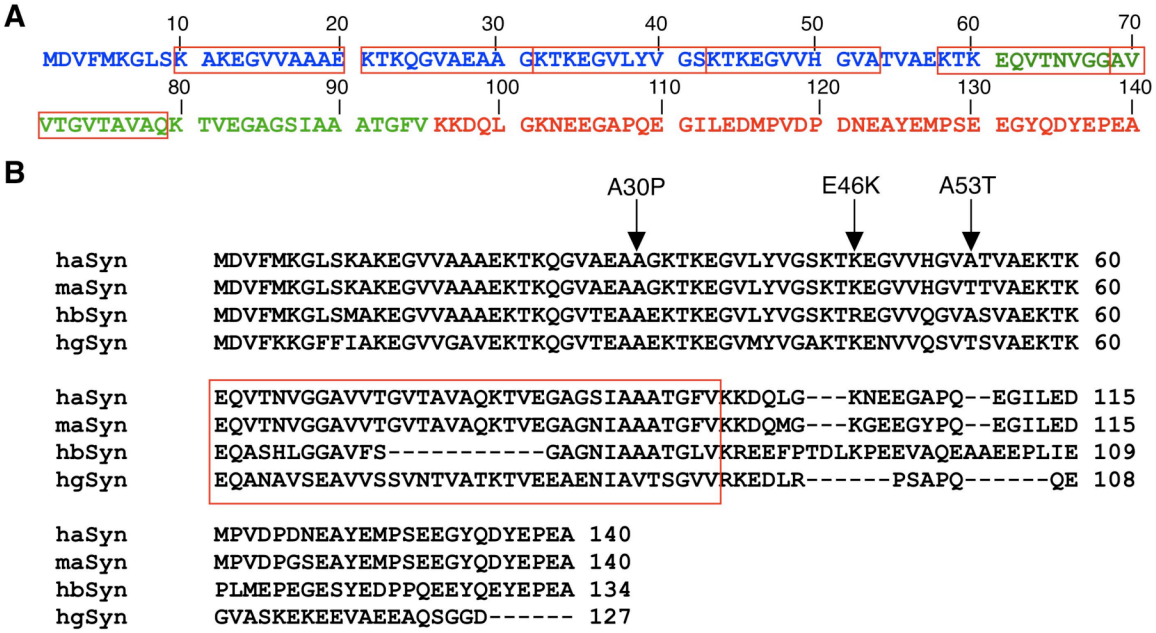

Figure 1.3 Primary amino acid sequences of human αSyn and variants.

A. The N-terminal, NAC and C-terminal regions of human αSyn are colored in blue, green and red, respectively. Imperfect 11-residue repeats are boxed. **B**. Sequences of human αSyn, mouse αSyn, human βSyn and human γSyn were aligned using ClustalW web server. The NAC region is boxed and positions of 3 genetic mutation points (A30P, E46K and A53T) are indicated by

arrows. The alignment shows that the N-terminal regions are very conserved and the NAC and the C-terminal regions are diverse.

Two homologous variants so called β-synuclein (βSyn) and γ-synuclein (γSyn) have been characterized in human. Little is known about the real biological functions of the two homologues. Similarly to αSyn, βSyn are predominately expressed in the central nervous system though γSyn are abundant in the peripheral nervous system and other tissues including breast cancer (Singh et al. 2007). Despite sharing highly conservative primary sequences with αSyn (figure 1.3), βSyn and γSyn are not found in Lewy body or Lewy neurite (Biere et al. 2000). The aggregation propensity of βSyn and γSyn are extremely disfavored. It has been shown βSyn is a non-amyloidogenic synuclein under normal condition and its aggregation is induced in the presence of metal ions (Yamin et al. 2005). γSyn exhibits very slow aggregation kinetics and has been implicated for breast cancer (Singh et al. 2007). Although the vast majority of PD cases are sporadic, three familial mutations (A30P (Kruger et al. 1998), E46K (Zarranz et al. 2004) and A53T (Polymeropoulos et al. 1997)) of αSyn linked to early onset PD have been identified in the recent 10 years. The genetic single point mutations, especially A53T, exhibit accelerated aggregation kinetics and the aggregation order among all synucleins from fastest to slowest is: mouse αSyn > αSyn A53T > αSyn E46K > *wt* αSyn , αSyn A30P >> γSyn > βSyn (Biere et al. 2000; Rochet et al. 2000; Rochet and Lansbury 2000; Serpell et al. 2000; Uversky et al. 2002; Choi et al. 2004; Greenbaum et al. 2005; Marsh et al. 2006). Mouse αSyn is also composed of 140-residue and shares 95% primary sequence identity with human αSyn (figure 1.3). Experimental results demonstrated from

Lansbury's group have shown that mouse αSyn aggregates and forms fibrils very rapidly and the aggregation may be retarded while mixing with human αSyn (Rochet et al. 2000; Volles and Lansbury 2002). In addition to the sequence-dependent effect on aggregation rates of αSyn, environmental factors including pH, salts, temperature, chemical ligands, metal ions and macromolecular crowding highly impact the aggregation kinetics of αSyn (Uversky 2007). Fink's group (University of California at Santa Barbara) and Lansbury's group (Harvard Medical School) have presented that low pH, high temperature, high salt, or crowding condition induces the αSyn aggregation and fibril formation very rapidly (Uversky et al. 2001a; b; Shtilerman et al. 2002; Goers et al. 2003; Yamin et al. 2003; Lowe et al. 2004; Munishkina et al. 2004b; Rochet et al. 2004; Yamin et al. 2005; Uversky 2007). Circular dichroism (CD) and small angle X-ray scattering (SAXS) analysis of αSyn at acidic pH (pH <3.0) further show transient β-strand and compact three-dimensional conformation, respectively (Uversky et al. 2001a).

A variety of biochemical and biophysical methods have been applied for the structural elucidation of intrinsically disordered proteins. αSyn has been studied using CD, SAXS, dynamic light scattering (DLS), fluorescence, Fourier transform-infrared (FT-IR) and heteronuclear NMR spectroscopy. CD (Uversky et al. 2001a) and NMR chemical shift-derived secondary structural propensity (Eliezer et al. 2001) have showed transient helical conformation of the free-state αSyn at neutral pH. SAXS (Uversky et al. 2001a), DLS and NMR (Bertoncini et al. 2007) have surprisingly shown a relatively compact hydrodynamic radius (R_h) (radius of gyration for SAXS) of αSyn at neutral pH. The R_h of αSyn is approximately 7 Å smaller than the theoretically predicted R_h of a 140-aa

random coil-like polypeptide under chemical denatured (8 M urea) condition (Wilkins et al. 1999; Bertoncini et al. 2007). Furthermore, paramagnetic relaxation enhancement (PRE) NMR experiments display transient tertiary long-range contacts between the amphiphathic N-terminal and acidic C-terminal regions of αSyn (Bertoncini et al. 2005a; Bertoncini et al. 2005b). Same applications on the familial mutants of αSyn and homologues (βSyn and γSyn) have shown similar helical structural trends in solution at neutral pH and increasing R_h values of αSyn mutants and βSyn (Bertoncini et al. 2007; Sung and Eliezer 2007). The hypothesis based on the current knowledge is that the aggregation of αSyn is initialized by the release of structural long-range contacts (Bertoncini et al. 2005a; Bertoncini et al. 2005b) however questions arise that non-amyloidogenic βSyn which has no long-range contacts is not matched to the simple hyopthesis. A clever and systematic study on the correlation between intra-molecular structural contacts of αSyn and aggregation kinetics must be carried out to elucidate the mechanism.

1.3 NMR spectroscopy and intrinsically disordered protein (IDP)

NMR spectroscopy is a powerful biophysical tool to determine protein structure, dynamics and conformational transition and interactions (Ferentz and Wagner 2000). It has been shown to be a very powerful tool for studying intrinsically disordered proteins at the atomic level (Radford et al. 2005; Mittag and Forman-Kay 2007; Wright and Dyson 2009)}. Liquid state NMR-based approaches developed in the recent 15 years are methods of choice for determining the structural details of proteins as folding intermediate and for looking at denaturation steps (Schulman et al. 1997; Klein-

Seetharaman et al. 2002; Dobson 2004) and are also suitable for intrinsically disordered proteins (IDPs). NMR parameters including chemical shifts, relaxation rates, diffusion coefficients, scalar coupling constants and dipolar coupling constants have been used to describe the secondary structural propensity, molecular motions, local structural rigidity, compactness and local and long-range interactions for partially folded or denatured proteins at equilibrium states. For NMR studies on IDPs, advantages and disadvantages of NMR parameters are briefly presented here. (1). ^{13}Carbon chemical shifts are sensitive indicators of sample helical or extended secondary structural propensity (Wishart and Sykes 1994; Eliezer 2009). It is important to have the correct reference offsets and select random coil references because the chemical shift deviations are quite small; inappropriate selection will lead to misinterpretation of data (Mittag and Forman-Kay 2007). Although $^{3}J_{HNHA}$ scalar coupling constants are also an indicator of residual structures (Kuboniwa et al. 1994; Vuister and Bax 1994). Obtaining accurate $^{3}J_{HNHA}$ values for IDPs are difficult because of serious overlays of diagonal peaks in the 3D HNHA spectrum. (2). Relaxation experiments including ^{15}N backbone relaxation (Palmer 2004) and paramagnetic relaxation enhancement (PRE) (Battiste and Wagner 2000) can show the motional information at ps-ns and μs-ms timescale and tertiary long-range contacts (intra-molecular and inter-molecular), respectively. Local structural clusters of denatured hen lysozyme (Klein-Seetharaman et al. 2002) and β_2-microglobulin (Smith et al. 2003) have been well characterized using ^{15}N backbone relaxation. Experimental conditions for aggregation-prone IDP must be carefully considered to avoid a rapid aggregation process and fast hydrogen exchange between water in solvent and amide protons of protein (Dempsey 2001). Indirect PRE measurement using simple peak ratios

in ^{15}N-^{1}H HSQC spectra is efficient, however, the incompletely spin labeled protein can elevate the peak ratios (Eliezer 2009). (3). Residual dipolar coupling (RDC) constants in IDPs have been used for defining local structural elements (Mohana-Borges et al. 2004) as well as long-range structural contacts (Bernado et al. 2005; Bertoncini et al. 2005b). Because of the heterogeneity of the IDP ensemble, individual conformers have different alignment frames and the incorporated RDC into calculations of disordered state ensembles.

1.4 Objectives

1.4.1. Characterization of sequence- and pH-dependent conformational ensembles of αSyn using NMR spectroscopy and implication for aggregation.

Although the NMR studies on αSyn genetic mutations have shown changes of secondary structural propensity, local structural dynamics and tertiary long-range contacts, it is still very unclear why single residue substitutions accelerates αSyn aggregation. Mouse αSyn was chosen for NMR characterization at neutral pH in order to provide comprehensive information on the sequence- or residues-dependent conformational ensemble and the implication for aggregation. Mouse αSyn is known as a rapid aggregator, approximately 5 times faster than human αSyn (Rochet et al. 2000; Volles and Lansbury 2002) and the sequence alignment in figure 1.3 shows that Thr found at position 53 of mouse αSyn may play the key role in rapid aggregation. Mouse αSyn not only consists of T53, the genetic mutant, but presents one substitution (N87) and 5 substitutions (M100, G103, Y107, G121 and S122) in the NAC and the C-terminal regions, respectively. Positions 121 and 122 in human αSyn have been identified as the divalent metal ion binding sites (Rasia et

al. 2005; Binolfi et al. 2006) suggesting that mouse αSyn may lose the capability of metal ion binding in the C-terminal region and the consequence of loss of metal ions on aggregation is not known. Thus NMR characterization of mouse αSyn and derived mutations which replaces mouse αSyn residues to human αSyn residues will provide structural insight into the sequence-dependent αSyn aggregation.

In addition to the comparison of human αSyn and mouse αSyn at neutral pH, residue-specific information of acidic pH-induced αSyn aggregator has not been presented yet. Although previous studies from Fink's group show global conformational changes of αSyn at acidic pH (Uversky et al. 2001a), the details of the conformational transition at atomic-level using NMR approaches will provide valuable information regarding the early steps of αSyn aggregation. Because the molecular conformation of αSyn becomes more compact at lower pH, it is clearly opposed to the "release-and-aggregation" hypothesis (Bertoncini et al. 2005a; Bertoncini et al. 2005b) that the conformation of aggregation-prone αSyn must be less compact. Therefore, the aggregation mechanism of αSyn at low pH may undergo a different pathway compared to the mechanism at neutral pH. NMR experiments including ^{13}C chemical shift measurements, ^{15}N backbone dynamics, pulse field gradient NMR for measurement of translational diffusion rates, residual dipolar coupling and paramagnetic relaxation enhancement for αSyn at a series of pH states from pH 7.4 to pH 2.0 will be applied to understand the altered trends of transient secondary structures, the local structural clusters, and the long-range contacts as a function of pH. Once the results are collected, the molecular basis of pH-dependent aggregation of αSyn will be clearly established.

1.4.2 Determination of interactions in early aggregation events

Formation of dimer or small oligomer is a necessary step in the molecular conversion pathway, however, intermolecular interactions of αSyn at the very early aggregation stage are poorly studied. The aggregation of monomeric αSyn has been shown to occur via a nucleation dependent conversion pathway (Wood et al. 1999; Conway et al. 2000). Moreover recent studies have concluded that small oligomers are toxic and the species are responsible for the PD and other neurodegenerative diseases (Volles and Lansbury 2003; Rochet et al. 2004). αSyn dimer or small oligomer in the early aggregation events, before the well-formed nucleus, are unstable and lowly populated in solution. The ultra-weak associated complex is short-lived and conventional NMR experiments such as chemical shift measurement or intermolecular-filtered NOESY spectroscopy are not sensitive enough to detect the sub-ensemble. Relaxation dispersion (Korzhnev et al. 2004; Korzhnev and Kay 2008; Neudecker et al. 2009; Vallurupalli et al. 2009) and paramagnetic relaxation enhancement (Clore et al. 2007; Iwahara et al. 2007; Clore 2008) are recently developed NMR approaches to characterize the invisible sub-ensemble and provide simulation constraints for visualization of the invisible, unstable structures. Cases have shown that paramagnetic NMR spectroscopy is a suitable approach for not only 3D structure determination of stable protein-protein complex (Rumpel et al. 2008) but also investigating intermolecular interactions of low populated DNA-protein or protein-protein heterodimer (Iwahara and Clore 2006; Tang et al. 2006; Clore et al. 2007; Iwahara et al. 2007; Clore 2008; Tang et al. 2008a; Tang et al. 2008b). Briefly, experiments demonstrated from Clore and co-workers were carried out by a mixture of sample consisting of an isotopically ^{15}N-labeled protein for heteronuclear NMR signal

and a natural abundant ^{14}N-labeled protein (or DNA) conjugated with a spin label molecule. NMR experiments have shown that ~300 μM αSyn is quite stable for months at 15 °C (Hsu et al. 2009) thus PRE measurements for detection of intermolecular interactions must be carried out at aggregation-prone conditions. Several aggregation-prone conditions (Uversky 2007) such as rapid aggregating variants, high concentration, low pH, high temperature, high salt, and macromolecular crowding are considered for the paramagnetic NMR experiments. Characterizing the residue-specific locations of the transient intermolecular interactions will be key information to understanding which residues or segments (regions) are crucial to initial αSyn aggregation.

Chapter 2 . Methods, materials and experimental procedures

This chapter describes all experimental procedures in protein expression, modification and spin labeling strategy. NMR experiments including triple resonance assignment, ^{15}N relaxation dynamics, residual dipolar couplings and pulse field gradient diffusion measurement are also detailed explained.

All used chemicals were purchased from Sigma-Aldrich (St. Louis, MO), Fisher Scientific (Pittsburgh, PA) and Acros organics (Morris Plain, NJ) except of mentioned special materials. Equipments for sample preparation include FPLC (GE Healthcare), UV-Visible spectrometer (Beckman), lyophilizor (LabConco), high-speed refrigerated centrifuge (Solvant, Fisher Scientific) and sonicator (Fisher Scientific). 800 MHz-grade NMR tubes were purchased from Wilmad (Buena, NJ) or Shigemi (Allison Park, PA) for regular or reduced volume, respectively.

2.1 Expression of αSyn and variants

Recombinant cDNA sequence containing human αSyn or mouse αSyn inserted into pT7-7 expression vector, an ampicillin resistant plasmid, was kind gifted from Dr. Peter Lansbury at Havard University. Constructs were separately transformed into *E.coli* BL21 DE3 expression system (strain purchased from Invitrogen Inc.) and cell lines were stored at -80 ºC.

Expression and purification of αSyn followed the published protocols (Weinreb et al. 1996). Protocols of αSyn expression are described here. Required buffer and media include:

1. -80 ºC stocked cell line in *E.coli* BL21 DE3 strain.
2. Sterile LB medium (Sigma-Aldrich) and/or M9 medium.
3. 1 M IPTG (stock concentration, 2.5 g in 10 ml distilled H_2O)

Steps of expression are:

1. Pick small piece of -80 ºC stocked *E.coli* cell line by 200 μl tip and transfer to 10 ml LB medium with proper amount of antibiotics (ampicillin of αSyn and homologs or kanamycin of βSyn, γSyn), overnight incubate in shaker at 37 ºC with 225~250 rpm
2. Prepare 500 ml sterile LB medium with proper antibiotics and transfer the overnight cultured *E.coli* BL21 DE3 strain to the 500 ml medium. Still incubate the *E.coli* in shaker at 37 ºC with 225~250 rpm rate.
3. About 3-4 hours passed, check the optical density (OD) by using UV-VIS spectrometer. The measured wavelength is 600 nm, and use distilled water as blank solution. To do over-expression, when the OD_{600} values reach to 0.6 (up to 1.0), add IPTG to the culturing medium. The final concentration of ITPG is 1 mM. Keep the culturing medium in shaker, same temperature and same agitation frequency for another 4 hours.
4. 4 hours after addition of IPTG, collect the *E.coli* pellet by centrifugation at 8500 rpm for 15 minutes at 4 ºC. For LB medium, supernatant looks like light beer and

discard the supernatant solution. Keep the pellet at -80 ºC freezer to disrupt the cell wall for protein purification.

For singly ^{15}N or doubly [^{15}N -^{13}C] labeled sample, change step 2 to the following steps:

I. Use 500 ml M9 medium which has 0.5 g/L $(^{15}NH_4)_2SO_4$ and 1-2 g/L ^{13}C glucose.
II. The LB culturing medium in step 1 has to be removed, thus do centrifugation at 3000 rpm for 10 minutes.
III. Discard the supernatant and gently re-suspend the *E.coli* pellet by M9 medium. Transfer the *E.coli* to M9 medium.
IV. Do steps 3 and 4 shown in the above protocol.

2.2 Purification of αSyn and variants

Required buffers (all are sterilized):

1. Lysis buffer: 10 mM Tris-HCl pH 8.0, 1 mM EDTA, 1 mM PMSF
2. Anion exchange buffers: Buffer A: 25 mM Tris-HCl, pH 7.7~8.0, Buffer B: 25 mM Tris-HCl, pH 7.7~8.0, 500 mM NaCl

Steps of purification are:

Part A. Heat and precipitate most cellular proteins.

1. Suspend the cell pellet which is stored at -80 °C by 30 ml lysis buffer. (mixed and stirred at 4 °C around 15 minutes, the solution is then mud-like.)
2. Run sonication on ice for 10 minutes

3. After step 2, spin the cell lysate at 13500 rpm and 4 °C for 30 minutes. Collect the supernatant for next step.
4. Add 10 mg/ml Streptomycin in the solution, stirring at 4 °C for 15 minutes to precipitate most nucleic acid and nucleic acid-bound proteins (ribosomal proteins). Run centrifugation at 13500 rpm and 4 °C for 30 minutes and collect the supernatant for next step.
5. Apply 360 mg/ml ammonium sulfate $(NH_4)_2SO_4$, in the solution and stir at 4 °C for at least 30 minutes to salt out synuclein. Centrifuge the mixture at 13500 rpm and 4 °C to collect the pellet which mainly contains salted out synuclein.
6. Reconstitute the pellet in step 5 by adding 30 ml buffer A depends on the concentration (or expression yield). It must be very careful to make all salted out proteins dissolved without making air bubbles prior load into FPLC injection loop. The solution should be filtered before applying to the superloop container for FPLC purification.
7. Transfer the solution in a boiling bath (~100 °C) for 10 minutes to denature most heat sensitive protein. Wait for cooling down to room temperature and run centrifugation at 13500 rpm and 4 °C to separate insoluble and soluble proteins. Synuclein is in the soluble part.
8. Cool solution from step 7 should be performed 40-fold volumetric dialysis by buffer A at 4 °C to ensure no salt residue for anion exchange.

Part B. Purification by FPLC using anion exchange column.

Anion exchange columns including HiPrep 20 mL DEAE column and HiTrap 5 mL Q column were purchased from GE Healthcare at Piscataway, NJ. Either DEAE or Q column does separation of synuclein and other heat-resistant protein in a similar manner. In order to save FPLC running time, purifications done in 2008 and 2009 were using the HiTrap Q column.

1. The Q column must be equilibrated by buffer A before injecting the solution from step A8.
2. After injection, using at least 5 column volume of buffer A to wash Q column, the flow through has some unknown proteins.
3. Apply gradient elution from (100% buffer A + 0% buffer B) to (0% buffer A + 100% buffer B), the synuclein is eluted at range of 200-300 mM NaCl. The elution length is typically 100 ml for 1-liter cultured products to have efficient separation of synuclein and undesired proteins.

Notes for anion exchange steps.

1. According to current experiences, streptomycin doesn't fully precipitate nucleic acid (streptomycin only binds nucleic acid-bound protein, thus free nucleic acid are still in solution). Nucleic acids stick in anion exchange column and will be eluted while [NaCl] is greater than 300 mM by monitor absorbance at 260 nm. Try to elongate the elution volume in the range of 150-250 mM to separate synuclein and nucleic acids.

2. For the preparation of NMR samples, dried proteins were dissolved to run size-exclusion gel filtration using a HiPrep 26/60 superdex75 column (GE healthcare, Piscataway, NJ) if the gel electrophoresis result showed dimers or oligomeric αSyn. The purity of αSyn was verified again by gel electrophoresis as a single band at 14.5 kDa.

Part C. Storage of αSyn

1. Solution containing purified αSyn from anion exchange column was dialyzed against 10 mM $(NH_4)_2SO_4$ at the 20-fold volumetric ratio for 4 times at 4 °C. Each time of dialysis was carried out at least 4 hours to ensure completely buffer exchanged. 20^4 ($1.6x10^5$) times of dilution is believed to have a salt-free solution for αSyn.
2. Salt-free solution removed from dialysis bag was quickly frozen by cryogenic liquid nitrogen and was applied for lyophilization (freeze-and-dry). Completely dried powder of αSyn looks like cotton and was stored at -20 °C freezer for future NMR experiments.

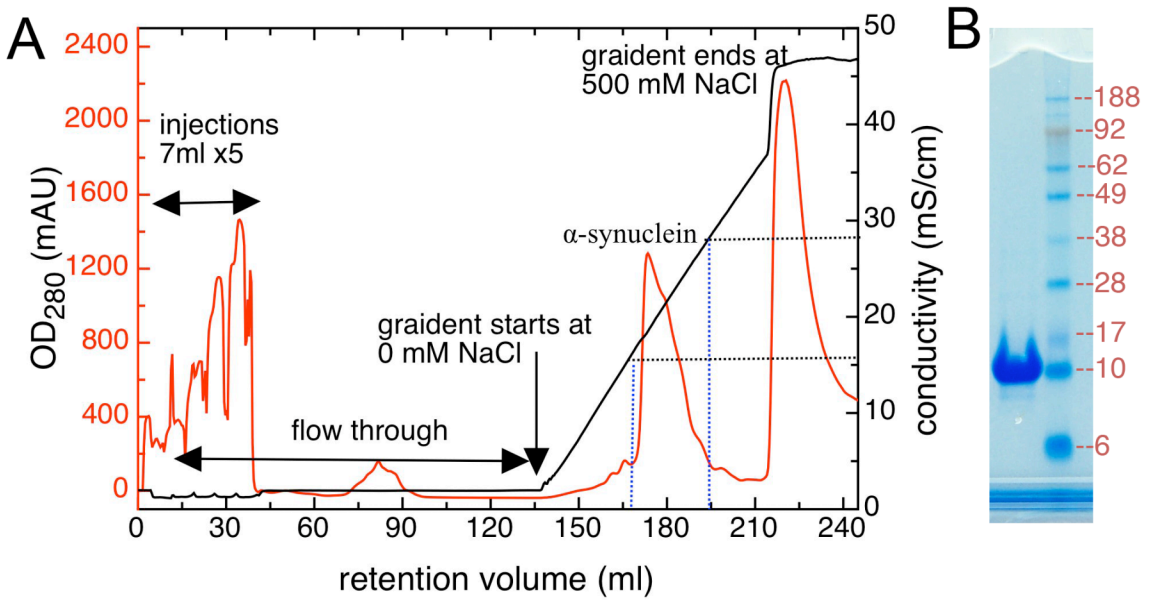

Figure 2.1 FPLC profile and SDS-PAGE of purified αSyn.

A. Purification of αSyn using HiTrap Q anion exchange column. Red and black curves are the signals of protein concentration and conductivity, respectively. 3 stages can be seen in the plot. (1). 5 times of 7-ml injection of impure αSyn was loaded into Q column (2) column was washed by buffer A and small amount of unbound protein was eluted around 70-90 retention volume. (3). Gradient of NaCl started at approximately 135 ml and αSyn was eluted (first peak) and separated from other nucleic acid and impurity (second peak) easily. Conductivity curve (black line) was used to monitor the gradient of [NaCl]. B. Proper amount of purified αSyn in panel A was loaded into SDS-PAGE (4-12% gradient precast gel from Inivitrogen). No other proteins were found except over-loaded αSyn located at 10-17 kDa.

2.3 Strategy of backbone assignment

2.3.1 ^{13}C-^{13}C connections

Strategies of backbone assignment of NMR spectra are well developed for globular folded proteins using ^{13}C-^{13}C connections including $^{13}C^{\alpha}$, $^{13}C^{\beta}$, and $^{13}C'$ (Ferentz and

Wagner 2000). Paired spectra including HNCACB/CBCA(CO)NH and HN(CA)CO/HNCO used in the ^{13}C-^{13}C connections are required to show connections between preceding and succeeding connections. The success using ^{13}C-^{13}C connections in folded protein is strongly counting on the well-dispersed chemical shifts in the regions of secondary structures. Deviations of ^{13}C chemical shifts from the random coil chemical shifts are typically 4-6 ppm. However, this conventional strategy is not perfect for NMR assignment of IDPs and denatured proteins. IDPs do not exhibit stable secondary structures therefore all ^{13}C chemical shifts ($^{13}C^{\alpha}$, $^{13}C^{\beta}$, and $^{13}C'$) are ambiguous and chemical shift deviations are quite small within the range of 0.5-1 ppm. To achieve accurate backbone assignment, new strategies including ^{15}N-^{15}N connections (Panchal et al. 2001) (section 2.3.2) and G-matrix Fourier transform NMR (GFT-NMR) (Kim and Szyperski 2003; 2004) had been employed to carry out spectral assignments.

2.3.2 ^{15}N-^{15}N connections

^{15}N chemical shifts compared to other ^{13}C and ^{1}H chemical shifts in denatured or disordered proteins are less sensitive to the effect on secondary/tertiary structures and exhibit wider range typically 100-135 ppm. Thus Hosur and his colleagues have developed a new assignment strategy (Panchal et al. 2001) for unfolded proteins according to this characteristic. Two pulses named HNN and HN(C)N were modified from HNCA and HN(CO)CA to perform ^{15}N-^{15}N connections. Unlike conventional approach using ^{13}C-^{13}C connections, Hosur's approach does not necessarily require paired 3D spectra for assignment because each of the two experiments (HNN and HN(C)N) is capable of providing complete backbone assignments independently.

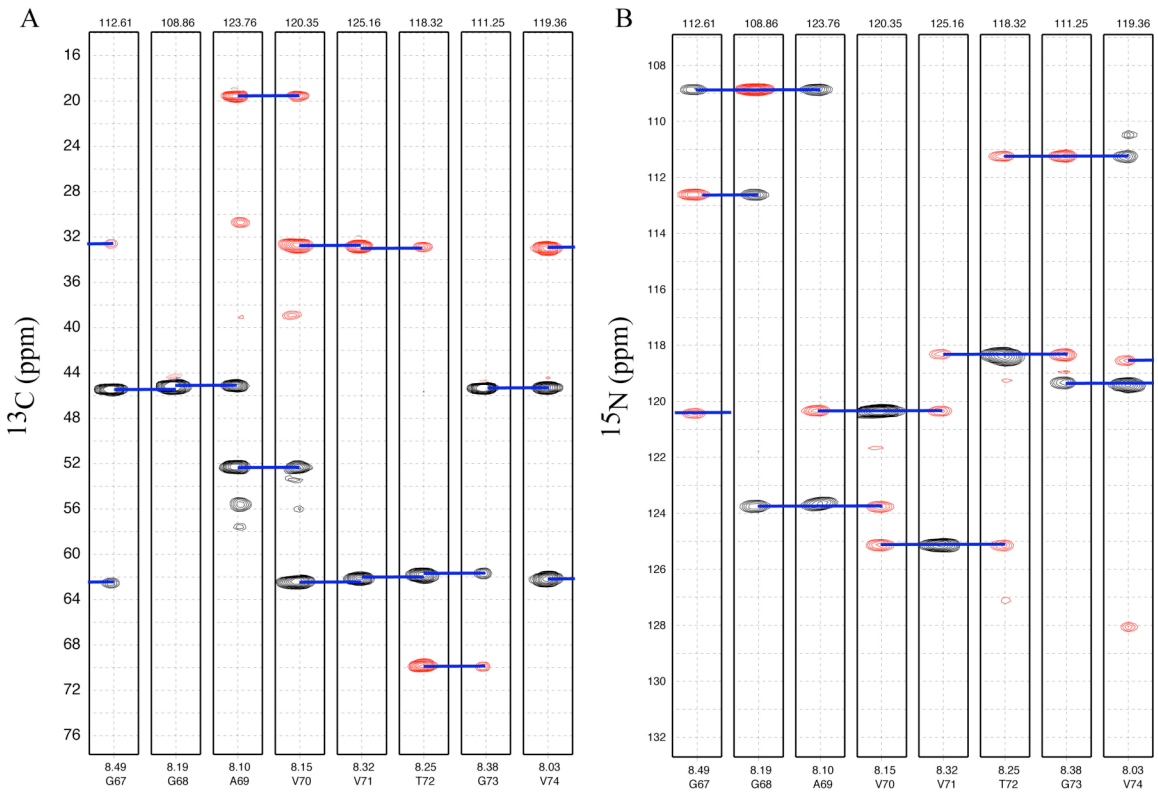

Figure 2.2 Examples of ^{13}C-^{13}C and ^{15}N-^{15}N connections for assignment.

Positive and negative peaks are colored in black and red, respectively. Resonance frequencies of H^N and ^{15}N in the F3 and F2 dimensions are labeled at the bottom and on the top of each strip, respectively. Range of ^{13}C or ^{15}N chemical shifts in F1 dimension is depicted. αSyn was dissolved in 2 M glucose solution. Data were collected at 15 °C on a Varian 800 MHz NMR and were plotted by NMRPipe. **A.** Strips of G^{67}-G-A-V-V-T-G-V^{74} extracted from HNCACB show very ambiguous $^{13}C^{\alpha}$ and $^{13}C^{\beta}$ chemical shifts of Val and Gly. **B.** Strips of G^{67}-G-A-V-V-T-G-V^{74} extracted from HNN show well-dispersed ^{15}N resonances. Several 3-residue connection patterns including GGX_3, GX_2X_3, X_1X_2G, and $X_1X_2X_3$ can be seen here.

Characteristics of HNN spectrum include 1). HNN retains *i*-1, *i* (diagonal peak) and *i*+1 correlation in each H^N except of several H^N which are connected to prolines or the last

residue and was chosen to perform most of the assignment tasks. 2). Spectral strips of H^N connected to prolines or last residue only show two peaks. 3). Diagonal and cross-peaks in each non-Gly and non-Pro H^N strip are positive and negative, respectively. 4). H^N strips of X_1-Gly-X_3 have positive cross-peak for succeeding residue (X_3), negative cross-peak for preceding residue (X_1) and negative diagonal peak. 5). While Gly positions at X_1 in point 4, the sign of peak reverses. Hosur et al. have summarized characteristics of HNN spectrum into 6 groups with 16 special patterns of peak signs. In summary, glycine and proline residues are good checkpoints and the 16 special patterns further assist sequential assignment rapidly. In addition, time of HNN data acquisition was shorter than 24 hours that is efficient for experiments under aggregation-prone conditions such as low pH, crowding, and high temperature.

2.4 Analysis of NMR relaxation data.

2.4.1 General information

All NMR ^{15}N backbone relaxation data were recorded on a Varian 800 MHz or a Varian 600 MHz spectrometer using different pulse sequences including longitudinal relaxation rate (R_1), transverse relaxation rates (R_2^{CPMG} and R_2^{HE}), steady state heteronuclear NOE, cross-correlation rate (η_{xy}), and $^1H^N$ transverse relaxation ($^1H^N$ R_2) (table 2.1). All data are stored as a pseudo 3D format and the interleaved FIDs were separated using a macro written in C language obtained from Lewis Kay (University of Toronto). Individual FID was then processed by NMRPipe (Delaglio et al. 1995) and was converted to Sparky format (Goddard and Kneller). All data were fitted using a single exponential decaying function plugged in Sparky.

Table 2.1 List of used NMR relaxation experiments

Type	Relaxation time	Data points	Recycle delays	Source	Reference
R_1	10 – 1800 ms	≥8	2 seconds	Varian	(Farrow et al. 1994)
R_2^{CPMG}	10 – 250 ms	≥8	2 seconds	Varian	(Farrow et al. 1994)
NOE	3 seconds	2	2 seconds	Varian	(Farrow et al. 1994)
R_2^{HE}	1-30 cycles 1 cycle = 7.68 ms	≥8	2 seconds	Homemade	(Wang and Palmer 2003)
η_{xy}	6, 8, 10, or 12 cycles 1 cycle = 7.68 ms	2 or 4	2 seconds	Homemade	(Kroenke et al. 1998)
$^1H^N$ R_2	6 – 55 ms	≥7	1.5 seconds	Homemade	(Donaldson et al. 2001)

2.4.2 Fitting relaxation data

Examples of ^{15}N backbone relaxation experiments including R_1, R_2^{CPMG} and R_2^{HE} and $^1H^N$ R_2 are shown in figure 2.3. Relaxation rates can be obtained using the following equation:

$$I = I_0 e^{(-t/T)}$$

where I_0 and T are unknown, I is the intensity at particular timing t. Relaxation rates R is a reverse value of T. Instead of getting deviations from multiple repeats, deviations (ΔR) of relaxation rates are simply converted from the fitting errors (ΔT).

$$\frac{\Delta T}{T} = \frac{\Delta R}{R},\ \Delta R = \frac{\Delta T}{T} \times R = \frac{\Delta T}{T} \times \frac{1}{T} = \frac{\Delta T}{T^2}$$

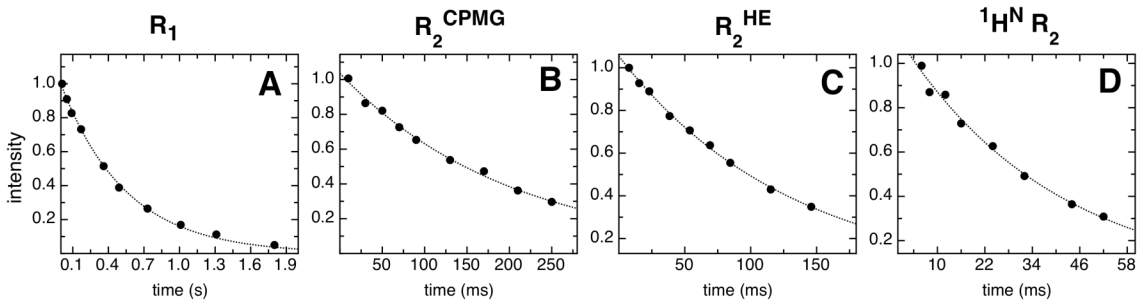

Figure 2.3 Example fitting data of the different relaxation parameters

Examples of four types of relaxation experiments are shown. The data points are fitted using a two-parameter single exponential decaying function to obtain the relaxation period "T". Relative intensity at Y-axis is used in the plots to conveniently inspect the degree of signal reductions.

2.4.3 Calculation of steady-state heteronuclear NOE

^{1}H-^{15}N steady-state heteronuclear NOE values collected under all used conditions were measured by recording spectra with or without a ^{1}H saturation period of 3 seconds. Residual NOE values are calculated by taking the ratios of intensities in the two spectra:

$$NOE = \frac{I_{sat}}{I_{ref}}$$

The uncertainties in the measured peak-height were set equal to the root-mean square baseline noise in the spectra, and the errors in NOE were the standard deviation of the two sets (Farrow et al. 1994).

2.4.4 Calculation of R_{ex}

To obtain the chemical exchange rate (R_{ex}) on the ms-μs timescale, approach developed from Palmer's group (Columbia University) was employed. This approach uses two

NMR parameter to derive R_{ex}: (1) the in-phase Hahn echo experiment (R_2^{HE}) (Wang et al. 2001; Wang et al. 2003)and (2) the η_{xy} (CSA/dipolar cross-correlation rate) experiment (Tjandra et al. 1996; Kroenke et al. 1998). R_2^{HE} is to with the R_2^{CPMG} experiment without suppression of chemical exchange. Each η_{xy} experiment was divided into two ^1H-^{15}N HSQC type spectra and the η_{xy} values was determined by following equation:

$$\frac{I_{cross}}{I_{auto}} = \tanh(\eta_{xy}\tau_{HE})$$

I_{cross} and I_{auto} are the peak intensity of cross- and auto- relaxation, respectively. τ_{HE} = n/J_{NH}, where n is a positive integer (e.g. 6 for 263K experiments) and J_{NH} is the scalar coupling constant of amide bond (93 Hz). Two more η_{xy} experiments were performed to get the average and standard error of the mean of each residue.

R_{ex} was defined as $R_{ex} = R_2^{HE} - R_2^0$, where $R_2^0 = \kappa\eta_{xy}$, and κ is an average value of the ratio of R_2^{HE}/η_{xy} for those residues not subjected to chemical exchange. To obtain the κ value for αSyn, weighted correlation fittings of R_2^{HE} and η_{xy} were calculated. Residues with differences of R_2^{HE} and η_{xy} greater than 2.5 were not included in the correlation fitting. Criterion "$R_2^{HE} - \eta_{xy} \leq 2.5$" is arbitrary and was chosen because of the better linear correlation in the R_2^{HE}/η_{xy} plot after iterated selection of reasonable cutoff.

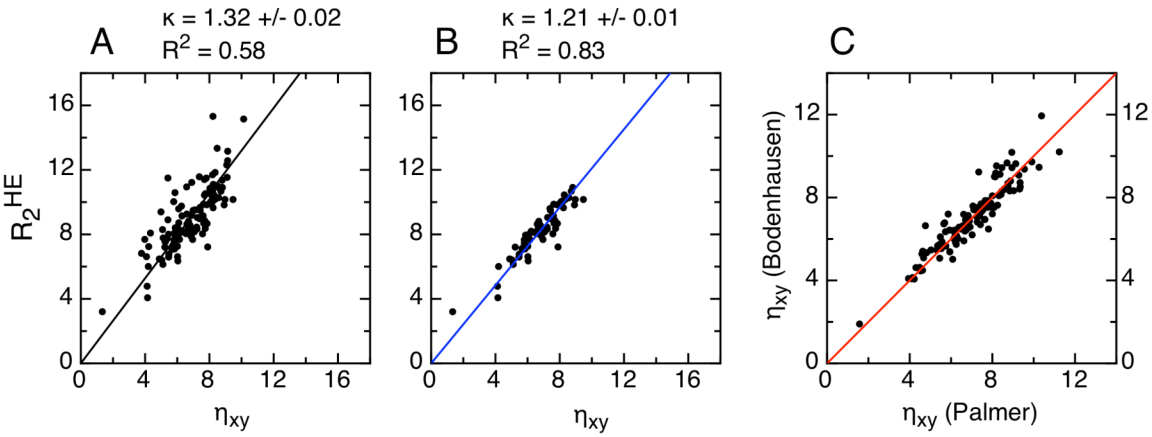

Figure 2.4 R_2^{HE} versus η_{xy} plot and correlation of η_{xy} from two pulse sequences.

The linear regression correlation values R of R_2^{HE} / η_{xy} using all data points in (A) and limited data points ($R_2^{HE} - \eta_{xy} \leq 2.5$) in (B) are 0.76 and 0.91, respectively. κ value is the weighted fitting of R_2^{HE} / η_{xy} which is the fitted slope. (C). η_{xy} values of αSyn at 263K obtaining from two NMR pulse sequences show good correlation.

Recently, a new η_{xy} pulse sequence proposed by Bodenhausen and his colleagues (Pelupessy et al. 2007) is believed being more accurate and does correct some values of αSyn at 15 °C. Symmetrical reconversion pulse train is embedded in the Bodenhausen's η_{xy} pulse sequence and the pseudo 3D spectrum is composed of 4 interleaved FIDs. Following equation is used to get the Bodenhausen's η_{xy} values:

$$\eta_{xy} = (\frac{J_{NH}}{n})\,\mathrm{atanh}\sqrt{\frac{I_2 I_3}{I_1 I_4}}$$

where J_{NH} is the scalar coupling of NH bond, n is an integer. Peak intensities of anti-phase and in-phase spectra are "I_2, I_3" and "I_1, I_4", respectively. For η_{xy} values at supercooled temperature, the two methods carried out similar results (figure 2.4C).

2.5 MTSL spin label reaction and PRE measurement

2.5.1 Spin label reaction

Side-directed mutagenesis of cysteine mutations including human αSyn A19C, A90C, G132C and mouse αSyn A19C and G132C were constructed by Dr. David Fela and Lijuan Kang. Expression and purification of cysteine variants were carried out by the same protocols described at sections 2.1 and 2.2. 5-10 mg dried αSyn cysteine variants was dissolved by PBS or buffer B with the treatment of DTT (20X molar ratio) for 4-6 hours at 4 °C to remove all cys-cys linked dimer. Sample was injected into desalting column to separate αSyn and DTT efficiently (figure 2.5). Excess MTSL (20-fold molar ratio) was immediately added to mixed with eluted αSyn cysteine variants. Spin label reaction was performed in dark at 4 °C overnight. I have discovered that 4 M urea was required for αSyn A19C mutant during the DTT treatment otherwise the spin label reaction did not success. MTSL purchased from Toronto Chemical Research (catalog #: O875000, Ontario, CA) was freshly dissolved by acetone (10 mg per 400 μl).

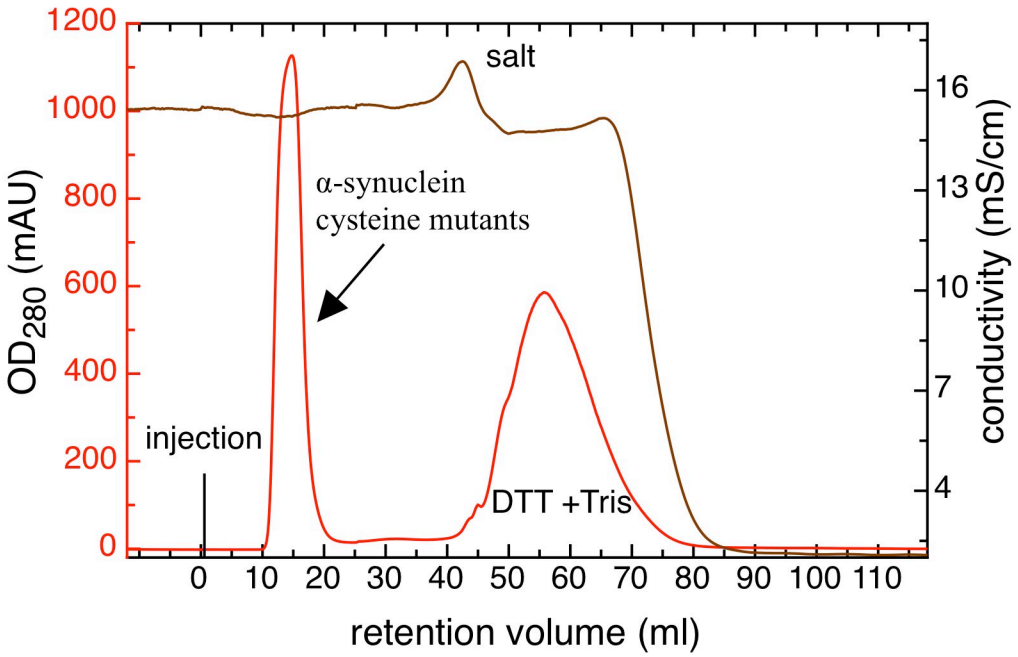

Figure 2.5 FPLC desalting process of αSyn cysteine variants for spin labeling.

HiPrep 16/60 desalting column (50 ml) was used to DTT from solution containing αSyn cysteine variants. The DTT treated solution was injected into column which was equilibrated by PBS. Injection volume was 2-5 ml depending on the amount of αSyn in solution (5-10 mg). After 10 ml retention volume, αSyn came out first and the eluted volume was ~10 ml. DTT came out lately as depicted in the plot. Conductivity was nearly 0.00 because water was used to wash the desalting column after seeing DTT.

Successfully MTSL labeled product is shown in figure 2.6 that the protein molecular weight is increased by 186. Excess un-reacted MTSL was removed by centrifugal column and aliquot was taken for mass spectrometer using ESI-MS (data not show).

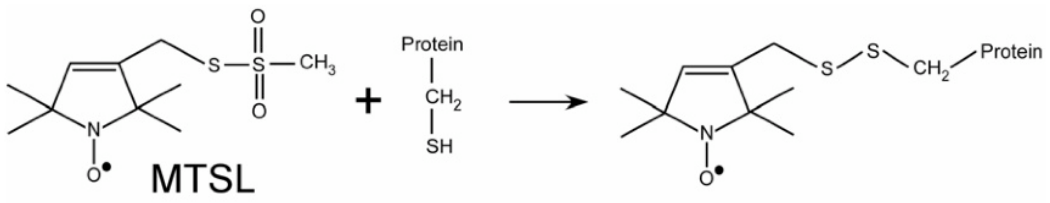

Figure 2.6 Chemical equation of spin label reaction

Chemical structure of MTSL is shown. MTSL contains a nitroxide free radical that caused paramagnetic effect during NMR data collection. MTSL mixed with protein that has a single reduced cysteine in solution results in conjugation on the protein via disulfide bond.

2.5.2 PRE measurement

Paramagnetic relaxation enhancement (PRE) can be simply obtained by calculating the intensity ratios (I_{para}/I_{dia} or I_{ox}/I_{red}) of cross-peaks under paramagnetic and diamagnetic conditions (figure 2.7). The peak intensity of ^{1}H-^{15}N HSQC cross-peaks is affected by PRE during the INEPT delays (9~10 ms depends on HSQC pulse sequences). Stronger PRE effect results in the broader linewidth, that is lower intensity. Theoretically, I_{para}/I_{dia} is within the range of 0 for very close distance and 1 for distance longer than 25 Å. The relationship of intensity of magnetization and PRE has been shown by Wanger and colleagues (Battiste and Wagner 2000):

$$\frac{I_{ox}}{I_{red}} = \frac{R_2 \exp(-\Gamma_2 t)}{R_2 + \Gamma_2}$$

where Γ_2 is the paramagnetic transverse relaxation enhancement.

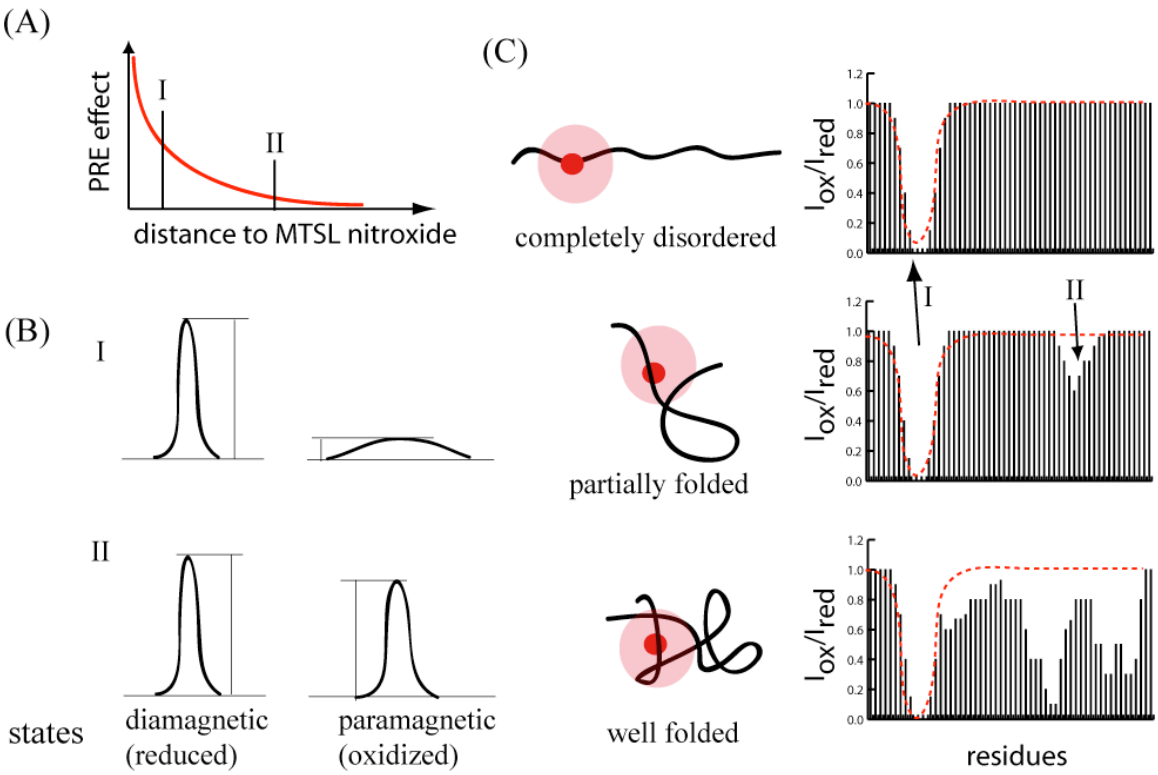

Figure 2.7 Schematic PRE application for IDP

A. The PRE effect on intensity ratio is relevant to the r^{-6} distance. B. Two sites (I and II) as picked in panel A present different linewidths affected by the distance-based PRE. Diamagnetic state linewidth (intensity) represent the reference signals for corresponding cross-peaks. C. The sensitive of PRE is used to characterize the tertiary long-range contacts of partially or unfolded protein. For a fully extended protein, the PRE effect is local and at the neighborhood of spin labeled residue (top). Partially and well-folded proteins show map dips with different amplitude in the PRE profiles. The reduction of intensity is related to the distances of amide protons and MTSL nitroxide.

The MTSL-induced PRE Γ_2 were converted into distances by using the following equation for the effect of nitroxide electron spin on nuclear magnetic relaxation (Kosen 1989; Gillespie and Shortle 1997; Battiste and Wagner 2000; Lietzow et al. 2002):

$$\Gamma_2 = \frac{K}{r^6}\left(4\tau_c + \frac{3\tau_c}{1+\omega_H^2\tau_c^2}\right)$$

where r is the distance from electron spin to amide protons, τ_c is the correlation time for the electron-nuclear interaction, ω_H is the Larmor frequency and K is 1.32×10^{-32} cm^6s^{-2}. The correlation τ_c is approximately equals the protein rotational time according to the following relationship:

$$\frac{1}{\tau_c} = \frac{1}{\tau_e} + \frac{1}{\tau_r} \approx \frac{1}{\tau_r}$$

where τ_e, the electron spin time, is ~100 times greater than τ_r which is the global correlation time of protein. For the PRE measurements of αSyn, τ_r is 2-3 ns at 15 °C and ω_H is either 600 or 800 MHz depending on the magnetic field.

2.5.3 Calculation of theoretical PRE intensity ratios of fully extended protein

Theoretical PRE curves were calculated by using XPLOR-NIH (Schwieters et al. 2003) to generate MTSL-attached (at A19C) fully extended structures. 400 structures were simulated without distance restraints at high temperature. Individual structures were inspected manually to select fully extended configurations to further extract the distances from MTSL nitroxide to each amide proton. Distances were then converted into the Γ_2 values assuming constant R_2 (10 s^{-1}) for each residue and correlation time of 3 ns. I_{para}/I_{dia} PRE values were finally calculated and used as a reference for an unfolded protein with no long-range interactions (Fieber et al. 2004). Since the PRE effect on a fully extended protein is limited to the neighboring residues, the theoretical A19C I_{para}/I_{dia} profile can be easily duplicated for other spin labeled sites (A90C and G132C).

2.6 Residual dipolar coupling experiments

2.6.1 Medium preparation

The bicelle medium developed by Otting et al. (Ruckert and Otting 2000) was used to perform RDC measurement in this thesis. Required Chemicals includes C8E5 (Sigma #: P4654-1ML), 1-otctanol (Sigma #: O4500-100ML), PBS buffer, Protein samples and D_2O (CIL, 99.9%)

Preparation of a 10% C8E5 stock medium which molar ratio of C8E5 (50 μL) : 1-octanol (14 μL) is 1.06.

1. 50 μL C8E5 + 450 μL PBS (containing 10% D_2O), mix well. The solution will be very clear, like water.
2. Add 4 μL 1-octanol into the aliquot and vortex the mixture for ~ 2 minutes. The solution is foamy.

   It must be careful in drawing octanol, it's very viscous. Try to remove the on-tip 1-octanol before the addition.
3. Add another 4 μL 1-octanol, vortex the solution > 5 minutes. The solution has a lot of small bubbles and is milky. Vortex time is very critical; the longer time for mixing, the better homogenous solution it is.
4. Add another 3 μL 1-octanol, vortex it for 5 ~ 10 minutes. At the moment, many bubbles are gone, and solution is less milky.
5. Add final 3 μL 1-octanol into the aliquot. Once the addition is done, the solution may become clear rapidly. Still, vortex it to mix all the solutes well. The final

solution is clear but viscous. Flip the small tube to see that tiny bubbles are floating in the solution. Using small centrifuge to remove the bubbles before NMR test. The prepared stock medium was leaving at room temperature for 3~4 hours to see if the medium is stable. If not stable, the solution is milky and bilayer again.

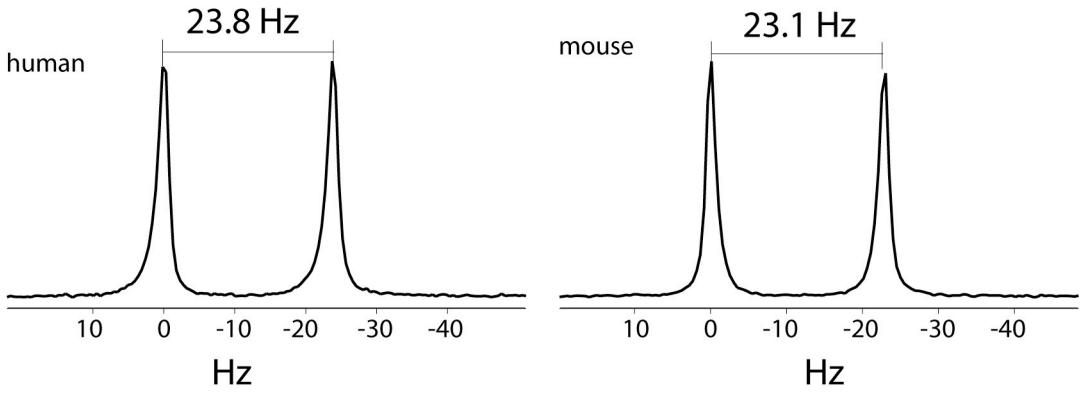

Figure 2.8 Measurement of quadrupolar deuterium splitting constant

Human or mouse αSyn aligned in 5% C8E5/octanol bicelle resulted in the quadrupolar splitting constants of 23.8 and 23.1 Hz at 15 °C, respectively. 1D spectra were processed and plotted by Felix 2000 (Accelrys, San Diego). Left peak is positioned at 0.0 Hz. The splitting values are very close suggesting nearly same alignment effect on human and mouse αSyn since splitting values is almost linearly with the bicelle concentration (Prestegard et al. 2000).

NMR test:

1. Mix 150 μL 10% C8E5 stock medium and 150 μL PBS (10% D_2O added, no proteins) well and test the quadrupolar deuterium splitting constant. The J values were within the range of 22~25 Hz.

2. If the splitting constant is good, mix the stock medium and protein solution by 1:1 ratio (final C8E5 concentration is 5%). Vortex the solution extensively at least 5 minutes, remove the bubbles and run NMR experiment. Quadrupolar deuterium splitting constant must be measured again to ensure the medium is anisotropic. Splitting profiles of human and mouse αSyn aligned in 5% C8E5 media are shown in figure 2.8.

2.6.2 NMR measurement of D_{NH}

To obtain the residual dipolar couplings of backbone amine protons (D_{NH}), Two ^{1}H-^{15}N HSQC spectra using IPAP (in phase-anti phase) pulse train are required. IPAP-HSQC (Ottiger et al. 1998) records two HSQC spectra without using decoupling pulse: one in-phase and one anti-phase. Addition and subtraction of the two spectra yield two new spectra each with one of the doublet. The separation of doublet NH cross-peaks eliminates overlapping problems during assignment; thus more unambiguous D_{NH} will be obtained. IPAP-HSQC spectra of human αSyn in PBS and in bicelle solution provide the values of scalar coupling constant J_{NH} and $J_{NH}+D_{NH}$, respectively. The differences of two measured coupling constants are the residual dipolar couplings as shown in figure 2.9.

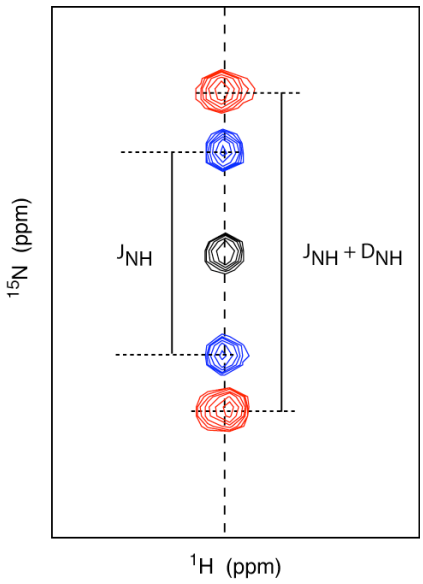

Figure 2.9 Illustrated spectra showing the measurement of D_{NH}

One residue is used to represent the concept of RDC D_{NH} measurement. Black cross-peak is the resonance frequency of decoupled NH proton. Blue doublet is the IPAP spectra in isotropic solution given J_{NH} value and red doublet provides the J_{NH}+D_{NH} value. Here, the combined value is greater than J_{NH} meaning D_{NH} is positive. In contrast, negative D_{NH} leads to product of J_{NH}+D_{NH} smaller than J_{NH}.

2.7 Translational diffusion coefficient

Winlkins et. al. (Wilkins et al. 1999) has used PFG-NMR to measure the R_h of more than 10 peptides and proteins ranging from 16 residues to 414 residues (and 494 residues for dimer) under the native state and the urea denatured unfolded state. In their report, they have established a relationship of size of R_h (in Å) and the length *N* of polypeptide chain at folded and unfolded states:

$R_h = (4.75 \pm 1.11)N^{0.29\pm0.02}$ for folded state

$R_h = (2.21 \pm 1.07)N^{0.57\pm0.02}$ for unfolded state.

For αSyn, the folded and unfolded R_h values are expected to be 19.9 and 37.0 Å, respectively.

PFG-NMR experiments incorporated with longitudinal Eddy current pulse schemes and convection compensation was used to measure the translational diffusion coefficients (D_{trans}) (Li et al. 2005b). Samples containing 300 μM αSyn and 35 mM 1,4-dioxane were dissolved in PBS buffers at pH 7.4 and 2.5 for PFG-NMR experiments at 15 °C. 25 1D PFG-NMR spectra were acquired over a range of gradient strengths of 2 to 17 G/cm or 5 to 50 G/cm for 1,4-dioxane or αSyn, respectively. In order to avoid strong water signals during data collection, samples for PFG-NMR experiments are suggested to be dissolved in 100% D_2O. Preparation of PBS buffer dissolved in 100% D_2O was carried out by lyophilization of fixed volume of PBS buffer (100% H_2O) and same volume of 100% D_2O was added in the completely dried tube. pD was not corrected.

NH fingerprint region is no longer useful and methyl group region (0-2.3 ppm) are chosen to perform volume integration and further analysis. Peak volumes of 1,4-dioxane and αSyn were integrated using VNMRJ 2.1 (Varian Inc., Palo Alto, CA) and were used to calculate D_{trans} (Li et al. 2005b) using GnuPlot 4.0 according to the following relationship:

$$I = I_0 \exp[-2D_{trans}\gamma^2 G^2 \delta^2 (\Delta + \frac{2}{3}\delta + \frac{3}{4}\tau)]$$

where γ is the proton gyromagnetic ratio (26752.22 $s^{-1}gauss^{-1}$), δ,Δ and τ are time delays used for data collection and factor 2 is included if pulse train of convection compensation

is used. The delay times for dioxane and αSyn were adjusted depending on the temperatures to get strong signals at low G and reasonable decays as the G increases. Since αSyn and dioxane were dissolved in one solution, the viscosity effect on $D_{trans}^{\alpha Syn}$ and $D_{trans}^{dioxane}$ can be ignored in the Stokes-Einstein equation:

$$D_{trans} = \frac{k_B T}{6\pi\eta R_h}$$

where k_B is the Boltzman constant, T is the temperature in Kelvin, η is the solvent viscosity and R_h is the effective hydrodynamic radius. Therefore, the equation can be simplified to get the hydrodynamic radius of αSyn by the relationship:

$$R_h^{\alpha Syn} D_{trans}^{\alpha Syn} = \frac{k_B T}{6\pi\eta} = R_h^{dioxane} D_{trans}^{dioxane}$$

where $R_h^{dixoane}$ is 2.12 Å.

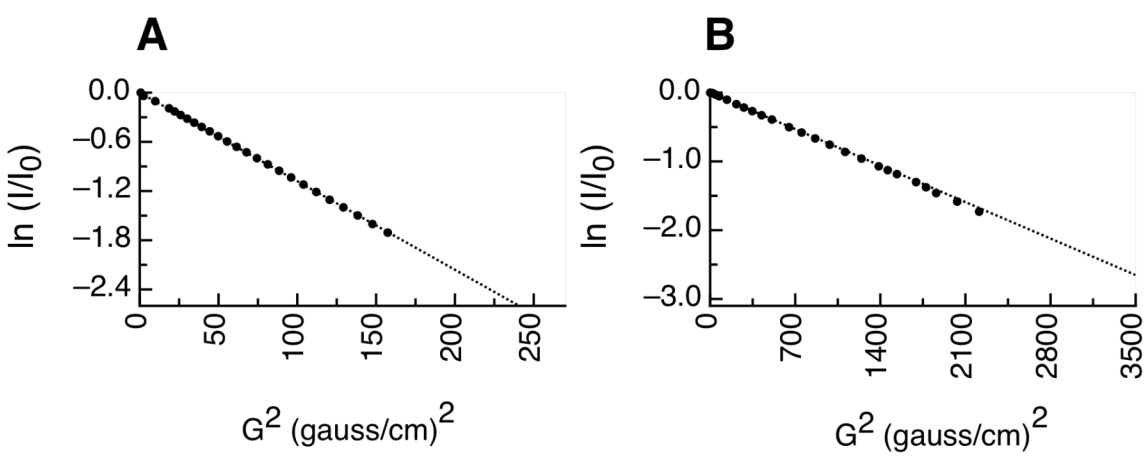

Figure 2.10 Examples of data fitting of 1D PFG-NMR spectra

Data fitting of 1,4-dioxane (A) and αSyn (B) are shown. Integrated peak volume (I) of dioxane and αSyn from 25 1D PFG-NMR spectra at different gradient strength (G) are used. Translational diffusion coefficient of dioxane and αSyn can been extracted from the slope of linear regression fit of $\ln(I/I_0)$ *versus* G^2 plot.

Chapter 3 . NMR Characterization of Intrinsically Disordered Human and Mouse α-Synuclein: implication for protein aggregation

3.1 Introduction

Natively unfolded or so called intrinsically disordered proteins can adopt a variety of conformational states and interconvert between them on a wide range of time scales (Dyson and Wright 2004; Mittag and Forman-Kay 2007). Identifying the range of conformations and timescales that can be accessed is important to understanding how natively unfolded proteins can be converted from their normally soluble form to insoluble fibers or plaques found in neurodegenerative diseases such as Alzheimer's disease, Parkinson's disease (PD), Huntington's disease and type II diabetes. Fluctuations within the ensemble of unfolded states are likely to be important in determining the pathway of folding to the aggregated form as conformational fluctuations provide a mechanism for different residues to come into contact with one another by exposing or protecting different regions of the protein to other proteins or to solvent.

Human αSyn is the primary protein component of the Lewy body deposits that are the diagnostic hallmark of PD (Spillantini et al. 1997). Aggregation of αSyn into fibrils is thought to play an important role in the pathogenesis of PD (Spillantini et al. 1998a; Spillantini et al. 1998b). The mechanism of conversion from soluble αSyn protein to amyloid fibril is proposed to arise via a nucleation dependent mechanism in which amyloidogenic proteins can access an unstable, partially ordered conformation prior to self assembly into insoluble protofibrils followed by the formation of amyloid fibrils

(Caughey and Lansbury 2003; Volles and Lansbury 2003). Human αSyn is natively unfolded in solution but is composed of conformational ensembles that are on average more compact than those expected for a random coil protein (Bussell and Eliezer 2001; Eliezer et al. 2001; Dedmon et al. 2005b; Sung and Eliezer 2007).

Human αSyn is highly homologous in amino acid sequence to mouse αSyn, human β-synuclein (βSyn) and γ-synuclein (γSyn), and variants involved in early onset disease including the human αSyn with point mutations A53T (Polymeropoulos et al. 1997), A30P (Kruger et al. 1998) and E46K (Zarranz et al. 2004). The amino acid sequence of human αSyn can be divided into three regions including the N and C-terminal regions and the central NAC. The N-terminal region (residues 1-60) consists of 11-residue repeats with a highly conserved hexamer motif KTK(E/Q)GV. The charged C-terminal region (96-140) has a high percentage of aspartate, glutuamate, and proline residues and the NAC region is a hydrophobic region. It has been shown that the rate of fibrillization is highly dependent on the sequence of the protein as well as the solution conditions (Narhi et al. 1999; Wood et al. 1999; Conway et al. 2000; Rochet et al. 2000). Mouse αSyn forms fibrils fastest relative to human αSyn, βSyn and γSyn as well as relative to the variants A53T and A30P involved in early onset of PD. Overall the rates of oligomer or fibril formation can be ordered from fastest to slowest in the order of mouse αSyn > human A53T αSyn > *wt* human αSyn, human A30P αSyn >> γSyn > βSyn (Conway et al. 1998; Rochet et al. 2000; Rochet and Lansbury 2000; Serpell et al. 2000; Volles and Lansbury 2003).

Mouse αSyn with 95% sequence identity to human αSyn and faster aggregation kinetics *in vitro* provides a good system to understand the sequence determinants of the conformation and dynamics of the disordered ensembles and their relationship to aggregation. There are seven substitutions between human and mouse αSyn including the A53T substitution that is the same as the one that has been linked to familial PD (figure 3.1). There is a single S87N substitution in the NAC region and the remaining five substitutions are found in the C-terminal region. One of C-terminal substitutions, D121G, is at a position characterized as a key metal ion binding site in human αSyn (Rasia et al. 2005). Structural characterization of mouse αSyn by CD shows a natively unfolded state in solution (Rochet et al. 2000) but little is known about the nature of the conformational ensembles that populate mouse αSyn.

```
       1         10        20        30        40        50        60        70
human  MDVFMKGLSKAKEGVVAAAEKTKQGVAEAAGKTKEGVLYVGSKTKEGVVHGVATVAEKTKEQVTNVGGAV
mouse  ..........................................................T.............

                 80        90       100       110       120       130       140
human  VTGVTAVAQKTVEGAGSIAAATGFVKKDQLGKNEEGAPQEGILEDMPVDPDNEAYEMPSEEGYQDYEPEA
mouse  ..........................N.............M..G...Y..............GS..................
```

Figure 3.1 Sequence alignment of human and mouse αSyn

Sequence alignment of human and mouse αSyn from the program ClustalW. Sequences of human and mouse αSyn are denoted as human and mouse, respectively. The seven non-identical residues in the mouse αSyn sequence are indicated, and identical residues to human αSyn are denoted by dots. The six KTK(E/Q)GV repeats are displayed in boxes and the NAC region (residues 61 to 95) is colored in red.

Comparison of the conformational fluctuations of human and mouse αSyn by nuclear magnetic resonance at room temperature (288K) and at supercooled temperatures (263K) are reported here in order to understand their sequence dependence and to relate these to the kinetics of fibril formation. Low temperatures were selected in order to freeze out motions and more clearly define the extent of restricted motion and nonrandom interactions in both proteins. ^{15}N backbone relaxation experiments which are sensitive indicators of local conformational restriction on the ps to ms timescale and paramagnetic relaxation enhancement (PRE) experiments (Kosen 1989; Gillespie and Shortle 1997) which allow the determination of long-range conformational contacts were correlated and show that mouse αSyn populates more extended conformations in solution than human αSyn. The NMR data indicate that regions of restricted mobility in human αSyn are correlated with regions that have transient long-range contacts to the C-terminal end of the protein whereas restricted mobility in mouse αSyn, which is prominent in the N-terminal region, does not show this correlation. The increased backbone motional restriction of the N-terminal region coupled with the flexible NAC region with a higher propensity of β conformation may explain the increased rate of fibril formation of mouse αSyn relative to human αSyn.

3.2 Material and methods

3.2.1 Chemicals

^{15}N labeled ammonium sulfate, ^{13}C labeled glucose and deuterium dioxide were purchased from Cambridge Isotope Laboratory (Andover, MA). MTSL (1-oxy-2,2,5,5-tetra-methyl-3-pyrroline-3-methyl-methanesulfonate) was purchased from Toronto

Research Chemicals (Toronto, On, Canada) and all other chemicals were purchased from Sigma-Aldrich (St. Louis, MO).

3.2.2 Protein preparation

Plasmids (pT7-7) encoded human and mouse αSyn cDNA sequences were gifts from Dr. Peter Lansbury (Harvard medical school, Cambridge, MA) and were transformed into *Escherichia coli* BL21 DE3 strain (Invitrogen Inc.). Expression and purification of αSyn followed the published protocols (Weinreb et al. 1996; Eliezer et al. 2001; Bertoncini et al. 2005b; Dedmon et al. 2005b) as describing in chapter 2.

3.2.3 NMR experiments

For NMR experiments in supercooled water at 288K and 263K, samples were prepared following the published protocols (Skalicky et al. 2000; Skalicky et al. 2001; Mills and Szyperski 2002). The proteins were dissolved in standard phosphate buffered saline (PBS: 8 mM Na_2HPO_4, 2 mM KH_2PO_4, 2.7 mM KCl, and 137 mM NaCl) at pH 7.4 and transferred into four 1.7 mm (outer diameter) capillary tubes (Wilmad labglass, Buena, NJ) and all capillary tubes were put into a regular 5 mm NMR tube with a cap. All NMR experiments were recorded at 288K and 263K on a Varian 800MHz spectrometer equipped with a warm probe. NMR data were processed with NMRPipe (Delaglio et al. 1995) with zero-filling and linear prediction if needed. Processed spectra were converted to NMRView (Johnson and Blevins 1994) or Sparky (Goddard and Kneller) file format for data analysis. Proton chemical shifts were referenced to DSS as 0.00 ppm and ^{15}N and

^{13}C chemical shifts were indirectly calibrated by the gyromagnetic ratios (Wishart et al. 2002).

The assignment of ^{1}H-^{15}N HSQC spectra and sequential assignments of human and mouse αSyn were first carried out at higher temperature (288K). Assignment of low temperature (263K) ^{1}H-^{15}N HSQC spectra of human and mouse αSyn were done by monitoring the movement of each cross-peak from 288K to 263K and also by using HNCACB to confirm the assignment. The secondary structure propensity (SSP) program has been developed by Marsh et al and gives a measure of the secondary structure populated (Marsh et al. 2006). The SSP scores of human and mouse αSyn were calculated using calibrated C^{α} and C^{β} chemical shifts at 263K as inputs.

150-200 μM samples were prepared for each ^{15}N backbone relaxation experiment. ^{1}H-^{15}N steady state heteronuclear NOE (^{1}H-^{15}N NOE), longitudinal relaxation (R_1) and transverse relaxation (R_2) experiments of human and mouse αSyn were recorded. ^{1}H-^{15}N steady-state heteronuclear NOE values at 288K and 263K were measured by recording spectra with or without a ^{1}H saturation period of 3 seconds. The uncertainties in the measured peak-height were set equal to the root-mean square baseline noise in the spectra, and the errors in ^{1}H-^{15}N NOE were the standard deviation of the two sets (Farrow et al. 1994). R_1 experiments at 288K and 263K were collected using the following relaxation delay times (in seconds) in a random order: 0.01, 0.05, 0.09, 0.17, 0.36, 0.49, 0.73, 1.01, 1.31, and 1.80. R_2 experiments at 288K and 263K were collected used the CPMG (Carr-Purcell-Meiboom-Gill) pulse train (Farrow et al. 1994), with an inter-pulse

delay of 625 μs and the relaxation delay times used were 0.01, 0.03, 0.05, 0.07, 0.09, 0.13, 0.17, 0.21, and 0.25 seconds. Two points were duplicated to have the proper error ranges for the R_1 and R_2 experiments. Recycle delays of R_1 and R_2 experiments are 2 seconds.

Chemical exchange R_{ex} was measured by taking the difference of two experiments; the in-phase Hahn echo experiment (R_2^{HE}) (Wang et al. 2001; Wang et al. 2003) and the η_{xy} (CSA/dipolar cross-correlation rate) experiment (Tjandra et al. 1996; Kroenke et al. 1998). Similarly to the R_2 experiment, R_2^{HE} experiments were performed by using several relaxation delays ranging from 15 ms to 150 ms. The relaxation rates were extracted by fitting the peak intensities to the equation $I(t) = I_0 \exp(-R_2 t)$ using the fitting function of Sparky. Relaxation delays and the recycle delay of the η_{xy} experiments at 263K were 46.08 ms and 2 seconds, respectively. Each η_{xy} experiment was divided into two ^{1}H-^{15}N HSQC type spectra and the η_{xy} values was determined by following equation:

$$\frac{I_{cross}}{I_{auto}} = \tanh(\eta_{xy}\tau_{HE}) \tag{3.1}$$

I_{cross} and I_{auto} are the peak intensity of cross- and auto- relaxation, respectively. $\tau_{HE} = n/J_{NH}$, where n is a positive integer (6 for 263K experiments) and J_{NH} is the scalar coupling constant of amide bond (93 Hz). Two more η_{xy} experiments were performed to get the average and standard error of the mean of each residue.

R_{ex} was defined as $R_{ex} = R_2^{HE} - R_2^0$, where $R_2^0 = \kappa\eta_{xy}$, and κ is an average value of the ratio of R_2^{HE}/η_{xy} for those residues not subjected to chemical exchange. To obtain the κ value for human and mouse αSyn, weighted correlation fittings of R_2^{HE} and η_{xy} were

calculated. Residues with differences of R_2^{HE} and η_{xy} greater than 2.5 were not included in the correlation fitting. The calculated κ values for both human and mouse αSyn are 1.22 ± 0.01.

The model of the theoretical R_2 values of a random coil like polypeptide chain was calculated as previously proposed (Schwalbe et al. 1997). R_2 values were fitted to the following equation:

$$R_2(i) = R_2^{\text{int}} \sum_{j=1}^{n} \exp(-\frac{|(i-j)|}{\lambda}) \tag{3.2}$$

where R_2^{int} is the intrinsic R_2, n is the residue numbers of the protein (140 for αSyn), λ is the window size of the persistence of the protein. For fitting the 263K R_2 data, R_2^{int} and λ are 0.33 and 12, respectively to provide a nice baseline.

Locally weighted scatterplot smoothing fitting (LOESS) (Cleveland and Devlin 1988) was used to smooth the R_2 data of human and mouse αSyn in order to define local deviations from the random coil R_2 values. Calculations of LOESS were performed by the curvefit toolbox of Matlab (The Mathworks Inc.) with a 5-point span.

Samples for measuring hydrodynamic radius (R_h, in angstroms) were dissolved in 90% D_2O (v/v) PBS at pH 7.4. The DOSY pulse sequence (Dbppste_cc) (Wu et al. 1995) in Varian BioPack library was used to obtain the translational diffusion coefficients (D_{trans}) of 0.2 mM human and mouse αSyn at 288K and 263K. Data was processed and analyzed by VNMRJ 2.12B. Convection compensation (Jerschow and Muller 1997) was applied to correct the temperature effects on D_{trans}. D_{trans} of 1,4-dioxane (1 mM in PBS) was also

measured at both temperatures as a reference molecule for calculating the R_h of human and mouse αSyn. Since both αSyn and 1,4-dioxane are dissolved in the same solution, it is not necessary to determine the viscosity to obtain R_h from the Stoke-Einstein equation. R_h of human and mouse αSyn can be calculated from the relationship:

$$R_h^{protei} = (D_{trans}^{dioxane}/D_{trans}^{protein})\ R_h^{dioxane} \quad (3.3)$$

where $R_h^{dioxane}$ is 2.12 Å and $D_{trans}^{dioxane}$ and $D_{trans}^{protein}$ are measurable parameters.

Bicelle RDC media for human and mouse αSyn were prepared as described in section 2.6. HSQC-IPAP experiments with 2048x512 complex points were carried out to collect isotropical and anisotropical states of human and mouse αSyn at 500 μM. Acquired spectra were processed by NMRPipe and converted to Sparky format for extracting the dipolar coupling constants without and with alignment in bicelle medium.

3.2.4 SDSL and PRE experiments

Two mutants were successfully constructed to replace the residues to cysteine (A19C and G132C) for each αSyn. DNA sequences were verified and proteins were expressed and purified as described for wild type αSyn. 5 mg lyophilized protein was dissolved in 1 ml PBS with 10 mM DTT and at least 4 hours incubation at room temperature to remove the disulfide bonds. The solution was transferred to a desalting column (GE Healthcare, Piscatway, NJ) to remove DTT. The DTT-free solution was immediately added to a 20-fold molar excess MTSL solution which was dissolved in acetone. The spin labeling reaction ran in the dark at 4 ºC for 16 hours or more and then the sample was concentrated to 250 μM for NMR experiments. The molecular weights of the four

cysteine mutants and the four spin labeled samples were verified by ESI Mass spectroscopy.

PRE experiments were performed by acquiring ^{1}H-^{15}N HSQC spectra in the absence and presence of MTSL spin labeling of each cysteine mutant. PRE experiments were first acquired at 288K to confirm the consistency of the published data (Bertoncini et al. 2005b; Sung and Eliezer 2007), then samples were quickly cooled to run data collection at low temperature. To control the reference more accurately, reference samples were prepared by adding DTT to the MTSL spin labeled samples after the MTSL-labeled ^{1}H-^{15}N HSQC acquisition. It should be noted that DTT-added solutions were kept at room temperature for 2-3 hours for complete reaction of removing the conjugated MTSL. Assigned peak intensities were extracted by Sparky to calculate the PRE ratios (I_{para} / I_{dia}) in the presence or absence MTSL attachment.

Theoretical PRE curves were calculated by using XPLOR-NIH (Schwieters et al. 2003)to generate MTSL-attached fully extended structures (see chapter 2). From these, I_{para} / I_{dia} PRE values were calculated and used as a reference for an unfolded protein with no long-range interactions (Fieber et al. 2004). To aid the eye the PRE data was smoothed using the LOESS approach similarly to the R_2 data. Since LOESS takes every 5 points to calculate and smooth the curve, residues in the predecessor or the successor positions of the A19C or G132C data were not included to perform fitting, respectively.

3.3 Results

3.3.1 NMR assignment and characterization of human and mouse αSyn at 15 °C.

The ^{1}H-^{15}N resonances of human and mouse αSyn are well resolved and have narrow chemical shift dispersion typical of natively unfolded proteins (figure 3.3). Backbone assignments of human and mouse αSyn were performed using a series of triple resonance experiments. Assignments were originally performed at 288K using standard triple resonance experiments (Ferentz and Wagner 2000) including HNCACB, CBCA(CO)NH, HNCO, HN(CA)CO, and C(CO)NH as well as (5,3D) HACACOCANH and (5,3D) HACACONH GFT-NMR (Kim and Szyperski 2003; 2004) in order to overcome ambiguities that arise in the standard experiments. Examples of sequential strips of HNCACB spectra of human and mouse αSyn from T64 to G73 in the NAC region are shown in figure 3.2. The poor dispersion of $^{13}C^{\alpha}$ and $^{13}C^{\beta}$ chemical shifts clearly presents that the conventional strategy for protein backbone assignment does not provide complete solution to rule out the ambiguous connections. Certain segments of the KTK(E/Q)GV repeats and several double repeats (AA, VV, GG, and EE) were not able to be assigned due to serious overlap. Published partially labeled HSQC spectra (Eliezer et al. 2001; Fernandez et al. 2004; Dedmon et al. 2005a) of human αSyn at 10 and 15 °C and published assignment of human αSyn at 10 °C using protonless technique (Bermel et al. 2006) were used as templates to help confirm or decide the ambiguous connections of human αSyn. In total, 118 resonances of the 134 assignable residues have been assigned for mouse αSyn and 117 residues assigned for human αSyn.

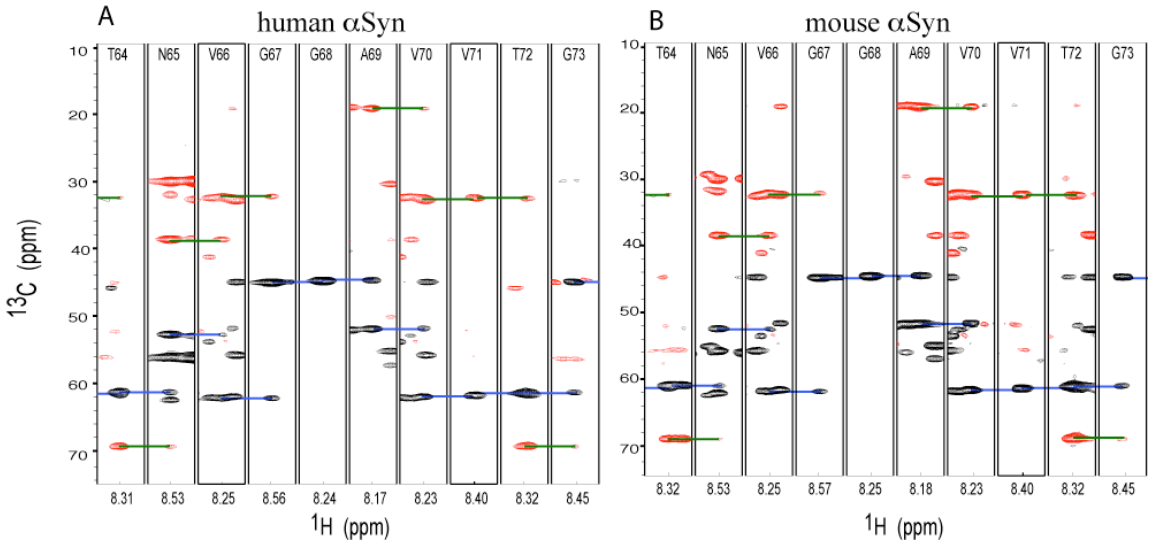

Figure 3.2 Examples of sequential strips of human and mouse αSyn at 15 °C

Sequential strips of HNCACB spectra of human and mouse αSyn from T64 to G73. C^{α} and C^{β} cross-peaks are in positive (black) and negative (red) phase, respectively. Connections of C^{α} and C^{β} cross-peaks are shown in light blue and green lines, respectively. Strips of HNCACB spectra were draw by NMRPipe.

Comparison of the ^{1}H-^{15}N chemical shifts of human and mouse αSyn indicates only small differences near the substitution sites indicating that there is no large global conformational change that takes place between the two proteins. $^{13}C^{\alpha}$ chemical shift deviation (CSD) of human and mouse αSyn were calculated to compare to the different secondary structural preferences along the proteins. Measured $^{13}C^{\alpha}$ chemical shifts of random coil-like peptides and proline neighboring effects were used as references (Wishart et al. 1995). $^{13}C^{\alpha}$ CSD profiles (figure 3.4) of human and mouse αSyn share common structural feature that the homologous proteins are intrinsically disordered and the ensembles in solution exhibit transient helical conformation in the N-terminal and NAC regions. The transient helical conformation of mouse αSyn at residues 55-70 is not

as strong as the same region in human αSyn. Although the slightly differences of helial propensity found in the amyloid core region (El-Agnaf et al. 1998; Chen et al. 2007; Vilar et al. 2008) between human and mouse αSyn, the correlation of aggregation kinetics and the secondary structural preferences remains unclear.

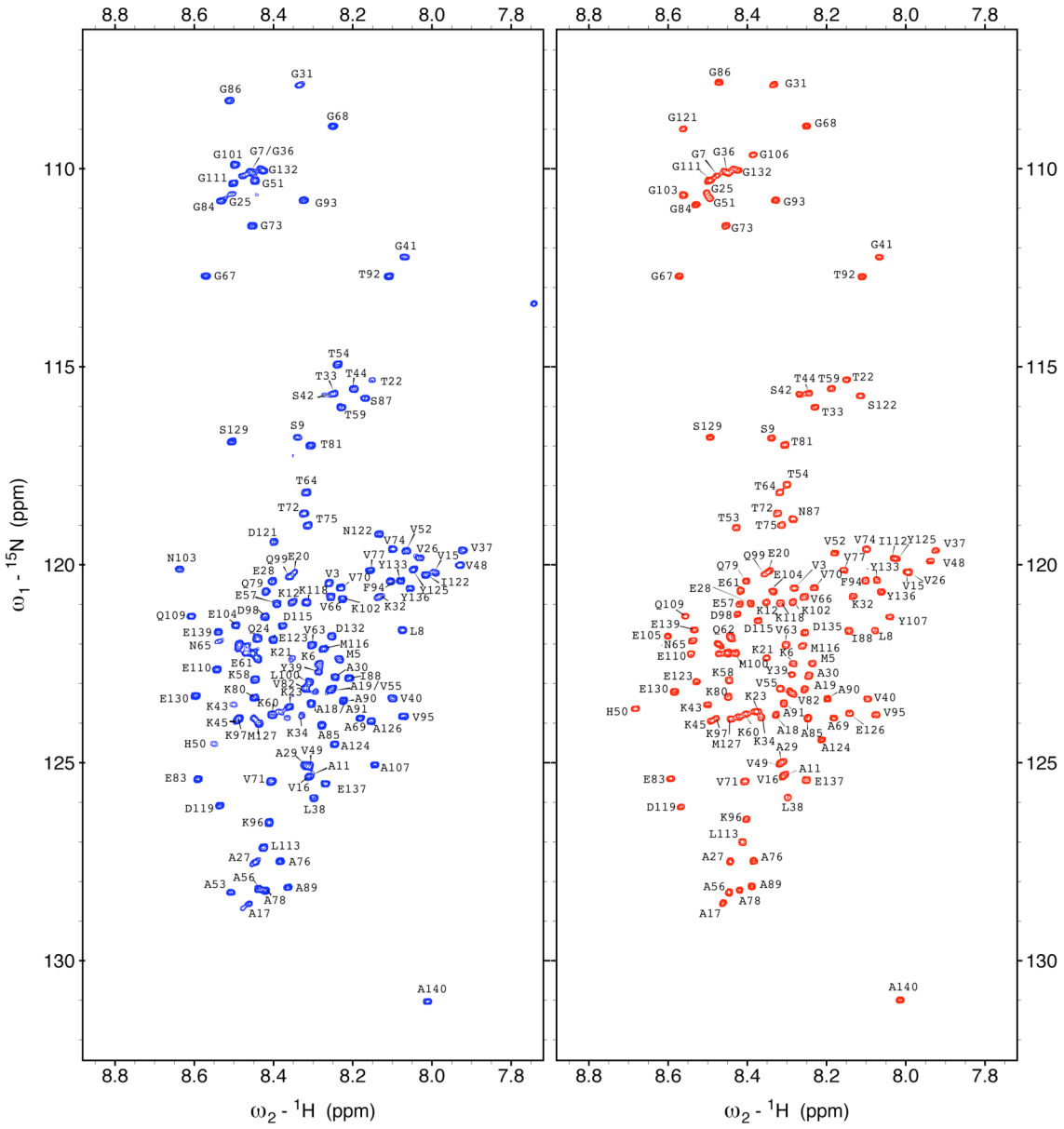

Figure 3.3 ^{1}H-^{15}N HSQC spectra of human and mouse αSyn at 15 °C

^{1}H-^{15}N HSQC spectra of human αSyn (left) and mouse αSyn (right) at 288K (15 °C).

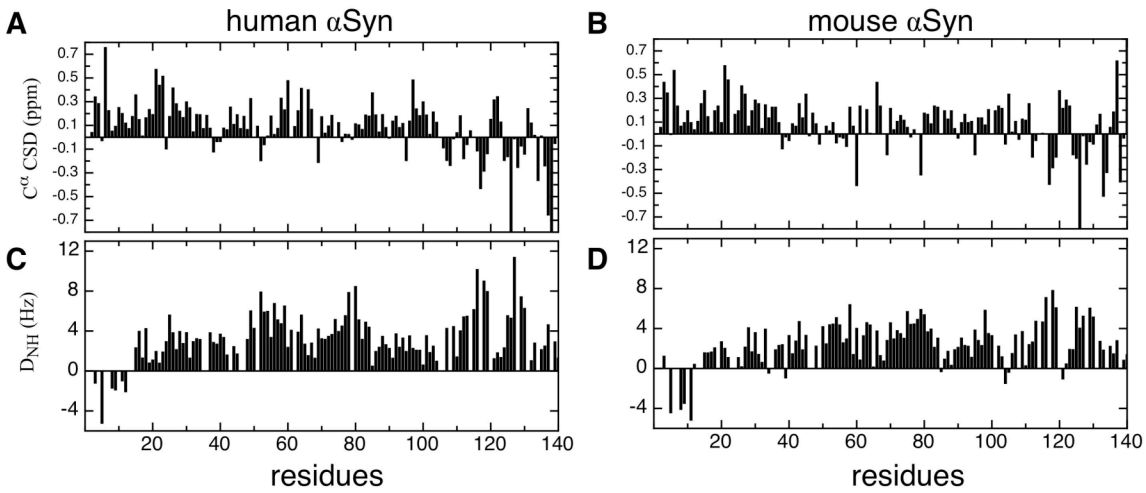

Figure 3.4 $^{13}C^{\alpha}$ CSD and D_{NH} RDC values of human and mouse αSyn.

The $^{13}C^{\alpha}$ chemical shift deviations of human and mouse αSyn were plotted in A and B, respectively. Residual dipolar coupling constants of NH bond of human and mouse αSyn were shown in panels C and D, respectively. The quadrupolar deuterium splitting constants of bicelle alignment media using for human and mouse αSyn are less than 10% different, thus the D_{NH} values are not proportionally scaled (Bertoncini et al. 2005b).

Residual dipolar coupling constants of NH bond (so called: D_{NH}) has been used to facilitate structural determination (Prestegard et al. 2000) as well as to determine the long-range structural contacts (Bertoncini et al. 2005b; Mittag and Forman-Kay 2007; Wright and Dyson 2009). Griesinger and co-workers have shown that changes in D_{NH} of human αSyn is linked to the release of long-range contacts (Bertoncini et al. 2005b). Here, the D_{NH} values of human and mouse αSyn at 15 °C were measured (figure 3.4) to characterize the differences caused by the residual substitutions. Two regions in the D_{NH} profiles between human and mouse αSyn show the distinct trends: residues 55-70 and 110-130. The distinct D_{NH} profiles in the C-terminal regions, as proposed by Bertoncini et al, suggest that mouse αSyn in solution exhibits very weak long-range contacts

between the N- and C-terminal regions. Different D_{NH} profiles in the leading portion of the NAC regions may be associated with the loss of transient helical conformation. Despite the characterized differences in CSD and D_{NH} profiles between human and mouse αSyn, the key residues that lead the mouse αSyn to aggregate faster than human αSyn is not clearly understood.

To further understand the effect of residue substitutions on the structures of the monomeric ensemble and the consequence of aggregation kinetics, ^{15}N backbone relaxation experiments including R_1, R_2 and NOE were measured. Differences in longitudinal relaxation parameters known as R_1 are typically responsive to the molecular weight. Thus R_1 is not useful for elucidating sequence effects because the molecular weights of human and mouse αSyn are close. The transverse relaxation parameter (so called R_2) is sensitive to molecular motion, however, published literature (Croke et al. 2008) and my recent work (section 6.3) suggests that the R_2 profiles at pH 7.4 are highly modulated by fast hydrogen exchange. That is, the differences of R_2 between human and mouse αSyn shown in figure 3.5 are not truly reflecting to the local structural motion or rigidity. The steady state heteronuclear NOE is believed to be free from effects of fast hydrogen exchange and can present the characteristics of local internal motion. In figure 3.5 both NOE profiles display that all residue-specific NOE values are small and most of them are negative consistent with the intrinsically disordered feature. Moreover, the NAC region is more flexible than the ends in solution and two segments can be defined according to the trends. The flexible NAC region in solution may provide low energy barriers to alter conformation and form ordered cross β-sheets in fibrils, however, more

structural evidence is required. In addition, very similar NOE profiles between human and mouse αSyn are not able to provide valuable information with respect to sequence determinant in aggregation kinetics.

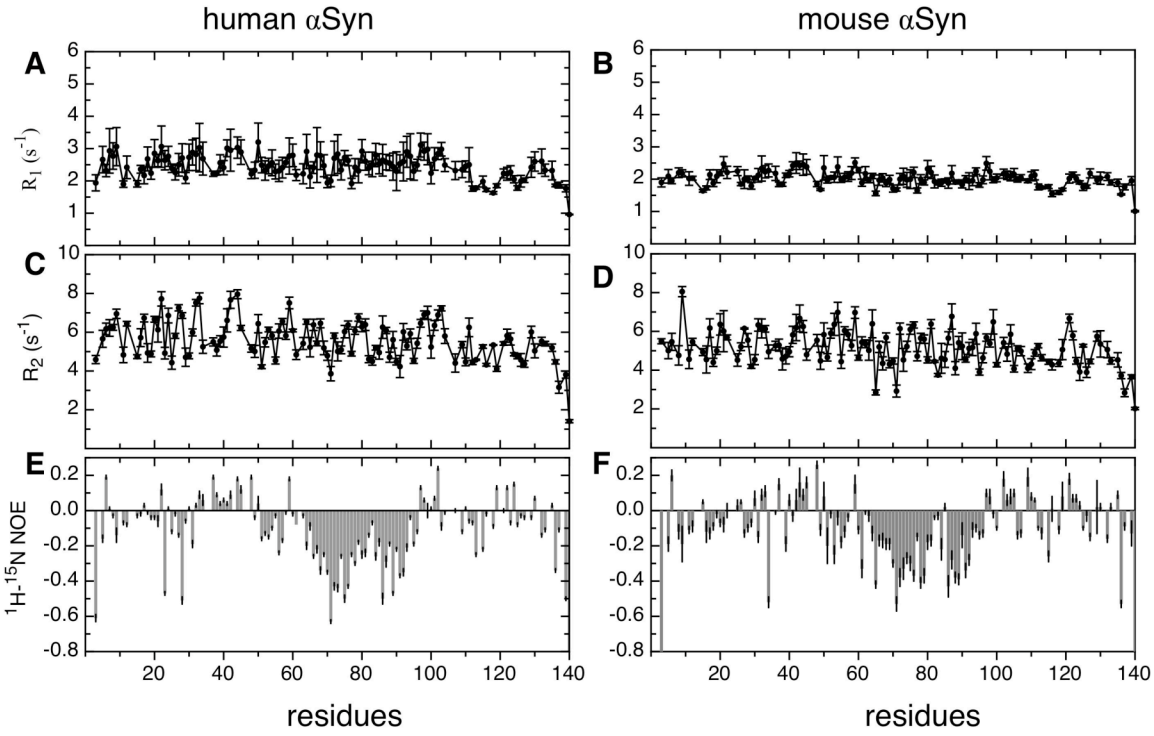

Figure 3.5 ^{15}N backbone dynamic profiles of human and mouse αSyn at 15 °C.

^{15}N backbone relaxation parameters including R_1, R_2 and NOE of human and mouse αSyn at pH 7.4 were shown. The data were acquired on a Varian 600 MHz spectrometry.

3.3.2 Assignments and secondary structural propensities of human and mouse αSyn at low temperature.

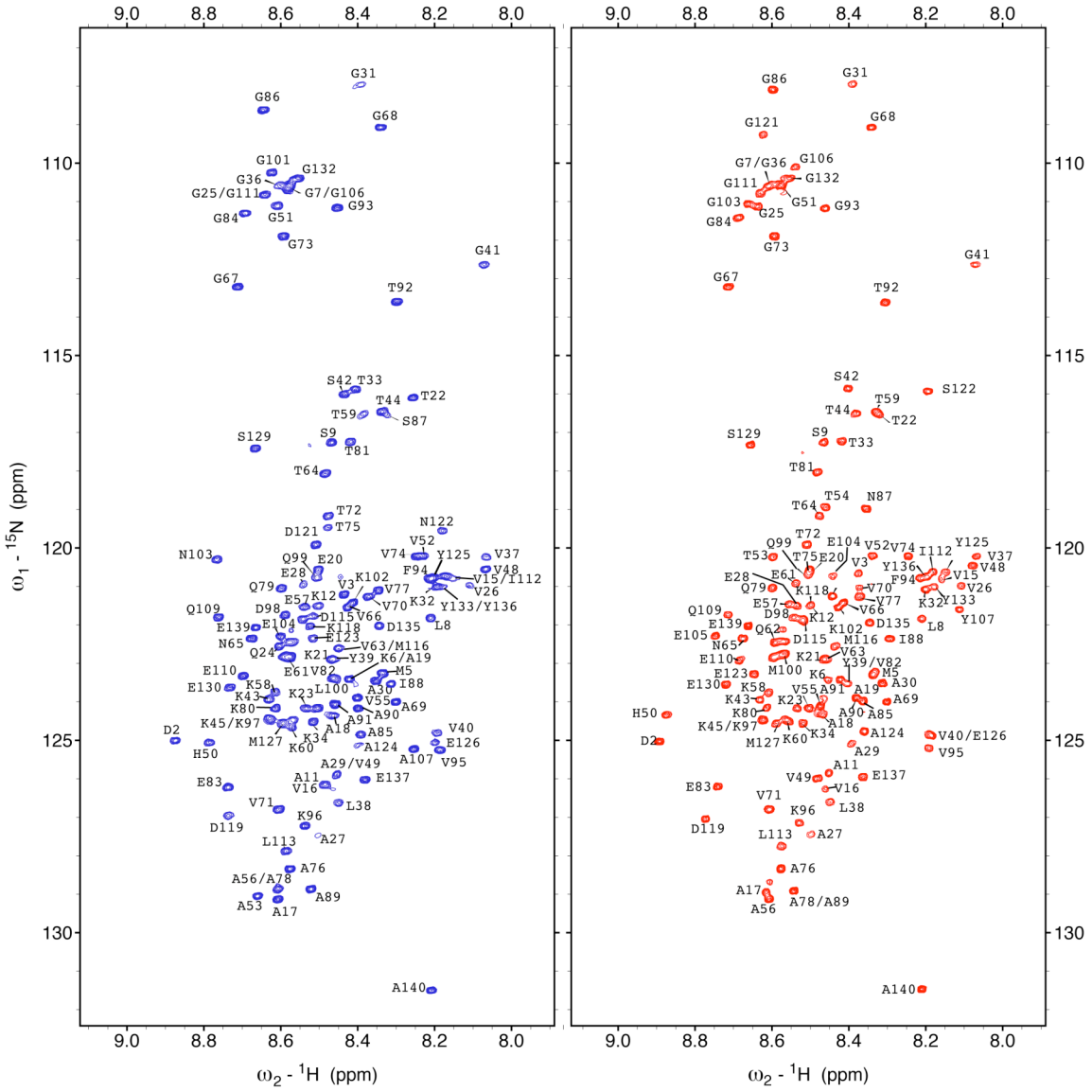

Figure 3.7 ^{1}H-^{15}N HSQC spectra of human and mouse αSyn at 263K.

^{1}H-^{15}N HSQC spectra of human αSyn (left) and mouse αSyn (right) at 263K. Both αSyn were dissolved in PBS buffer at pH 7.4. Both spectra were acquired on a Varian 800 MHz NMR and assignments are indicated on the figure.

Low temperature (263K) spectra were assigned by a temperature titration and the assignments confirmed by HNCACB experiments. NMR chemical shifts are frequently used to probe the propensity of natively unfolded proteins to sample different regions of conformational space (Yao et al. 1997; Eliezer et al. 2001; Bertoncini et al. 2005b; Marsh et al. 2006; Sung and Eliezer 2007). Kim et al have reported averaged C^{α} and C' chemical shifts for human αSyn at -15 ˚C and show that residues 38-98 as well as the C-terminal residues have predominantly negative chemical shifts (Kim et al. 2007). Here we use the secondary structure propensity score (SSP) that has been used for the comparison of human αSyn and γSyn at 5 ˚C to compare the propensity to secondary structure of human and mouse αSyn at low temperature (Marsh et al. 2006).

Although there are only minor differences in the ^{1}H-^{15}N HSQC spectra between human and mouse αSyn at low temperature, the SSP profile shows certain important differences between the two proteins (figure 3.7). The SSP profile of human αSyn shows very little propensity to helical conformation along the protein sequence, but does show a mild propensity of β conformation from residue 30 to 140. In contrast, mouse αSyn shows more propensity overall of secondary structure with some helical propensity at positions 33-37, at the substitution site A53T and at residues 100 to 105 which include substitutions sites L100M, N103G and A107Y. In addition, mouse αSyn shows more propensity to form β conformation in particular in the NAC region at residues 75 to 82 and 85 to 97 and in the N-terminal region from residues 25-30. Many of the SSP changes occur in the regions around the substitution sites indicating that local conformational propensities are sensitive to the substitutions. However there are also changes in SSP in

regions that contain no substitutions such as the changes for residues 33-37 in the N-terminal region.

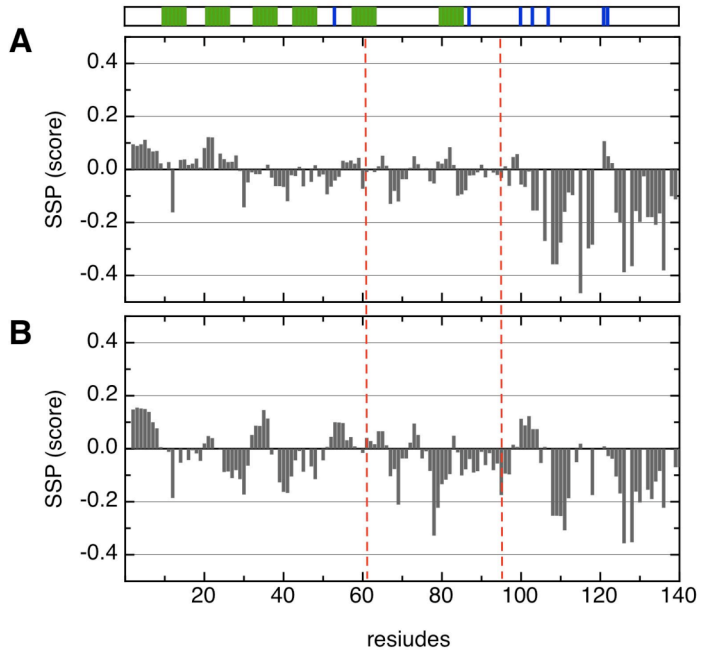

Figure 3.7 Secondary structure propensity of human and mouse αSyn at 263K.

C^{α} and C^{β} chemical shifts were used to calculate the residue-specific SSP scores of human αSyn (A) and mouse αSyn (B). Positive values ranging from 0 to 1 and negative values from 0 to -1 represent the propensities of α and β structures, respectively. A schematic of the sequence containing the positions of the repeats and the point substitutions are indicated on top with repeats shown with green boxes and point substitutions shown by blue lines. The red dashed lines indicate the separation of the N-terminal, NAC and C-terminal regions.

3.3.3 Backbone dynamics of human and mouse αSyn at 263K

^{15}N relaxation experiments (figure 3.5) are performed to explore the dynamics of the natively unfolded states of human and mouse αSyn on the fast ps-ns timescales as well as on the slower millisecond timescale. In human αSyn the R_1 data are extremely uniform

across the sequence whereas the R_2 data show distinct regions of variability (figure 3.8A, 3.8B). The R_2 data range from 8.0 sec^{-1} which are approximately the values expected for the random coil values (Schwalbe et al. 1997) and increase to values as high as 13 sec^{-1} suggesting that human αSyn has significant heterogeneity in backbone dynamics at low temperature. In order to define the variable regions in the R_2 data, locally weighted scatterplot smoothing fitting (LOESS) (Cleveland and Devlin 1988) has been performed to smooth the R_2 data and five qualitative clusters of deviations from the random coil R_2 have been assigned to the sequence (Table 3.1).

Table 3.1. The local clusters defined by R_2 profiles of human and mouse αSyn [a].

No. of clusters	Human αSyn	Mouse αSyn
I	A11 ~ G31	L8 ~ Q33
II	V37 ~ T64	V37 ~ T64
III	G73 ~ G86	N/A[b]
IV	V95 ~ L100	F94 ~ M100
V	G111 ~ M127	E105 ~ Y133

[a]: Local nonrandom structural clusters are characterized based on the R_2 values greater than 8.5 sec^{-1} at supercooled temperatures. The first and last residues of each cluster are indicated by types of amino acid and position numbers for each αSyn.

[b]: This cluster was defined according to human αSyn since mouse αSyn has near random coil R_2 values at this region.

Clusters I and II in the N-terminal end from residues 11 to 31 and 37 to 64 respectively display increased R_2 values on the order of 8 s^{-1} and 14 s^{-1}. Cluster III which is in the NAC region is clearly defined by low R_2 values at the two edges and increased values in the center. Cluster IV at the C-terminal edge of the NAC region displays relatively flat R_2 values consistent with random coil like R_2 values and the final cluster V shows

increased values for R_2 on the order of 10 sec^{-1} to 11 sec^{-1}. ^1H-^{15}N NOE data are in the range of 0.5 and are relatively uniform across the sequence; there is a small dip around residues 107 to 116 (figure 3.8E).

^{15}N relaxation experiments in mouse αSyn show similar features to human αSyn in R_1 values (average is 1.48 ± 0.14 $sec^{-1}$and 1.49 ± 0.12 sec^{-1} in human and mouse respectively) but significantly different patterns and amplitudes in the R_2 values with values ranging from 8 to 16 sec^{-1} and average values of 8.74 ± 1.72 sec^{-1} and 9.50 ± 1.96 sec^{-1} for human and mouse αSyn respectively (figure 3.8B, 3.8D). Cluster I in the N-terminal region is highly elevated relative to the random coil values (R_2 values on the order of 12 sec^{-1} to 16 sec^{-1}) and relative to the same cluster in human αSyn. Cluster II with some restricted mobility appears to be similar to cluster II in human αSyn. Cluster III in the NAC region shows values that are very close to the random coil indicating a flexible region in mouse different from the NAC region in human αSyn that has more restricted mobility. Cluster IV in mouse αSyn just carboxyl terminal to the NAC region has increased R_2 values relative to the same region in human and cluster V in the charged C-terminal has slightly larger R_2 values over a wider of residues (from 94 to 100 in mouse versus 95 to 100 in human αSyn). The ^1H-^{15}N NOEs average values of human and mouse αSyn are similar with 0.47 ± 0.08 and 0.49 ± 0.08 respectively. ^1H-^{15}N NOE values are slightly elevated relative to human αSyn in the N-terminal region but slightly decreased in the NAC and C-terminal regions indicating restricted motion in the N-terminal region (figure 3.8F).

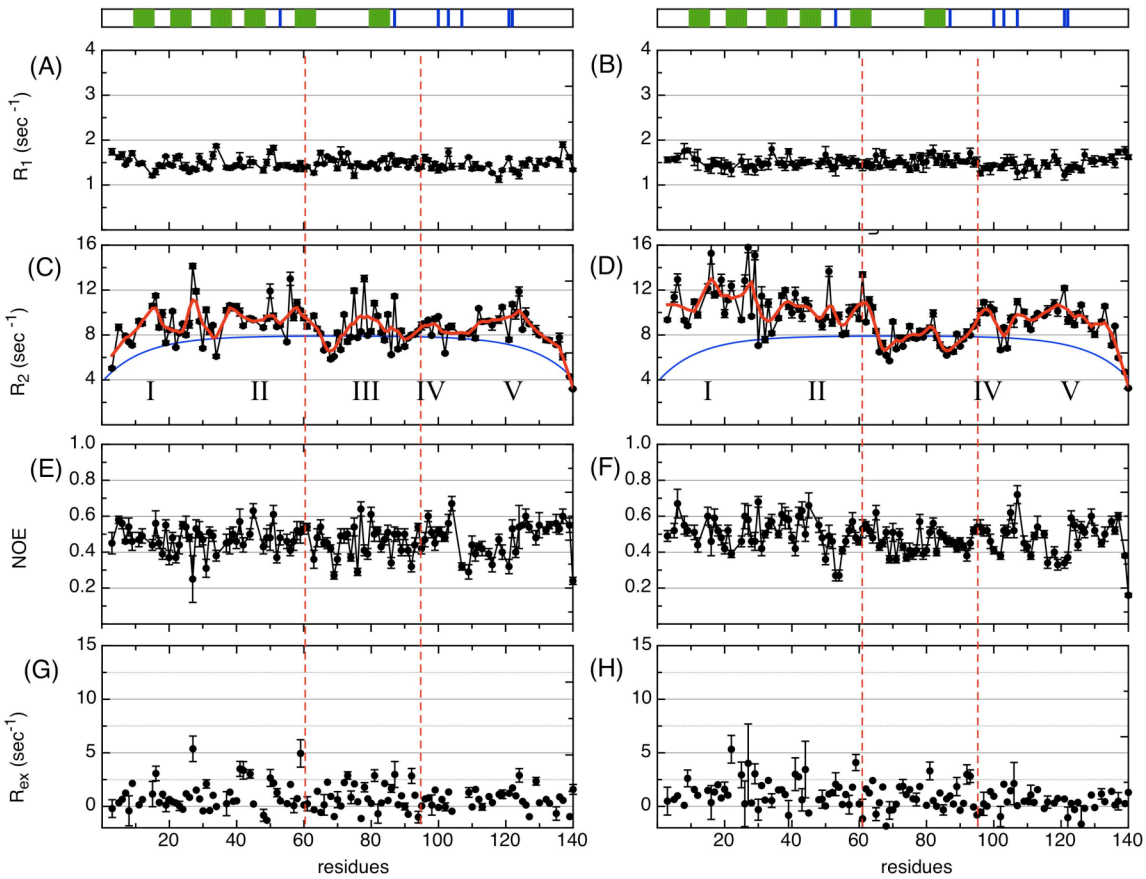

Figure 3.8 ^{15}N Relaxation parameters of human and mouse αSyn at 263K.

The relaxation data R_1 (A), R_2 (C), ^{1}H-^{15}N NOE (E) and R_{ex} (G) of human αSyn and the relaxation data R_1 (B), R_2 (D), ^{1}H-^{15}N NOE (F) and R_{ex} (H) of mouse αSyn at 263K are shown in the left and right panels, respectively. 150~200 μM samples were freshly prepared to record the four relaxation experiments for each αSyn on a Varian 800MHz NMR spectrometer. The schematic of the sequence is placed above the data to show the positions of KTK(E/Q)GV repeats and the seven non-identical point substitutions. R_1 plots of human and mouse αSyn are presented in panels (A) and (B), correspondingly. Relaxation rates calculated for a random coil (Schwalbe et al. 1997) are presented in both human and mouse αSyn R_2 plots (C, D) to provide a baseline. Smoothing curves (red) of human and mouse αSyn were calculated by using a locally weighted scatterplot smoothing method (LOESS) with a span of 5 points. Clusters derived from the deviation of the smoothed curves relative to the calculated random coil values are denoted

beneath the experimental R_2 values. ^1H-^{15}N NOE plots of human and mouse αSyn are shown in (E) and (F) respectively. R_{ex} plots (G,H) were obtained from the difference of R_2^{HE} - $\kappa\eta_{xy}$ experiments where κ is 1.22 ± 0.01 for both human and mouse αSyn (see Methods). Error bars are shown for every three points and for any point with R_{ex} values greater than 2.5 for clarity.

Elevated R_2 relaxation rates indicate increased lower frequency motions or slower backbone motions which could arise from a number of factors including restricted motion due to transient secondary structure, local clustering effects, clustering effects due to long-range contacts, or conformational exchange in the μs to ms timescale (Klein-Seetharaman et al. 2002; Wirmer et al. 2006). In order to identify whether residues that have elevated R_2 rates are undergoing conformational exchange on the μs-ms timescale and to derive the chemical exchange rate (R_{ex}) for these residues, the difference of two experiments is required. One experiment, the η_{xy} (CSA/dipolar cross-correlation rate) experiment (Tjandra et al. 1996; Kroenke et al. 1998) is designed to quantify the intrinsic (R_2^0), which is the condition under which chemical exchange is totally suppressed and the second experiment, the in-phase Hahn echo experiment (R_2^{HE}) (Wang et al. 2001; Wang et al. 2003) is designed to measure R_2 under conditions where the full exchange contribution to relaxation is obtained. R_{ex} values derived from the difference in these two experiments shows that for human αSyn R_{ex} are primarily in the range of -1 ~ 1.5 (sec^{-1}) suggesting minimal or no chemical exchange across the protein sequence (figure 3.8G). The R_{ex} values of human and mouse αSyn are very similar suggesting that differences in the R_2 values do not arise from differences in chemical exchange in the μs-ms timescale for these proteins at low temperature (figure 3.8H). In both proteins, Ser, Thr and Gly residues tend to have slightly higher R_{ex} values closer to 2.5 s^{-1} which is seen for example

with residues G41, S42 and T44 (R_{ex} values of 2.5 to 3.5 s^{-1}). The higher R_{ex} values of Gly, Ser and Thr may be related to solvent water exchange and experiments are underway to investigate this relationship. There are a very small number of residues that have larger exchange rates on the order of 5 s^{-1}, in particular residues A27 and T59 in human and mouse αSyn.

Because of the minimal nature of the chemical exchange and the similarity of the R_{ex} values in the two proteins, the difference in the R_2 rates in human and mouse is attributed primarily to a clustering effect or to transient secondary structures. The most significant differences between the R_2 values of human and mouse αSyn are seen in the more rigid N-terminal region and more rigid cluster IV just C-terminal to the NAC region and the more flexible NAC region of mouse αSyn.

3.3.4 Long-range interactions from the C-terminal to the N-terminal and hydrophobic NAC region are eliminated in mouse αSyn.

PRE experiments have been used to locate residual long-range interactions in natively unfolded human αSyn, βSyn and γSyn (Bertoncini et al. 2005b; Dedmon et al. 2005b; Kim et al. 2007; Sung and Eliezer 2007). PREs are employed here to map the tertiary long-range contacts of human and mouse αSyn at low temperature (figure 3.9). Two positions, A19 and G132, were chosen to construct a cysteine mutation in human and mouse αSyn. The spin label nitroxide, MTSL, was conjugated to the thiol group of Cys by forming a disulfide bond. The peak linewidth of the amide proton becomes broadened when the distance of the HN-to-MTSL is within 25 Å of another residue and PRE effects

(I_{para} / I_{dia}) can be easily observed by acquiring HSQC spectra in the oxidized or reduced state of the MTSL spin label.

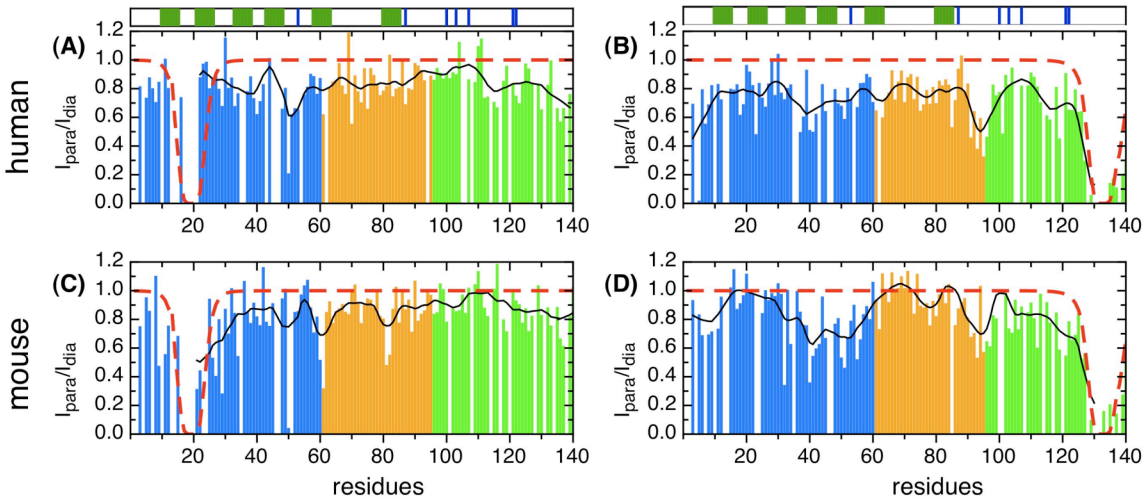

Figure 3.9 PRE profiles of amide protons in human and mouse αSyn

PRE experiments using MTSL spin labels were done at 263K for cysteine mutants human A19C αSyn (A), human G132C αSyn (B), mouse A19C αSyn (C) and mouse G132C αSyn (D). Measured PRE intensity ratios (I_{para} / I_{dia}) of human and mouse αSyn are presented in top and bottom panels, respectively**.** N-terminal, NAC and C-terminal regions are colored light blue, orange and green respectively. Red dashed lines in each plot show the broadening expected from a random coil polypeptide (see section 2.5.3) to provide a reference to map long-range contacts. Smoothing curves were calculated by using LOESS with a span of 5 points and they are shown in thin lines over the colored bars.

Spin labeling of the N terminus at residue A19C (figure 3.9A) leads to weak signal attenuation across most of the protein except for residues at the edge of the C-terminal which have signal attenuation on the order of I_{para} / I_{dia} of 0.8 and signal attenuation in a small region of the N-terminal at approximately residue 50. Placing the spin label at position G132C in the C-terminal region (figure 3.9B) shows that human αSyn exhibits a

wide range of transient long-range contacts from the C-terminal end to the rest of the protein. In particular, there is strong signal attenuation, in the range of I_{para} / I_{dia} of 0.6-0.7, just the carboxyl terminal to the NAC region at residues 92 to 100 and at the N-terminal region of the protein at residues 37 to 53. In addition to these strong regions of signal attenuation there is also weaker signal attenuation across the entire protein sequence in the range of I_{para} / I_{dia} of 0.8 suggesting that the C-terminal end of the protein is making transient contact with many regions of the rest of the protein.

Although human and mouse αSyn have some PRE effects in common, they have very different long-range interactions between the C-terminus and the rest of the protein. With the spin label attached at residue 132 (figure 3.9D), comparison of mouse and human αSyn shows that the strong signal attenuation to the N-terminal region at positions 30 to 50 is maintained as well as the strong signal attenuation C-terminal to the NAC. However human and mouse αSyn show a difference in the signal attenuation at the N-terminal between residues 10 and 30, at positions 60 to 90 in the NAC region and at positions 100 to 110 in the C-terminal region. In mouse αSyn, there is no signal attenuation in these three regions indicating that the C-terminal is not interacting with the first two hexamer repeats of the N-terminal region, the majority of the NAC region or the small region at position 100 just C-terminal to the NAC region. Labeling at the N-terminal end at residue A19C shows more subtle differences between human (figure 3.9A) and mouse αSyn (figure 3.9C). Overall there is less signal attenuation in mouse αSyn than human αSyn with exposure of the NAC region. The differences in the signal attenuation of the C-terminal spin label in mouse and human αSyn suggests that the long-

range contacts within the two proteins differ from one another. In particular, there is elimination of long-range interactions from the C-terminal end to the hydrophobic NAC region and the N-terminal region in mouse and the transient interactions from the C-terminal end to these regions are eliminated in mouse αSyn relative to human αSyn.

Pulse field gradient NMR translational diffusion experiments are performed on human and mouse αSyn in order to obtain the hydrodynamic radius of the proteins at low temperature (Wu et al. 1995). Mouse αSyn has a greater hydrodynamic radius (R_h = 29.5 Å) than huam αSyn (R_h= 28.1 Å) indicating that mouse protein is less compact than human αSyn. These results are consistent with the PRE experiments that show fewer long-range contacts from the C-terminal end of mouse αSyn to the NAC and N-terminal region relative to human αSyn.

3.4 Discussion

There is significant interest in the conformation and dynamics of human αSyn, its homologs βSyn and γSyn as well as the variants that contain single substitutions that result in early onset disease. Understanding the role and sensitivity of sequence changes to the nature of the conformational ensembles of these natively unfolded proteins has provided insight into the propensity of different synucleins to aggregate and form fibrils (Bussell and Eliezer 2001; Bertoncini et al. 2005a; Bertoncini et al. 2005b; Dedmon et al. 2005b; Sung and Eliezer 2007). Mouse αSyn with only seven substitutions relative to human αSyn is a good system to identify the role of a small number of residues in redistributing the conformational fluctuations relative to human αSyn. Backbone

relaxation experiments and PRE experiments at high temperature (288K) showed only very small differences between the two proteins but significant differences were observed at supercooled temperatures (263K) allowing a more detailed investigation of the differences between the conformational ensembles of human and mouse αSyn.

Working at low temperature may shift the thermodynamics or the kinetics of the system or both. This will result in changes in distributions of populations and/or changes in the kinetics of inter-conversion towards conformational ensembles that are less averaged and more easily characterized by NMR relaxation and PRE methods. In the kinetic limit, the effect of the low temperature will be to induce changes in inter-conversion rates between the conformers allowing the characterization of the same states that are present at physiological temperatures. In the thermodynamic limit, there may be a shift in the population balance toward a more easily characterized state. While that state may not be the major conformation at physiological temperatures undoubtedly it still has some significant population and is energetically accessible at high temperature. Therefore, these low temperature conformations may provide novel insight into the types of interactions that can exist in αSyn conformers but that may be difficult or impossible to detect under high temperature conditions.

3.4.1 Correlation of transient long-range tertiary contacts and restricted mobility in human αSyn

Despite the similar amino acid sequences of human and mouse αSyn, NMR measurements indicate that restricted mobility on the ps-ns timescale and long-range

contacts within the proteins are significantly different from one another. A schematic illustration of the combined R_2 and PRE effects of human and mouse αSyn illustrates the differences between them (figure 3.10). PRE effects are shown by a color gradient with dark blue indicating a strong loss of signal intensity and red indicating no loss of signal intensity from the PRE probe. Human αSyn has a wide range of C-terminal contacts along the protein as evidenced by the primarily blue/light pink tone of the human sequence. Regions of most contact to the C-terminal probe include cluster II and cluster IV, with other regions showing lighter colors suggestive of interactions that are not as strong but that still exist transiently. In human αSyn there is a strong correlation between regions of restricted mobility and the PRE from the C-terminal label to the rest of the protein. The PRE effects are primarily in regions that have been identified as having restricted mobility from the R_2 data (residues represented as surface residues). The residues that are identified as mobile on the ps-ns timescale (residues shown in stick), such as the edges of the NAC region which are composed of Gly residues and the residues in the C-terminal end, have weaker PRE contacts from the C-terminal end (pinker color). This correlation between the regions of restricted mobility and the strong signal attenuation from the spin label suggests that the restriction of motion in clusters I, II and III and IV arises predominantly from the long-range contacts with the C-terminal end and that restriction of motion arises primarily from transient clustering of residues within the protein.

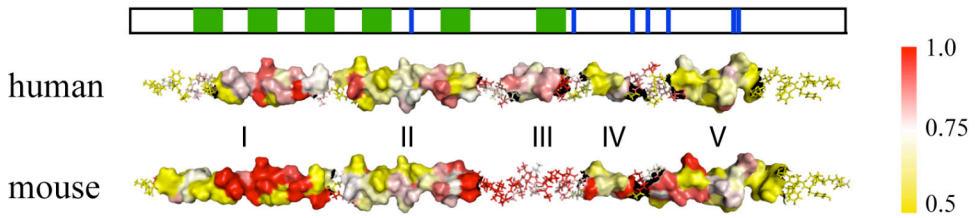

Figure 3.10 Model representations of structural clusters and long-range contacts of human and mouse αSyn

Schematic illustration along the protein sequence of the combined R_2 and C-terminal PRE data for human (top) and mouse αSyn (bottom). Residues assigned to clusters derived from R_2 data (clusters are shown in figure 3.8, and defined in table 3.1) are illustrated in surface and residues that do not belong to clusters are shown in stick. Experimental PRE values from 1.0 to 0.5 are represented by a color gradient of red to white to yellow. This model was made by PyMOL 0.99 (http://pymol.sourceforge.net).

The picture that emerges from our data for human αSyn at low temperature is one for which the C-terminal end of the protein makes contact with many different parts of the protein suggesting that αSyn is composed of a large number of different compact structures that populate the ensemble averaged conformation. Previous studies by Kim et al have suggested that the effect of low temperature is to remove the transient long-range interactions in human αSyn (Kim et al. 2007). This is based on the measurement of the hydrodynamic radius of human αSyn at -15˚C which is increased relative to high temperature, and PRE experiments from the N-terminal labels that show minimal long-range interactions. Our measurements at -10˚C have shown similar PRE results to Kim's with the spin label at the N-terminal region, however additional experiments where the PRE probe is placed at the C-terminal end extend the data and show that human αSyn

exhibits a wide range of transient long-range contacts from the C-terminal end to the rest of the protein. At this point we propose that the discrepancy between the two laboratories may be due to measurement under different solution conditions; in particular measurement under very different buffer/salt concentrations (Kim 50mM phosphate buffer, pH 7.4, 300 mM NaCl; Wu 10mM phosphate buffer, pH 7.4, 137mM NaCl). Fink et al. have shown that the rate of fibrillation of human αSyn is extremely sensitive to salt concentration suggesting that the two laboratories may be investigating distinct conformational ensembles due to the dissimilar salt conditions (Munishkina et al. 2004a). Further work is required to clarify these issues.

3.4.2 Loss of long-range contacts in mouse αSyn relative to human αSyn

In contrast to human αSyn, mouse αSyn does not exhibit a strong correlation between regions of restricted mobility as defined by increased R_2 values and the PRE effects from the C-terminal end. The large cluster at the N-terminal end, cluster I, shows the most restricted backbone mobility and yet has no PRE contacts with the C-terminal end. A second region that exhibits markedly different behavior from human αSyn is the flexible NAC region which also does not have any long-range contacts with the C-terminal end of the protein as observed by PRE experiments. Decreased contacts from the C-terminus allows both the NAC and the N-terminus to be exposed; however these two regions show very different degrees of restricted motion with the NAC region flexible, while the N-terminus is highly restricted in motion. In addition, the NAC region shows increased propensity to β conformation while cluster I of the N-terminal shows little propensity to secondary structure. It has been suggested that residual helical propensity in the N-

terminal region in human αSyn may stabilize long-range interactions and interfere with intermolecular association (Sung and Eliezer 2007). In mouse αSyn, the converse may be true where the destabilization of the N-terminal helical propensity along with the absence of long-range contacts to the C-terminal end may increase aggregation rates. In contrast to human αSyn the picture that emerges for mouse αSyn is one that has fewer C-terminal contacts across the protein, may have missing elements of the ensemble relative to human αSyn and fewer compact structures that populate the ensemble averaged conformation. The larger hydrodynamic radius of mouse αSyn relative to human αSyn is consistent with this picture.

The lack of correlation between regions of restricted mobility and C-terminal long-range contacts suggests that the restricted mobility of the N-terminal region in mouse does not arise through a clustering effect from transient long-range intra-chain interactions but rather may arise from transient secondary structure, a local clustering effect or transient aggregation. Examination of the SSP data does not indicate a high propensity to secondary structure in cluster I and R_{ex} data does not show significant restricted mobility due to chemical exchange on the ms timescale in this region. In addition, it is unlikely that the restricted mobility arises from long-range intra-chain interactions as there are no other regions of the protein that exhibit the same magnitude of R_2 values. In light of the lack of secondary structure propensity and the lack of a long-range interactions, suggestions for the origin of the N-terminal slower backbone motions of cluster I may be from back folding of the hexamer repeats or from transient protein-protein aggregation at the N-terminal end.

3.4.3 Implications for aggregation

Conformational and dynamics comparison of human and mouse αSyn are undertaken in order to determine the differences between the natively unfolded ensembles of the proteins and to relate these to the aggregation propensities of the proteins. It has been hypothesized that the C-terminal region of αSyn acts like a binding partner and interacts with the repeating fragments of the N-terminal and the hydrophobic NAC region (Hoyer et al. 2004). It has also been shown that C-terminal truncation variants aggregate much faster than the wild type confirming that the C-terminal end is important for directing fibril formation (Li et al. 2005a). In mouse αSyn, substitutions in the C-terminal end, L100M, N103G and A107Y enhance the propensity to α-helical conformation at residues 100 to 104 and show restricted mobility. In human αSyn, the same region is very flexible based on R_2 data. The extent of broadening due to the C-terminal spin label between residues 100-104 is greater in human versus mouse synuclein suggesting that the sequence changes in mouse are responsible for the altered secondary structure and increased rigidity. The limited flexibility and the secondary structure propensity of residues 100-104 (the N-terminal end of cluster V) in mouse versus human αSyn may be a key determinant in preventing the C-terminal region of the mouse αSyn from interacting with the N-terminal region.

The loss of long-range interactions to the NAC region in mouse αSyn at low temperature is similar to what is observed for the familial mutations of human αSyn, A30P or A53T mutations at high temperature (Bertoncini et al. 2005a; Bertoncini et al. 2005b). Because the A53T mutation exists in mouse αSyn it is interesting to compare the single mutation

variant to mouse αSyn. It has been proposed that the A53T mutation may stabilize alternative structures relative to the folded over structures and shift the population of conformers away from the folded over structures towards conformational ensembles that are more likely to aggregate (Bertoncini et al. 2005a). The same destabilization mechanism may be important for mouse αSyn but in addition, the increased rigidity of the "hinge" region (cluster IV) between the C-terminal and the rest of the protein that arises from the L100M, N103G and A107Y substitutions further enhances the exposure of the NAC and N-terminal. Therefore, an idea is proposed that the restricted mobility in cluster I of the N terminal region may arise from transient interchain interactions suggesting that the N-terminal KTK(E/Q)GV hexamer repeats may serve as initiation sites for aggregation in mouse αSyn. Increased interaction between the N-terminal regions suggests a lower barrier to aggregation. These N-terminal repeats have been shown to be very important as deletion or removal of N-terminal repeats impacts dramatically on the rate of fibril formation (Kessler et al. 2003). Another factor that has been suggested to be important for the rate of fibril formation is the extent of secondary structure propensity in the NAC region (Bussell and Eliezer 2001; Marsh et al. 2006). It appears that the sequence of mouse αSyn optimizes the effects that are important for rapid fibril formation; transient interchain interactions of the N-terminal region coupled with a NAC region that is both more exposed and has a higher propensity to β structure may explain the increased rate of fibril formation of mouse αSyn relative to human αSyn and A53T αSyn.

Chapter 4 . Structural Reorganization of Acid-induced α-Synuclein Characterized by NMR Spectroscopy

4.1 Introduction

Many human diseases are associated with proteins that convert from their normally soluble form to aggregates that accumulate in the affected organs. The final forms of the aggregates include fibrillar plaques known as amyloid. This disease class includes Alzheimer's disease, Parkinson's disease, Huntington's disease, Prion disease, and type II diabetes (Dobson 1999; Lansbury 1999; Perutz 1999; Chiti and Dobson 2006). Parkinson's disease (PD) is the second most prevalent of the late onset neurodegenerative diseases (Siderowf and Stern 2003). αSyn is the primary protein component of the Lewy body deposits that are the diagnostic hallmark of PD and is expressed in high levels in the brain (Rochet and Lansbury 2000). αSyn can adopt two forms, the free form found in the cytoplasm and a highly helical membrane bound form (Davidson et al. 1998; Jo et al. 2000). The membrane-bound αSyn may be crucial for physiological functions (George et al. 1995; Jenco et al. 1998; Abeliovich et al. 2000; Cooper et al. 2006) and has been shown to be associated with the recruitment of dopamine in the presynapse and with the synaptic signal transmission (Yavich et al. 2004). The aggregation of αSyn has been shown to occur via a nucleation dependent mechanism during which there is an initial lag phase followed by a growth phase (Wood et al. 1999). The rate of fibrillization is highly dependent on the sequence identity of the protein as well as the solution conditions and the details of the mechanism remain unclear.

One approach to understanding the progression of fibril formation is to study human αSyn and variants under different conditions in order to define the distribution of conformational states in the monomeric ensemble and how these may be related to the aggregation propensities. Human αSyn in the free form has been shown to be an intrinsically disordered protein (IDP) (Eliezer et al. 2001) (Weinreb et al. 1996) and like other IDPs is characterized by a low sequence complexity, low overall hydrophobicity and high net charge (Uversky 2003). It consists of three regions: an N-terminal region (residues 1-60) with a highly conserved hexamer motif KTKEGV forms α-helices in association with membranes (Jo et al. 2000; Bussell and Eliezer 2003; Ulmer et al. 2005). A central hydrophobic region, known as the "non-amyloid β component" (NAC) (residues 61-95) is proposed to be primarily responsible for aggregation (El-Agnaf et al. 1998). The C-terminal region (residues 96-140) is acidic, proline-rich (Kim et al. 2002) and also contains three highly conserved tyrosine residues. The charged residues are unevenly distributed within the sequence as a function of pH (Figure 4.1) and result in a net charge of -9 at neutral pH (Table 4.1). The N-terminus has a high charge density at neutral pH (18 charged residues out of 60), but the balance between positive and negative charges leads to a net charge of +4, while the NAC, with a net charge of -1, only has three charged residues. The C-terminus at neutral pH has an even higher percentage of charged residues than the N-terminus (18 out of 45 residues), and a preponderance of negatively charged Asp and Glu residues results in a net charge of -12. The uneven distribution of charges within the three regions implies that the charge profile of αSyn is strongly dependent on pH. The charge distribution of the NAC, which has very few

charged residues, is not greatly effected by the change in pH. However, the N-terminus region which contains the highest fraction of positively charged residues, becomes the region with the highest charge density at low pH, while the C-terminus, at low pH becomes more like the NAC, with both a low charge density and a low net charge.

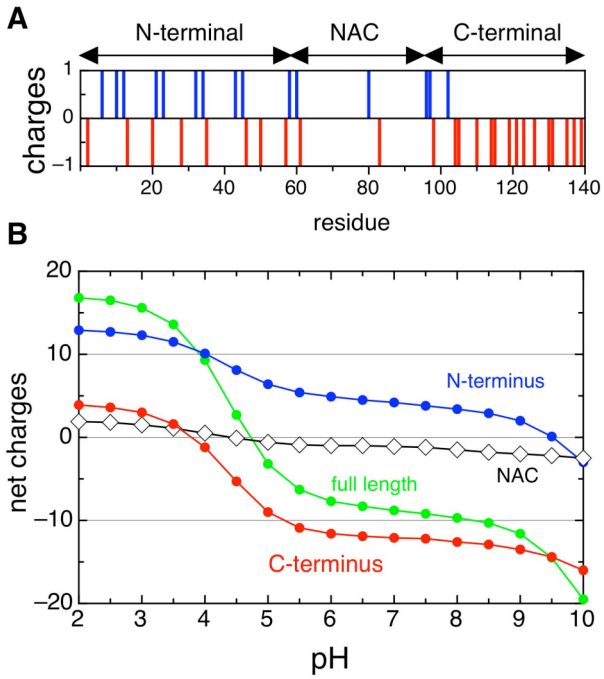

Figure 4.1 Distribution of charged residues of αSyn and the pH-dependency.

A. The distribution of positive (blue) and negative (red) charged residues of αSyn at pH 7.4 is shown. B. pH-dependent net charges of full length αSyn and its individual regions are shown. Charges of residues at each pH point were calculated at an online server (http://www.scripps.edu/~cdputnam/protcalc.html).

Developing a better understanding of how sequence dependent effects alter the conformational propensities of monomeric αSyn, and correlating these effects with changes in aggregation rates, can provide insights into the mechanistic basis for abnormal

folding and human disease. The conformational states of the synuclein family, consisting of human αSyn (Eliezer et al. 2001), βSyn (Bertoncini et al. 2007; Sung and Eliezer 2007) and γSyn (Marsh et al. 2006) as well as the familial mutations of synuclein A53T (Bussell and Eliezer 2001; Bertoncini et al. 2005a), A30P (Bussell and Eliezer 2001; Bertoncini et al. 2005a) and E46K (Bussell and Eliezer 2004; Rospigliosi et al. 2009) and mouse αSyn (Wu et al. 2008), which contains seven mutations relative to human αSyn, have been studied extensively using NMR and other spectroscopic approaches. Human αSyn at neutral pH has a relatively more compact conformation than is expected for a random coil conformation and transient α-helical structure has been detected in the N-terminal region of the protein (Uversky et al. 2001a; Bertoncini et al. 2005b; Bertoncini et al. 2007; Sung and Eliezer 2007; Wu et al. 2008). Transient long-range interactions between the C- and N-terminal regions and also between the C-terminal and NAC regions have been proposed based on paramagnetic relaxation enhancement (PRE) measurements (Bertoncini et al. 2005b; Dedmon et al. 2005b; Sung and Eliezer 2007; Wu et al. 2008; Bisaglia et al. 2009). Observation of these long-range interactions have led to the proposal that the contacts between the NAC and the C-terminal regions shield the hydrophobic NAC region and therefore delay the aggregation of αSyn under these conditions (Bertoncini et al. 2005b; Dedmon et al. 2005b; Sung and Eliezer 2007). Destabilization of these long range contacts in mouse αSyn (Wu et al. 2008) and in A53T and A30P mutations (Bertoncini et al. 2005a) involved in early onset disease have been correlated with faster aggregation supporting the notion that protection of the NAC region may be important for delaying aggregation (Bertoncini et al. 2005a). An alternative view is that there is little difference in long-range contacts between the *wt* and

mutant forms of αSyn that changes in aggregation rate can be attributed to local changes in the physico-chemical properties of individual residues (Rospigliosi et al. 2009).

Table 4.1 Distribution of charges in the sequence of αSyn

pH	N			NAC			C			αSyn		
	Net	Total	%	Net	Total	%	Net	Total	%	Net	Total	%
Neutral	+4	18	30.0	-1	3	8.6	-12	18	40.0	-9	39	27.8
Low	+11	11	18.3	+1	1	2.9	+3	3	6.7	+15	15	10.7

Net charge, total charge (total number of charged residues), and percentage of charged residues in the N, NAC, and C regions, and the full αSyn sequence at neutral pH and low pH.

At low pH, αSyn has been shown to aggregate faster than at neutral pH with fibrils taking days to form rather than several weeks (Uversky et al. 2001a). Fink and his colleagues have observed, via CD, FT-IR, and SAXS measurements, a 1.3-fold compaction in the radius of gyration of αSyn at pH 3.0 as well as an increase in β structure (Uversky et al. 2001a). The data suggested that the compaction of the protein into a partially folded conformation is responsible for the increased rate of aggregation at low pH.

NMR spectroscopy (Bracken et al. 2004; Mittag and Forman-Kay 2007; Eliezer 2009; Wright and Dyson 2009) has been developed in recent years to characterize conformational ensembles of IDPs. Here NMR approaches are applied to compare the conformational ensembles of αSyn at neutral and low pH. These studies help identify the role of electrostatic interactions in the pH dependent structural changes of αSyn and to relate these to the different aggregation propensities as a function of pH. NMR measurements provide the structural information of the conformational ensemble of αSyn at low pH. The results suggest that there is a significant structural reorganization relative

to the neutral pH ensemble in terms of long-range intra-chain contacts and hydrodynamic radius. At neutral pH the highly charged C-terminal tail makes contact with the other regions of the protein in only a small population of structures. In contrast, at low pH, the C-terminus is locally collapsed. The secondary structure propensity and exposure of the NAC region to solvent is not affected by the pH change. The structural changes observed at low pH highlight the effects that the very different charge characteristics in the N-terminal, NAC, and C-terminal chain segments have on the pH dependent structural reorganization of αSyn. In addition to NMR studies, replica exchange molecular dynamic (REMD) simulation of αSyn at neutral and acidic pH states were also performed in collaboration with Levy group (Chitra Narayanana and Daniel S. Weinstock) to present pictures of αSyn ensemble.

4.2 Material and methods

4.2.1 Sample preparation

Expression and purification of human αSyn in *E.coli* were followed by described protocol in section 2.x and published results (Wu et al. 2008). Further purification using DEAE or Q anion exchange chromatography was applied to ensure high purity of αSyn for low pH studies. αSyn was eluted at 200-300 mM NaCl gradient. Solution containing pure αSyn was dialyzed against with 20 volumetric times of PBS (pH 7.4) at 4 °C and repeated 3 times. Dialyzed and concentrated αSyn (200 μM) was transferred to 1.5 ml tubes and quickly frozen by cryogenic liquid nitrogen for -80 °C storage. For each NMR sample, the -80 °C stored proteins were unfrozen at 4 °C, polished using a 100 kDa filter

(Millipore), and then dialyzed to pH 2.5 (10 mM phosphate, 140 mM NaCl) with the addition of 10% D_2O.

4.2.2 NMR experiments for assignment

NMR experiments including triple resonance experiments and ^{15}N backbone dynamics experiments were performed on a Varian 800 MHz spectrometer equipped with triple gradient probe. PFG-NMR diffusion, PRE and RDC measurements were acquired on a Varian 600 MHz spectrometer with a cold probe or on a Bruker 700 MHz spectrometer. Acquired spectra were processed by NMRPipe (Delaglio et al. 1995) and analyzed by Sparky (Goddard and Kneller).

650 μM ^{13}C-^{15}N labeled αSyn at pH 2.5 was used to perform triple resonance experiments for backbone assignment at 15 °C. The 3D spectra were acquired via the conventional strategy (Ferentz and Wagner 2000) using HNCACB, CBCA(CO)NH, HNCO, and HN(CA)CO, and a new approach using HNN (Panchal et al. 2001) via ^{15}N-^{15}N connections. Data collection time for each 3D spectrum at 15 °C is shorter than 20 hour (with 8 or 16 transient scans) to avoid aggregation during acquisition. HSQC spectra were collected to check the stability of αSyn before acquiring the next 3D spectrum.

4.2.3 Translational diffusion coefficients and hydrodynamic radii

PFG-NMR experiments incorporated with longitudinal Eddy current pulse schemes and convection compensation was used to measure the translational diffusion coefficients

(D_{trans}) (Li et al. 2005b). Samples containing 300 μM αSyn and 35 mM 1,4-dioxane were dissolved in PBS buffers at pH 7.4 and 2.5 (100% D_2O, pD is uncorrected) for PFG-NMR experiments at 15 °C. 25 1D PFG-NMR spectra were acquired over a range of gradient strengths of 2 to 17 G/cm or 5 to 50 G/cm for 1,4-dioxane or αSyn, respectively. Integrated peak volumes of 1,4-dioxane and αSyn (methyl groups only) were fitted using VNMRJ 2.1 (Varian Inc. CA) and used to calculate D_{trans} (Li et al. 2005b). Since αSyn and dioxane were dissolved in one solution, the viscosity effect on D_{trans} can be ignored. Therefore, the Stokes-Einstein equation can be simplified to get the hydrodynamic radius of αSyn by the relationship:

R_h(αSyn) x D_{trans} (αSyn) = R_h (dioxane) x D_{trans} (dixoane)

where R_h(dixoane) is 2.12 Å.

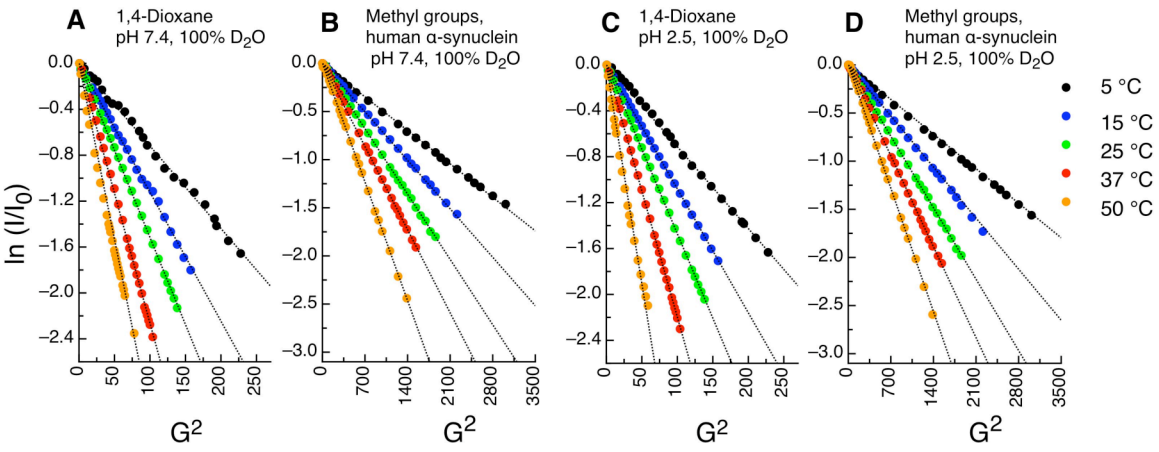

Figure 4.2 PFG-NMR data fitting of dioxane and αSyn.

Five temperature points (5, 15, 25, 37 and 50 °C) were chosen to acquire PFG-NMR spectra of 1,4-dixoane and αSyn at pH 7.4 and 2.5. Methyl groups of αSyn in each spectrum were integrated for fitting. Detailed experimental parameters are described in section 4.2.3.

4.2.4 ^{15}N backbone relaxation experiments

^{15}N R_2^{CPMG} relaxation experiments were acquired using 250 μM ^{15}N labeled αSyn at pH 2.5 and 6.1. Complex points for each spectrum were 1024x256 in the ^{1}H and ^{15}N dimensions, respectively. The relaxation times for R_2^{CPMG} were 0.01, 0.03, 0.05, 0.09, 0.13, 0.17, 0.19, 0.21 and 0.25 seconds. Recycle delays for each experiment were 2 second. Data were processed by NMRPipe and analyzed by Sparky.

4.2.5 Site-directed spin label

Methods for MTSL (Toronto Research Chemicals, Ontario, Canada) spin labeled ^{15}N-αSyn A19C, A90C, or G132C were done as described in chapter 2 and 3 and also in previous work (Wu et al. 2008). In brief, 250 μM MTSL labeled αSyn cysteine mutants were dialyzed to pH 2.5 or 7.4 and were divided to equal volume for experiments at paramagnetic (oxidized) and diamagnetic (reduced) states. Addition of 10 mM L-ascorbate (pH 2.5) or 10 mM dithiothreitol (DTT) (pH 7.4) was applied for generating the diamagnetic samples. It is not possible to use DTT or L-ascorbate as a reducing reagent at both pHs. DTT cannot be used at low pH as the disulfide bond is not efficiently broken at pH 2.5 because the thiol groups are highly protonated. At neutral pH, significant signal enhancements and changes of ^{1}H and ^{15}N chemical shifts in the presence of L-ascorbate were observed. PRE ratios (I_{ox}/I_{red}) were calculated as the intensity ratios of the same residue in the absence (I_{ox}) or in the presence (I_{red}) of L-ascorbate or DTT. At low pH all mutant samples were normalized against L-ascorbate and at neutral pH all samples were normalized against DTT.

4.2.6 RDC measurements

N-alkyl-poly(ethylene glycol)/n-alkyl alcohol mixture (Ruckert and Otting 2000) was chosen to prepare the liquid crystalline medium for residual dipolar coupling experiments. 5% C8E5 (pentaethylene glycol monooctyl ether) and 1-octanol were mixed with PBS buffer at pH 2.5 or 7.4. The molar ratio of C8E5 and 1-octanol is 1.05. The quadrupolar deuterium splitting constants are 23.8 and 22.7 Hz at pH 7.4 and 2.5, respectively. High resolution HSQC_IPAP spectra in the absence or in the presence of an alignment medium were collected at 15 °C with complex points of 2048 (*t2*) x 512 (*t1*) and 16 transient scans.

4.3 Results

4.3.1 Acid-induced changes in structure and dynamics probed by NMR

Singly ^{15}N labeled and doubly ^{13}C-^{15}N labeled αSyn dissolved in phosphate buffer at pH 2.5 were used to collect ^{15}N backbone dynamics, RDC measurement, and triple resonance data for sequential assignment. The ^{1}H-^{15}N HSQC spectrum at pH 2.5 (figure 4.3) and 15 °C exhibits similar spectral features to the HSQC spectrum at pH 7.4 (Eliezer et al. 2001); the narrow $^{1}H^{N}$ chemical shift range and poor dispersion suggest that αSyn is intrinsically disordered at pH 2.5. Backbone assignments were carried out based on ^{15}N-^{15}N connections using the 3D HNN triple resonance experiments (Panchal et al. 2001). 134 out of 140 residues (no Met^{1} and 5 Prolines) were assigned in the ^{1}H-^{15}N HSQC spectrum and most of the ^{1}H and ^{15}N chemical shift changes arise in the C-terminal region of the protein (Figure 4.4A) where there are 3 Asp and 12 Glu residues. Chemical shifts were calibrated using DSS dissolved at pH 2.5 as a reference (Wishart et al. 2002).

Comparing the secondary structural propensity using the C^{α} chemical shifts deviation from the random coil shifts is not appropriate since the random coil C^{α} chemical shifts measured at pH 5.0 (Wishart et al. 1995) and 2.3 (Schwarzinger et al. 2000; Schwarzinger et al. 2001) exhibit significant differences. Directly monitoring the changes of C^{α} chemical shifts ($\Delta\delta C^{\alpha} = \delta C^{\alpha}_{7.4} - \delta C^{\alpha}_{2.5}$) was used to inspect the secondary structure propensities at pH 7.4 and 2.5. The major changes in C^{α} shifts ($\Delta\delta C^{\alpha}$, Figure 4.4B) from pH 7.4 to pH 2.5 can be directly tied to the protonation of Asp and Glu residues at pH 2.5. Once those changes are accounted for, the remaining small $\Delta\delta C^{\alpha}$'s in the N-terminus and NAC regions alternate between positive and negative values, indicating the secondary structure propensities are essentially the same at low and neutral pH. There is however a stretch of small negative values in the C-terminus region which represents a small decrease in the β propensity in this region of the protein at low pH.

Residual dipolar coupling constants of backbone NH bond (D_{NH}) have been employed to probe the local structural ordering (Mohana-Borges et al. 2004; Kristjansdottir et al. 2005) and also long-range contacts (Bertoncini et al. 2005b; Meier et al. 2008) of IDPs. The D_{NH} values of αSyn at pH 7.4 and pH 2.5 using an n-alkyl-poly(ethylene glycol)/n-alkyl alcohol mixture (C8E5/1-octanol) as the alignment medium were measured. Significant differences can be seen in the RDC profiles at pH 7.4 and pH 2.5 particularly at the C-terminus and the leading portion of the N-terminus (Figure 4.4C). At pH 2.5, the D_{NH} values are close to zero or negative at residues 100-127 and even more negative (~ -8 to -10 Hz) at the end of C-terminus. The D_{NH} values in the NAC region and the N-

terminal region are similar to the D_{NH} values measured at pH 7.4 indicating that these regions are relatively insensitive to the environmental changes.

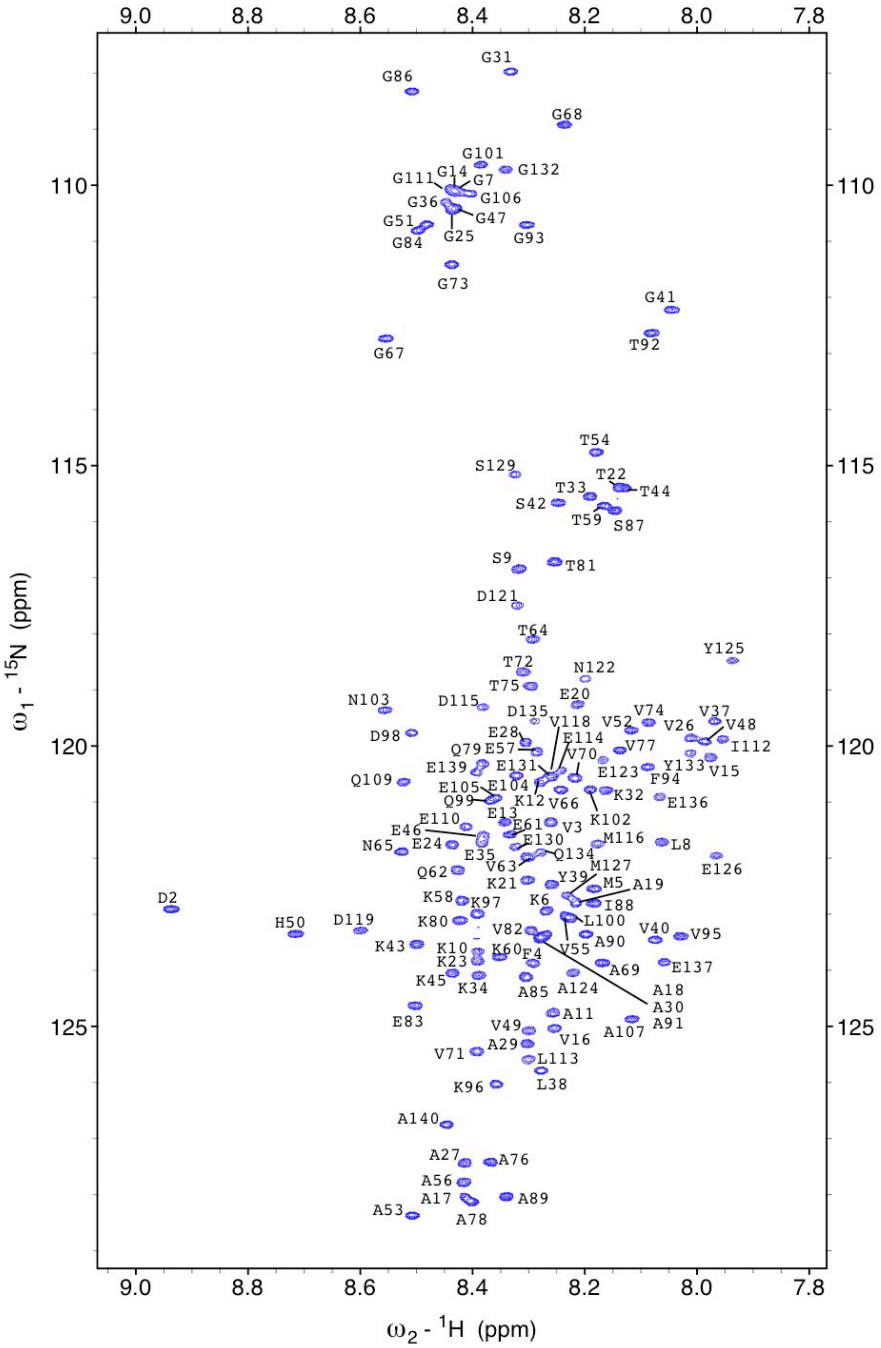

Figure 4.3 ^{1}H-^{15}N HSQC spectrum of αSyn dissolved in phosphate buffet at pH 2.5.

^{1}H-^{15}N HSQC spectrum was collected on a Varian 800 MHz NMR at 15 °C. Sidechain cross-peaks are not shown here. Each backbone cross-peak is labeled by the single-letter residue type and the position number.

^{15}N backbone transverse relaxation experiments using the CPMG pulse train (R_2^{CPMG}) indicate that the low and near neutral pH forms of αSyn exhibit different local dynamics along the sequence (figure 4.4D). R_2^{CPMG} experiments at pH 2.5 and pH 6.1 were compared rather than pH 7.4 as discussed in chapter 6 that the intrinsic R_2^{CPMG} values at pH 7.4 are modulated by the fast hydrogen exchange rates that exist at this pH. A more accurate view of the intrinsic R_2^{CPMG} values can be obtained at pH 6.1 where the hydrogen exchange rates are slower. The R_2^{CPMG} values can be classified into 5 segments (10-25, 32-42, 52-62, 93-105, and 109-136) using R_2^{CPMG} =3.0 Hz as cutoff. The overall features of the R_2^{CPMG} data are similar for the two pH values with the exception of the C-terminal end from residues 105 to the end of the protein. Here the R_2^{CPMG} values are uniformly greater at pH 2.5 than at pH 6.1 suggesting that the C-terminal end of the protein is experiencing restricted motion and is more rigid at low pH. In the NAC region, for both pHs, the R_2^{CPMG} values are the smallest indicating that this region is the most flexible.

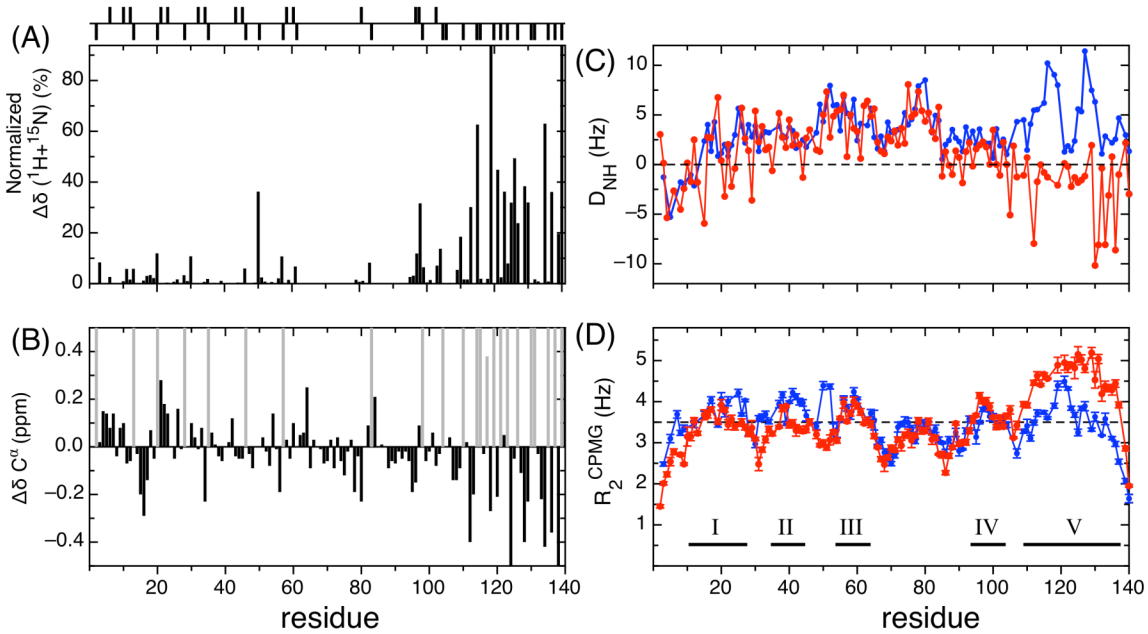

Figure 4.4 NMR parameters for αSyn at pH 7.4 and 2.5

Distribution of charged residues shown in figure 4.1 is displayed at the top of the figure. Comparison of chemical shifts (A, B), RDC (C) and R_2^{CPMG} (D) data of αSyn at acidic and neutral pH. (A) Average differences of H^N and ^{15}N chemical shifts at pH 2.5 and 7.4 with the formula: $\Delta\delta=\sqrt{\{[(\Delta H^N)^2+0.2(\Delta^{15}N)^2)]/2\}}$ and the values are normalized. (B) C^α chemical shift differences between pH 7.4 and 2.5 ($\Delta\delta C^\alpha = \delta C^\alpha_{7.4} - \delta C^\alpha_{2.5}$) are shown. Asp and Glu residues are colored in light gray. (C) ^1H-H^N residual dipolar couplings at pH 2.5 and 7.4 are shown in red and blue dot-lines, respectively. (D) R_2^{CPMG} relaxation rates at pH 2.5 and 6.1 are displayed with red and blue dot-lines, respectively. Average value (3.5 Hz) of R_2^{CPMG} at pH 2.5 is indicated. Regions of five defined segments are shown in bars and numbered.

4.3.2 The C-terminus is structurally collapsed at pH 2.5

Site-directed spin labeling and paramagnetic relaxation enhancement (PRE) at three positions, A19, A90 and G132, are used to obtain information about long-range

interactions within the unfolded protein. The PRE effects are compared at pH 7.4 and pH 2.5 and show differences, especially in terms of the interactions observed at the C-terminal end of the protein. At pH 7.4 (Figure 4.5A) the spin label at A19C results in diminished intensity throughout the entire sequence with a maximum observed value of I_{ox}/I_{red} ~0.8. At the N-terminus, there is a slow increase in I_{ox}/I_{red} up to residue 60 at which point the intensity plateaus at ~0.8. The same spin label at pH 2.5 (Figure 4.5D), has a progressively faster increase in PRE intensity at the N-terminus and plateaus at a higher level close to 1.0 in the NAC region and C-terminal to it. There is a small reduction in intensity (I_{ox}/I_{red} ~0.8) at the very end of the C-terminus from residues 110-140. At neutral pH there are numerous short range contacts between residue 19 and the N-terminus as well as transient contacts between residue 19 and the NAC and C-terminal regions consistent with previous experimental results (Bertoncini et al. 2005b; Sung and Eliezer 2007). At low pH the N-terminal region has fewer interactions with the N-terminal spin label, the NAC region is not interacting with the N-terminal spin label and is only making very local transient contact at a small region of the C terminal (residues 115-130).

The PRE results at A90C in the NAC region (Figure 4.5B, 4.5E) show distinct features at neutral and low pH. At pH 7.4, the PRE I_{ox}/I_{red} pattern is similar to the published data obtained by placing the PRE label at position A85 (Rospigliosi et al. 2009) or A90 (Bertoncini et al. 2005b). The A90C spin label probe at pH 7.4 interacts primarily with the second half of the N-terminal region (40-60) as well as with the C-terminal region. In contrast at pH 2.5 there are essentially no interactions with the N-terminal region and increased interactions with the C-terminal (I_{ox}/I_{red} 0.4-0.6) relative to the neutral pH.

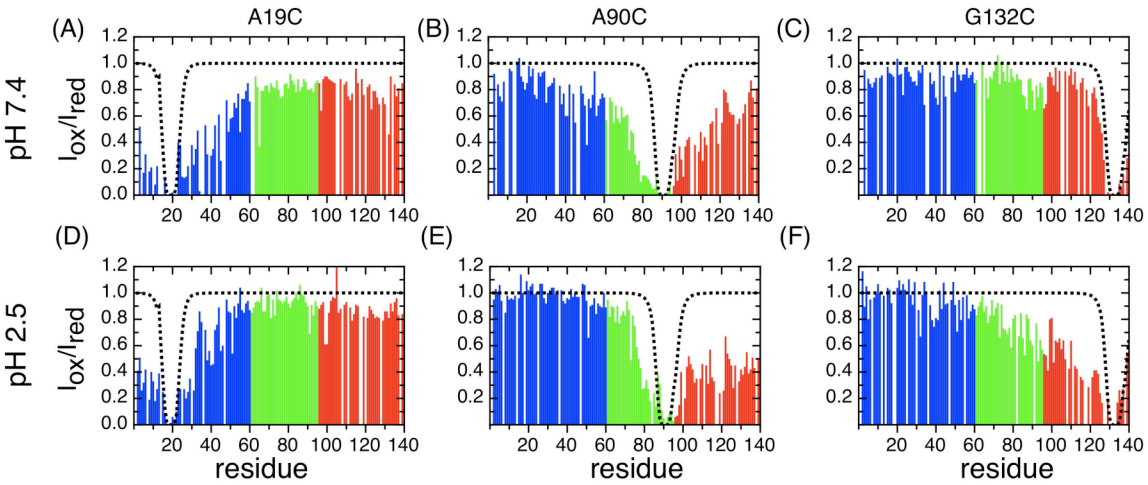

Figure 4.5 PRE profiles of spin-labeled αSyn at neutral and low pH

Paramagnetic relaxation experiments of amide protons in human αSyn at pH 7.4 (A, B and C) and pH 2.5 (D, E and F) using MTSL spin labels for cysteine mutants A19C, A90C and G132C. Measured PRE intensity ratios (I_{ox} / I_{red}) are presented in the top (pH 7.4) and bottom (pH 2.5) panels. White gaps in each plot are unassignable residues including 5 prolines. N-terminal, NAC and C-terminal regions are colored in blue, green and red respectively. Dashed lines are the theoretical PRE values of αSyn without any long-range contacts calculated as described (Wu et al. 2008).

The spin label at position G132C (Figure 4.5C, 4.5F) has a very different intensity profile at neutral and low pH in particular in the C-terminal region of the protein. At neutral pH the spin label does not lead to strong signal attenuation anywhere in the sequence. Three small dips in the intensity ratio (I_{ox}/I_{red} = ~0.8) are observed, one in the NAC region from residues 80-100 and two in the N-terminus, around residues 30-40 and near residue 5. This profile has similar trends to those seen by Zweckstetter (Bertoncini et al. 2005b) and Eliezer (Sung and Eliezer 2007) who have studied the effects of spin labels at positions A140C and P120C respectively, however the decrease in the intensity ratio is somewhat

smaller for the data observed here with the spin label at position 132. The PRE effects due to the G132C spin label at low pH (Figure 4.5F) are quite different; there is no signal attenuation in the N-terminus, but there is strong signal attenuation in the C-terminus (I_{ox}/I_{red} ~0.4) which continues, gradually weakening (I_{ox}/I_{red} goes from 0.4 to 0.9), into the NAC region. The weak signal attenuation from G132C at neutral pH suggests that the protein is making infrequent transient C- to N-terminal contacts. However, the pH 2.5 the PRE profile shows a cluster of long-range contacts between the C-terminal spin label and the C-terminal end and NAC region.

Pulse-field gradient NMR (PFG-NMR) translational diffusion experiments were performed at low and neutral pH in order to obtain the effective hydrodynamic radius (R_h) of the proteins. NMR peaks at the aliphatic region were used to collect integrated volume as a function of gradient strength and fitted slopes were used to obtain the R_h (see 2.7 and 4.2.3). The R_h value at 15 °C and pH 2.5 (R_h=30.1 Å) is smaller than that at pH 7.4 (R_h=31.7 Å) suggesting that low pH induces a conformational compaction relative to the neutral pH value. As the temperature is increasing to 37 °C and higher (50 °C), the R_h values of αSyn at low and neutral pH become bigger and are close to 37 Å which is the predicted R_h of urea-denatured 140-aa suggesting a more unfolded and pH-independent ensemble of αSyn at the physiological body temperature. Fink and his colleagues has also observed a compaction at low pH relative to neutral pH (Uversky et al. 2001a); they have observed a decrease in the radius of gyration from 40 Å at pH 7.5 to 30 Å at pH 3.0. The large gap in the radius of gyration (R_g) values relative to the R_h is because the R_g, which measures the average distance of each residue from the center of mass of the protein, is

more sensitive to the extension of the chain than the hydrodynamic radius, which approximates the radius of a sphere whose diffusion constant equals that of the protein (Wilkins et al. 1999).

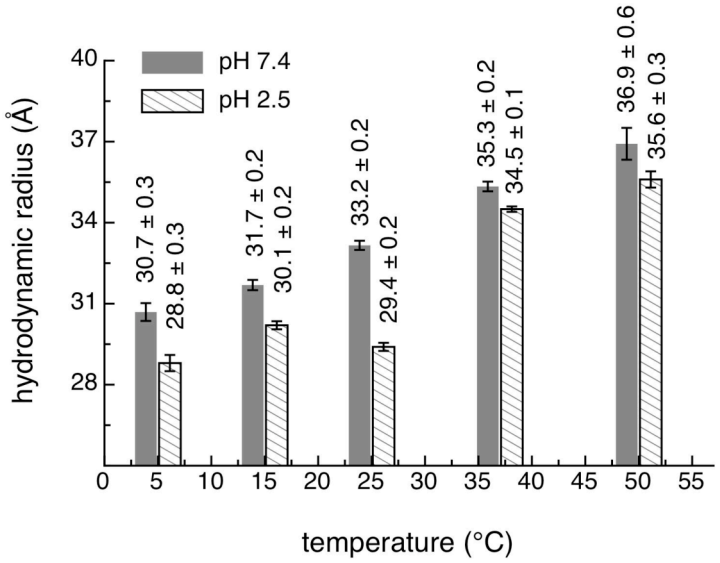

Figure 4.6 Hydrodynamic radii of αSyn at pH 7.4 and 2.5 from 5 to 50 °C.

PFG-NMR derived translational diffusion coefficients were used to calculate the hydrodynamic radii of αSyn at pH 7.4 and 2.5 and at 5 temperature points (5, 15, 25, 37 and 50 °C). Values and error ranges of R_h were depicted.

4.4 Discussion

NMR spectroscopy approaches were used to characterize the conformational ensembles of the IDP αSyn at both neutral and low pH. Chemical shifts, RDCs, R_2^{CPMG}, and PREs of αSyn were measured at pH 7.4 and 2.5 in order to compare the secondary structure and long-range interactions within the protein and to explore differences in dynamics. αSyn at neutral pH has been extensively studied by NMR (Eliezer et al. 2001; Bertoncini et al. 2005b; Dedmon et al. 2005b; Wu et al. 2008). The experimental measurements at pH 7.4 reproduce the same general features observed in previous studies. The effect of

the N-terminal spin label is seen throughout the remainder of the N-terminus and results in a small, uniform reduction in the intensity ratio in both the NAC and the C-terminus. It is a reflection of the heterogeneity of the structural ensemble since it implies that A19C is not involved in unique long-range contacts with any particular residues in the C-terminal part of the protein. An alternative explanation for the plateau is that there is a scaling problem between the oxidized and reduced experiments that lowers the baseline but is not indicative of any actual contact between A19C and the residues of the NAC and C-terminal regions.

NMR experiments indicate that there is a significant structural reorganization within the low pH ensemble relative to that at neutral pH in terms of long-range contacts, hydrodynamic radius, and the amount of heterogeneity within the conformational ensembles. The PRE profiles show that the largest change takes place in the C-terminus. Whereas the C-terminal region in the neutral pH ensemble is largely extended, only making contact with the other regions transiently, at low pH there are numerous contacts between the C-terminus and the tailing portion of the NAC (figure 4.5E, 4.5F). The C-terminus at low pH is also more compact, has decreased flexibility based on ^{15}N relaxation data, and is less exposed to the solvent than at neutral pH. The response of the N-terminal region to the change in pH is less dramatic. While the N-terminus at low pH is both more extended and more exposed to solvent than at neutral pH, neither of these changes are as large as those observed in the C-terminus. These results highlight the change in the long range interactions between the neutral and low pH ensembles; at neutral pH there is a very heterogeneous ensemble with transient contacts between the N-

terminus and the NAC, however at low pH there is a more homogeneous ensemble which exhibits strong contacts between the NAC and the C-terminus. Transient contacts between the N- and C-termini are observed at both pHs.

NMR experiments show that the low pH ensemble of αSyn has a smaller average hydrodynamic radius than the neutral pH ensemble. From the experimental data it is clear that there is no global collapse of the protein at low pH but rather the compaction is local and exists primarily in the C-terminal domain and the C-terminal region of the NAC. Fink has proposed, based on CD and FT-IR measurements, that the low pH form of αSyn has increased β content relative to the neutral pH form, a relatively compact conformation and can be thought of as a pre-molten globule state (Uversky et al. 2001a). The detailed atomic description presented here indicates that the compaction is primarily restricted to the last 60 residues of the protein and that the N-terminal region is more exposed. In addition there is no evidence at the individual residue level of an increase in β conformation in the low pH ensemble relative to the neutral pH ensemble.

In collaboration with Dr. Levy's group, the results of molecular simulations allow for the visualization of individual structures within the conformational ensembles. The conformations from the neutral-pH ensemble shown in figure 4.7 represent more than 53% of the ensemble. The representative structures from the low-pH ensemble represent more than 60% of the total population, provide the first visualization of structures from an ensemble consistent with experimental observations at low pH. These figures highlight the structural changes at low pH relative to neutral pH previously observed in both the PRE measurements and the contact maps for the simulation ensembles, namely, the compaction

of the C-terminal region at low pH coupled with an N-terminal region, which is less extended than the C-terminus at neutral pH.

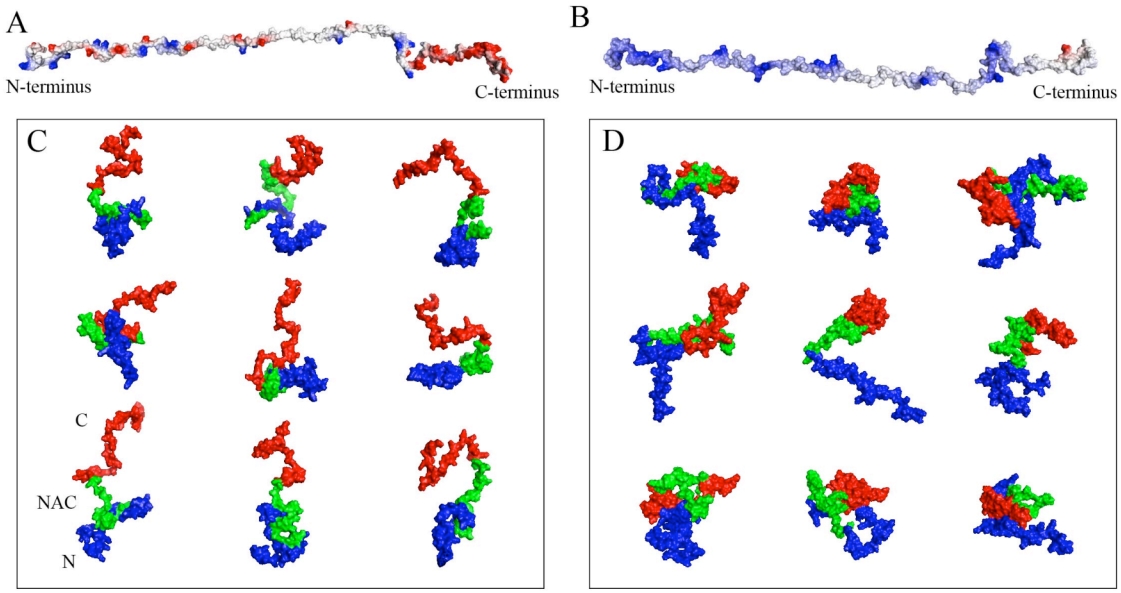

Figure 4.7 Selected representative simulated conformation of αSyn ensemble.

Fully extended αSyn at neutral and low pH states with electrostatic surface potential are colored in (A) and (B), respectively. Blue, white and red stand for positive, no and negative charges, respectively. Representative structures chosen from (C) the top four clusters of the neutral-pH ensemble and (D) the top three clusters from the low-pH ensemble. These clusters account for more than 53% and 60% of the respective structural ensembles. The N-terminus is shown in blue, the NAC is shown in green, and the C-terminus is shown in red.

The structural reorganization at pH 2.5 can be rationalized by considering the distribution of charges that exist in the low pH-induced form relative to the neutral pH form. As seen in the charge density table (table 4.1) and the pH-dependent net charges (figure 4.1B), the three regions of αSyn are impacted differently by lowering the pH. In particular, there is

a large change in the total charge density in the C-terminus that decreases from 40% charged residues at neutral pH to only 6.7% charged residues at low pH. In contrast, the effect of low pH on the N-terminus is less pronounced with a shift from 30% charged residues at neutral pH to 18.3% charged residues at low pH, and a total charge that is high at both pHs. Overall, the decrease in the total charge density of the C-terminus is considerably more than the change at the N-terminus and accounts for the fact that the reorganization of the C-terminus is the most pronounced, and that of the N-terminus less so.

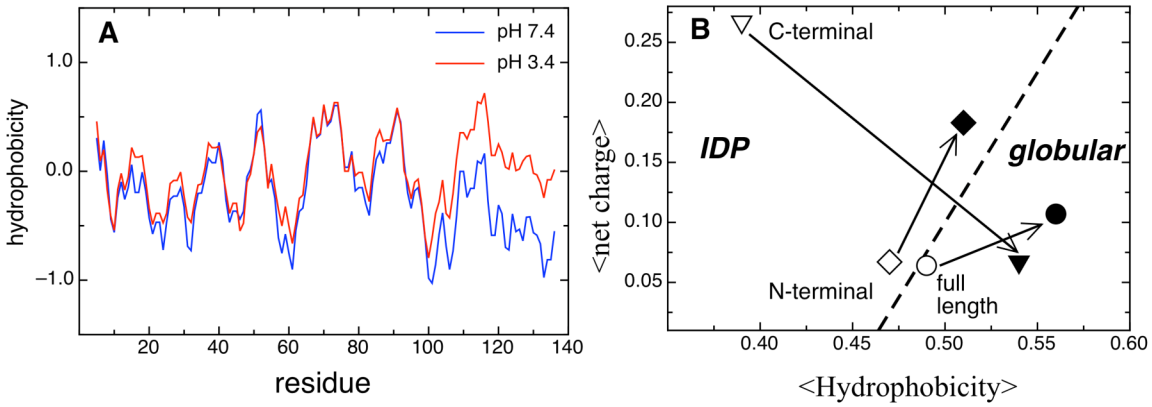

Figure 4.8 Hydrophobcity profiles and charge-hydrophobicity correlation of αSyn. **(A).** Hydrophobicity profiles of αSyn at pH 7.4 and 3.4 normalized from 1.0 to -1.0 standing for hydrophobic and hydrophilic respectively are shown. The hydrophobicity values for αSyn were calculated using the Cowan-Whittaker hydropathy indices (Cowan and Whittaker 1990) for the low and neutral pH conditions using a window size of 5 amino acids. Changes in the C-terminal region respond to increase hydrophobicity upon pH transition. **(B).** Charge-hydrophobicity characteristics of αSyn at low (filled symbols) and neutral (opened symbols) pH. The hydrophobicity values for the individual amino acids were normalized to scale of 0-1. The mean net hydrophobicity (net charge) was calculated as the sum of normalized hydrophobicity (charge at specfic pH) divided by the total number of residues in αSyn. The black line represents the

boundary between globular proteins and IDPs determined using a list of these proteins, an analysis similar to that performed by Uversky et al (Uversky et al. 2000).

It has empirically observed that IDPs and globular proteins fall into two distinct regions as a function of their mean net hydrophobicity versus mean net charge (Uversky et al. 2000). In the plot of hydrophobicity versus charge αSyn is one of the few examples of an IDP that is just over the line into the ordered region of the plot (Figure 4.8). However, by considering the three functional regions of αSyn separately, it has been noted that the C-terminal region at neutral pH, with a net charge of -12, resides very definitively in the IDP region of the Uversky plot. At low pH however, the C-terminus loses most of its net charge and becomes highly hydrophobic. The very dramatic movement of the C-terminus to the ordered region may be due to the high density of glutamates in the sequence that become very hydrophobic at low pH. The globular like quality of the C-terminus that is predicted in the plot is reflected in the NMR experiments where the C-terminal compaction is seen both in the experimental PRE measurements and the contact map of the simulated low pH ensemble. The full αSyn sequence at low pH moves more fully into the ordered region of the charge versus hydrophobicity plot due to an increase in hydrophobicity. This shift is mirrored by the smaller hydrodynamic radius observed at low pH. Interestingly, because of the balance between positively and negatively charged residues in the N-terminus at neutral pH, the N-terminus has both a higher net charge and slightly higher net hydrophobicity at low pH and remains in the IDP region of the plot.

αSyn has been shown to aggregate more rapidly at low pH and a comparison of the structural and dynamical differences may aid in understanding which factors are critical

to aggregation. Aggregation may be affected by a number of properties including propensity to form transient secondary structure (Sung and Eliezer 2007), the distribution of long-range interactions (Bertoncini et al. 2005b; Dedmon et al. 2005b), the hydrodynamic radius of the protein (Uversky et al. 2001a), the flexibility of different regions and their exposure to solvent (Hoyer et al. 2004; Wu et al. 2008), and the distribution of charges along the protein (Rivers et al. 2008). The C^{α} chemical shifts of the neutral and low pH forms are quite similar suggesting that secondary structure propensity is not a driving force to increase the aggregation rate at low pH. It has previously been suggested that the increased rates of aggregation observed for single point mutations (Bertoncini et al. 2005a) or upon binding of divalent metal ions (Binolfi et al. 2006) or polycations (Fernandez et al. 2004; Bertoncini et al. 2005b) are due to the release of the long range N- to C-terminal contacts and subsequent exposure of the NAC. However, the PRE results suggest that the NAC region has comparable exposure to solvent at both neutral and low pH; R_2^{CPMG} measurements suggest that the NAC region has comparable flexibility in both pH forms.

At low pH where the charge profiles of both the N- and C-termini are significantly different from their neutral pH counterparts it is possible that initiation of aggregation may arise through a different mechanism. Previously it has been proposed for mouse αSyn at neutral pH that aggregation may be initiated through intermolecular N-terminal contacts. While the N-terminus has a balance of positively and negatively charged residues at neutral pH in both mouse and human αSyn, it carries a large positive charge at low pH. Without complementary negative charges anywhere in the sequence, it is

reasonable to assume that the N-terminus is unlikely to initiate intermolecular contacts at low pH. One scenario that is consistent with the structural changes and charge distribution at low pH is that the locally collapsed C-terminus, which loses its net charge and becomes highly hydrophobic under these conditions, is involved in the earliest stages of αSyn aggregation at low pH. These data indicate the importance of the charge distribution in directing both the mechanism and the rates of aggregation (Rivers et al. 2008).

Chapter 5 . Detection of transient intermolecular contacts of α-synuclein using paramagnetic NMR spectroscopy

5.1 Introduction

Many human diseases are associated with proteins that convert from their normally soluble form to aggregates that accumulate in the affected organs. The final forms of the aggregates include fibrillar plaques known as amyloid (Chiti and Dobson 2006). Parkinson's disease (PD) is the second most prevalent of the late onset neurodegenerative diseases. αSyn is the primary protein component of the Lewy body deposits that are the diagnostic hallmark of PD (Arawaka et al. 1998). Like other amyloidogenic proteins, the formation of fibrillar αSyn consists of two states: (1) the nucleation state and (2) the assembling elongation state (Fink 2006). Solid state NMR (Heise et al. 2005; Vilar et al. 2008) and EPR (Der-Sarkissian et al. 2003; Chen et al. 2007) studies have presented the structural elements and core region of αSyn fibrils. However, the conversion of fibrils from monomer to oligomer and then to polymer is poorly understood. Formation of dimer or small oligomer is a necessary step in the molecular conversion pathway, however, intermolecular interactions of αSyn at the very early aggregation stage are poorly studied. The aggregation of monomeric αSyn has been shown to occur via a nucleation dependent conversion pathway (Wood et al. 1999; Conway et al. 2000). Moreover recent studies have concluded that small oligomers are toxic and the species are responsible for the PD and other neurodegenerative diseases (Volles and Lansbury 2003; Rochet et al. 2004). Determination of the intermolecular interactions of αSyn in the very early steps will

provide valuable information for therapeutic application. αSyn dimer or small oligomer in the early aggregation events, before the well-formed nucleus, are unstable and lowly populated in solution. In order to capture the transient intermolecular interactions, a mixed labeled sample using paramagnetic relaxation enhancement (PRE) technique is introduced here. Recently, the low populated transient complexes (Iwahara and Clore 2006; Tang et al. 2006; Tang et al. 2008b) as well as the ultra-weak self-associated protein (Tang et al. 2008a) have been successfully detected by the PRE measurements (Donaldson et al. 2001; Iwahara et al. 2007). In this chapter, a variety of PRE experiments are applied to characterize the transient intermolecular contacts of human αSyn at neutral and acidic pH and other extreme conditions.

5.2 Material and Methods

Expression and purification of αSyn in *E.coli* and MTSL (Toronto Research Chemicals, ON, CA) spin labeling reaction were carried out as described in chapter 2 (Wu et al. 2008; Wu et al. 2009).

5.2.1 Preparation of mixed labeled samples

As shown in figure 5.1, equivalent ^{14}N-labeled αSyn MTSL-conjugated cysteine mutant (A19C, A90C or G132C) and ^{15}N-labeled αSyn were mixed in desired solution and then was concentrated to 350 μL and then was transferred to Shigemi tube to perform NMR R_2 data collection. Paramagnetic $^{1}H^{N}$ R_2 (R_2^p) data of different mixed samples in variable buffers (pH 2.5, pH 6.0, 100 mg/ml mixed PEG, and 2 M glucose) were acquired at 15 °C on a Varian 800 MHz spectrometer using a homemade pulse sequence (figure 5.2).

400 μM ^{15}N-/^{14}N-labeled mixed αSyn prepared in buffers were used to collect the diamagnetic $^{1}H^{N}$ R_2 (R_2^d). The paramagnetic relaxation enhancement (PRE) on $^{1}H^{N}$ on the same condition is defined by: $^{1}H^{N}$ $\Gamma_2 = R_2^p - R_2^d$. At least 7 relaxation delays ranging 6-52 ms with 1.5 second recycle delay were used for all R_2 measurements. Interleaved R_2 data were processed, analyzed and fitted using the same protocol as described in chapters 2 and 3.

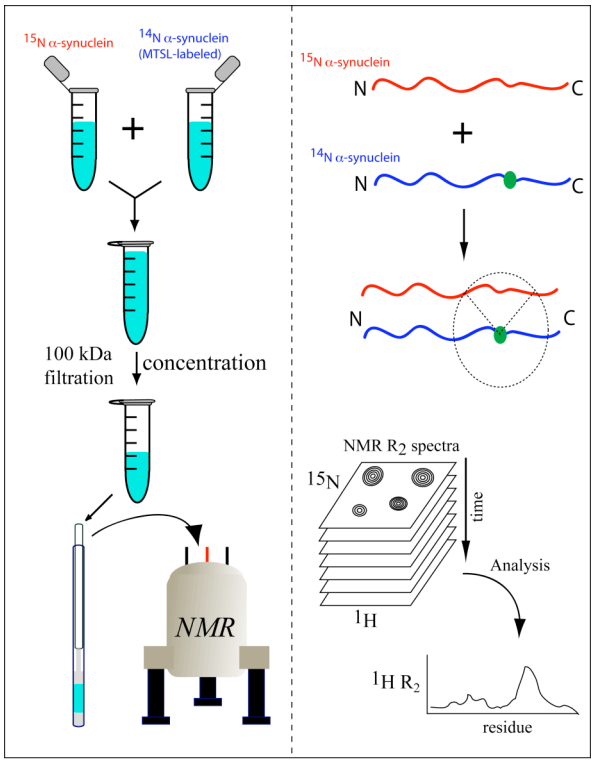

Figure 5.1 Schematic of intermolecular PRE measurement using mixed samples.

Equivalent ^{15}N-labeled and ^{14}N-labeled αSyn were mixed in a test tube. A 100-kDa cut-off membrane was used to remove invisible small aggregates and the final volume was reduced to 350 μl for NMR experiments in Shigemi tubes. MTSL (green dots) spin labeled samples (A19C, A90C or G132C) or ^{14}N-labeled *wt* αSyn were prepared and equally mixed with the ^{15}N-labeled *wt* αSyn for paramagnetic and diamagnetic studies, respectively.

5.2.2 Macromolecular crowding solution and highly viscous solution

To prepare macromolecular crowding solution, polyethylene glycol (PEG) was chosen to be the co-solute in NMR running buffer. PEG is an inert polymer and commercially available in different molecular size from 100 Da to 20 kDa depending on the length of polymerization. To be comparable with most of the intracellular molecules are proteins which molecular weight is commonly greater than 10 kDa, larger PEG molecules ranging from 1 kDa to 20 kDa were used to create a macromolecular crowding solution. 2X (200 mg/ml) concentrated PEG molecules (12.5% PEG 1K, 12.5% PEG 4K, 25% PEG 8K, 50% PEG 20K) were dissolved in solution (10 mM MES, 100 mM NaCl, 20 % D_2O and pH 6) as a stock solution. 300 μl 2X PEG and 300 μl mixed αSyn were combined and transfer into regular NMR tube for NMR studies including ^{15}N R_2 and intermolecular PRE measurements.

High concentration of glucose is very viscous and inert to biological molecules including αSyn. A series of glucose solution from 60 mM to 2.5 M dissolved in PBS buffer were prepared to measure the translational diffusion coefficients which are inverse proportional to the viscosity assuming that temperature is constant. 2 M (360 g/l) glucose was found to be viscous enough for NMR αSyn studies for cytosol-like environmental viscosity. Backbone assignments were carried out by ^{15}N-^{15}N connections using HNN spectrum and by ^{13}C-^{13}C connections using HNCACB, CBCACONH, HNCO and HNCACO spectra. ^{15}N backbone dynamics including R_1, R_2 and NOE and intermolecular PRE measurements were collected. All NMR spectra of αSyn dissolved in 2 M glucose

were acquired at 15 °C on a Varian 800 MHz spectrometer, processed using NMRPipe, and analyzed using Sparky.

5.3 Results

5.3.1 Theory of ^{1}H R_2 and its application for PRE measurement

The conventional approach to measure the intra-molecular PRE effect is comparing the ^{1}H-^{15}N correlation intensities in two ^{15}N-edited HSQC spectra at paramagnetic (I_{para}) and diamagnetic (I_{dia}) states. The ratio (I_{para}/I_{dia}) has been approximately correlated with diamagnetic R_2 and it's paramagnetic relaxation enhancement Γ_2 (Battiste and Wagner 2000):

$$\frac{I_{para}}{I_{dia}} = \frac{R_2^{dia}\exp(-\Gamma_2 t)}{R_2^{dia} + \Gamma_2}$$

where R_2^{dia} is the R_2 value under diamagnetic conditions, Γ_2 is the R_2 enhanced by paramagnetic effect, and t is the INEPT magnetization transfer time which is 9~10 ms depending on the type of HSQC and on Varian or Bruker NMR system. The relationship of Γ_2 and distances from MTSL nitroxide free radical to H^N atoms is:

$$r = \left[\frac{K}{\Gamma_2}(4\tau_c + \frac{3\tau_c}{1+\omega_H^2\tau_c^2})\right]^{1/6}$$

where K is a constant ($1.23\text{x}10^{-32}$ cm^6s^{-2}), ω_H is the Larmor frequency and τ_c is the PRE correlation time and τ_c approximately equal the protein rotational time (τ_r) because the τ_e of MTSL nitroxide is 100 times greater than τ_c thus, $\tau_c \approx \tau_r$ ($1/\tau_c = 1/\tau_e + 1/\tau_r$).

The same approach using intensity ratios can be applied to detect the contact sites and

orientations of protein-protein interactions, especially for weak binding systems (Volkov et al. 2006). In order to measure the PRE effect on a 1:1 mixed heterodimer system, Zweckstetter et al. (Rumpel et al. 2008) has proposed a correction to obtain the intermolecular PRE effect from the measured intensity ratios (denoted by "m") which have mixed signal contributions from bound and unbound ^{15}N-labeled proteins:

$$\left(\frac{I_{para}}{I_{dia}}\right)_r = 2\left(\frac{I_{para}}{I_{dia}}\right)_m - 1 = \frac{R_2^{dia}\exp(-\Gamma_2 t)}{R_2^{dia} + \Gamma_2}$$

This convenient approach can be carried out rapidly from 30 minutes to few hours, however, it exhibits some potential problems and drawbacks. Drawbacks of using intensity ratios to obtain Γ_2 and derived distances are: 1). The R_2^{dia} was assumed to be constant for all residues and independent of the position in the protein and on the free/bound states (Fieber et al. 2004). It is well known that N-terminal and C-terminal residues are usually more flexible than the other residues in protein thus R_2^{dia} values at the two ends should be smaller. In contrast, R_2^{dia} values should be elevated in secondary structural elements. Ignoring the variation of R_2^{dia} leads to decreased and increased Γ_2 values at the flexible and structural regions, respectively. Therefore, the data will be mis-interpreted and the converted distances will be wrong. 2). The relationship of Zweckstetter's proposed correction strongly counts on fixed orientation of a "static" heterodimer. In IDP systems, orientations of protein-protein interactions may not be fixed and the self-association rate is ultra weak. Thus the PRE effect on NMR peak intensities under the paramagnetic is heterogeneous and is too weak to be distinguished from the data at diamagnetic state. Direct data collection of R_2 values seems to be the best choice for studying (ultra-weak) self-association of IDPs in order to avoid misinterpretations

from intensity ratios.

The effects of paramagnetic relaxation enhancement on the R_1 and R_2 have been shown by Kosen (Kosen 1989):

$$\Gamma_1 = \frac{1}{15}\left(\frac{\mu_0}{4\pi}\right)^2 \gamma_I^2 g_I^2 \mu_B^2 S(S+1) r^{-6}\left(\frac{6\tau_c}{1+(\omega_H\tau_c)^2}\right) = \left[\frac{K}{r^6}\left(\frac{6\tau_c}{1+\omega_h^2\tau_c^2}\right)\right] \quad (5.1)$$

$$\Gamma_2 = \frac{1}{15}\left(\frac{\mu_0}{4\pi}\right)^2 \gamma_I^2 g_I^2 \mu_B^2 S(S+1) r^{-6}\left(4\tau_c + \frac{3\tau_c}{1+(\omega_H\tau_c)^2}\right) = \left[\frac{K}{r^6}\left(4\tau_c + \frac{3\tau_c}{1+\omega_h^2\tau_c^2}\right)\right] \quad (5.2)$$

where r is the effective distance, μ_0 is the permeability of vacuum, μ_B is the electron Bohr magneton, g is the electron g-factor, τ_c is the PRE correlation time and γ_I is the gyromagnetic ratio.

By calculating the ratio of Γ_2/Γ_1 assuming data collection on an 800 MHz NMR spectrometer and assuming 3 ns for τ_c, Γ_2 is ~5-fold more sensitive than Γ_1 and the theoretical sensitivity is independent on the secondary and tertiary structural elements. According to equations 5.1 and 5.2, Γ_2 is proportional to γ^2 (^{1}H or ^{15}N) thus measurement of ^{1}H R_2 will be 100 times more sensitive than the measurement of ^{15}N R_2. In summary, the order of sensitivity of the NMR parameters for PRE experiments is: ^{1}H R_2 > ^{1}H R_1 > ^{15}N R_2.

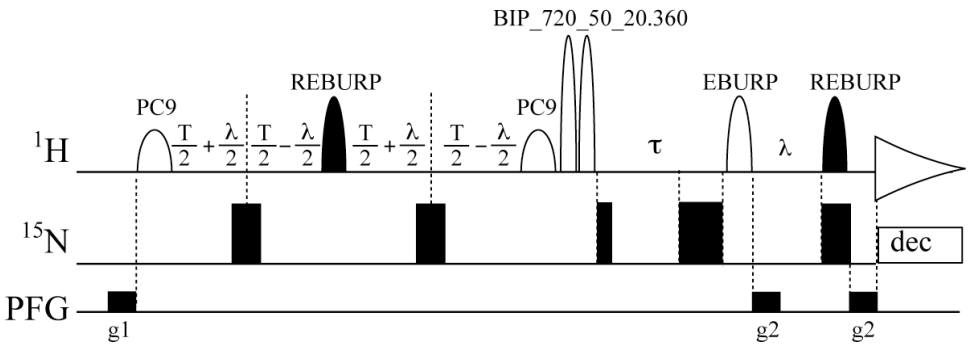

Figure 5.2 ^{1}H R_2 pulse sequence

The ^{1}H R_2 pulse sequence modified from Best-HSQC (Lescop et al. 2007). Periods of soft pulses are 2.2 ms for PC9, 1.5 ms for REBURP, 1.4 ms for EBURP and 78.4 ms for BIP_720_50_20.360. Thicknesses of rectangles at the ^{15}N channel represent times of 90 degree; 1 (90°), 2 (180°) and 3 (270°). λ and τ are 2.4 ms and 0.2 ms, respectively. Garp/WURST decoupling scheme is used at the ^{15}N channel during the data acquisition.

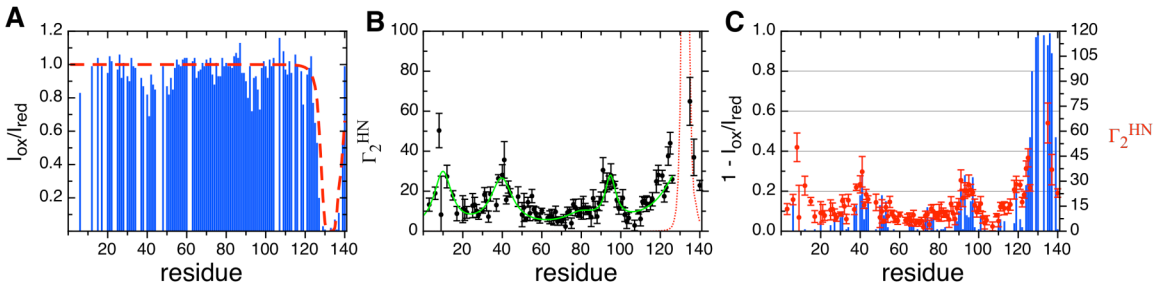

Figure 5.3 Correlation of reduction in intensity and enhancement in R_2 at pH 6.0.

Diamagnetic and paramagnetic (using G132C probe) samples were prepared to collect ^{15}N-edited HSQC and ^{1}H R_2 spectra. The PRE profiles using intensity ratio and R_2 enhancement are shown in panels A and B, respectively. Dashed lines in (A) and (B) are the theoretical values of a 140-aa protein without any long-range contacts. Gaussian function was used to generate a smooth curve which fits the trends of Γ_2 data. Overlay of reduction of intensity ($1-I_{ox}/I_{red}$) and R_2 enhancement (Γ_2) is shown as blue bars and red dots respectively in (C).

A NMR pulse sequence (figure 5.2) was made to measure ^{1}H R_2 rates using Best-HSQC (Lescop et al. 2007) pulse sequence as a template. The written pulse is similar to the published version by Kay et al (Donaldson et al. 2001). Intra-molecular PRE measurements were first applied to evaluate the confidence of this homemade ^{1}H R_2 pulse sequence. The comparison (figure 5.3) using intensity ratios and using the ^{1}H R_2 enhancement are in good agreement. For instance, 20% signal reduction of peak intensity corresponds to ~25 Hz increase of ^{1}H R_2.

5.3.2 Transient intermolecular contacts at pH 2.5

As described in section 5.2.1, samples (total concentration of each is 700 μM) including (1) ^{15}N αSyn + ^{14}N αSyn A19C-MTSL (2) ^{15}N αSyn + ^{14}N αSyn A90C-MTSL and (3) ^{15}N αSyn + ^{14}N αSyn G132C-MTSL dissolved at pH 2.5 were prepared to obtain the $^{1}H^{N}$ R_2 at paramagnetic state and one sample composed of ^{15}N αSyn + ^{14}N αSyn was used to collect the $^{1}H^{N}$ R_2 at diamagnetic state. Paramagnetic relaxation enhancement on $^{1}H^{N}$ R_2 (so called $^{1}H^{N}$ Γ_2) is defined as the elevated $^{1}H^{N}$ R_2 values from diamagnetic to paramagnetic states. As shown in figure 5.4, the 3 mixed samples at pH 2.5 present significant transient intermolecular contacts, especially in the C-terminal region. The C-terminal PRE probe (G132C, Fig. 5.4C) presents the most intense $^{1}H^{N}$ Γ_2 values that are greater than any residual $^{1}H^{N}$ Γ_2 probing at NAC (A90C, Fig. 5.4B) and N-terminal region (A19C, Fig. 5.4A). From the collected $^{1}H^{N}$ Γ_2 profiles, several intermolecular contacts were observed: (1) A19C to residues 110-140 (2) A90C to residues 100-140 and (3) G132C to residues 90-140. A portion of N-terminal and NAC regions have been shown as the core region of αSyn fibril and may be expected to participate in

intermolecular interaction in the early steps of aggregation. However, some expected intermolecular contacts including (1) A90C to NAC region and (2) A90C to residue 40-60 were not seen. Cartoon plots of representative monomeric αSyn and 5 possible contact orientations of αSyn at pH 2.5 are proposed in figure 5.4. Model 1 shows in-register parallel αSyn which is not matched to the observed information. N-terminus of αSyn at pH 2.5 is highly positively charged and is disfavored for inter-chain aggregation. Model 2 presents an antiparallel packing orientation that must exhibit pronounced N- to C-terminal contacts, however, no such information were characterized. Model 3 shows a head-to-head contact scheme that is not possible because of lack of N- to N-terminal contacts. Model 4 assumes NAC-to-NAC only contacts at pH 2.5 however the probe at A90C induces great ^{1}H R_2 enhancement at the C-terminus suggesting that model 4 is not correct. Model 5 presents a tail-to-tail contact orientation leaving the N-terminal and NAC regions free from direct intermolecular contacts. Model 5 matches the observed PRE-based contacts and presents the most plausible conformation for the transient dimer. The $^{1}H^{N}$ Γ_2 profiles illuminate a picture that αSyn encounters transient C-terminal to C-terminal (tail-to-tail) intermolecular interactions leaving free N-terminal and NAC regions in solution.

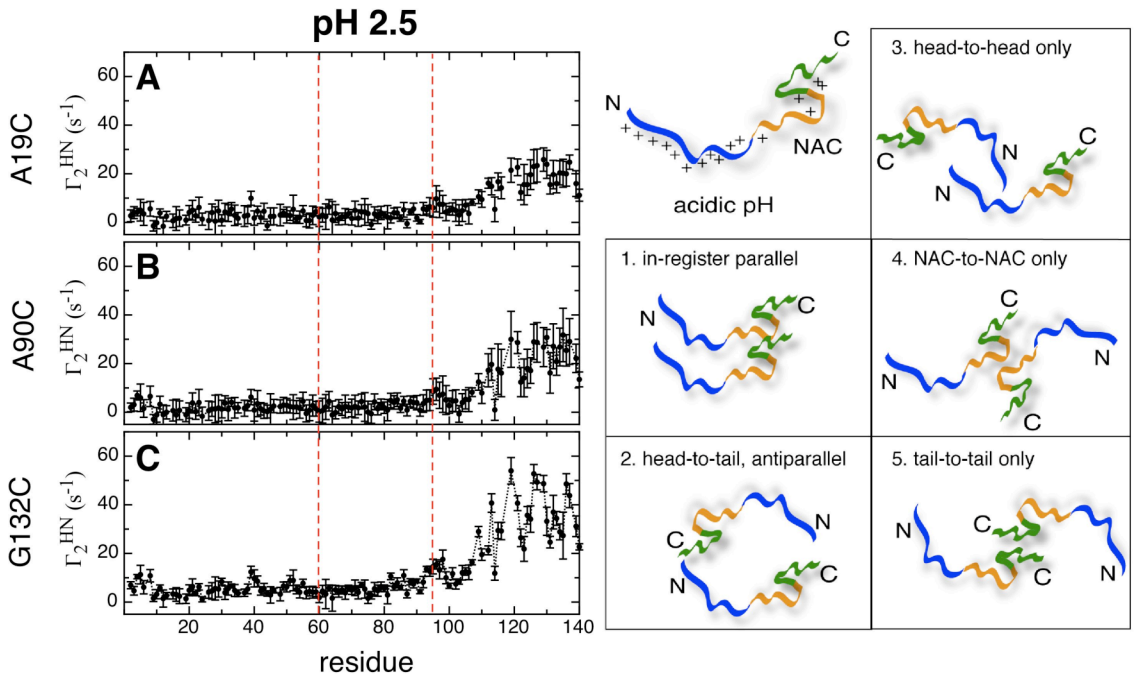

Figure 5.4 Intermolecular PRE profiles and possible dimeric contacts at pH 2.5. $^{1}H^{N}$ Γ_2 rates of 1:1 mixed αSyn (^{14}N-αSyn MTSL labeled: ^{15}N αSyn) at pH 2.5 (A,B,C) 3 probing sites (A19C, A90C, and G132C). Two dashed red lines are used to separate N-terminal, NAC and C-terminal regions. Monomeric conformation and possible models of transient contacts are shown on the right sides.

5.3.3 Transient intermolecular contacts at pH 6.0

The ^{15}N transverse relaxation of αSyn is highly impacted by fast hydrogen exchange (HX) rate at pH 7.4 but it becomes HX-free at pH 6.0 as further discussed in chapter 6. To ensure that $^{1}H^{N}$ R_2 values of αSyn at paramagnetic and diamagnetic states not HX-modulated, all relaxation data were collected at pH 6.0. The residual $^{1}H^{N}$ Γ_2 values at pH 6.0 (Fig. 5.5) using highly concentrated sample (1100 μM) are uniformly smaller than values under the aggregation-prone condition (pH 2.5) suggesting very disfavored protein-protein interactions at neutral pH. Pronounced transient intermolecular

interactions characterized from figure 5.5 are (1) A19C to C-terminal residues 110-140, (2) A90C to residues 34-50 and (3) G132C to residues 1-20 and 35-50. Similarly to the results at pH 2.5, no significant PRE effect at neutral pH has been seen in the NAC region using the 3 probes. Proposed models of possible interacting orientations of αSyn at neutral pH are shown in figure 5.5. Model 1 shows an in-register parallel contact which is the known structural alignment in the αSyn fibrils, however, the obtained PRE profiles do not support this structural pair. Model 2 assumes that tail-to-tail contact are the only transient interacting sites but all $^{1}H^{N}$ Γ_2 values in the C-terminus probed by G132C are flat and close to 0.0 implying that model 2 is not correct. Model 3 presents a head-to-head contact that is not consistent with the experimental results because no elevated R_2 are observed in the N-terminus region in figure 5.5A. Model 4 shows that NAC-to-NAC is the only transient contact place but A90C probe does not show any relaxation enhancement in the NAC region. Model 5 displays an antiparallel head-to-tail structural alignment and the NAC region may be or not be directly involved in transient contacts. The experimental $^{1}H^{N}$ Γ_2 profiles at neutral pH exhibit clear N-terminal to C-terminal relaxation enhancement and *vice versa* meaning that head-to-tail contact model displays consistent intermolecular interactions with experimental results.

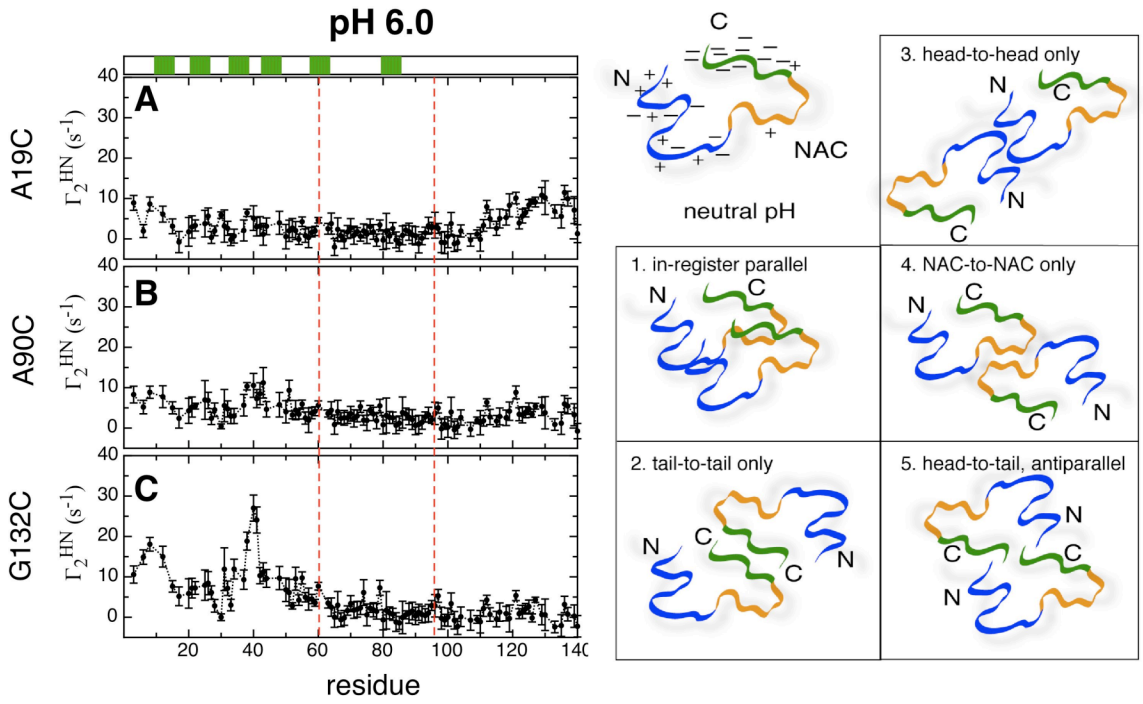

Figure 5.5 Intermolecular PRE profiles and possible dimeric contacts at pH 6.0. $^{1}H^{N}$ Γ_2 rates of 1:1 mixed αSyn (^{14}N-αSyn MTSL labeled: ^{15}N αSyn) at pH 6 (A,B,C) 3 probing sites (A19C, A90C, and G132C). Two dashed red lines are used to separate n-terminal, NAC and C-terminal regions. Sequence scheme including six imperfect repeats shown in green boxes are on top of panel A. Monomeric conformation and possible models of transient contacts are shown on the right sides.

5.3.4 Concentration-dependent PRE and PRE-derived local structural conformation

Studies (Uversky et al. 2001b; Uversky 2007) have shown that the αSyn aggregation rates are highly correlated with the concentration of αSyn: higher concentration results in shorter nucleation time and faster aggregation kinetics. Thus the frequencies of intermolecular contacts during the very early nucleation time are expected to be concentration dependent. Figure 5.6A and 5.6B present the concentration-dependent

PRE profiles at pH 6 and pH 2.5, respectively. At neutral pH, the transient interactions are not significantly observed using 700 μM 1:1 mixed samples and the $^{1}H^{N}$ Γ_2 values are more intense around residue 40 and its neighbors while higher concentration (1:1 mixed 1100 μM) sample was used. At pH 2.5, the aggregation-prone state, intermolecular αSyn interactions are more frequent, spontaneous and favorable thus 1:1 mixed samples (total is 700 μM) are concentrated enough to observe very pronounced $^{1}H^{N}$ Γ_2 values. Changing the sample concentration from 700 μM to 400 μM at pH 2.5 reduces the intermolecular contact frequencies, thus weaker $^{1}H^{N}$ Γ_2 values are obtained (figure 5.6B). Although the residual $^{1}H^{N}$ Γ_2 intensities are reduced using a low concentration sample, the specific intermolecular contacts include residues 115-122, 125-130, and 133-140 are the same.

The intensities of measured $^{1}H^{N}$ Γ_2 values are proportional to r^{-6} according to equation 5.2. That is, stronger or weaker $^{1}H^{N}$ Γ_2 values of corresponding residues exhibit shorter or longer distances, respectively, from the MTSL nitroxide to the backbone amide protons. The observed up-down trends in Fig. 5.4C reflect short and long distances from the $^{1}H^{N}$ to the nitroxide free radical, respectively. From the distance-derived information, the C-terminal residues L113, V118, D119, D121 Y125, M127, D135 and Y136 are points very close to the spin label nitroxide and residues E114, N122, E123, E131, G132 and Y133 are far away from the PRE probe. The distance information strongly suggests that the C-terminus of αSyn at pH 2.5 exhibits several bending segments and the possible bending conformation is pictured in figure 5.6C. The bending conformation of the C-terminus is novel that has not been observed using intra-molecular PRE experiments. Intra-molecular

PRE probe at position G132C is nearby the center of collapsed C-terminus implying distances that from C-terminal amide protons to MTSL nitroxide may all be shorter than 15 Å thus the intra-molecular PRE effect on all NH is too strong to properly display the differences of effective distances. In addition, detailed analysis of the bending sequence shows that 4 prolines (P117, P120, P128, and P138) may play role in kinking residues 113-140 into 4 hairpin-like conformations.

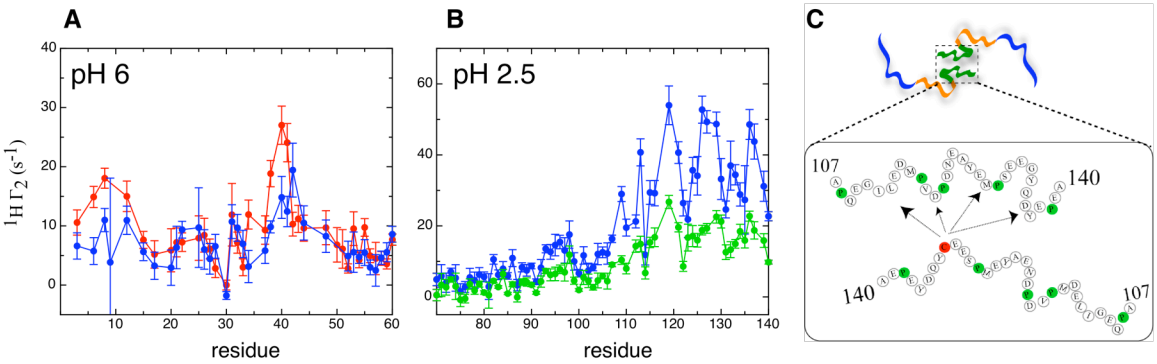

Figure 5.6 Concentration-dependent PRE profiles and detailed local C-terminal conformation at pH 2.5

The intermolecular $^1H^N$ Γ_2 rates are concentration dependent as measured at 6.0 (A) and pH 2.5 (B) using 1100 μM (red), 700-710 μM (blue) and 400 μM (green) mixed αSyn Both plots have paramagnetic probe at G132C. Comprehensive local topology in the C-terminus of αSyn at pH 2.5 is shown in (C). Residues G132C and prolines are colored in red and green, respectively. Arrows indicate the shortest distances derived from strongest ^{1}H Γ_2.

5.3.5 Macromolecular crowding effect enhances the transient intermolecular interactions

As shown in section 5.3.4 that the concentration-dependent effect on the intermolecular

interactions of αSyn concludes that $^{1}H^{N}$ Γ_2 values, a distance-based magnitude of protein-protein interaction, are uniformly enhanced in concentrated samples. The results can be explained by the increased protein-protein pairs in solution or a crowding effect on Brownian motion. To evaluate the crowding effect on the PRE of αSyn, samples composed of αSyn and very crowded macromolecules are prepared for NMR studies. Inert polyethelyne glycol (PEG) and polysaccharide (e.g. dextran, ficoll) have been used to create macromolecular crowding effect on αSyn aggregation resulting in shorter nucleation time and faster elongation rates (Shtilerman et al. 2002; Munishkina et al. 2004a). A solution consisting of 400 μM mixed αSyn has been prepared to perform NMR measurements under heterogeneous macromolecular crowding condition at pH 7.4 (100 mg/ml mixed PEG, see methods). Strong HX-modulated $^{1}H^{N}$ R_2 of αSyn mixed with PEG at pH 7.4 was obtained (Figure. 5.7A) implying that the crowding effect does not reduce or stop the exchange between amide protons and water protons. However, ^{1}H R_2 profile of αSyn at pH 6.0 in the PEG solution exhibits clean and HX-free results. In addition, the PEG-induced macromolecular crowding effect does not alter chemical shifts of the ^{1}H-^{15}N correlation resonances at pH 6.0 thus structural and dynamic features of αSyn in crowded solution are expected to be very similar with those in dilute solution. The ^{15}N R_2 profile of αSyn in crowded PEG solution, as predicted, does not change the features but values are uniformly elevated by 2-4 Hz. Thus the non HX-modulated intermolecular PRE measurements under the macromolecular crowding condition were all carried out at pH 6.0 (10 mM MES, 100 mM NaCl).

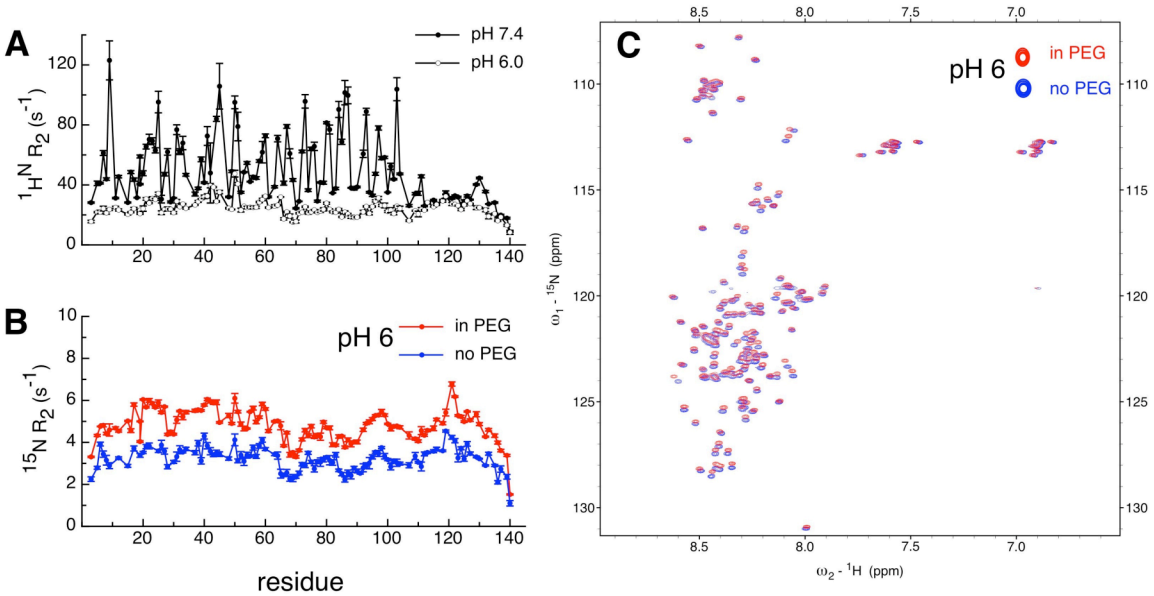

Figure 5.7 ^{1}H and ^{15}N R_2 profiles and HSQC spectrum of αSyn in crowded PEG solution.

A. ^{1}H R_2 profile of αSyn mixed with crowded PEG solution at pH 7.4 (filled dot-line) shows residues 1-100 exhibit strong signal modulation by hydrogen exchange. While changing the pH to 6.0 in same crowded PEG environment (open dot-line), the collected ^{1}H R_2values are not fluctuated as seen at pH 7.4. **B.** ^{15}N R_2 profiles of αSyn under crowded (red) and non-crowded (blue) solution are sharing the same curve pattern although the ^{15}N R_2 profile of αSyn in crowded PEG is uniformly enhanced. **C.** Overlaid ^{1}H-^{15}N HSQC spectra of αSyn in PEG and in PEG-free solution at pH 6.0 show that PEG does not change the chemical environment greatly because there are no significant shifts observed.

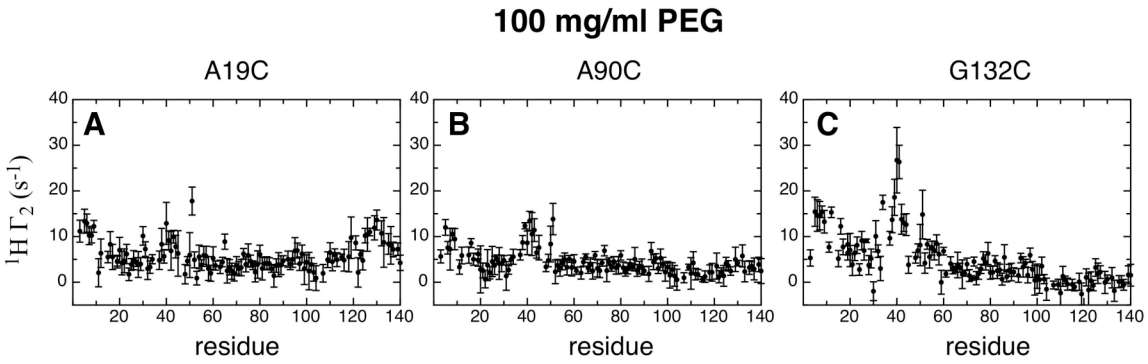

Figure 5.8 Intermolecular PRE profiles of αSyn in PEG crowded solution.

The intermolecular $^1H^N$ Γ_2 rates of αSyn in 100 mg/ml crowded PEG solution are obtained using MTSL probes located at A19C (A), A90C (B) and G132C (C). Samples composed of approximate 400 μM mixed αSyn were prepared for paramagnetic NMR experiments.

The profiles of head-to-tail transient intermolecular contacts of αSyn in crowded PEG solution display similar patterns to those seen in diluted solution at neutral pH (figure 5.5). The characterized intermolecular contacts include (1) A19C MTSL to C-terminal residues 120-140 (2) A90C MTSL to residues 35-50 and (3) G132C MTSL to N-terminal residues 1-20 and 35-50 suggesting that αSyn dissolved in PEG-induced macromolecular crowded solution maintains its head-to-tail antiparallel intermolecular contacts. As proposed earlier, heterogeneous crowding effect can be taken as one kind of concentration effect that enhances the intermolecular interaction greatly. In the crowding studies, each sample is composed of 400 μM αSyn and 100 mg/ml PEG which is approximately 12 mM. More frequent protein-protein interactions and rapid aggregation in crowding environment based on the excluded volume effect have been predicted (Zhou et al. 2008). In addition, high concentration αSyn (~700 μM) sample has been prepared for crowded solution, however, the proteins precipitated immediately in PEG solution.

Although macromolecular crowding raises the tendency of intermolecular interactions, the NMR results still show a free and non-interacting NAC regions.

5.3.6 Viscosity effect on the transient intermolecular interactions

Besides the macromolecular crowding effect, viscosity also plays an important role in the cytosolic protein network. Viscosity in the cytosol has been shown to be approximately 3-fold greater than buffer viscosity in test tubes (Serber et al. 2005). It has been found that the mixed PEG crowding solution is not viscous enough to create intracellular-like viscosity for NMR experiments. In addition, αSyn precipitated immediately in 150 mg/ml PEG (same mixed ratios) which is more viscous. In order to create a highly viscous solution with high solubility of αSyn, glucose was chosen as a solute. By measuring the concentration-dependent translational diffusion coefficients of glucose in PBS buffer (figure 5.9A), 2 M glucose (360 mg/ml) exhibits approximately 3.5 times reduction and is the best condition to mimic viscous cytosolic environment for NMR experiments. Macromolecular crowding effect in this solution is not considered since glucose is a small inert biomolecule (MW: 180 dalton) to protein. Secondary structural propensity (figure 5.9C) and ^{1}H-^{15}N HSQC spectrum (figure. 5.9D) show that αSyn retains its disordered characteristics in highly viscous solution, the ^{15}N R_2 profile (figure 5.10A) in glucose are similar to those obtained at supercooled -10 °C (chapter 3) (Wu et al. 2008). Both ^{15}N R_2 data consistently indicate that the NAC is the flexible region in the whole protein.

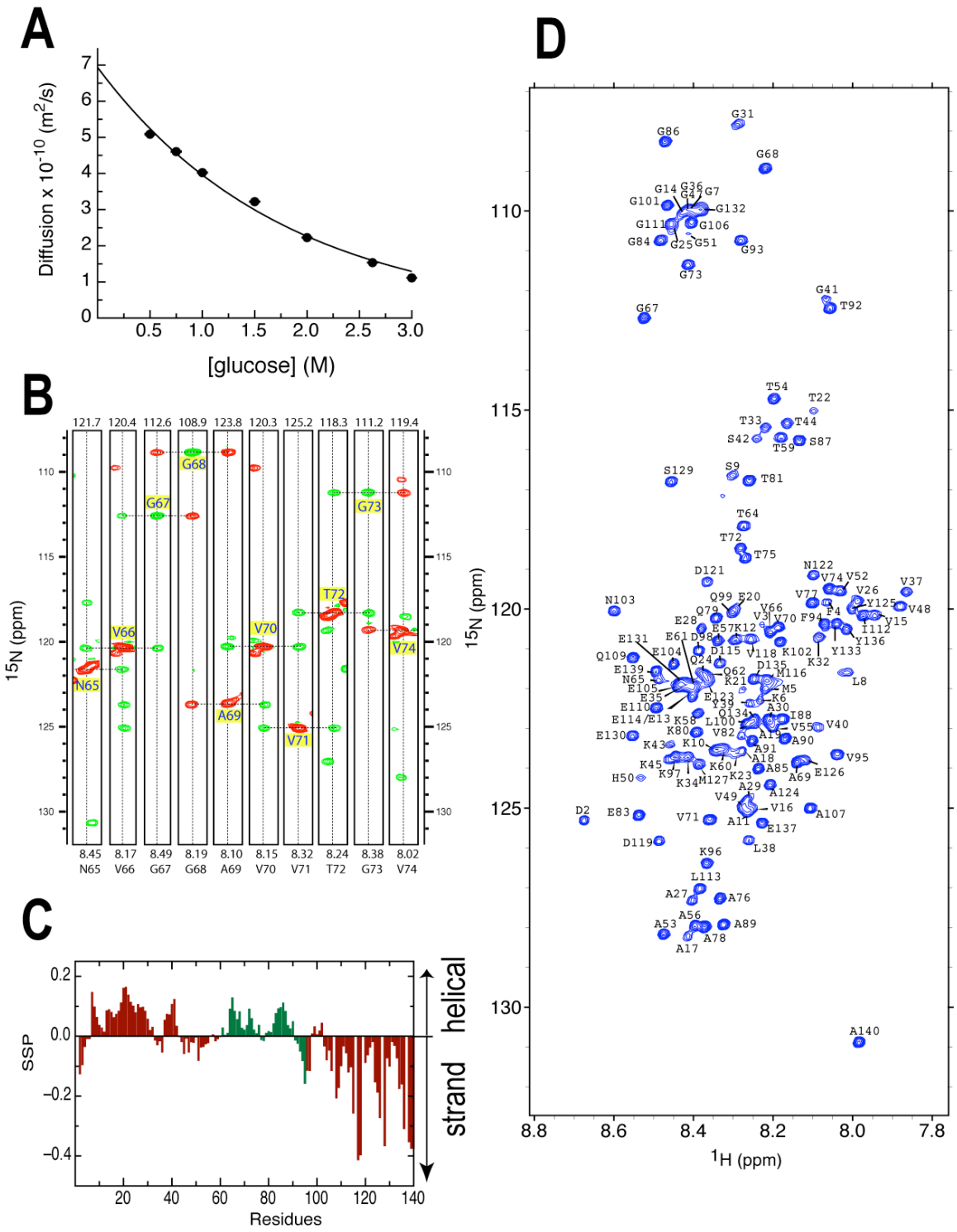

Figure 5.9 NMR spectral assignment and SSP scores of αSyn in 2 M glucose.

(A). Concentration-dependent translational diffusion coefficients of glucose were measured using PFG-NMR technique. Measurements were carried out at 15 °C on a Varian 600 MHz NMR. Data

process, peak integration and fitting were done as described in section 2.7. Obtained D_{trans} of glucose were used to fit a single exponential decaying function in order to predict the D_{trans} of very dilute glucose (e.g. 10 mM). The reduction of D_{trans} from very dilute glucose to 2 M glucose is approximately 3.5 times. **(B).** HNN connections of αSyn are shown from N65 to V74. Positive and negative peaks are colored in green and red, respectively. Diagonal peaks are indicated and labeled in each strip. **(C).** SSP scores of αSyn in 2 M glucose solution are shown. Positive and negative scores correspond extend and helical propensities. NAC region is colored in green and N- and C-terminal regions are colored in red. **(D).** Assigned ^{1}H-^{15}N HSQC of αSyn dissolved in 2 M glucose solution at 15 °C. Labels of cross-peaks are indicated as abbreviated residue type and corresponding numbers.

The diamagnetic ^{1}H R_2 of αSyn in 2 M glucose at pH 7.4 are greatly elevated ranging from 30-80 Hz suggesting that the backbone dynamic of αSyn is very restricted in such a viscous solution. Unlike the result reported in section 5.3.5 that diamagnetic ^{1}H R_2 of αSyn in 100 mg/ml PEG at pH 7.4 are highly HX-modulated, there is no strong, significant HX-modulation on the ^{1}H or ^{15}N R_2 of αSyn. Therefore, PRE-based characterizations of intermolecular contacts were carried out at the physiological pH states (pH 7.4). $^{1}H^{N}$ Γ_2 values of 400 μM mixed αSyn in viscous solution (2 M glucose) (figure 5.11) are uniformly ~2-fold enhanced relative to 400 μM αSyn dissolved in 100 mg/ml mixed PEG. The observed transient intermolecular contacts by using 3 different probes are: (1) A19C MTSL to C-terminal residues 113-135, (2) A90C MTSL to N-terminal residues 8-12 and 35-50 and residues 67-97 in NAC region and (3) G132C MTSL to N-terminal residues 2-20 and 30-60. PRE-based information shows that αSyn in viscous glucose solution at pH 7.4 undergoes transient antiparallel intermolecular

contacts and the transient intermolecular contacts are more pronounced than same observed contacts in other environment at neutral pH. Hotspots 3-20 and 30-60 (figure. 5.11C) also seen in dilute and PEG solutions are greatly enhanced in viscous glucose solution suggesting that the contact frequencies are increased and the life time of transient dimmer/oligomer is long. The extremely slow diffused medium also shows very weak NAC-to-NAC intermolecular contacts (figure 5.10). For instance, MTSL probe located at A90C shows small ^{1}H R_2 enhancement at residues 67-97 (< 15 Hz). The A90C PRE result provides novel information that the NAC region is the second place encountering intermolecular interactions and contacts are antiparallel consistent with previous information.

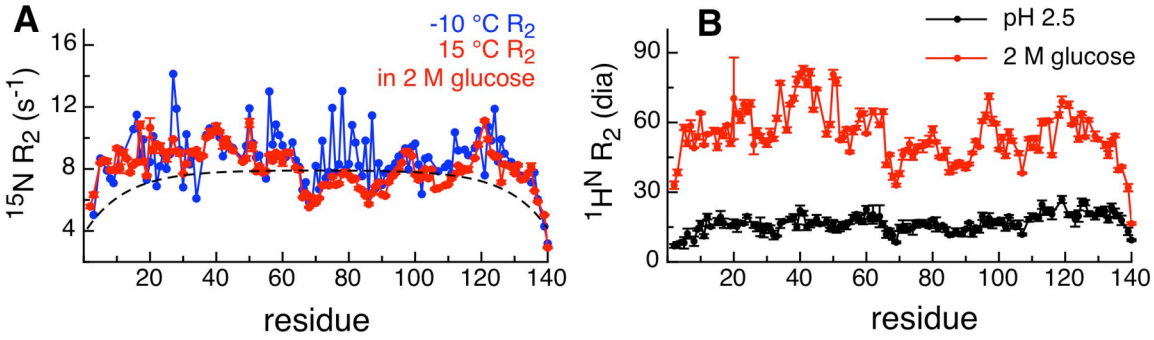

Figure 5.10 Comparison of ^{15}N R_2 of αSyn in 2 M glucose and at -10 °C and diamagnetic ^{1}H R_2 of αSyn in 2 M glucose.

(A). Measured ^{15}N R_2 of αSyn dissolved in 2 M glucose (red) and cooled at -10 °C (blue). Dashed line is the theoretical R_2 values of a 140-aa random coil (section 3.3) (Wu et al. 2008). **(B).** The diamagnetic ^{1}H R_2 of αSyn in viscous glucose solution also reflects that the NAC region is more flexible than the N- and C-terminal residues although all ^{1}H R_2 values are highly elevated compared to that measured in diluted solution (e.g. at pH 2.5).

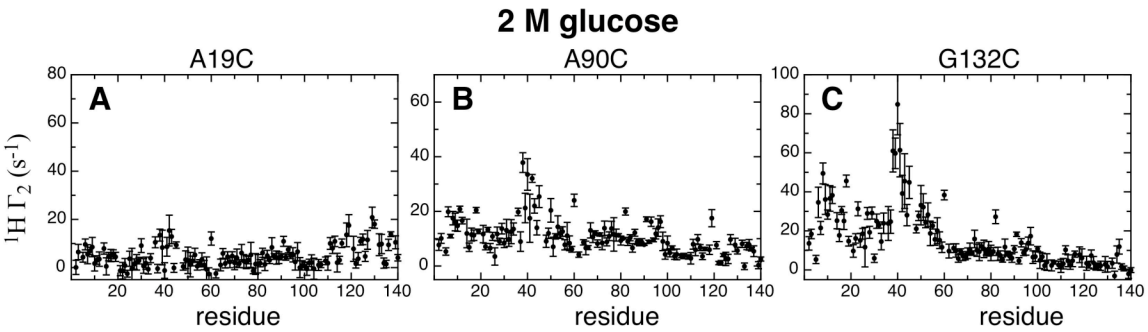

Figure 5.11 Intermolecular PRE profiles of αSyn in viscous glucose solution.

The intermolecular $^1H^N$ Γ_2 rates of αSyn in viscous 2 M glucose solution are obtained using MTSL probes located at A19C (A), A90C (B) and G132C (C). Samples composed of approximate 400 μM mixed αSyn were prepared for paramagnetic NMR experiments.

5.4 Conclusion and discussion

The schematic of the transient intermolecular interactions at low and neutral pH is illustrated in Fig. 5.12. αSyn at pH 2.5 consists of a highly positively charged N-terminus and collapsed NAC and C-terminal regions (Cho et al. 2009; McClendon et al. 2009). Hydrophobic packing at the C-terminus and part of NAC region is the major driving force of intermolecular interactions. The repulsive electrostatic feature of the N-terminus because of 18 positively charged residues (pH 2.5) results in the N-termini are being from one other. Thus the C-terminal and a portion of the NAC region are the only segments responsible for intermolecular contacts in a "tail-to-tail" manner. The details of up-down trends as seen in figure 5.12 comprehensively display that the hairpin-like units are kinked by prolines in the C-terminus. The bending feature may lead to a close intermolecular contact of αSyn (at low pH) perhaps followed by the lock-and-key model. According to the results coupled with the known distinct charge profiles at neutral and low pH, the aggregation of αSyn at low pH probably goes to a separate pathway to form

oligomer and fibrils. The core region and its secondary structural elements in the fibril may be different from those at neutral pH (Der-Sarkissian et al. 2003; Heise et al. 2005; Vilar et al. 2008). More experiments including hydrogen exchange of DMSO-dissolved αSyn fibrils (low pH incubated), EPR and solid state NMR experiments are necessary to provide clear insight into the structural aligment of αSyn fibrils at acidic pH.

Transient intermolecular contacts observed at neutral pH are very weak, consistent with current knowledge that aggregation is not favored at neutral and basic pH (Uversky et al. 2001a). Based on the mixed labeled PRE measurements, it is known now that self-association of αSyn at neutral pH is strongly based on the electrostatic attractions and picture of antiparallel head-to-tail pairing ensembles is proposed (Fig. 5.5). The ultra-weak intermolecular contacts between the N-terminal and the C-terminal regions are also known as intra-molecular αSyn contacts (Der-Sarkissian et al. 2003; Lee et al. 2004; Bertoncini et al. 2005b). The highly negatively charged C-terminus favors interactions with the N-terminal regions at two positions: 3-15 and 35-50. No noticeable NAC to NAC intermolecular contacts are detected at neutral pH implying that electrostatic charge-charge attractions instead of hydrophobic contact is the main driving force in the early stages of aggregation of αSyn under this condition. The data suggest that, at neutral pH, intermolecular and intra-molecular N- and C-terminal electrostatic interactions are competing with each other resulting in a very low tendency of αSyn aggregation. Moreover, an aggregation-disfavored variant of αSyn (Kessler et al. 2003) by adding two more N-terminal repeats at the N-terminus (9 repeats in total) may fit the theory that more complicated electrostatic intra-molecular and inter-molecular interactions lead to

slower aggregation kinetics. The additional repeats should have tendency like the first 2 N-terminal repeat to interact with the C-terminal residues thus there are two kinds of intra-molecular C-/N-terminal interactions and two kinds of inter-molecular C-/N-terminal contacts. In other words, there are many different interactions competing to form a relatively stable monomeric or dimeric ensemble in solution. Therefore a very long nucleation time was given. At here, it has been shown that the effects of macromolecular crowding and viscosity on αSyn at neutral pH dramatically enhance the transient inter-molecular contacts without changing the interface sites. Changes of excluded volume and decreased translational diffusion rates as studied here (figure 5.9A) confirm that the occurrences of inter-molecular interactions *in vivo* can be largely increased. NAC region known as the central core of αSyn fibril as characterized using solid state NMR (Heise et al. 2005; Vilar et al. 2008) and EPR (Der-Sarkissian et al. 2003; Chen et al. 2007) is not primarily in charge of the earliest interaction at either acidic or neutral pH but may be the second interface site of inter-molecular interactions at neutral pH as shown in figures 5.8 and 5.11.

The distribution of positive charges of the N-terminus at pH 2.5 keeps the N-terminal region away from other N-terminal regions. The NAC and C-terminal regions are more hydrophobic and favor association with another αSyn in the tail-to-tail contact manner. Core of fibrils and numbers of β-strands of αSyn amyloid fibrils incubated at low pH are unknown leaving an open question about the structural alignment and secondary structural segments of αSyn fibrils growing at neutral and low pH are similar or very distinct.

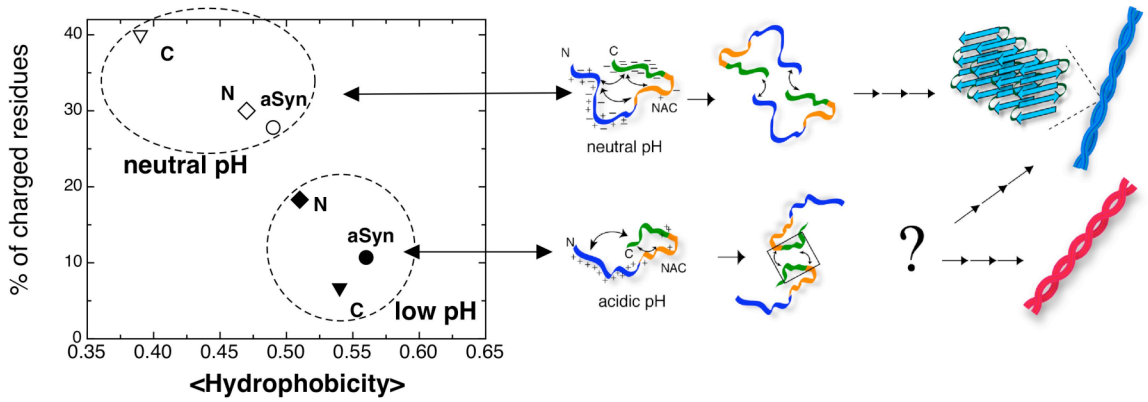

Figure 5.12 Plot of charge density and mean hydrophobicity and schematic of αSyn aggregation.

Correlation of percentage of charged residues and the mean hydrophbocity of αSyn, individual N- and C-terminal regions at neutral (pH 7.4) and low pH (pH 3.0) is shown. Diamond, inverse triangle and circle denote the N-terminal, C-terminal and full length of αSyn, respectively. Open and filled symbols represent the neutral and low pH states, respectively. At neutral pH, full length αSyn and the N- and C-termini are composed of 30-40% positively and negatively charged residues, however, all of them lose the negatively charged residue while protein goes to pH 3.0. Therefore αSyn and the two termini at acidic pH contain less than 20% charged residues but the corresponding mean hydrophobicity is increased. αSyn at neutral pH exhibits intra-molecular weak N-/C-terminal interactions as well as inter-molecular N-/C-terminal contacts. The head-to-tail contacts are primarily formed by the electrostatic attractions. NAC region as a core inside fibril and cross-β structures (5 strands) are illustrated according to earlier studies (Der-Sarkissian et al. 2003; Chen et al. 2007; Vilar et al. 2008).

Lindquist and colleagues have used fluorescence approach to reveal that head and tail regions of Sup35 (Krishnan and Lindquist 2005), a prion-like protein in yeast, are

responsible for oligomerization leaving the untouched central core during the self-association process. The studies on αSyn using paramagnetic NMR method also demonstrate similar results that the core region in fibrils aggregated from disordered protein is not necessary to be the primary element for self-association. In-register parallel structure constituting as a major class of amyloid fibrils of several intrinsically disordered proteins including αSyn has been concluded (Margittai and Langen 2008). However, molecular conversion from monomeric ensemble to cross-β amyloid fibril is not clear. Here, the characterized transient inter-molecular contacts of αSyn provide a novel structural insight into the earliest steps of αSyn aggregation at two distinct pH states. The next step with respect to understanding the details of molecular assembly of the polymer are important to understand the conformational conversion from head-to-tail packing to formation of in-register parallel NAC-NAC hydrophobic core.

Chapter 6 . Fast Hydrogen Exchange Reaction Modulates ^{15}N Backbone Transverse Relaxation in Intrinsically Disordered Protein

6.1 Introduction

NMR is a powerful tool to investigate protein backbone and sidechain dynamics. ^{15}N backbone transverse relaxation experiments (R_2) using the CPMG pulse train (^{15}N R_2^{CPMG}) have been used to investigate dynamics of the globular protein backbone amides on the ps to ms timescale (Kay et al. 1989; Mandel et al. 1995; Palmer 2004). The R_2 rates empirically provide information regarding the local structural mobility and chemical exchange process. Recently, this experiment has been applied for NMR dynamics studies of intrinsically disordered proteins (IDPs) (Buevich and Baum 1999; Buevich et al. 2001; Mittag and Forman-Kay 2007; Eliezer 2009; Wright and Dyson 2009) which have attracted significant attention in recent years as these proteins are functional as a disordered form and some of them are implicated in misfolding or aggregation diseases (Dyson and Wright 2005; Chiti and Dobson 2006). It has been shown by Bertini's group (Bertini et al. 2002) and Kay's group (Tugarinov and Kay 2003) that the ^{15}N R_2^{CPMG} rates of flexible loops of globular protein at neutral pH are modulated by fast hydrogen change (HX) rates. Residues with fast HX in folded proteins are always located at the solvent accessible surface area and the residues are often more flexible than other residues in the secondary structural elements. Since IDPs are random-coil like ensembles in solution, the NMR backbone dynamics of IDPs at neutral pH and higher temperature would be strongly modulated by fast HX. Here, α-synuclein, an IDP associated to Parkinson's disease, is chosen to demonstrate the relationship of fast HX and the ^{15}N R_2^{CPMG} rates at

different pH states. Briefly, the apparent ^{15}N R_2^{CPMG} values shown in figure 6.1 increased relatively by changing pH from 6.1 to 7.4 at 15 °C. Since the measured hydrogen exchange (HX) rates of α-synuclein is significantly high at neutral pH especially in the first 100 residues (Croke et al. 2008), the data in figure 6.1 imply that the fast hydrogen exchange rates of amide protons may modulate the measured ^{15}N R_2^{CPMG} values. Deconvolution of this fast HX effect on ^{15}N relaxation rates is important to obtain the correct ^{15}N R_2^{CPMG} relaxation rates for natively unfolded proteins. A demonstration using intrinsically disordered αSyn shows that ^{15}N relaxation rates that are affected by fast HX can be corrected quantitatively. The pH-dependent procedures shown here could be applied to other IDPs or partially folded proteins that are studied at neutral pH to avoid misinterpreting conformational and dynamic characteristics.

6.2 Materials and methods

6.2.1 αSyn preparation and NMR data acquisition

The expression and purification of ^{15}N-labeled αSyn were done by described protocols in sections 2.1. Lyophilized αSyn was dissolved in phosphate buffer at pH 7.4 or 6.1 (10 mM phosphate, 137 mM NaCl, 2 mM KCl). Prior to applying NMR experiments, samples were filtered by a 100 kDa filter (Millipore) to remove invisible small aggregates. Final sample concentrations were adjusted to 250 μM with 10% (v/v) D_2O for all NMR experiments.

The ^{15}N R_2^{CPMG} experiment was performed using the pulse sequence of gNhsqc in the Varian BioPack library; the ^{15}N R_2^{CPMG} relaxation is followed by the refocused INEPT

(insensitive nuclei enhancement via polarization transfer) transfer from ^{1}H to ^{15}N and the signal decay is measured by ^{1}H detection after the reverse INEPT. The NMR data were collected at a proton frequency of 800 MHz and 15 °C. Relaxation time delays (in seconds) for R_2^{CPMG} experiments were 0.01, 0.03, 0.05, 0.07, 0.09, 0.13, 0.17, 0.21, and 0.25. Interpulse delays and recycle delays were 625 μs and 2 seconds, respectively. Spectral complex points were 1024 and 256 in the t_2 and t_1 dimensions, respectively. Data were processed and analyzed by NMRPipe (Delaglio et al. 1995).

The relaxation data were fit with a single exponential function to measure the apparent R_2^{CPMG} values. The intrinsic R_2^{CPMG} values free from the HX effect were obtained as discussed in the results.

6.2.2 indole-^{15}N-labeled tryptophan preparation and NMR data collection

Indole-^{15}N-labeled tryptophan was purchased from Cambridge Isotope Laboratory (Andover, MA). 10mM indole-^{15}N-labeled tryptophan sample was prepared in 20mM Na-phosphate buffer and 90%/10% H_2O/D_2O at various pH states including pH 7.34, 6.86, 6.38, 5.86 and 5.38. The ^{15}N R_2^{CPMG} NMR pulse sequence was the same as that for αSyn and was performed on a Varian 800 MHz spectrometer with the relaxation time delays of 0.01, 0.03, 0.07, 0.11, 0.17, 0.21, and 0.25 (s). The apparent ^{15}N R_2^{CPMG} values affected by HX were obtained by the single exponential fit and the deconvolution of the HX effect on R_2^{CPMG} values was described in results. The ^{1}H-^{15}N R_{1zz} experiment based on Skrynnikov and Ernst (Skrynnikov and Ernst 1999) was modified to include the gradient sensitivity enhancement used in gNhsqc. The R_{1zz} experiment was performed

with the same arrays of relaxation delays and the intensity decays of R_{1zz} relaxation data were fitted with the single exponential decay to measure apparent N_zH_z R_{1zz} values which are the sum of intrinsic R_{1zz} and k_{HX}.

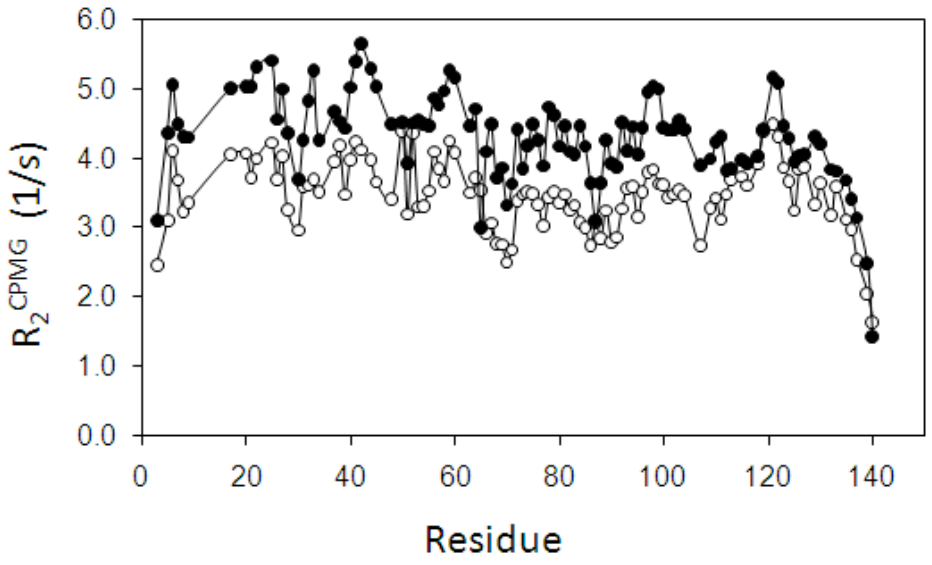

Figure 6.1 Distinct patterns of measured R_2^{CPMG} values of αSyn at two neutral pHs. Apparent R_2^{CPMG} values of αSyn at 15°C and at pH 7.4 (filled circles) and pH 6.1 (open circles). The R_2^{CPMG} relaxation data were fit with a single exponential decay function.

6.3 Results

αSyn is an intrinsically disordered protein (IDP) with less compactly folded structure and the backbone amide protons are not protected from the solvent (Weinreb et al. 1996; Eliezer et al. 2001; Uversky 2003; Wu et al. 2008). To study αSyn by NMR, protein samples have been prepared at pH 7.4 close to the physiological condition, but data are obtained at a low temperature (15°C) to reduce the tendency of aggregation. The apparent ^{15}N R_2^{CPMG} values of αSyn were acquired at pH 7.4 and pH 6.1 and plotted in Figure 6.1.

The apparent R_2^{CPMG} values at pH 7.4 were elevated relatvie to those at pH 6.1 and also showed some sequence-specific differences. The N-terminal residues had larger values than the C-terminal residues. However, the ^{1}H and ^{15}N chemical shifts of αSyn at pH 6.1 and 7.4 are indistinguishable suggesting no specific conformational changes between the two pH states. It is difficult to determine whether the pH-dependent differences in ^{15}N R_2^{CPMG} come from the nature of the protein dynamics which may be sensitive to a change of pH or from other physicochemical properties such as the hydrogen exchange (HX) rates which may impact on the NMR pulse sequence such as the ^{15}N R_2^{CPMG} NMR experiment. As shown in chapters 4 and 5, the apparent ^{15}N R_2^{CPMG} values of αSyn were quite variable depending on sample conditions such as pH (chapter 5) (Wu et al. 2009) and temperatures (chapter 4) (Wu et al. 2008). Similar results of distinct ^{15}N R_2^{CPMG} values of mouse αSyn at pH 7.4 and pH 6.0 were observed (data not shown) and fast HX kinetics of human αSyn at 10 °C were reported (Croke et al. 2008), sequence or region-dependence is not considered and fast HX effects on ^{15}N R_2^{CPMG} is further discussed in this chapter.

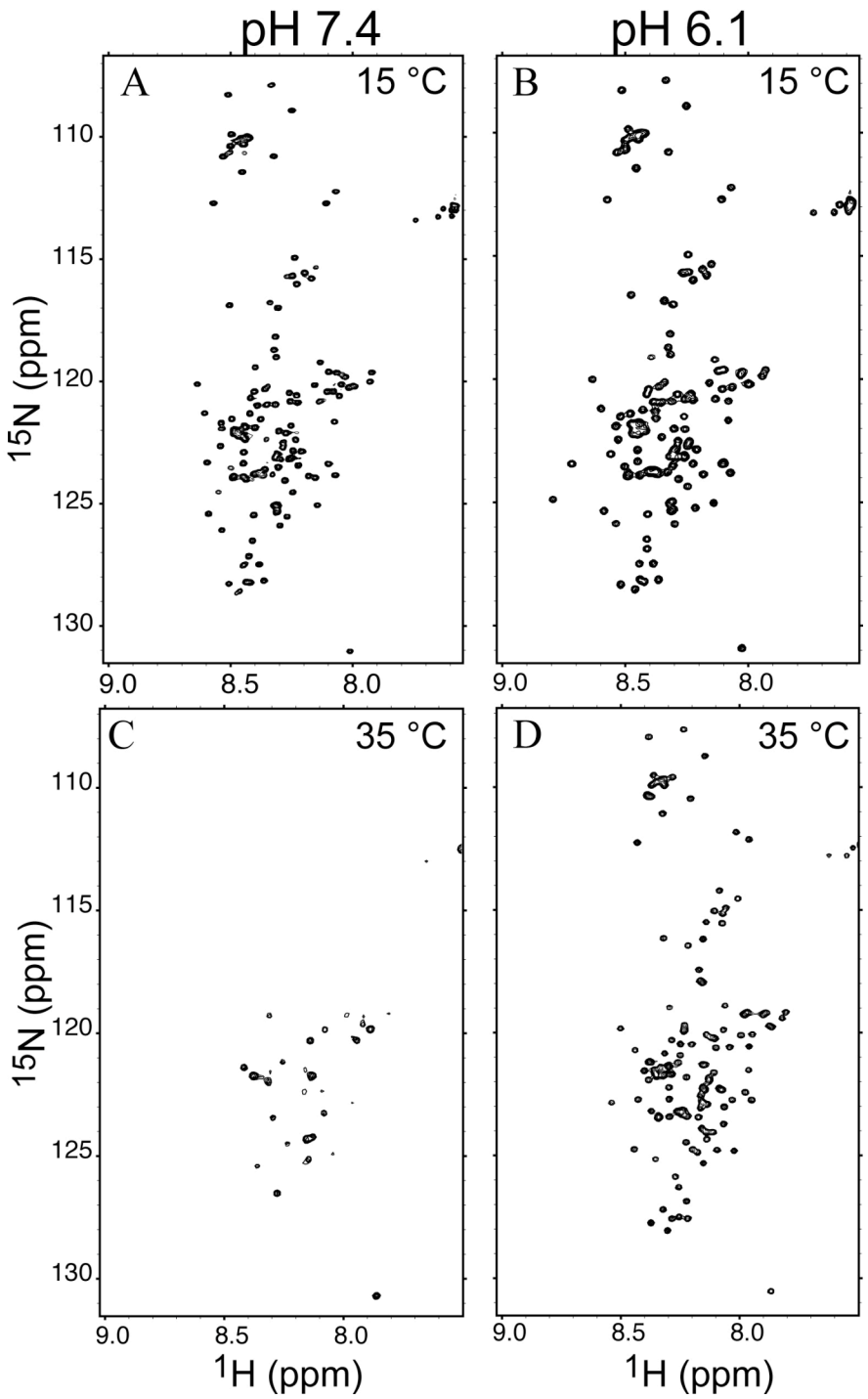

Figure 6.2 ^{1}H-^{15}N HSQC spectra at different pH and temperature.

^{1}H-^{15}N HSQC spectra of αSyn at different sample conditions; (A) pH 7.4 and 15 °C, (B) pH 6.1 and 15 °C, (C) pH 7.4 and 35 °C, and (D) pH 6.1 and 35 °C.

As shown in figure 6.2, ^{1}H-^{15}N HSQC of αSyn at pH 7.4 and 15 °C was compared to HSQC acquired under other experimental conditions. The HSQC of αSyn at pH 7.4 and 35 °C indicated reduced signal intensities and many missing amide resonances, but the HSQC spectrum acquired at pH 6.1 and 35 °C showed that all of the amide resonances were back. The chemical shits of amide resonances at 15 °C between pH 7.4 and pH 6.1 were indistinguishable except for His 50 and its flanking sequences. Similarly the chemical shifts at pH 6.1 between 15 °C and 35 °C were also invariant over the change of temperature. The chemical shifts of amide resonances were basically an upfield shift with increasing temperature at pH 7.4 and 6.1 but the intensities of the cross-peaks were sensitive to the changing conditions. A quick inspection of the HSQC spectra leads to a hypothesis that the fast HX might result in the large difference in signal intensities at pH 7.4 between 15 °C and 35 °C but the fast HX kinetics in αSyn may be suppressed significantly at pH 6.1. Thus, the fast HX of unprotected amide proteins could be the main contributor to the increase of the apparent R_2^{CPMG} values in Figure 6.1.

HX-affected NMR relaxations experiments have been reported and some relaxation experiments were developed to find the fast HX rates (Zhang et al. 1995; Dempsey 2001). The following two experiments describe the relationship between HX and the ^{15}N relaxation rates. In the R_{1zz} relaxation experiment of two spin order (N_zH_z) (Skrynnikov and Ernst 1999), the HX effect is the complete decorrelation of the N_zH_z spin operator and this results in the combined HX and R_{1zz} relaxation rate. In the ^{15}N R_2 relaxation experiment by the HCN-type coherence transfer (Kateb et al. 2007), the fast HX effect dephasing the ^{15}N spin operator is mediated through the $^{1}J_{NH}$ coupling evolution and the

HX. The presence or absence of ^{1}H decoupling during the relaxation time results in a significant difference in the HX effect on ^{15}N R_2 relaxation rates. Based on this experimental background, the ^{15}N R_2^{CPMG} relaxation rate measured by the HSQC-type NMR experiment is expected to be modified by the fast HX but the amount of the effect must be determined because of the different magnetization transfer from ^{15}N R_{1zz} or HCN-type ^{15}N R_2 experiment.

To describe the HX effect on the ^{15}N R_2^{CPMG} NMR experiment, the behavior of ^{15}N magnetization during the relaxation time period after the refocused INEPT is considered. When fast HX kinetics happens on the in-phase spin operator, the in-phase ^{15}N magnetization itself is not affected. However, the inter-converting anti-phase magnetization during the refocusing CPMG pulse train undertakes the signal decay by HX. Using the single spin operators for the amide proton (H) and the water proton (W) under HX,

$$NxH^{\alpha} \xrightarrow{W^{\alpha/\beta}} NxW^{\alpha} + NxW^{\beta}$$
$$NxH^{\beta} \xrightarrow{W^{\alpha/\beta}} NxW^{\alpha} + NxW^{\beta}$$

the HX effect on the in-phase magnetization is,

$$Nx = 0.5NxH^{\alpha} + 0.5NxH^{\beta} \xrightarrow{W^{\alpha/\beta}} 0.5NxW^{\alpha} + 0.5NxW^{\beta} = Nx$$

and the HX effect on the anti-phase magnetization is,

$$2NxHz = NxH^{\alpha} - NxH^{\beta} \xrightarrow{W^{\alpha/\beta}} zero$$

During the basic element of the CPMG pulse train in the ^{15}N R_2^{CPMG} NMR experiment, delay (0.5τ) – 180° Nx pulse – delay(0.5τ), the $^1J_{NH}$ coupling evolution can be described in the equation (1).

$$Nx \xrightarrow{NzHz\pi J\tau} \xrightarrow{\pi Nx} \xrightarrow{NzHz\pi J\tau} Nx\cos(0.5\pi J\tau)^2 + Nx\sin(0.5\pi J\tau)^2 \qquad (1)$$

Before applying the trigonometric identity ($\cos^2 x + \sin^2 x = 1$), the origin of cosine and sine terms needs to be emphasized; the cosine term is the fraction retained from the initial in-phase spin operator and the sine term is the fraction resulting from the anti-phase operator through the $^1J_{NH}$ coupling evolution. As mentioned, the anti-phase term undertakes the HX, so only the sine term is affected by HX for the duration of τ. The HX is treated as the first order chemical reaction in the initial rate because of the excess amount of the water solvent in the sample. If the HX rate is assumed to be in the slower exchange regime compared to the $^1J_{NH}$ coupling constant, it ensures the smooth exponential decay of the anti-phase term by HX.

$$(1) \xrightarrow{HX} \cos(0.5\pi J\tau)^2 + Nx\sin(0.5\pi J\tau)^2 e^{-k_{HX}\tau} \qquad (2)$$

When the R_2 relaxation during τ is applied to (2),

$$(2) \xrightarrow{\mathrm{Re}laxation} Nx\{\cos(0.5\pi J\tau)^2 + \sin(0.5\pi J\tau)^2 e^{-k_{HX}\tau}\}e^{-R_2\tau} \qquad (3)$$

The equation 3 implies that the HX effect on R_2 is mediated through the coupling evolution and it is suppressed by the spin-lock which maintains the cosine term. The stronger the CPMG spin-lock RF field strength, the more suppressed the HX effect on R_2. However, this is valid when the exchanging water magnetization is completely on the z-axis during the relaxation time. If the water magnetization is partially on the x-y plane,

the NMR signal from the cosine term will also be affected by HX because the experiment detects the proton signal after the reverse INEPT.

$$Nx = 0.5NxH^{\alpha} + 0.5NxH^{\beta} \xrightarrow{W^{x/y}} NxW^{x/y} \rightarrow \text{ Not observable}$$

Moreover, when the D_2O in the solvent is involved in the HX exchange, the HX effect on the cosine term is also to be involved.

$$NH \xrightarrow{D_2O} ND \rightarrow \text{ Not observable}$$

Thus the total HX effect on the ^{15}N R_2^{CPMG} NMR experiment using HSQC results from the contributions from the sum of contents of the anti-phase magnetization, no z-axis water magnetization, and the amount of D_2O in the sample solvent (v/v). Without quantifying these individual effects, a factor was used to simplify the correlation and Q is defined as the remaining portion of R_2 signals which are not affected by HX.

Since the total HX effect is suppressed by Qk_{HX} when k_{HX} is the HX rate, the corresponding kinetic model can be proposed in Scheme 1 as the consecutive and parallel kinetics of R_2 and Qk_{HX}.

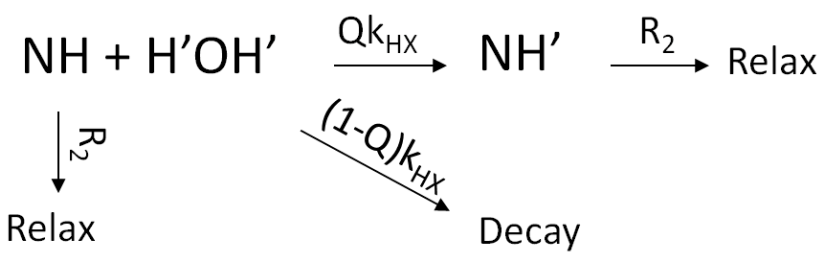

Scheme 1. The hydrogen exchange effect on the R_2 relaxation

The relevant rate equations for Scheme 1 are,

$$\frac{d[NH]}{dt} = -k_{HX}[NH] - R_2[NH]$$

$$\frac{d[NH']}{dt} = Qk_{HX}[NH] - R_2[NH']$$

The integral forms of these equations with I_0 (the initial concentration) are,

$$[NH] = I_0 e^{-(k_{HX}+R_2)t}$$

$$[NH'] = I_0 Q(e^{-R_2 t} - e^{-(k_{HX}+R_2)t})$$

When the NMR observable (I) is proportional to the sum of [NH] and [NH'], the signal decay is,

$$I = I_0\{Q + (1-Q)e^{-k_{HX}t}\}e^{-R_2 t} \qquad (4)$$

Equation 4 represents the multi-exponential decay of R_2 and k_{HX} and the measured relaxation rate can span between the intrinsic R_2 and $k_{HX} + R_2$ depending on the complete HX effect (Q = 0) and the fully suppressed effect (Q = 1). In case of the R_2^{CPMG} experiment, it may have a large Q value with $0 < Q < 1$. In the R_{1zz} experiment, Q = 0 due to the complete decorrelation of two spin order (N_zH_z) by HX.

$$I = I_0 e^{-(k_{HX}+R_{1zz})t} \qquad (5)$$

Since the relaxation decay data in the R_2^{CPMG} experiment needs to be fit with four parameters (I_0, Q, k_{HX}, and R_2) in equation 4, it is proposed to use Q and k_{HX} values as fixed parameter values prior to the data analysis. The parameter Q of the HX effect on

R_2^{CPMG} was estimated with the pre-determined k_{HX} by the R_{1zz} experiment. Two relaxation experiments (R_{1zz} and R_2^{CPMG}) were run at multiple pH conditions with a well-known model compound such as indole-^{15}N-labeled tryptophan. In case of the R_{1zz} experiment, the apparent R_{1zz} rate by a single exponential decay (Equation 5) is the sum of the intrinsic R_{1zz} and k_{HX} and this leads to evaluating the difference of k_{HX} values at different pH's by fitting the intensity ratios of two R_{1zz} relaxation decay data which cancel intrinsic the R_{1zz}. The difference of k_{HX} values allowed estimating k_{HX} values at different pH's with the approximation of the base-catalysis HX mechanism by $k_{HX}10^{\Delta pH}$ where ΔpH is the difference of pH. As shown in Figure 6.3A, the measured R_{1zz} values could be deconvoluted into the intrinsic R_{1zz} and k_{HX} and the majority of the measured R_{1zz} values were from the HX effect.

To estimate the Q value of the R_2^{CPMG} experiment, pH-dependent R_2^{CPMG} relaxation data of Trp were modeled by Equation 4 with known k_{HX} values from the R_{1zz} experiment. The resulting Q values were calculated as 0.75 +/- 0.03. Using the average Q = 0.75 and the k_{HX} value at each pH, the R_2^{CPMG} relaxation data were fit with Equation 4 again to obtain the intrinsic R_2^{CPMG} values. Figure 6.3B showed these intrinsic R_2^{CPMG} values from Equation 4 and apparent R_2^{CPMG} values obtained from the single exponential fit. The observable pH-dependence of the apparent R_2^{CPMG} values (from the single exponential fit) was removed in the intrinsic R_2^{CPMG} values although small errors in the intrinsic R_2^{CPMG} values were present due to the fixed Q value. The average Q = 0.75 seemed to be the sum of the HX effects by the average population ($\cos^2(0.5\pi J\tau) = 0.96$) of the in-phase ^{15}N magnetization with τ = 1.25 ms in the CPMG pulses, the 90% H_2O content of the

sample solvent, and about 87% of the z-axis water magnetization, in which the total Q may come from 0.96×0.9×0.87.

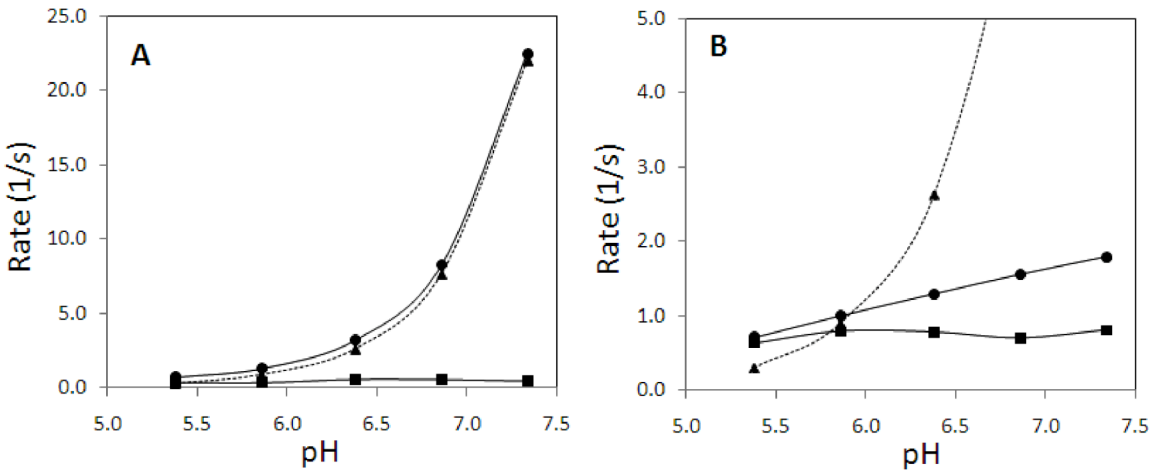

Figure 6.3 pH-dependent R_{1zz} and R_2^{CPMG} of indole-^{15}N-labeled tryptophan

(A) The apparent R_{1zz} values (circles) of indole-^{15}N-labeled tryptophan were decomposed into k_{HX} (triangles) and intrinsic R_{1zz} (squares) using the pH dependency of k_{HX} ($k_{HX}' = k_{HX}10^{\Delta pH}$). (B) The apparent R_2^{CPMG} values (circles) of indole-^{15}N-labeled tryptophan were obtained from the single exponential fit of the R_2^{CPMG} relaxation data. With known k_{HX} rates (triangles) from the R_{1zz} experiment and Q = 0.75, the relaxation data were fit with Equation 4 and resulted intrinsic R_2^{CPMG} values (squares) were plotted.

Since the Q value is known in the R_2^{CPMG} experiment, measuring k_{HX} values for other samples can be accomplished by acquiring pH-dependent R_2^{CPMG} experiments and fitting the intensity ratios of R_2^{CPMG} relaxation decay data by Equation 6 with the fixed Q value (0.75) and the pH dependency of k_{HX}.

$$I'/I = I'_0/I_0\{Q + (1-Q)e^{-10^{\Delta pH} k_{HX} t}\}/\{Q + (1-Q)e^{-k_{HX} t}\} \qquad (6)$$

Without performing the R_{1zz} experiments, this method was applied to the R_2^{CPMG} relaxation data of αSyn acquired at two different pH's while the k_{HX} at pH 7.4 is approximated from the k_{HX} at pH 6.1 by multiplying $10^{\Delta pH} = 10^{1.3}$. The resulting k_{HX} values at pH 6.1 and 7.4 were plotted in Figure 6.4A. Comparing to apparent R_2^{CPMG} values (Figure 6.1) obtained from the single exponential decay, overall k_{HX} values at pH 7.4 were much greater than the difference of apparent R_2^{CPMG} values between pH7.4 and 6.1, which indicate that the R_2^{CPMG} experiment suppresses a large amount of the HX effect although the HX effect is still observable on the apparent R_2^{CPMG} values. When these indirectly calculated k_{HX} values from the R_2^{CPMG} relaxation values are compared to other published data (Croke et al. 2008) estimated by the CLEANEX (Hwang and Shaka 1998; Hwang et al. 1998) experiment, the values were similar to each other.

However, it is not recommended to use the R_2^{CPMG} relaxation experiment to measure k_{HX} values since the largely suppressed condition of the HX effect on the R_2^{CPMG} relaxation makes it hard to extract correct k_{HX} values. MEXICO (Gemmecker et al. 1993), CLEANEX or R_{1zz} experiments are designed to measure the k_{HX} values. Instead of using pH dependent R_2^{CPMG} data, independent measurement of k_{HX} values using these techniques may have an advantage in accuracy. Figure 6.4A showed large errors in estimated k_{HX} values at pH 7.4 indicating that the errors looked proportionally larger with the k_{HX} values. This implies that estimating correct k_{HX} values becomes harder with increasing k_{HX} values. Since the time delays of the R_2^{CPMG} relaxation experiment are governed by the R_2^{CPMG} rates, the efficient HX effect convoluted into the R_2^{CPMG} rates happens when the k_{HX} rate is close to the R_2^{CPMG} rate. Thus, ideal range of k_{HX} values

largely influential to the R_2^{CPMG} relaxation may be $0.1 < k_{HX}/R_2^{CPMG} < 10$. Outside of this regime, the HX effect on the R_2^{CPMG} relaxation will become hard to measure. Furthermore, the HSQC signal itself is not observable when $k_{HX} > {}^1J_{NH}$.

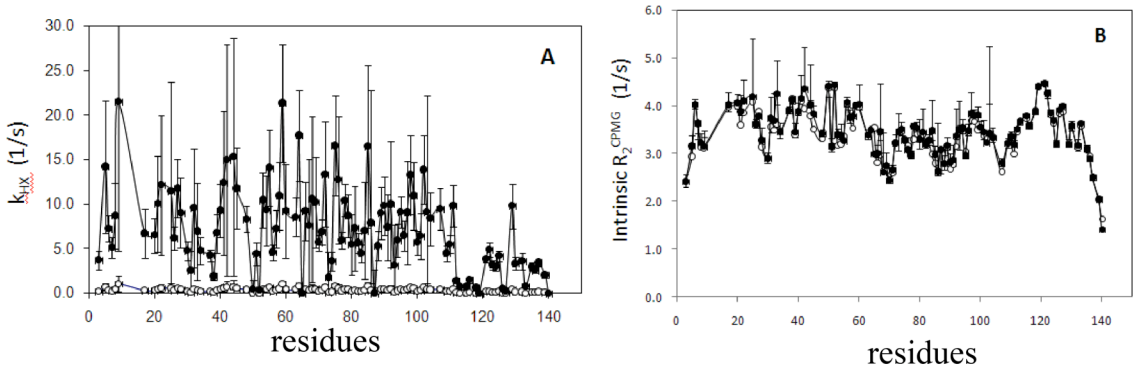

Figure 6.4 k_{HX} values and corrected R_2^{CPMG} at pH 6.1 and 7.4

(A) k_{HX} values at pH 6.1 (open circles) and 7.4 (filled circles). The k_{HX} values were estimated from the intensity ratios of the R_2^{CPMG} relaxation data by fitting Equation 6 with the fixed Q = 0.75. At residues 65, 119, and 140, observable k_{HX} were not found from the R_2^{CPMG} relaxation data. The errors of k_{HX} values at pH 6.1 were similar to the size of symbols and the errors at pH 7.4 were plotted symmetric upper- and lower-bounds. (B) Intrinsic R_2^{CPMG} values at pH 6.1 (open circles) and 7.4 (filled circles). The R_2^{CPMG} relaxation data were fit with the multi-exponential equation shown in Equation 4 while the k_{HX} values were fixed as shown at Figure 6.4A and Q = 0.75 was also fixed. The fit errors were estimated using upper- and lower-bounds of k_{HX} values. The fit errors of intrinsic R_2^{CPMG} values at pH 6.1 were within the size of symbols. The fit errors of intrinsic R_2^{CPMG} values at pH 7.4 were relatively larger than those at pH 6.1 but much more suppressed than the errors in k_{HX} values. The large upper-bound errors in intrinsic R_2^{CPMG} values at pH 7.4 were from the lower-bound k_{HX} values.

Since Q and k_{HX} values are known, the multi-exponential fit by Equation 4 was applied for the R_2^{CPMG} relaxation data at pH 6.1 and 7.4 to find out the intrinsic R_2^{CPMG} values

free from the HX effect. The resulting intrinsic R_2^{CPMG} values at pH 6.1 and 7.4 in Figure 6.4B were quite similar with each other and the large discrepancies in apparent R_2^{CPMG} values of αSyn shown in Figure 6.1 were eliminated by correcting the HX effect. The asymmetric error bars on the intrinsic R_2^{CPMG} values at pH 7.4 were estimated from the upper- and lower-bound k_{HX} values shown as symmetric error bars around the k_{HX} values. The small lower-bound errors in R_2^{CPMG} values were estimated from the upper-bound k_{HX} values and the large upper-bound ones in R_2^{CPMG} values were from the lower-bound k_{HX} values. Since the upper-bounds of k_{HX} (k_{HX} + error) values did not degrade the fit of R_2^{CPMG} relaxation data by Equation 4, the errors from the larger k_{HX} values were not directly propagated to the errors in R_2^{CPMG} values. This can be explained by the almost logarithmic suppression of k_{HX} in the R_2^{CPMG} values as shown in the Trp data (Figure 6.3B).

To demonstrate the HX effect on the R_2^{CPMG} relaxation as a conclusion, an example of the relaxation data was plotted in Figure 6.5A. The fit line (3) on the relaxation data (filled circles) was by Equation 4 with the fixed Q (=0.75) and k_{HX}, and the fit line (4) was by the single exponential function of an apparent R_2^{CPMG} value. As shown in Figure 6.5A, the fit of relaxation data using Equation 4 was better and the resulted intrinsic R_2^{CPMG} value became reduced. To show the goodness of fit, the ratio of SSE's (sum of squared errors) between the multi-exponential fit (Equation 4) and the single exponential fit was plotted for each residue in Figure 6.5B. For most of the residues, the multi-exponential fits were favorable due to the pH dependent HX effect on R_2^{CPMG} relaxation.

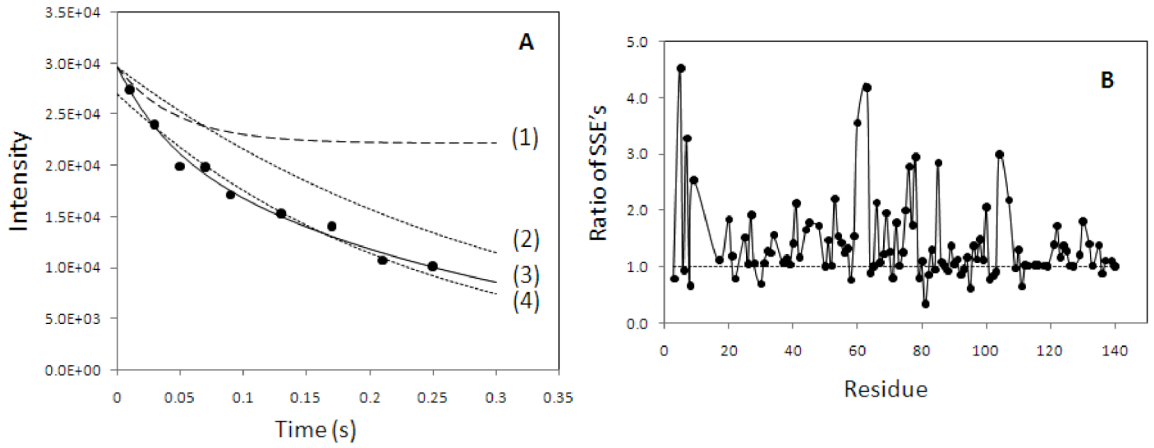

Figure 6.5 Example fitting and correction curves and fitting errors.

(A) The R_2^{CPMG} relaxation decay data at the residue Ser 9 affected by HX at pH 7.4 (filled circles) were plotted. The line (1) is the intensity decay by HX with $I_0(Q+(1-Q)\exp(-k_{HX}t))$, the line (2) is the relaxation decay by $I_0\exp(-R_2^{CPMG}t)$ with the intrinsic R_2^{CPMG}, and the line (3) is from Equation 4, $I_0(Q+(1-Q)\exp(-k_{HX}t))\exp(-R_2^{CPMG}t)$, to fit the data (filled circles). If the data was fit by a single exponential decay, $I_0\exp(-R_2^{CPMG}t)$, shown in the line (4), the sum of squared errors for fit was 2.5 times greater than the fit by the line (3). The parameter values and equations for each fit line were (2.96E+04)exp(-21.49t) for line (1), (2.96E+04)exp(-3.148t) for line (2), (2.96E+04)(0.75+0.25exp(-21.49t))exp(-3.148t) for line (3), and (2.70E+4)exp(-4.301t) for line (4). (B) Ratio of SSE's (sum of squared errors) between the multi-exponential fit (Equation 4) and the single exponential fit. The ratios larger than 1.0 indicate that fit by Equation 4 is favorable.

6.4 Conclusion and discussion

Based on the analysis of the HX effect on the ^{15}N R_2^{CPMG} NMR experiment, the mechanisms of HX effects were due to various sources and quite experiment specific: The anti-phase magnetization during the relaxation period was from the incomplete spin-lock of CPMG pulses, the fraction of none z-axis water magnetization was due to the

partial perturbation of the water magnetization, and the deuterium content was from the sample preparation. Remarkably, the last two effects are the major contributors and looked inevitable for the HSQC-based ^{15}N relaxation experiments since the hydrogen exchange process happens spontaneously during the relaxation period between the INEPT (from H to N) and the reverse INEPT (from N to H). These two effects could be ignored when the ^{15}N magnetization was prepared by HCN-type out-and-back INEPT in which HN was not involved in the observable (Kateb et al. 2007) or the ^{15}N magnetization under relaxation was in the two spin order such as N_zH_z (Skrynnikov and Ernst 1999). Thus the total HX effect on a specific NMR experiment depends on the nature of the coherence under relaxation and the coherence transfer pathways in addition to the status of the water magnetization.

Generally pH- or temperature- dependent R_2 measurements on unprotected amides of IDPs and loop regions in globular folded protein are prone to have the HX effect. Without correcting the HX effect, the elevated apparent R_2^{CPMG} values would be mis-interpreted as a result of other contributions such as conformational exchange or protein aggregation. Conformational exchange of αSyn induced by elevated temperature at 37 °C has been proposed (McNulty et al. 2006), however the protonless NMR experiments for αSyn at 37 °C done in the Dobson group has shown little changes in the ^{13}C chemical shifts (Hsu et al. 2009) suggesting consistent information with the data presented here that fast hydrogen exchange process in αSyn modulates the NMR signals and misleads to wrong conclusion. More accurate relaxation rates need to be obtained by working under conditions for which fast HX does not exist. When experimental conditions of fast

HX are inevitable, quantitative correction of the ^{15}N relaxation rates for fast HX is required. An alternative approach to avoid the signal modulation by the HX effect is to decrease the temperature to 5 °C or lower would slow down the HX kinetics a lot. The NMR studies of αSyn at supercooled temperatures in chapter 3 are showing perhaps HX-free ^{15}N R_2^{CPMG} values. Although the HX effect was demonstrated on the ^{15}N R_2^{CPMG} experiment, other NMR experiments that have long evolution times necessary to measure relaxations and diffusions are also known to have the fast HX effect (Dempsey 2001). Thus, extreme experimental conditions such as high pH and high temperature affecting the HX rates should be avoided when amide protons of proteins are susceptible to the HX effect. In addition to IDPs, the susceptible protein samples may include globular proteins with unstructured elements such as large loop regions or partially folded proteins that have great amount of amides exposed to the solvent.

Chapter 7 . Conclusion

7.1 Aggregation-prone αSyn ensemble

In chapters 3 and 4, the aggregation-prone ensembles of αSyn impacted by sequence or pH state have been thoroughly studied using NMR spectroscopy and the results provide novel insight into the correlation of structural reorganization and aggregation kinetics. Objectives as proposed in chapter 1 intend to decode the residue-specific effect on the aggregation kinetics, however, two sets of NMR data (mouse and human) can not clearly explain and point out which one (or more than one) among the 7 substitutions dominate the aggregation process. A combinatorial library consisting of single, double and triple-point residue substitutions from mouse αSyn to human αSyn or *vice versa* must be created for a systematic search. Approaches including biophysical characterizations using NMR spectroscopy and kinetic measurements using ThT fluorescence spectrometry are necessary to collect enough clues for the determination of sequence dependence. Bioinformatic tools such as TANGO (Fernandez-Escamilla et al. 2004; Linding et al. 2004; Rousseau et al. 2006), SALSA (shell script appendix A9) (Zibaee et al. 2007), Aggrescan (Conchillo-Sole et al. 2007) and Zyggregator (Pawar et al. 2005) algorithms have shown successful cases of accurate predictions of sequence-dependent aggregation and can efficiently assist the design of the combinatorial library.

In addition to the sequence- and pH-dependent aggregation-prone ensembles, reports from several groups have shown other environmental factors such as high salts (Munishkina et al. 2004b), high temperature (Uversky et al. 2001a), metal ions (Uversky

et al. 2001b; Yamin et al. 2003; Rasia et al. 2005; Binolfi et al. 2006) and marcromolecular crowding (Shtilerman et al. 2002; Munishkina et al. 2004a) drive αSyn aggregation rapidly. The extreme condition dramatically enhances the subtle aggregation-prone ensemble from low to high populated. NMR characterization of αSyn under these conditions will support more comprehensive details with aspects of secondary structural preferences and conformational rearrangements of aggregation-prone ensembles.

7.2 Transient inter-molecular contacts of αSyn

In chapter 5, the novel information of transient inter-molecular contacts at pH 2.5, pH 6 and macromolecular/viscous solution point out that the aggregation of αSyn at neutral pH is initially driven by the electrostatic interactions rather than the hydrophobic interactions. The studies using paramagnetic probes at three difference sites were performed at 15 °C. Molecular dynamic simulations using distance constraints derived from the PRE Γ_2 values will reveal the first visualization of temporarily lived αSyn dimer. Perhaps, additional PRE data probing at other sites are required to improve the quality and quantity of computational results. A systematic investigation of transient inter-molecular contacts using the developed mixed labeled PRE approach under different conditions including sequence, pH, temperature, salt, and macromolecular crowding must be carried out to show not only the exact contact model of transient dimer but also how the sequence and environmental factors influence on the inter-molecular interactions. The systematic studies described in sections 7.1 and 7.2 will shed light on the early molecular mechanism of αSyn fibril formation.

7.3 Future consideration

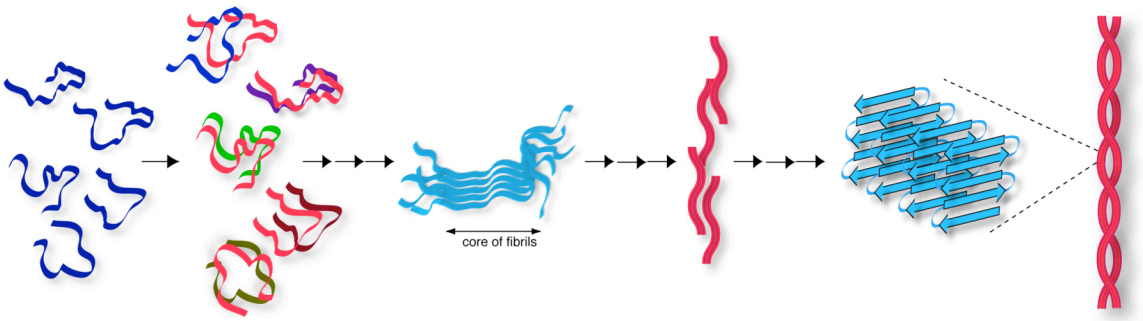

Figure 7.1 Schematic of αSyn aggregation

The results presented in chapters 3, and 4 provide more structural information of monomeric αSyn ensembles under aggregation-prone conditions and the results in chapter 5 further indicate the potential dimeric contact orientation. Molecular conversion from transient dimer, to nucleated oligomer, protofibrils, and then mature fibrils is not fully understood yet.

Figure 7.1 presents the simple schematic pathway of molecular conversion of fibril formation. For αSyn, the unfolded monomeric ensemble is heterogeneous in solution. The following step commonly known as nucleation, forming stable dimer or small oligomer, is believed to be the rate determining step. Assembling nucleated oligomers and elongated protofibrils are then presented. Current molecular and structural understanding of the conversion pathway are concentrated at the early and end stages showing the conformational characteristics of monomeric ensembles and the molecular alignment and rigid structural segments in the fibrils, respectively. Questions regarding the (1) the formation of nucleus (2) molecular mechanism of elongation (3) secondary, ternary and quaternary structural features of oligomers are not solved. Oligomers in the intermediate stages are very distinct in molecular size, conformation and structures. In addition, results in chapter 5 indicates that the head-to-tail antiparallel interactions of

transient dimers at neutral pH do not fit the current concept that αSyn fibril is packed in an in-register parallel structure suggesting that molecular rearrangements must exist during the nucleation or elongation states. Understanding the conformation of stable oligomer is needed. A sophisticated method must be developed to synchronize the molecular assembling process for NMR measurements of small oligomers and protofibrils. An alternative is using single molecule techniques with fluorescence, dynamic light scattering and atomic force microscopy to monitor the protein-protein interactions and fibril growth and provide complementary data to NMR-based information.

Reference

Abeliovich, A., Schmitz, Y., FariÒas, I., Choi-Lundberg, D., Ho, W.-H., Castillo, P.E., Shinsky, N., Verdugo, J.M.G., Armanini, M., Ryan, A., et al. 2000. Mice Lacking alpha-Synuclein Display Functional Deficits in the Nigrostriatal Dopamine System. *Neuron* **25:** 239-252.

Anfinsen, C.B. 1973. Principles that Govern the Folding of Protein Chains. *Science* **181:** 223-230.

Arawaka, S., Saito, Y., Murayama, S., and Mori, H. 1998. Lewy body in neurodegeneration with brian iron accumulation type 1 is immunoreactive for alpha-synuclein. *Neurology* **51:** 887-889.

Battiste, J.L., and Wagner, G. 2000. Utilization of site-directed spin labeling and high-resolution heteronuclear nuclear magnetic resonance for global fold determination of large proteins with limited nuclear overhauser effect data. *Biochemistry* **39:** 5355-5365.

Bermel, W., Bertini, I., Felli, I.C., Lee, Y.M., Luchinat, C., and Pierattelli, R. 2006. Protonless NMR experiments for sequence-specific assignment of backbone nuclei in unfolded proteins. *J Am Chem Soc* **128:** 3918-3919.

Bernado, P., Bertoncini, C.W., Griesinger, C., Zweckstetter, M., and Blackledge, M. 2005. Defining long-range order and local disorder in native alpha-synuclein using residual dipolar couplings. *J Am Chem Soc* **127:** 17968-17969.

Bertini, I., Carrano, C.J., Luchinat, C., Piccioli, M., and Poggi, L. 2002. A 15N NMR mobility study on the dicalcium P43M calbindin D9k and its mono-La3+-substituted form. *Biochemistry* **41:** 5104-5111.

Bertoncini, C.W., Fernandez, C.O., Griesinger, C., Jovin, T.M., and Zweckstetter, M. 2005a. Familial mutants of alpha-synuclein with increased neurotoxicity have a destabilized conformation. *J Biol Chem* **280:** 30649-30652.

Bertoncini, C.W., Jung, Y.S., Fernandez, C.O., Hoyer, W., Griesinger, C., Jovin, T.M., and Zweckstetter, M. 2005b. Release of long-range tertiary interactions potentiates aggregation of natively unstructured alpha-synuclein. *Proc Natl Acad Sci U S A* **102:** 1430-1435.

Bertoncini, C.W., Rasia, R.M., Lamberto, G.R., Binolfi, A., Zweckstetter, M., Griesinger, C., and Fernandez, C.O. 2007. Structural Characterization of the Intrinsically Unfolded Protein beta-Synuclein, a Natural Negative Regulator of alpha-Synuclein Aggregation. *Journal of molecular biology* **372:** 708-722.

Biere, A.L., Wood, S.J., Wypych, J., Steavenson, S., Jiang, Y., Anafi, D., Jacobsen, F.W., Jarosinski, M.A., Wu, G.M., Louis, J.C., et al. 2000. Parkinson's disease-associated alpha-synuclein is more fibrillogenic than beta- and gamma-synuclein and cannot cross-seed its homologs. *J Biol Chem* **275:** 34574-34579.

Binolfi, A., Rasia, R.M., Bertoncini, C.W., Ceolin, M., Zweckstetter, M., Griesinger, C., Jovin, T.M., and Fernandez, C.O. 2006. Interaction of alpha-synuclein with divalent metal ions reveals key differences: a link between structure, binding specificity and fibrillation enhancement. *J Am Chem Soc* **128:** 9893-9901.

Bisaglia, M., Mammi, S., and Bubacco, L. 2009. Structural insights on physiological functions and pathological effects of alpha-synuclein. *FASEB J.* **23:** 329-340.

Bracken, C., Iakoucheva, L.M., Romero, P.R., and Dunker, A.K. 2004. Combining prediction, computation and experiment for the characterization of protein disorder. *Curr Opin Struct Biol* **14:** 570-576.

Buevich, A.V., and Baum, J. 1999. Dynamics of Unfolded Proteins: Incorporation of Distributions of Correlation Times in the Model Free Analysis of NMR Relaxation Data. *J Am Chem Soc* **121:** 8671-8672.

Buevich, A.V., Shinde, U.P., Inouye, M., and Baum, J. 2001. Backbone dynamics of the natively unfolded pro-peptide of subtilisin by heteronuclear NMR relaxation studies. *Journal of biomolecular NMR* **20:** 233-249.

Bussell, R., Jr., and Eliezer, D. 2001. Residual structure and dynamics in Parkinson's disease-associated mutants of alpha-synuclein. *J Biol Chem* **276:** 45996-46003.

Bussell, R., Jr., and Eliezer, D. 2003. A structural and functional role for 11-mer repeats in alpha-synuclein and other exchangeable lipid binding proteins. *Journal of molecular biology* **329:** 763-778.

Bussell, R., Jr., and Eliezer, D. 2004. Effects of Parkinson's disease-linked mutations on the structure of lipid-associated alpha-synuclein. *Biochemistry* **43:** 4810-4818.

Bussell, R., Jr., Ramlall, T.F., and Eliezer, D. 2005. Helix periodicity, topology, and dynamics of membrane-associated alpha-synuclein. *Protein Sci* **14:** 862-872.

Caughey, B., and Lansbury, P.T. 2003. Protofibrils, pores, fibrils, and neurodegeneration: separating the responsible protein aggregates from the innocent bystanders. *Annu Rev Neurosci* **26:** 267-298.

Chen, M., Margittai, M., Chen, J., and Langen, R. 2007. Investigation of alpha-Synuclein Fibril Structure by Site-directed Spin Labeling. *J Biol Chem* **282:** 24970-24979.

Chiti, F., and Dobson, C.M. 2006. Protein misfolding, functional amyloid, and human disease. *Annual review of biochemistry* **75:** 333-366.

Cho, M.K., Nodet, G., Kim, H.Y., Jensen, M.R., Bernado, P., Fernandez, C.O., Becker, S., Blackledge, M., and Zweckstetter, M. 2009. Structural characterization of alpha-synuclein in an aggregation prone state. *Protein Sci* **18:** 1840-1846.

Choi, W., Zibaee, S., Jakes, R., Serpell, L.C., Davletov, B., Crowther, R.A., and Goedert, M. 2004. Mutation E46K increases phospholipid binding and assembly into filaments of human alpha-synuclein. *FEBS Lett* **576:** 363-368.

Cleveland, W.S., and Devlin, S.J. 1988. Locally Weighted Regression:An Approach to Regression Analysis by Local Fitting. *J Am Chem Soc* **83:** 596-610.

Clore, G.M. 2008. Visualizing lowly-populated regions of the free energy landscape of macromolecular complexes by paramagnetic relaxation enhancement. *Molecular bioSystems* **4:** 1058-1069.

Clore, G.M., Tang, C., and Iwahara, J. 2007. Elucidating transient macromolecular interactions using paramagnetic relaxation enhancement. *Curr Opin Struct Biol* **17:** 603-616.

Conchillo-Sole, O., de Groot, N.S., Aviles, F.X., Vendrell, J., Daura, X., and Ventura, S. 2007. AGGRESCAN: a server for the prediction and evaluation of "hot spots" of aggregation in polypeptides. *BMC Bioinformatics* **8:** 65.

Conway, K.A., Harper, J.D., and Lansbury, P.T. 1998. Accelerated in vitro fibril formation by a mutant alpha-synuclein linked to early-onset Parkinson disease. *Nat Med* **4:** 1318-1320.

Conway, K.A., Lee, S.J., Rochet, J.C., Ding, T.T., Williamson, R.E., and Lansbury, P.T., Jr. 2000. Acceleration of oligomerization, not fibrillization, is a shared property of both alpha-synuclein mutations linked to early-onset Parkinson's disease: implications for pathogenesis and therapy. *Proc Natl Acad Sci U S A* **97:** 571-576.

Cooper, A.A., Gitler, A.D., Cashikar, A., Haynes, C.M., Hill, K.J., Bhullar, B., Liu, K., Xu, K., Strathearn, K.E., Liu, F., et al. 2006. alpha-Synuclein Blocks ER-Golgi Traffic and Rab1 Rescues Neuron Loss in Parkinson's Models. *Science* **313:** 324-328.

Cowan, R., and Whittaker, R. 1990. Hydrophobicity indices for amino acid residues as determined by high-performance liquid chromatography. *Pept. Res* **3:** 75-80.

Croke, R.L., Sallum, C.O., Watson, E., Watt, E.D., and Alexandrescu, A.T. 2008. Hydrogen exchange of monomeric alpha-synuclein shows unfolded structure persists at physiological temperature and is independent of molecular crowding in Escherichia coli. *Protein Sci* **17:** 1434-1445.

Davidson, W.S., Jonas, A., Clayton, D.F., and George, J.M. 1998. Stabilization of alpha-synuclein secondary structure upon binding to synthetic membranes. *J Biol Chem* **273:** 9443-9449.

Dedmon, M.M., Christodoulou, J., Wilson, M.R., and Dobson, C.M. 2005a. Heat shock protein 70 inhibits alpha-synuclein fibril formation via preferential binding to prefibrillar species. *J Biol Chem* **280:** 14733-14740.

Dedmon, M.M., Lindorff-Larsen, K., Christodoulou, J., Vendruscolo, M., and Dobson, C.M. 2005b. Mapping long-range interactions in alpha-synuclein using spin-label NMR and ensemble molecular dynamics simulations. *J Am Chem Soc* **127:** 476-477.

Delaglio, F., Grzesiek, S., Vuister, G.W., Zhu, G., Pfeifer, J., and Bax, A. 1995. NMRPipe: a multidimensional spectral processing system based on UNIX pipes. *Journal of biomolecular NMR* **6:** 277-293.

Dempsey, C.E. 2001. Hydrogen exchange in peptides and proteins using NMR spectroscopy. *Progress in Nuclear Magnetic Resonance Spectroscopy* **39:** 135-170.

Der-Sarkissian, A., Jao, C.C., Chen, J., and Langen, R. 2003. Structural Organization of alpha-Synuclein Fibrils Studied by Site-directed Spin Labeling. *J Biol Chem* **278:** 37530-37535.

Dinner, A.R., Sali, A., Smith, L.J., Dobson, C.M., and Karplus, M. 2000. Understanding protein folding via free-energy surfaces from theory and experiment. *Trends in biochemical sciences* **25:** 331-339.

Dobson, C.M. 1999. Protein misfolding, evolution and disease. *Trends in biochemical sciences* **24:** 329-332.

Dobson, C.M. 2001. The structural basis of protein folding and its links with human disease. *Philosophical transactions of the Royal Society of London* **356:** 133-145.

Dobson, C.M. 2003. Protein folding and misfolding. *Nature* **426:** 884-890.

Dobson, C.M. 2004. Experimental investigation of protein folding and misfolding. *Methods (San Diego, Calif* **34:** 4-14.

Donaldson, L.W., Skrynnikov, N.R., Choy, W.Y., Muhandiram, D.R., Sarkar, B., Forman-Kay, J.D., and Kay, L.E. 2001. Structural characterization of proteins

with an attached ATCUN motif by paramagnetic relaxation enhancement NMR spectroscopy. *J Am Chem Soc* **123:** 9843-9847.

Dyson, H.J., and Wright, P.E. 2004. Unfolded proteins and protein folding studied by NMR. *Chemical reviews* **104:** 3607-3622.

Dyson, H.J., and Wright, P.E. 2005. Intrinsically unstructured proteins and their functions. *Nature reviews* **6:** 197-208.

El-Agnaf, O.M., Bodles, A.M., Guthrie, D.J., Harriott, P., and Irvine, G.B. 1998. The N-terminal region of non-A beta component of Alzheimer's disease amyloid is responsible for its tendency to assume beta-sheet and aggregate to form fibrils. *European journal of biochemistry / FEBS* **258:** 157-163.

Eliezer, D. 2009. Biophysical characterization of intrinsically disordered proteins. *Curr Opin Struct Biol* **19:** 23-30.

Eliezer, D., Kutluay, E., Bussell, R., Jr., and Browne, G. 2001. Conformational properties of alpha-synuclein in its free and lipid-associated states. *Journal of molecular biology* **307:** 1061-1073.

Farrow, N.A., Muhandiram, R., Singer, A.U., Pascal, S.M., Kay, C.M., Gish, G., Shoelson, S.E., Pawson, T., Forman-Kay, J.D., and Kay, L.E. 1994. Backbone dynamics of a free and phosphopeptide-complexed Src homology 2 domain studied by 15N NMR relaxation. *Biochemistry* **33:** 5984-6003.

Ferentz, A.E., and Wagner, G. 2000. NMR spectroscopy: a multifaceted approach to macromolecular structure. *Quarterly reviews of biophysics* **33:** 29-65.

Fernandez, C.O., Hoyer, W., Zweckstetter, M., Jares-Erijman, E.A., Subramaniam, V., Griesinger, C., and Jovin, T.M. 2004. NMR of alpha-synuclein-polyamine complexes elucidates the mechanism and kinetics of induced aggregation. *The EMBO journal* **23:** 2039-2046.

Fernandez-Escamilla, A.M., Rousseau, F., Schymkowitz, J., and Serrano, L. 2004. Prediction of sequence-dependent and mutational effects on the aggregation of peptides and proteins. *Nat Biotechnol* **22:** 1302-1306.

Fieber, W., Kristjansdottir, S., and Poulsen, F.M. 2004. Short-range, long-range and transition state interactions in the denatured state of ACBP from residual dipolar couplings. *Journal of molecular biology* **339:** 1191-1199.

Fink, A.L. 2006. The aggregation and fibrillation of alpha-synuclein. *Acc Chem Res* **39:** 628-634.

Forman, M.S., Trojanowski, J.Q., and Lee, V.M. 2004. Neurodegenerative diseases: a decade of discoveries paves the way for therapeutic breakthroughs. *Nat Med* **10:** 1055-1063.

Gemmecker, G., Jahnke, W., and Kessler, H. 1993. Measurement of fast proton exchange rates in isotopically labeled compounds. *J Am Chem Soc* **115:** 11620-11621.

George, J.M., Jin, H., Woods, W.S., and Clayton, D.F. 1995. Characterization of a novel protein regulated during the critical period for song learning in the zebra finch. *Neuron* **15:** 361-372.

Gillespie, J.R., and Shortle, D. 1997. Characterization of long-range structure in the denatured state of staphylococcal nuclease. I. Paramagnetic relaxation enhancement by nitroxide spin labels. *Journal of molecular biology* **268:** 158-169.

Goddard, T.D., and Kneller, D.G. Sparky 3. University of California, San Francisco.

Goedert, M. 2001. Alpha-synuclein and neurodegenerative diseases. *Nature Reviews Nueroscience* **2:** 492-501.

Goers, J., Uversky, V.N., and Fink, A.L. 2003. Polycation-induced oligomerization and accelerated fibrillation of human alpha-synuclein in vitro. *Protein Sci* **12:** 702-707.

Greenbaum, E.A., Graves, C.L., Mishizen-Eberz, A.J., Lupoli, M.A., Lynch, D.R., Englander, S.W., Axelsen, P.H., and Giasson, B.I. 2005. The E46K mutation in alpha-synuclein increases amyloid fibril formation. *J Biol Chem* **280:** 7800-7807.

Heise, H., Hoyer, W., Becker, S., Andronesi, O.C., Riedel, D., and Baldus, M. 2005. Molecular-level secondary structure, polymorphism, and dynamics of full-length alpha-synuclein fibrils studied by solid-state NMR. *Proc Natl Acad Sci U S A* **102:** 15871-15876.

Hoyer, W., Cherny, D., Subramaniam, V., and Jovin, T.M. 2004. Impact of the acidic C-terminal region comprising amino acids 109-140 on alpha-synuclein aggregation in vitro. *Biochemistry* **43:** 16233-16242.

Hsu, S.T., Bertoncini, C.W., and Dobson, C.M. 2009. Use of protonless NMR spectroscopy to alleviate the loss of information resulting from exchange-broadening. *J Am Chem Soc* **131:** 7222-7223.

Hwang, T.L., and Shaka, A.J. 1998. Multiple-pulse mixing sequences that selectively enhance chemical exchange or cross-relaxation peaks in high-resolution NMR spectra. *J Magn Reson* **135:** 280-287.

Hwang, T.L., van Zijl, P.C., and Mori, S. 1998. Accurate quantitation of water-amide proton exchange rates using the phase-modulated CLEAN chemical EXchange (CLEANEX-PM) approach with a Fast-HSQC (FHSQC) detection scheme. *Journal of biomolecular NMR* **11:** 221-226.

Iwahara, J., and Clore, G.M. 2006. Detecting transient intermediates in macromolecular binding by paramagnetic NMR. *Nature* **440:** 1227-1230.

Iwahara, J., Tang, C., and Marius Clore, G. 2007. Practical aspects of 1H transverse paramagnetic relaxation enhancement measurements on macromolecules. *J Magn Reson B* **184:** 185-195.

Jenco, J.M., Rawlingson, A., Daniels, B., and Morris, A.J. 1998. Regulation of Phospholipase D2: Selective Inhibition of Mammalian Phospholipase D Isoenzymes by alpha- and beta-Synucleins. *Biochemistry* **37:** 4901-4909.

Jerschow, A., and Muller, N. 1997. Suppression of Convection Artifacts in Stimulated-Echo Diffusion Experiments. Double-Stimulated-Echo Experiments. *J Magn Reson B* **125:** 372-375.

Jo, E., McLaurin, J., Yip, C.M., St George-Hyslop, P., and Fraser, P.E. 2000. alpha-Synuclein membrane interactions and lipid specificity. *J Biol Chem* **275:** 34328-34334.

Johnson, B.A., and Blevins, R.A. 1994. NMR View: A computer program for the visualization and analysis of NMR data. *Journal of biomolecular NMR* **4:** 603-614.

Karplus, M. 1997. The Levinthal paradox: yesterday and today. *Folding and Design* **2:** S69-S75.

Kateb, F., Pelupessy, P., and Bodenhausen, G. 2007. Measuring fast hydrogen exchange rates by NMR spectroscopy. *J Magn Reson* **184:** 108-113.

Kay, L.E., Torchia, D.A., and Bax, A. 1989. Backbone dynamics of proteins as studied by 15N inverse detected heteronuclear NMR spectroscopy: application to staphylococcal nuclease. *Biochemistry* **28:** 8972-8979.

Kessler, J.C., Rochet, J.C., and Lansbury, P.T., Jr. 2003. The N-terminal repeat domain of alpha-synuclein inhibits beta-sheet and amyloid fibril formation. *Biochemistry* **42:** 672-678.

Kim, H.Y., Heise, H., Fernandez, C.O., Baldus, M., and Zweckstetter, M. 2007. Correlation of Amyloid Fibril beta-Structure with the Unfolded State of alpha-Synuclein. *Chembiochem* **8:** 1671-1674.

Kim, S., and Szyperski, T. 2003. GFT NMR, a new approach to rapidly obtain precise high-dimensional NMR spectral information. *J Am Chem Soc* **125:** 1385-1393.

Kim, S., and Szyperski, T. 2004. GFT NMR experiments for polypeptide backbone and 13Cbeta chemical shift assignment. *Journal of biomolecular NMR* **28:** 117-130.

Kim, T.D., Paik, S.R., and Yang, C.H. 2002. Structural and functional implications of C-terminal regions of alpha-synuclein. *Biochemistry* **41:** 13782-13790.

Klein-Seetharaman, J., Oikawa, M., Grimshaw, S.B., Wirmer, J., Duchardt, E., Ueda, T., Imoto, T., Smith, L.J., Dobson, C.M., and Schwalbe, H. 2002. Long-range interactions within a nonnative protein. *Science* **295:** 1719-1722.

Korzhnev, D.M., and Kay, L.E. 2008. Probing invisible, low-populated States of protein molecules by relaxation dispersion NMR spectroscopy: an application to protein folding. *Acc Chem Res* **41:** 442-451.

Korzhnev, D.M., Salvatella, X., Vendruscolo, M., Di Nardo, A.A., Davidson, A.R., Dobson, C.M., and Kay, L.E. 2004. Low-populated folding intermediates of Fyn SH3 characterized by relaxation dispersion NMR. *Nature* **430:** 586-590.

Kosen, P.A. 1989. Spin labeling of proteins. *Methods Enzymol* **177:** 86-121.

Krishnan, R., and Lindquist, S.L. 2005. Structural insights into a yeast prion illuminate nucleation and strain diversity. *Nature* **435:** 765-772.

Kristjansdottir, S., Lindorff-Larsen, K., Fieber, W., Dobson, C.M., Vendruscolo, M., and Poulsen, F.M. 2005. Formation of native and non-native interactions in ensembles of denatured ACBP molecules from paramagnetic relaxation enhancement studies. *Journal of molecular biology* **347:** 1053-1062.

Kroenke, C.D., Loria, J.P., Lee, L.K., Rance, M., and Palmer, A.G. 1998. Longitudinal and Transverse 1H-15N Dipolar/15N Chemical Shift Anisotropy Relaxation Interference: Unambiguous Determination of Rotational Diffusion Tensors and Chemical Exchange Effects in Biological Macromolecules. *J Am Chem Soc* **120:** 7905-7915.

Kruger, R., Kuhn, W., Muller, T., Woitalla, D., Graeber, M., Kosel, S., Przuntek, H., Epplen, J.T., Schols, L., and Riess, O. 1998. Ala30Pro mutation in the gene encoding alpha-synuclein in Parkinson's disease. *Nature genetics* **18:** 106-108.

Kuboniwa, H., Grzesiek, S., Delaglio, F., and Bax, A. 1994. Measurement of HN-H alpha J couplings in calcium-free calmodulin using new 2D and 3D water-flip-back methods. *Journal of biomolecular NMR* **4:** 871-878.

Lansbury, P.T., Jr. 1999. Evolution of amyloid: what normal protein folding may tell us about fibrillogenesis and disease. *Proc Natl Acad Sci U S A* **96:** 3342-3344.

Lee, J.C., Langen, R., Hummel, P.A., Gray, H.B., and Winkler, J.R. 2004. alpha-Synuclein structures from fluorescence energy-transfer kinetics: Implications for

the role of the protein in Parkinson's disease. *Proc Natl Acad Sci U S A* **101:** 16466-16471.

Lescop, E., Schanda, P., and Brutscher, B. 2007. A set of BEST triple-resonance experiments for time-optimized protein resonance assignment. *J Magn Reson* **187:** 163-169.

Levinthal, C. 1968. Are there pathways for protein folding. *J. Chim. Physique* **65:** 44-45.

Li, W., West, N., Colla, E., Pletnikova, O., Troncoso, J.C., Marsh, L., Dawson, T.M., Jakala, P., Hartmann, T., Price, D.L., et al. 2005a. Aggregation promoting C-terminal truncation of alpha-synuclein is a normal cellular process and is enhanced by the familial Parkinson's disease-linked mutations. *Proc Natl Acad Sci U S A* **102:** 2162-2167.

Li, Y., Kim, S., Brodsky, B., and Baum, J. 2005b. Identification of partially disordered peptide intermediates through residue-specific NMR diffusion measurements. *J Am Chem Soc* **127:** 10490-10491.

Lietzow, M.A., Jamin, M., Jane Dyson, H.J., and Wright, P.E. 2002. Mapping long-range contacts in a highly unfolded protein. *Journal of molecular biology* **322:** 655-662.

Linding, R., Schymkowitz, J., Rousseau, F., Diella, F., and Serrano, L. 2004. A comparative study of the relationship between protein structure and beta-aggregation in globular and intrinsically disordered proteins. *Journal of molecular biology* **342:** 345-353.

Lowe, R., Pountney, D.L., Jensen, P.H., Gai, W.P., and Voelcker, N.H. 2004. Calcium(II) selectively indeces alpha-synuclein annular oligomers via interacyion with the C-terminal domain. *Protein Sci* **13:** 3245-3252.

Mandel, A.M., Akke, M., and Palmer, A.G., 3rd. 1995. Backbone dynamics of Escherichia coli ribonuclease HI: correlations with structure and function in an active enzyme. *Journal of molecular biology* **246:** 144-163.

Margittai, M., and Langen, R. 2008. Fibrils with parallel in-register structure constitute a major class of amyloid fibrils: molecular insights from electron paramagnetic resonance spectroscopy. *Quarterly reviews of biophysics* **41:** 265-297.

Marsh, J.A., Singh, V.K., Jia, Z., and Forman-Kay, J.D. 2006. Sensitivity of secondary structure propensities to sequence differences between alpha- and gamma-synuclein: implications for fibrillation. *Protein Sci* **15:** 2795-2804.

McClendon, S., Rospigliosi, C.C., and Eliezer, D. 2009. Charge neutralization and collapse of the C-terminal tail of alpha-synuclein at low pH. *Protein Sci* **18:** 1531-1540.

McNulty, B.C., Tripathy, A., Young, G.B., Charlton, L.M., Orans, J., and Pielak, G.J. 2006. Temperature-induced reversible conformational change in the first 100 residues of alpha-synuclein. *Protein Sci* **15:** 602-608.

Meier, S., Blackledge, M., and Grzesiek, S. 2008. Conformational distributions of unfolded polypeptides from novel NMR techniques. *The Journal of chemical physics* **128:** 052204.

Mills, J.L., and Szyperski, T. 2002. Protein dynamics in supercooled water: the search for slow motional modes. *Journal of biomolecular NMR* **23:** 63-67.

Mittag, T., and Forman-Kay, J.D. 2007. Atomic-level characterization of disordered protein ensembles. *Curr Opin Struct Biol* **17:** 3-14.

Mohana-Borges, R., Goto, N.K., Kroon, G.J., Dyson, H.J., and Wright, P.E. 2004. Structural characterization of unfolded states of apomyoglobin using residual dipolar couplings. *Journal of molecular biology* **340:** 1131-1142.

Munishkina, L.A., Cooper, E.M., Uversky, V.N., and Fink, A.L. 2004a. The effect of macromolecular crowding on protein aggregation and amyloid fibril formation. *J Mol Recognit* **17:** 456-464.

Munishkina, L.A., Henriques, J., Uversky, V.N., and Fink, A.L. 2004b. Role of protein-water interactions and electrostatics in alpha-synuclein fibril formation. *Biochemistry* **43:** 3289-3300.

Narhi, L., Wood, S.J., Steavenson, S., Jiang, Y., Wu, G.M., Anafi, D., Kaufman, S.A., Martin, F., Sitney, K., Denis, P., et al. 1999. Both familial Parkinson's disease mutations accelerate alpha-synuclein aggregation. *J Biol Chem* **274:** 9843-9846.

Neudecker, P., Lundstrom, P., and Kay, L.E. 2009. Relaxation dispersion NMR spectroscopy as a tool for detailed studies of protein folding. *Biophys J* **96:** 2045-2054.

Onuchic, J.N., and Wolynes, P.G. 2004. Theory of protein folding. *Current Opinion in Structural Biology* **14:** 70-75.

Ottiger, M., Delaglio, F., and Bax, A. 1998. Measurement of J and dipolar couplings from simplified two-dimensional NMR spectra. *J Magn Reson* **131:** 373-378.

Palmer, A.G., 3rd. 2004. NMR characterization of the dynamics of biomacromolecules. *Chemical reviews* **104:** 3623-3640.

Panchal, S.C., Bhavesh, N.S., and Hosur, R.V. 2001. Improved 3D triple resonance experiments, HNN and HN(C)N, for HN and 15N sequential correlations in (13C, 15N) labeled proteins: application to unfolded proteins. *Journal of biomolecular NMR* **20:** 135-147.

Pawar, A.P., Dubay, K.F., Zurdo, J., Chiti, F., Vendruscolo, M., and Dobson, C.M. 2005. Prediction of "aggregation-prone" and "aggregation-susceptible" regions in proteins associated with neurodegenerative diseases. *Journal of molecular biology* **350:** 379-392.

Pearl, L.H., and Prodromou, C. 2006. Structure and Mechanism of the Hsp90 Molecular Chaperone Machinery. *Annual review of biochemistry* **75:** 271-294.

Pelupessy, P., Ferrage, F., and Bodenhausen, G. 2007. Accurate measurement of longitudinal cross-relaxation rates in nuclear magnetic resonance. *The Journal of chemical physics* **126:** 134508.

Perutz, M.F. 1999. Glutamine repeats and neurodegenerative diseases: molecular aspects. *Trends in biochemical sciences* **24:** 58-63.

Polymeropoulos, M.H., Lavedan, C., Leroy, E., Ide, S.E., Dehejia, A., Dutra, A., Pike, B., Root, H., Rubenstein, J., Boyer, R., et al. 1997. Mutation in the alpha-synuclein gene identified in families with Parkinson's disease. *Science* **276:** 2045-2047.

Prestegard, J.H., al-Hashimi, H.M., and Tolman, J.R. 2000. NMR structures of biomolecules using field oriented media and residual dipolar couplings. *Quarterly reviews of biophysics* **33:** 371-424.

Radford, S.E., Gosal, W.S., and Platt, G.W. 2005. Towards an understanding of the structural molecular mechanism of beta(2)-microglobulin amyloid formation in vitro. *Biochim Biophys Acta* **1753:** 51-63.

Rasia, R.M., Bertoncini, C.W., Marsh, D., Hoyer, W., Cherny, D., Zweckstetter, M., Griesinger, C., Jovin, T.M., and Fernandez, C.O. 2005. Structural characterization of copper(II) binding to alpha-synuclein: Insights into the bioinorganic chemistry of Parkinson's disease. *Proc Natl Acad Sci U S A* **102:** 4294-4299.

Rivers, R.C., Kumita, J.R., Tartaglia, G.G., Dedmon, M.M., Pawar, A., Vendruscolo, M., Dobson, C.M., and Christodoulou, J. 2008. Molecular determinants of the aggregation behavior of alpha- and beta-synuclein. *Protein Sci* **17:** 887-898.

Rochet, J.C., Conway, K.A., and Lansbury, P.T., Jr. 2000. Inhibition of fibrillization and accumulation of prefibrillar oligomers in mixtures of human and mouse alpha-synuclein. *Biochemistry* **39:** 10619-10626.

Rochet, J.C., and Lansbury, P.T., Jr. 2000. Amyloid fibrillogenesis: themes and variations. *Curr Opin Struct Biol* **10:** 60-68.

Rochet, J.C., Outeiro, T.F., Conway, K.A., Ding, T.T., Volles, M.J., Lashuel, H.A., Bieganski, R.M., Lindquist, S.L., and Lansbury, P.T. 2004. Interactions among alpha-synuclein, dopamine, and biomembranes: some clues for understanding neurodegeneration in Parkinson's disease. *J Mol Neurosci* **23:** 23-34.

Rospigliosi, C.C., McClendon, S., Schmid, A.W., Ramlall, T.F., BarrÈ, P., Lashuel, H.A., and Eliezer, D. 2009. E46K Parkinson's-Linked Mutation Enhances C-Terminal-to-N-Terminal Contacts in alpha-Synuclein. *Journal of molecular biology* **388:** 1022-1032.

Rousseau, F., Schymkowitz, J., and Serrano, L. 2006. Protein aggregation and amyloidosis: confusion of the kinds? *Curr Opin Struct Biol* **16:** 118-126.

Ruckert, M., and Otting, G. 2000. Alignment of Biological Macromolecules in Novel Nonionic Liquid Crystalline Media for NMR Experiments. *J Am Chem Soc* **122:** 7793-7797.

Rumpel, S., Becker, S., and Zweckstetter, M. 2008. High-resolution structure determination of the CylR2 homodimer using paramagnetic relaxation enhancement and structure-based prediction of molecular alignment. *Journal of biomolecular NMR* **40:** 1-13.

Schulman, B.A., Kim, P.S., Dobson, C.M., and Redfield, C. 1997. A residue-specific NMR view of the non-cooperative unfolding of a molten globule. *Nature structural biology* **4:** 630-634.

Schwalbe, H., Fiebig, K.M., Buck, M., Jones, J.A., Grimshaw, S.B., Spencer, A., Glaser, S.J., Smith, L.J., and Dobson, C.M. 1997. Structural and dynamical properties of a denatured protein. Heteronuclear 3D NMR experiments and theoretical simulations of lysozyme in 8 M urea. *Biochemistry* **36:** 8977-8991.

Schwarzinger, S., Kroon, G.J., Foss, T.R., Chung, J., Wright, P.E., and Dyson, H.J. 2001. Sequence-dependent correction of random coil NMR chemical shifts. *J Am Chem Soc* **123:** 2970-2978.

Schwarzinger, S., Kroon, G.J., Foss, T.R., Wright, P.E., and Dyson, H.J. 2000. Random coil chemical shifts in acidic 8 M urea: implementation of random coil shift data in NMRView. *Journal of biomolecular NMR* **18:** 43-48.

Schwieters, C.D., Kuszewski, J.J., Tjandra, N., and Clore, G.M. 2003. The Xplor-NIH NMR molecular structure determination package. *J Magn Reson* **160:** 65-73.

Serber, Z., Corsini, L., Durst, F., and Dotsch, V. 2005. In-cell NMR spectroscopy. *Methods Enzymol* **394:** 17-41.

Serpell, L.C., Berriman, J., Jakes, R., Goedert, M., and Crowther, R.A. 2000. Fiber diffraction of synthetic alpha-synuclein filaments shows amyloid-like cross-beta conformation. *Proc Natl Acad Sci U S A* **97:** 4897-4902.

Shtilerman, M.D., Ding, T.T., and Lansbury, P.T., Jr. 2002. Molecular crowding accelerates fibrillization of alpha-synuclein: could an increase in the cytoplasmic protein concentration induce Parkinson's disease? *Biochemistry* **41:** 3855-3860.

Siderowf, A., and Stern, M. 2003. Update on Parkinson Disease. *Ann Intern Med* **138:** 651-658.

Singh, V.K., Zhou, Y., Marsh, J.A., Uversky, V.N., Forman-Kay, J.D., Liu, J., and Jia, Z. 2007. Synuclein-gamma targeting peptide inhibitor that enhances sensitivity of breast cancer cells to antimicrotubule drugs. *Cancer research* **67:** 626-633.

Skalicky, J.J., Mills, J.L., Sharma, S., and Szyperski, T. 2001. Aromatic ring-flipping in supercooled water: implications for NMR-based structural biology of proteins. *J Am Chem Soc* **123:** 388-397.

Skalicky, J.J., Sukumaran, D.K., Mills, J.L., and Szyperski, T. 2000. Toward Structural Biology in Supercooled Water. *J Am Chem Soc* **122:** 3230-3231.

Skrynnikov, N.R., and Ernst, R.R. 1999. Detection of intermolecular chemical exchange through decorrelation of two-spin order. *J Magn Reson* **137:** 276-280.

Smith, D.P., Jones, S., Serpell, L.C., Sunde, M., and Radford, S.E. 2003. A systematic investigation into the effect of protein destabilisation on beta 2-microglobulin amyloid formation. *Journal of molecular biology* **330:** 943-954.

Spillantini, M.G., Crowther, R.A., Jakes, R., Cairns, N.J., Lantos, P.L., and Goedert, M. 1998a. Filamentous alpha-synuclein inclusions link multiple system atrophy with Parkinson's disease and dementia with Lewy bodies. *Neuroscience letters* **251:** 205-208.

Spillantini, M.G., Crowther, R.A., Jakes, R., Hasegawa, M., and Goedert, M. 1998b. alpha-Synuclein in filamentous inclusions of Lewy bodies from Parkinson's disease and dementia with lewy bodies. *Proc Natl Acad Sci U S A* **95:** 6469-6473.

Spillantini, M.G., Schmidt, M.L., Lee, V.M., Trojanowski, J.Q., Jakes, R., and Goedert, M. 1997. Alpha-synuclein in Lewy bodies. *Nature* **388:** 839-840.

Sung, Y.H., and Eliezer, D. 2007. Residual Structure, Backbone Dynamics, and Interactions within the Synuclein Family. *Journal of molecular biology* **372:** 689-707.

Tang, C., Ghirlando, R., and Clore, G.M. 2008a. Visualization of transient ultra-weak protein self-association in solution using paramagnetic relaxation enhancement. *J Am Chem Soc* **130:** 4048-4056.

Tang, C., Iwahara, J., and Clore, G.M. 2006. Visualization of transient encounter complexes in protein-protein association. *Nature* **444:** 383-386.

Tang, C., Louis, J.M., Aniana, A., Suh, J.Y., and Clore, G.M. 2008b. Visualizing transient events in amino-terminal autoprocessing of HIV-1 protease. *Nature* **455:** 693-696.

Tjandra, N., Szabo, A., and Bax, A. 1996. Protein Backbone Dynamics and 15N Chemical Shift Anisotropy from Quantitative Measurement of Relaxation Interference Effects. *J Am Chem Soc* **118:** 6986-6991.

Tugarinov, V., and Kay, L.E. 2003. Quantitative NMR studies of high molecular weight proteins: application to domain orientation and ligand binding in the 723 residue enzyme malate synthase G. *Journal of molecular biology* **327:** 1121-1133.

Tycko, R. 2006. Molecular structure of amyloid fibrils: insights from solid-state NMR. *Quarterly reviews of biophysics* **39:** 1-55.

Ulmer, T.S., Bax, A., Cole, N.B., and Nussbaum, R.L. 2005. Structure and dynamics of micelle-bound human alpha-synuclein. *J Biol Chem* **280:** 9595-9603.

Uversky, V.N. 2003. A Protein-Chameleon: Conformational Plasticity of alpha-Synclein, a Disordered Protein Involved in Neurodegenerative Disorders. *Journal of Biomolecular Structure & Dynamics* **21:** 211-234.

Uversky, V.N. 2007. Neuropathology, biochemistry, and biophysics of alpha-synuclein aggregation. *Journal of neurochemistry* **103:** 17-37.

Uversky, V.N., Gillespie, J.R., and Fink, A.L. 2000. Why are "natively unfolded" proteins unstructured under physiologic conditions? *Proteins* **41:** 415-427.

Uversky, V.N., Li, J., and Fink, A.L. 2001a. Evidence for a partially folded intermediate in alpha-synuclein fibril formation. *J Biol Chem* **276:** 10737-10744.

Uversky, V.N., Li, J., and Fink, A.L. 2001b. Metal-triggered structural transformations, aggregation, and fibrillation of human alpha-synuclein. A possible molecular NK between Parkinson's disease and heavy metal exposure. *J Biol Chem* **276:** 44284-44296.

Uversky, V.N., Li, J., Souillac, P., Millett, I.S., Doniach, S., Jakes, R., Goedert, M., and Fink, A.L. 2002. Biophysical properties of the synucleins and their propensities to fibrillate: inhibition of alpha-synuclein assembly by beta- and gamma-synucleins. *J Biol Chem* **277:** 11970-11978.

Vallurupalli, P., Hansen, D.F., Lundstrom, P., and Kay, L.E. 2009. CPMG relaxation dispersion NMR experiments measuring glycine 1H alpha and 13C alpha chemical shifts in the 'invisible' excited states of proteins. *Journal of biomolecular NMR* **45:** 45-55.

Vilar, M., Chou, H.T., Luhrs, T., Maji, S.K., Riek-Loher, D., Verel, R., Manning, G., Stahlberg, H., and Riek, R. 2008. The fold of alpha-synuclein fibrils. *Proc Natl Acad Sci U S A* **105:** 8637-8642.

Volkov, A.N., Worrall, J.A., Holtzmann, E., and Ubbink, M. 2006. Solution structure and dynamics of the complex between cytochrome c and cytochrome c peroxidase determined by paramagnetic NMR. *Proc Natl Acad Sci U S A* **103:** 18945-18950.

Volles, M.J., and Lansbury, P.T., Jr. 2002. Vesicle permeabilization by protofibrillar alpha-synuclein is sensitive to Parkinson's disease-linked mutations and occurs by a pore-like mechanism. *Biochemistry* **41:** 4595-4602.

Volles, M.J., and Lansbury, P.T., Jr. 2003. Zeroing in on the pathogenic form of alpha-synuclein and its mechanism of neurotoxicity in Parkinson's disease. *Biochemistry* **42:** 7871-7878.

Vuister, G.W., and Bax, A. 1994. Measurement of four-bond HN-H alpha J-couplings in staphylococcal nuclease. *Journal of biomolecular NMR* **4:** 193-200.

Wang, C., Grey, M.J., and Palmer, A.G., 3rd. 2001. CPMG sequences with enhanced sensitivity to chemical exchange. *Journal of biomolecular NMR* **21:** 361-366.

Wang, C., and Palmer, A.G., 3rd. 2003. Solution NMR methods for quantitative identification of chemical exchange in 15N-labeled proteins. *Magnetic Resonance in Chemistry* **41:** 866-876.

Wang, C., Rance, M., and Palmer, A.G., 3rd. 2003. Mapping chemical exchange in proteins with MW > 50 kD. *J Am Chem Soc* **125:** 8968-8969.

Weinreb, P.H., Zhen, W., Poon, A.W., Conway, K.A., and Lansbury, P.T., Jr. 1996. NACP, a protein implicated in Alzheimer's disease and learning, is natively unfolded. *Biochemistry* **35:** 13709-13715.

Wilkins, D.K., Grimshaw, S.B., Receveur, V., Dobson, C.M., Jones, J.A., and Smith, L.J. 1999. Hydrodynamic radii of native and denatured proteins measured by pulse field gradient NMR techniques. *Biochemistry* **38:** 16424-16431.

Wirmer, J., Berk, H., Ugolini, R., Redfield, C., and Schwalbe, H. 2006. Characterization of the unfolded state of bovine alpha-lactalbumin and comparison with unfolded states of homologous proteins. *Protein Sci* **15:** 1397-1407.

Wishart, D.S., Bigam, C.G., Holm, A., Hodges, R.S., and Sykes, B.D. 1995. 1H, 13C and 15N random coil NMR chemical shifts of the common amino acids. I. Investigations of nearest-neighbor effects. *Journal of biomolecular NMR* **5:** 67-81.

Wishart, D.S., Case, D.A., and Thomas L. James, V.D.U.S. 2002. Use of chemical shifts in macromolecular structure determination. In *Methods Enzymol*, pp. 3-34. Academic Press.

Wishart, D.S., and Sykes, B.D. 1994. The 13C chemical-shift index: a simple method for the identification of protein secondary structure using 13C chemical-shift data. *Journal of biomolecular NMR* **4:** 171-180.

Wood, S.J., Wypych, J., Steavenson, S., Louis, J.C., Citron, M., and Biere, A.L. 1999. alpha-synuclein fibrillogenesis is nucleation-dependent. Implications for the pathogenesis of Parkinson's disease. *J Biol Chem* **274:** 19509-19512.

Wright, P.E., and Dyson, H.J. 2009. Linking folding and binding. *Curr Opin Struct Biol* **19:** 31-38.

Wu, D.H., Chen, A.D., and Johnson, C.S. 1995. An Improved Diffusion-Ordered Spectroscopy Experiment Incorporating Bipolar-Gradient Pulses. *J Magn Reson A* **115:** 260-264.

Wu, K.-P., Weinstock, D.S., Narayanan, C., Levy, R.M., and Baum, J. 2009. Structural Reorganization of alpha-Synuclein at Low pH Observed by NMR and REMD Simulations. *Journal of molecular biology* **391:** 784-796.

Wu, K.P., Kim, S., Fela, D.A., and Baum, J. 2008. Characterization of conformational and dynamic properties of natively unfolded human and mouse alpha-synuclein ensembles by NMR: implication for aggregation. *Journal of molecular biology* **378:** 1104-1115.

Yamin, G., Glaser, C.B., Uversky, V.N., and Fink, A.L. 2003. Certain metals trigger fibrillation of methionine-oxidized alpha-synuclein. *J Biol Chem* **278:** 27630-27635.

Yamin, G., Munishkina, L.A., Karymov, M.A., Lyubchenko, Y.L., Uversky, V.N., and Fink, A.L. 2005. Forcing nonamyloidogenic beta-synuclein to fibrillate. *Biochemistry* **44:** 9096-9107.

Yao, J., Dyson, H.J., and Wright, P.E. 1997. Chemical shift dispersion and secondary structure prediction in unfolded and partly folded proteins. *FEBS Lett* **419:** 285-289.

Yavich, L., Tanila, H., Vepsalainen, S., and Jakala, P. 2004. Role of alpha-synuclein in presynaptic dopamine recruitment. *J Neurosci* **24:** 11165-11170.

Zarranz, J.J., Alegre, J., Gomez-Esteban, J.C., Lezcano, E., Ros, R., Ampuero, I., Vidal, L., Hoenicka, J., Rodriguez, O., Atares, B., et al. 2004. The new mutation, E46K, of alpha-synuclein causes Parkinson and Lewy body dementia. *Annals of neurology* **55:** 164-173.

Zhang, Y.Z., Paterson, Y., and Roder, H. 1995. Rapid amide proton exchange rates in peptides and proteins measured by solvent quenching and two-dimensional NMR. *Protein Sci* **4:** 804-814.

Zhou, H.-X., Rivas, G.n., and Minton, A.P. 2008. Macromolecular Crowding and Confinement: Biochemical, Biophysical, and Potential Physiological Consequences*. *Annu Rev Biocphys* **37:** 375-397.

Zibaee, S., Jakes, R., Fraser, G., Serpell, L.C., Crowther, R.A., and Goedert, M. 2007. Sequence Determinants for Amyloid Fibrillogenesis of Human alpha-Synuclein. *Journal of molecular biology* **374:** 454-464.

Appendix

A.1 Backbone assignment of human α-synuclein at 15 °C and pH 7.4

Res		#	HN	HA	^{15}N	CA	CB	CO
Met	M	1						
Asp	D	2				54.25	41.52	175.77
Val	V	3	8.27	4.01	120.52	62.55	32.68	175.29
Phe	F	4				57.99	39.01	175.77
Met	M	5	8.23	4.24	122.43	55.37	32.78	175.82
Lys	K	6	8.28	4.20	122.47	56.96	32.82	176.99
Gly	G	7	8.43	3.92	110.03	45.33		174.18
Leu	L	8	8.07	4.35	121.59	55.16	42.52	177.63
Ser	S	9	8.33		116.75	58.40	63.71	174.74
Lys	K	10	8.49	4.28	123.49	56.46	33.06	176.58
Ala	A	11	8.31	4.28	125.35	52.71	19.25	177.91
Lys	K	12	8.35	4.25	120.90	56.32	32.99	176.68
Glu	E	13	8.47		121.93	56.68	30.27	176.91
Gly	G	14				45.28		173.99
Val	V	15	7.99	4.09	120.16	62.56	32.72	176.49
Val	V	16	8.30	4.05	125.28	62.35	32.79	175.99
Ala	A	17	8.45	4.22	128.49	52.52	19.18	177.67
Ala	A	18	8.32	4.10	123.73	52.67	19.18	177.80
Ala	A	19	8.29	4.28	123.10	52.74	19.16	178.18
Glu	E	20	8.34	4.22	120.11	56.80	30.18	177.14
Lys	K	21	8.34	4.31	122.30	56.78	32.85	177.19
Thr	T	22	8.14	4.25	115.29	62.24	69.76	174.65
Lys	K	23	8.37	4.29	123.64	56.72	32.97	176.64
Gln	Q	24	8.43	4.24	121.77	55.60	29.60	176.73
Gly	G	25	8.49	3.93	110.57	45.28		173.92
Val	V	26	7.98	4.07	120.15	62.62	32.82	176.35
Ala	A	27	8.44	4.29	127.43	52.79	19.08	177.64
Glu	E	28	8.40	4.21	120.36	56.83	29.81	176.33
Ala	A	29	8.31	4.25	124.95	52.67	19.15	177.69
Ala	A	30	8.28	4.26	122.47	52.80	19.11	178.46
Gly	G	31	8.32	3.92	107.81	45.35		174.21
Lys	K	32	8.12	4.37	120.73	56.25	33.20	176.99
Thr	T	33	8.24	4.29	115.62	62.00	68.88	174.67
Lys	K	34	8.36	4.28	123.81	56.40	33.00	176.68
Glu	E	35	8.46		121.99	56.68	30.27	176.91
Gly	G	36				45.29		173.96
Val	V	37	7.91	4.05	119.57	62.28	32.78	175.91
Leu	L	38	8.29	4.28	125.83	54.97	42.49	176.65

Res		#	HN	HA	^{15}N	CA	CB	CO
Tyr	Y	39	8.28	4.57	122.70	57.86	38.86	175.57
Val	V	40	8.09	3.98	123.34	62.16	32.87	176.15
Gly	G	41	8.06	3.91	112.18	45.18		173.96
Ser	S	42	8.25	4.40	115.63	58.37	63.81	174.75
Lys	K	43	8.49	4.29	123.45	56.46	32.99	176.87
Thr	T	44	8.18	4.28	115.49	61.91	69.83	174.69
Lys	K	45	8.48	4.28	123.87	56.40	33.10	176.51
Glu	E	46	8.45		122.17	56.68	30.27	176.91
Gly	G	47				45.28		173.92
Val	V	48	7.93	4.06	119.85	62.27	32.79	176.06
Val	V	49	8.29	4.04	125.21	62.53	32.93	176.05
His	H	50	8.54		124.90	56.84	30.21	176.99
Gly	G	51	8.44	3.90	110.23	45.20		174.25
Val	V	52	8.02	4.07	119.78	62.00	32.98	175.93
Ala	A	53	8.51	4.37	128.26	52.43	19.32	177.81
Thr	T	54	8.24	4.29	114.91	61.82	69.93	174.62
Val	V	55	8.25	4.08	123.08	62.38	32.90	175.93
Ala	A	56	8.43	4.27	128.12	52.53	19.22	177.76
Glu	E	57	8.38	4.19	120.92	56.68	30.41	176.70
Lys	K	58	8.44	4.29	122.85	56.53	33.09	176.98
Thr	T	59	8.22	4.24	115.98	62.04	69.08	174.67
Lys	K	60	8.39	4.28	123.72	56.68	32.92	176.65
Glu	E	61	8.44	4.24	122.19	55.26	29.51	176.81
Gln	Q	62				55.80	29.54	175.94
Val	V	63	8.30	4.16	121.97	62.43	32.78	176.31
Thr	T	64	8.31	4.32	118.11	62.22	69.82	174.05
Asn	N	65	8.53	4.75	121.84	53.10	38.91	175.24
Val	V	66	8.25	4.07	120.75	62.61	32.60	176.86
Gly	G	67	8.56	3.93	112.65	45.34		174.66
Gly	G	68	8.24	3.92	108.85	45.10		173.73
Ala	A	69	8.17	4.25	123.79	52.28	19.36	177.65
Val	V	70	8.23	4.08	120.53	62.38	32.72	176.33
Val	V	71	8.40	4.17	125.43	62.24	32.82	176.36
Thr	T	72	8.32	4.32	118.66	61.90	69.80	174.90
Gly	G	73	8.45	3.97	111.37	45.29		173.93
Val	V	74	8.09	4.13	119.56	62.20	32.92	176.51
Thr	T	75	8.31	4.32	118.95	61.93	69.75	174.07
Ala	A	76	8.38	4.32	127.43	52.46	19.31	177.56
Val	V	77	8.15	4.05	120.10	62.23	32.85	175.93
Ala	A	78	8.42	4.27	128.17	52.53	19.22	178.12
Gln	Q	79	8.41	4.20	120.59	55.68	29.50	175.95
Lys	K	80	8.44	4.32	123.29	56.32	33.15	176.67
Thr	T	81	8.30	4.34	116.94	61.91	69.83	174.44
Val	V	82	8.31	4.09	123.07	62.27	32.86	176.15
Glu	E	83	8.58	4.25	125.35	56.79	30.25	177.01

Res		#	HN	HA	^{15}N	CA	CB	CO
Gly	G	84	8.52	3.92	110.74	45.28		174.14
Ala	A	85	8.27	4.27	123.97	52.88	19.22	178.49
Gly	G	86	8.50	3.94	108.21	45.29		174.30
Ser	S	87	8.16	4.45	115.72	58.35	63.83	174.72
Ile	I	88	8.20	4.16	122.80	61.30	38.66	176.27
Ala	A	89	8.36	4.23	128.08	52.59	19.08	177.55
Ala	A	90	8.22	4.20	123.37	52.49	19.20	177.77
Ala	A	91	8.30	4.28	123.45	52.64	19.16	178.12
Thr	T	92	8.10	4.28	112.65	61.98	69.80	175.15
Gly	G	93	8.32	3.89	110.73	45.19		173.65
Phe	F	94	8.10	4.57	120.35	57.82	39.72	175.47
Val	V	95	8.06	4.01	123.78	62.00	33.11	175.40
Lys	K	96	8.40	4.20	126.45	56.34	33.11	176.49
Lys	K	97	8.48	4.27	123.86	56.69	33.24	176.40
Asp	D	98	8.41	4.52	121.23	54.44	41.10	176.20
Gln	Q	99	8.35	4.26	120.24	55.89	29.48	176.02
Leu	L	100	8.30	4.29	122.88	55.40	42.22	177.99
Gly	G	101	8.49	3.92	109.83	45.29		174.09
Lys	K	102	8.22	4.29	120.78	56.23	33.00	176.46
Asn	N	103	8.63	4.66	120.02	53.32	38.80	175.29
Glu	E	104	8.48	4.23	121.44	56.73	30.19	176.78
Glu	E	105						
Gly	G	106				45.01		173.43
Ala	A	107	8.14	4.55	124.97	50.48	18.19	177.23
Pro	P	108				63.06	32.06	177.08
Gln	Q	109	8.60	4.27	121.21	55.68	29.64	175.98
Glu	E	110	8.53	4.26	122.55	56.64	30.50	176.58
Gly	G	111	8.49	3.92	110.30	45.29		173.80
Ile	I	112	8.01	4.09	120.16	60.92	38.65	176.30
Leu	L	113	8.42	4.36	127.03	55.03	42.37	177.23
Glu	E	114				56.66	30.28	175.86
Asp	D	115	8.37	4.53	121.43	54.21	41.10	175.75
Met	M	116	8.26	4.76	122.04	53.18	32.46	
Pro	P	117				62.86	32.17	176.70
Val	V	118	8.31	4.04	120.88	61.91	33.06	175.76
Asp	D	119	8.53	4.86	125.98	52.06	41.08	174.77
Pro	P	120				63.46	32.16	176.91
Asp	D	121	8.39	4.58	119.28	54.52	40.88	176.14
Asn	N	122	8.12	4.66	119.15	53.45	39.33	175.39
Glu	E	123	8.39	4.20	121.77	56.73	30.09	176.06
Ala	A	124	8.24	4.26	124.77	52.30	19.19	177.21
Tyr	Y	125	8.03	4.50	119.97	57.73	38.96	175.34
Glu	E	126	8.13	4.24	123.80	55.59	30.65	175.42
Met	M	127	8.42	4.32	123.88	53.28	32.63	174.59
Pro	P	128				63.04	32.21	176.88

Res		#	HN	HA	^{15}N	CA	CB	CO
Ser	S	129	8.49	4.38	116.77	58.22	63.83	174.80
Glu	E	130	8.58	4.28	123.19	56.45	30.27	176.51
Glu	E	131				56.85	30.22	176.99
Gly	G	132	8.42	3.88	109.98	45.23		173.85
Tyr	Y	133	8.07	4.51	120.33	57.92	38.88	174.86
Gln	Q	134				55.33	29.84	
Asp	D	135	8.25	4.50	121.66	54.22	41.10	175.48
Tyr	Y	136	8.05	4.51	120.60	57.65	38.96	175.07
Glu	E	137	8.25	4.50	125.40	53.54	30.16	173.63
Pro	P	138				61.77	32.21	176.80
Glu	E	139	8.53	4.20	121.60	56.54	30.21	175.38
Ala	A	140	8.01	4.08	130.93	53.80	20.20	174.63

A.2 Backbone assignment of mouse α-synuclein at 15 °C and pH 7.4

Res		#	HN	HA	^{15}N	CA	CB	CO
Met	M	1						
Asp	D	2				54.26	41.56	
Val	V	3	8.27	4.01	120.47	62.64	32.97	
Phe	F	4				58.05	39.05	
Met	M	5	8.23	4.37	122.40	55.39	32.76	
Lys	K	6	8.28	4.14	122.49	56.74	33.28	
Gly	G	7				45.34		174.20
Leu	L	8	8.07	4.36	121.60	55.17	42.52	177.66
Ser	S	9	8.33	4.36	116.73	58.40	63.70	174.56
Lys	K	10	8.37	4.28	123.63	56.40	32.92	176.66
Ala	A	11	8.30	4.28	125.28	52.60	19.22	
Lys	K	12	8.35	4.22	120.90	56.24	32.97	
Glu	E	13				56.71	30.31	
Gly	G	14				45.36		173.89
Val	V	15	7.99	4.12	120.13	62.57	32.75	176.28
Val	V	16	8.31	4.05	125.29	62.35	32.78	175.98
Ala	A	17	8.46	4.22	128.50	52.52	19.21	177.68
Ala	A	18	8.33	4.09	123.74	52.70	19.10	177.86
Ala	A	19	8.29	4.08	123.17	52.74	19.17	178.65
Glu	E	20	8.34	4.24	120.08	56.70	30.27	176.92
Lys	K	21	8.47	4.28	122.30	56.78	32.92	177.13
Thr	T	22	8.15	4.24	115.30	62.26	69.76	174.73
Lys	K	23						
Gln	Q	24				55.87	29.72	
Gly	G	25	8.49	3.92	110.25	45.30		173.91
Val	V	26	7.99	4.12	120.13	62.61	32.67	176.34
Ala	A	27	8.44	4.29	127.44	52.84	19.03	177.18
Glu	E	28	8.39	4.20	120.92	56.67	30.51	177.67
Ala	A	29	8.31	4.24	125.01	52.70	19.17	177.79
Ala	A	30	8.24	4.24	122.76	52.79	19.11	178.46
Gly	G	31	8.33	3.93	107.81	45.36		174.26
Lys	K	32	8.13	4.40	120.74	56.25	33.21	177.07
Thr	T	33	8.23	4.28	115.99	62.05	69.81	174.70
Lys	K	34	8.49	4.27	123.80	56.34	32.90	
Glu	E	35				56.83	30.27	
Gly	G	36	8.45	3.93	110.03	45.33		174.02
Val	V	37	7.92	4.05	119.59	62.30	32.79	176.04
Leu	L	38	8.29	4.28	125.84	54.97	42.50	176.65
Tyr	Y	39	8.28	4.56	122.60	57.87	38.86	175.65
Val	V	40	8.09	4.01	123.35	62.14	32.90	176.13
Gly	G	41	8.06	3.93	112.19	45.19		173.98
Ser	S	42	8.26	4.42	115.63	58.37	63.85	174.74

Res		#	HN	HA	^{15}N	CA	CB	CO
Lys	K	43	8.50	4.36	123.48	56.46	33.08	177.01
Thr	T	44	8.24	4.29	115.64	61.94	69.92	174.76
Lys	K	45	8.48	4.25	123.90	56.54	33.08	
Glu	E	46				56.58	30.19	
Gly	G	47				45.28		173.89
Val	V	48	7.93	4.05	119.91	62.29	32.80	176.20
Val	V	49	8.30	4.24	125.25	62.11	32.58	175.97
His	H	50	8.59	4.28	124.21	56.01	30.30	174.92
Gly	G	51	8.46	3.93	110.69	45.17		173.89
Val	V	52	8.14	4.20	119.63	62.23	32.94	176.55
Thr	T	53	8.42	4.44	118.97	61.90	69.75	174.57
Thr	T	54	8.29	4.32	117.92	61.72	69.88	174.38
Val	V	55	8.31	4.09	123.08	62.17	32.87	176.09
Ala	A	56	8.44	4.24	128.23	52.46	19.37	177.58
Glu	E	57	8.42	4.24	120.96	56.49	30.39	176.71
Lys	K	58	8.44	4.22	122.89	56.43	33.09	176.88
Thr	T	59	8.19	4.28	115.53	61.87	69.85	174.65
Lys	K	60	8.40	4.28	123.70	55.76	32.69	178.09
Glu	E	61	8.41	4.48	120.60	56.84	29.72	176.69
Gln	Q	62	8.44	4.24	121.79	56.50	29.63	175.97
Val	V	63	8.30	4.16	121.99	62.41	32.80	176.25
Thr	T	64	8.32	4.32	118.13	61.81	69.85	174.03
Asn	N	65	8.53	4.75	121.63	53.10	38.91	175.27
Val	V	66	8.25	4.09	120.77	62.64	32.54	176.85
Gly	G	67	8.57	3.93	112.65	45.34		174.67
Gly	G	68	8.25	3.93	108.67	45.10		173.77
Ala	A	69	8.18	4.28	123.80	52.32	19.34	177.67
Val	V	70	8.23	4.09	120.54	62.42	32.73	176.31
Val	V	71	8.40	4.20	125.44	62.24	32.75	176.38
Thr	T	72	8.32	4.32	118.66	61.91	69.81	174.88
Gly	G	73	8.45	3.97	113.38	45.26		174.03
Val	V	74	8.09	4.16	119.54	62.32	32.89	176.52
Thr	T	75	8.31	4.32	118.98	61.86	69.74	174.07
Ala	A	76	8.38	4.28	127.43	52.47	19.29	177.57
Val	V	77	8.16	4.01	120.11	62.24	32.90	176.07
Ala	A	78	8.42	4.24	128.19	52.50	19.22	177.61
Gln	Q	79	8.40	4.24	120.37	55.35	29.64	175.89
Lys	K	80	8.45	4.28	123.29	56.38	33.14	176.65
Thr	T	81	8.30	4.32	116.93	61.97	69.85	174.41
Val	V	82	8.29	4.08	123.17	62.29	32.87	176.20
Glu	E	83	8.59	4.24	125.37	56.84	30.26	177.02
Gly	G	84	8.53	3.93	110.86	45.33		174.01
Ala	A	85	8.24	4.28	123.80	54.80	19.28	178.40
Gly	G	86	8.47	3.89	107.75	45.30		174.00
Asn	N	87	8.28	4.67	118.78	53.23	38.85	175.36

Res		#	HN	HA	^{15}N	CA	CB	CO
Ile	I	88	8.14	4.12	121.62	61.30	38.75	176.18
Ala	A	89	8.39	4.24	128.08	52.55	19.10	177.55
Ala	A	90	8.20	4.24	123.33	52.46	19.21	177.77
Ala	A	91	8.30	4.28	123.46	52.60	19.18	178.16
Thr	T	92	8.11	4.28	112.68	61.97	69.80	175.20
Gly	G	93	8.32	3.89	110.73	45.20		173.65
Phe	F	94	8.09	4.59	120.34	57.81	39.73	175.48
Val	V	95	8.07	4.01	123.78	62.02	33.10	175.49
Lys	K	96	8.40	4.20	126.39	56.34	33.13	176.54
Lys	K	97	8.48	4.25	123.87	56.34	33.97	
Asp	D	98	8.37	4.56	121.42	54.28	41.16	176.24
Gln	Q	99	8.35	4.29	120.17	55.91	29.43	176.95
Met	M	100	8.45	4.35	122.21	56.72	32.95	175.92
Gly	G	101				45.30		174.21
Lys	K	102	8.28	4.20	120.88	56.44	32.92	177.27
Gly	G	103	8.56	3.93	110.63	45.32		174.30
Glu	E	104	8.33	4.24	120.63	56.51	30.31	176.72
Glu	E	105	8.60	4.20	127.78	56.94	30.15	176.85
Gly	G	106	8.38	3.86	109.60	45.12		174.00
Tyr	Y	107	8.04	4.75	121.64	55.91	38.14	174.09
Pro	P	108				63.25	32.09	176.86
Gln	Q	109	8.56	4.28	121.29	55.83	29.68	176.07
Glu	E	110	8.54	4.28	122.25	56.72	30.36	176.91
Gly	G	111	8.49	3.90	110.24	45.36		174.26
Ile	I	112	8.00	4.05	120.19	60.90	38.68	176.36
Leu	L	113	8.41	4.36	127.20	55.04	42.35	178.14
Glu	E	114						
Asp	D	115	8.37	4.54	121.42	54.21	41.17	
Met	M	116	8.26	4.75	122.02	53.30	32.67	
Pro	P	117				62.87	32.24	176.73
Val	V	118	8.32	4.05	120.95	61.91	33.08	175.84
Asp	D	119	8.57	4.83	126.13	52.00	41.31	174.79
Pro	P	120				63.67	32.13	177.69
Gly	G	121	8.56	3.93	108.96	45.32		174.60
Ser	S	122	8.11	4.40	115.67	58.59	63.92	174.79
Glu	E	123	8.53	4.24	122.94	56.84	29.96	176.14
Ala	A	124	8.21	4.24	124.40	52.32	19.25	177.13
Tyr	Y	125	8.03	4.48	119.89	57.69	38.97	175.42
Glu	E	126	8.14	4.24	123.80	55.64	30.73	175.47
Met	M	127	8.43	4.67	123.84	53.28	32.44	176.52
Pro	P	128				63.04	32.25	176.90
Ser	S	129	8.50	4.40	116.80	58.23	63.83	174.83
Glu	E	130	8.59	4.28	123.22	56.51	30.34	176.54
Glu	E	131	8.62	4.20	122.50	56.68	30.27	176.84
Gly	G	132	8.43	3.85	110.02	45.27		173.44

Res		#	HN	HA	^{15}N	CA	CB	CO
Tyr	Y	133	8.05	4.52	120.54	57.37	39.20	175.12
Gln	Q	134				55.37	29.88	174.86
Asp	D	135	8.25	4.52	121.73	54.26	41.17	175.47
Tyr	Y	136	8.07	4.52	120.33	58.09	38.85	175.73
Glu	E	137	8.26	4.52	125.45	53.58	30.28	173.68
Pro	P	138				62.89	32.21	176.89
Glu	E	139	8.53	4.20	121.63	56.56	30.32	176.34
Ala	A	140	8.01	4.09	130.96	53.82	20.22	173.41

A.3 Backbone assignment of human α-synuclein at -10 °C and pH 7.4

Res		#	HN	^{15}N	CA	CB	HA
Met	M	1			54.13	32.63	
Asp	D	2			54.07	41.33	4.69
Val	V	3	8.44	121.2	62.52	32.56	
Phe	F	4			58.06	38.77	
Met	M	5	8.34	123.3	55.26	32.66	
Lys	K	6	8.42	123.4	56.85	32.66	
Gly	G	7	8.58	110.6	45.20		
Leu	L	8	8.21	121.8	54.94	42.34	4.50
Ser	S	9	8.47	117.3	58.38	63.56	4.36
Lys	K	10					
Ala	A	11	8.49	126.2	52.72	19.04	
Lys	K	12	8.50	121.5	56.37	32.78	
Glu	E	13					
Gly	G	14			45.07		
Val	V	15	8.16	120.8	62.92	32.57	
Val	V	16	8.47	126.2	62.16	32.65	4.23
Ala	A	17	8.61	129.1	52.47	19.01	4.23
Ala	A	18	8.47	124.3	52.52	19.04	
Ala	A	19	8.43	123.4	52.52	19.04	
Glu	E	20	8.50	120.6	56.81	29.37	4.29
Lys	K	21	8.47	122.9	56.42	32.88	
Thr	T	22	8.26	116.1	62.00	69.65	4.42
Lys	K	23	8.53	124.2			
Gln	Q	24	8.60	122.5	56.64	30.08	
Gly	G	25	8.64	110.8	45.07		3.92
Val	V	26	8.11	121.0	62.91	33.00	
Ala	A	27	8.50	127.5	52.96	18.85	
Glu	E	28	8.54	121.0	56.42	30.01	4.18
Ala	A	29	8.46	125.9	52.69	19.04	
Ala	A	30	8.35	123.5	52.78	19.00	
Gly	G	31	8.39	108.0	45.16		3.95
Lys	K	32	8.20	121.1	56.12	33.24	
Thr	T	33	8.41	115.9	62.17	69.67	4.26
Lys	K	34	8.52	124.5	57.05	32.81	
Glu	E	35					
Gly	G	36			45.08		
Val	V	37	8.07	120.2	62.26	32.71	4.05
Leu	L	38	8.45	126.6	54.84	42.25	4.32
Tyr	Y	39	8.46	122.9	57.89	39.06	
Val	V	40	8.19	124.8	61.85	33.00	4.02

Res		#	HN	^{15}N	CA	CB	HA
Gly	G	41	8.07	112.6	44.96		3.93
Ser	S	42	8.44	116.0	58.27	63.68	4.26
Lys	K	43			56.37	32.98	
Thr	T	44	8.34	116.5	62.00	69.65	4.30
Lys	K	45	8.64	124.4	56.37	32.98	
Glu	E	46					
Gly	G	47			45.08		
Val	V	48	8.07	120.6	62.26	32.71	4.04
Val	V	49	8.45	125.8	62.05	32.61	4.23
His	H	50	8.79	125.1	55.48	29.07	4.66
Gly	G	51	8.61	111.1	45.07		3.96
Val	V	52	8.23	120.2	61.79	32.87	4.15
Ala	A	53	8.66	129.1	52.37	19.13	4.36
Thr	T	54			61.84	69.85	
Val	V	55	8.40	123.9	62.17	32.65	4.26
Ala	A	56	8.60	128.8	52.47	19.01	4.32
Glu	E	57	8.54	121.5	56.37	29.50	
Lys	K	58	8.62	123.8	56.27	32.98	4.32
Thr	T	59	8.39	116.5	61.97	69.82	4.31
Lys	K	60	8.57	124.5	56.65	32.83	
Glu	E	61	8.59	122.9	56.64	30.05	
Gln	Q	62			55.26	29.37	
Val	V	63	8.45	122.6	62.37	32.70	
Thr	T	64	8.48	118.1	61.98	69.66	4.30
Asn	N	65	8.67	122.4	52.98	38.77	4.75
Val	V	66	8.42	121.5	62.52	32.70	
Gly	G	67	8.72	113.2	45.20		3.98
Gly	G	68	8.34	109.1	44.87		3.97
Ala	A	69	8.30	124.0	52.20	19.19	4.31
Val	V	70	8.37	121.3	62.08	32.83	
Val	V	71	8.61	126.8	62.11	32.73	4.17
Thr	T	72	8.48	119.2	61.80	69.71	4.57
Gly	G	73	8.59	111.9	45.05		3.92
Val	V	74	8.25	120.2	62.16	32.81	4.15
Thr	T	75	8.48	119.5	61.89	69.68	4.30
Ala	A	76	8.58	128.3	52.35	19.15	4.32
Val	V	77	8.35	121.1	62.16	32.65	
Ala	A	78	8.61	128.9	52.47	19.00	4.32
Gln	Q	79	8.60	121.0	55.53	29.58	4.22
Lys	K	80	8.62	124.2	56.33	32.03	
Thr	T	81	8.42	117.2	62.21	69.68	-4.26
Val	V	82	8.46	123.4	62.11	32.72	
Glu	E	83	8.74	126.2	56.68	30.08	4.22
Gly	G	84	8.69	111.3	45.09		3.95

Res		#	HN	^{15}N	CA	CB	HA
Ala	A	85	8.39	124.8	52.52	19.04	4.22
Gly	G	86	8.65	108.6	45.10		3.95
Ser	S	87	8.33	116.5	58.32	63.70	4.30
Ile	I	88	8.32	123.5	61.02	38.50	4.22
Ala	A	89	8.52	128.9	52.55	18.92	
Ala	A	90	8.40	124.2	52.31	18.91	4.26
Ala	A	91	8.46	124.1	52.47	19.05	
Thr	T	92	8.30	113.6	62.01	69.70	4.29
Gly	G	93	8.45	111.2	44.97		3.92
Phe	F	94	8.22	120.8	57.89	39.06	
Val	V	95	8.19	125.3	61.85	33.00	4.02
Lys	K	96	8.54	127.2	56.42	33.00	4.21
Lys	K	97	8.63	124.5	56.37	32.10	
Asp	D	98	8.59	121.7	54.35	40.98	
Gln	Q	99	8.50	120.8	55.61	29.34	4.29
Leu	L	100	8.46	123.4	55.59	42.12	
Gly	G	101	8.62	110.2	45.07		3.91
Lys	K	102	8.41	121.4	56.06	33.03	
Asn	N	103	8.77	120.3	53.24	38.66	4.68
Glu	E	104	8.60	122.3	56.64	30.05	
Glu	E	105					
Gly	G	106			44.80		
Ala	A	107	8.25	125.2	50.50	17.91	4.58
Pro	P	108			62.93	31.99	
Gln	Q	109	8.76	121.8	55.47	29.56	4.27
Glu	E	110	8.70	123.3	56.54	30.35	4.25
Gly	G	111	8.64	110.8	45.07		3.92
Ile	I	112	8.17	120.7	60.84	38.52	
Leu	L	113	8.58	127.9	54.88	42.18	
Glu	E	114					
Asp	D	115	8.52	122.0	53.04	40.81	
Met	M	116	8.44	122.6	54.32	32.77	4.76
Pro	P	117			61.82	32.77	
Val	V	118	8.51	121.8	62.11	32.72	
Asp	D	119	8.74	127.0	52.02	40.93	4.82
Pro	P	120					
Asp	D	121	8.51	119.9	54.62	40.70	4.29
Asn	N	122	8.18	119.6	53.25	39.28	4.68
Glu	E	123	8.52	122.4	56.69	29.97	
Ala	A	124	8.40	125.1	52.31	18.92	
Tyr	Y	125	8.20	120.8	57.89	39.13	
Glu	E	126	8.19	125.0	55.24	30.69	
Met	M	127	8.59	124.6	53.30	32.98	

Res		#	HN	^{15}N	CA	CB	HA
Pro	P	128			62.84	32.28	
Ser	S	129	8.67	117.4	58.21	63.72	4.36
Glu	E	130	8.73	123.7	56.32	30.11	4.27
Glu	E	131			56.69	30.08	
Gly	G	132	8.56	110.4	45.07		
Tyr	Y	133	8.19	121.0	57.94	38.74	
Gln	Q	134			55.25	29.78	
Asp	D	135	8.35	122.0	54.14	40.98	4.47
Tyr	Y	136	8.18	121.0	57.60	38.78	
Glu	E	137	8.38	126.0	53.41	30.11	4.49
Pro	P	138			62.70	32.20	
Glu	E	139	8.67	122.1	56.34	30.14	4.17
Ala	A	140	8.21	131.5	53.84	19.85	4.08

A.4 Backbone assignment of mouse α-synuclein at -10 °C and pH 7.4

Res		#	HN	^{15}N	HA	CA	CB	CO
Met	M	1						
Asp	D	2				54.26	41.56	
Val	V	3	8.27	120.47	4.01	62.64	32.97	
Phe	F	4				58.05	39.05	
Met	M	5	8.23	122.40	4.37	55.39	32.76	
Lys	K	6	8.28	122.49	4.14	56.74	33.28	
Gly	G	7				45.34		174.20
Leu	L	8	8.07	121.60	4.36	55.17	42.52	177.66
Ser	S	9	8.33	116.73	4.36	58.40	63.70	174.56
Lys	K	10	8.37	123.63	4.28	56.40	32.92	176.66
Ala	A	11	8.30	125.28	4.28	52.60	19.22	
Lys	K	12	8.35	120.90	4.22	56.24	32.97	
Glu	E	13				56.71	30.31	
Gly	G	14				45.36		173.89
Val	V	15	7.99	120.13	4.12	62.57	32.75	176.28
Val	V	16	8.31	125.29	4.05	62.35	32.78	175.98
Ala	A	17	8.46	128.50	4.22	52.52	19.21	177.68
Ala	A	18	8.33	123.74	4.09	52.70	19.10	177.86
Ala	A	19	8.29	123.17	4.08	52.74	19.17	178.65
Glu	E	20	8.34	120.08	4.24	56.70	30.27	176.92
Lys	K	21	8.47	122.30	4.28	56.78	32.92	177.13
Thr	T	22	8.15	115.30	4.24	62.26	69.76	174.73
Lys	K	23						
Gln	Q	24				55.87	29.72	
Gly	G	25	8.49	110.25	3.92	45.30		173.91
Val	V	26	7.99	120.13	4.12	62.61	32.67	176.34
Ala	A	27	8.44	127.44	4.29	52.84	19.03	177.18
Glu	E	28	8.39	120.92	4.20	56.67	30.51	177.67
Ala	A	29	8.31	125.01	4.24	52.70	19.17	177.79
Ala	A	30	8.24	122.76	4.24	52.79	19.11	178.46
Gly	G	31	8.33	107.81	3.93	45.36		174.26
Lys	K	32	8.13	120.74	4.40	56.25	33.21	177.07
Thr	T	33	8.23	115.99	4.28	62.05	69.81	174.70
Lys	K	34	8.49	123.80	4.27	56.34	32.90	

Res		#	HN	^{15}N	HA	CA	CB	CO
Glu	E	35				56.83	30.27	
Gly	G	36	8.45	110.03	3.93	45.33		174.02
Val	V	37	7.92	119.59	4.05	62.30	32.79	176.04
Leu	L	38	8.29	125.84	4.28	54.97	42.50	176.65
Tyr	Y	39	8.28	122.60	4.56	57.87	38.86	175.65
Val	V	40	8.09	123.35	4.01	62.14	32.90	176.13
Gly	G	41	8.06	112.19	3.93	45.19		173.98
Ser	S	42	8.26	115.63	4.42	58.37	63.85	174.74
Lys	K	43	8.50	123.48	4.36	56.46	33.08	177.01
Thr	T	44	8.24	115.64	4.29	61.94	69.92	174.76
Lys	K	45	8.48	123.90	4.25	56.54	33.08	
Glu	E	46				56.58	30.19	
Gly	G	47				45.28		173.89
Val	V	48	7.93	119.91	4.05	62.29	32.80	176.20
Val	V	49	8.30	125.25	4.24	62.11	32.58	175.97
His	H	50	8.59	124.21	4.28	56.01	30.30	174.92
Gly	G	51	8.46	110.69	3.93	45.17		173.89
Val	V	52	8.14	119.63	4.20	62.23	32.94	176.55
Thr	T	53	8.42	118.97	4.44	61.90	69.75	174.57
Thr	T	54	8.29	117.92	4.32	61.72	69.88	174.38
Val	V	55	8.31	123.08	4.09	62.17	32.87	176.09
Ala	A	56	8.44	128.23	4.24	52.46	19.37	177.58
Glu	E	57	8.42	120.96	4.24	56.49	30.39	176.71
Lys	K	58	8.44	122.89	4.22	56.43	33.09	176.88
Thr	T	59	8.19	115.53	4.28	61.87	69.85	174.65
Lys	K	60	8.40	123.70	4.28	55.76	32.69	178.09
Glu	E	61	8.41	120.60	4.48	56.84	29.72	176.69
Gln	Q	62	8.44	121.79	4.24	56.50	29.63	175.97
Val	V	63	8.30	121.99	4.16	62.41	32.80	176.25
Thr	T	64	8.32	118.13	4.32	61.81	69.85	174.03
Asn	N	65	8.53	121.63	4.75	53.10	38.91	175.27
Val	V	66	8.25	120.77	4.09	62.64	32.54	176.85
Gly	G	67	8.57	112.65	3.93	45.34		174.67
Gly	G	68	8.25	108.67	3.93	45.10		173.77
Ala	A	69	8.18	123.80	4.28	52.32	19.34	177.67
Val	V	70	8.23	120.54	4.09	62.42	32.73	176.31

Res		#	HN	^{15}N	HA	CA	CB	CO
Val	V	71	8.40	125.44	4.20	62.24	32.75	176.38
Thr	T	72	8.32	118.66	4.32	61.91	69.81	174.88
Gly	G	73	8.45	113.38	3.97	45.26		174.03
Val	V	74	8.09	119.54	4.16	62.32	32.89	176.52
Thr	T	75	8.31	118.98	4.32	61.86	69.74	174.07
Ala	A	76	8.38	127.43	4.28	52.47	19.29	177.57
Val	V	77	8.16	120.11	4.01	62.24	32.90	176.07
Ala	A	78	8.42	128.19	4.24	52.50	19.22	177.61
Gln	Q	79	8.40	120.37	4.24	55.35	29.64	175.89
Lys	K	80	8.45	123.29	4.28	56.38	33.14	176.65
Thr	T	81	8.30	116.93	4.32	61.97	69.85	174.41
Val	V	82	8.29	123.17	4.08	62.29	32.87	176.20
Glu	E	83	8.59	125.37	4.24	56.84	30.26	177.02
Gly	G	84	8.53	110.86	3.93	45.33		174.01
Ala	A	85	8.24	123.80	4.28	54.80	19.28	178.40
Gly	G	86	8.47	107.75	3.89	45.30		174.00
Asn	N	87	8.28	118.78	4.67	53.23	38.85	175.36
Ile	I	88	8.14	121.62	4.12	61.30	38.75	176.18
Ala	A	89	8.39	128.08	4.24	52.55	19.10	177.55
Ala	A	90	8.20	123.33	4.24	52.46	19.21	177.77
Ala	A	91	8.30	123.46	4.28	52.60	19.18	178.16
Thr	T	92	8.11	112.68	4.28	61.97	69.80	175.20
Gly	G	93	8.32	110.73	3.89	45.20		173.65
Phe	F	94	8.09	120.34	4.59	57.81	39.73	175.48
Val	V	95	8.07	123.78	4.01	62.02	33.10	175.49
Lys	K	96	8.40	126.39	4.20	56.34	33.13	176.54
Lys	K	97	8.48	123.87	4.25	56.34	33.97	
Asp	D	98	8.37	121.42	4.56	54.28	41.16	176.24
Gln	Q	99	8.35	120.17	4.29	55.91	29.43	176.95
Met	M	100	8.45	122.21	4.35	56.72	32.95	175.92
Gly	G	101				45.30		174.21
Lys	K	102	8.28	120.88	4.20	56.44	32.92	177.27
Gly	G	103	8.56	110.63	3.93	45.32		174.30
Glu	E	104	8.33	120.63	4.24	56.51	30.31	176.72
Glu	E	105	8.60	127.78	4.20	56.94	30.15	176.85
Gly	G	106	8.38	109.60	3.86	45.12		174.00

Res		#	HN	^{15}N	HA	CA	CB	CO
Tyr	Y	107	8.04	121.64	4.75	55.91	38.14	174.09
Pro	P	108				63.25	32.09	176.86
Gln	Q	109	8.56	121.29	4.28	55.83	29.68	176.07
Glu	E	110	8.54	122.25	4.28	56.72	30.36	176.91
Gly	G	111	8.49	110.24	3.90	45.36		174.26
Ile	I	112	8.00	120.19	4.05	60.90	38.68	176.36
Leu	L	113	8.41	127.20	4.36	55.04	42.35	178.14
Glu	E	114						
Asp	D	115	8.37	121.42	4.54	54.21	41.17	
Met	M	116	8.26	122.02	4.75	53.30	32.67	
Pro	P	117				62.87	32.24	176.73
Val	V	118	8.32	120.95	4.05	61.91	33.08	175.84
Asp	D	119	8.57	126.13	4.83	52.00	41.31	174.79
Pro	P	120				63.67	32.13	177.69
Gly	G	121	8.56	108.96	3.93	45.32		174.60
Ser	S	122	8.11	115.67	4.40	58.59	63.92	174.79
Glu	E	123	8.53	122.94	4.24	56.84	29.96	176.14
Ala	A	124	8.21	124.40	4.24	52.32	19.25	177.13
Tyr	Y	125	8.03	119.89	4.48	57.69	38.97	175.42
Glu	E	126	8.14	123.80	4.24	55.64	30.73	175.47
Met	M	127	8.43	123.84	4.67	53.28	32.44	176.52
Pro	P	128				63.04	32.25	176.90
Ser	S	129	8.50	116.80	4.40	58.23	63.83	174.83
Glu	E	130	8.59	123.22	4.28	56.51	30.34	176.54
Glu	E	131	8.62	122.50	4.20	56.68	30.27	176.84
Gly	G	132	8.43	110.02	3.85	45.27		173.44
Tyr	Y	133	8.05	120.54	4.52	57.37	39.20	175.12
Gln	Q	134				55.37	29.88	174.86
Asp	D	135	8.25	121.73	4.52	54.26	41.17	175.47
Tyr	Y	136	8.07	120.33	4.52	58.09	38.85	175.73
Glu	E	137	8.26	125.45	4.52	53.58	30.28	173.68
Pro	P	138				62.89	32.21	176.89
Glu	E	139	8.53	121.63	4.20	56.56	30.32	176.34
Ala	A	140	8.01	130.96	4.09	53.82	20.22	173.41

A.5 Backbone assignment of human α-synuclein at 15 °C and pH 2.5

Res		#	HN	^{15}N	CA	CB	CO
Met	M	1			54.89	32.79	
Asp	D	2	8.94	122.9	52.74	38.20	174.56
Val	V	3	8.27	121.3	62.53	32.68	175.67
Phe	F	4	8.30	123.8	57.84	39.38	175.65
Met	M	5	8.19	122.5	55.22	32.91	175.81
Lys	K	6	8.27	122.9	56.88	32.87	177.08
Gly	G	7	8.43	110.0	45.19		174.16
Leu	L	8	8.07	121.7	55.20	42.62	177.62
Ser	S	9	8.32	116.8	58.31	63.76	174.67
Lys	K	10	8.40	123.6	56.35	32.80	176.69
Ala	A	11	8.26	124.7	52.78	19.08	178.03
Lys	K	12	8.28	120.6	56.39	32.85	176.79
Glu	E	13	8.35	121.3	56.05	28.72	176.60
Gly	G	14	8.44	110.1	45.31		174.05
Val	V	15	7.98	120.2	62.76	32.72	176.62
Val	V	16	8.26	125.0	62.65	32.72	176.18
Ala	A	17	8.42	128.0	52.66	19.12	177.68
Ala	A	18	8.28	123.2	52.60	19.13	178.00
Ala	A	19	8.22	122.7	52.79	19.00	178.16
Glu	E	20	8.22	119.2	55.97	28.71	176.36
Lys	K	21	8.31	122.3	56.50	32.88	177.00
Thr	T	22	8.15	115.3	62.07	69.86	174.52
Lys	K	23	8.40	123.8	56.58	32.90	176.70
Gln	Q	24	8.44	121.7	56.27	29.42	176.45
Gly	G	25	8.45	110.3	45.33		174.24
Val	V	26	8.01	119.8	62.46	32.72	176.30
Ala	A	27	8.42	127.4	52.80	19.01	177.98
Glu	E	28	8.31	119.9	55.85	28.83	176.07
Ala	A	29	8.31	125.2	52.67	19.03	177.61
Ala	A	30	8.30	123.4	52.70	19.11	178.44
Gly	G	31	8.34	107.9	45.32		174.24
Lys	K	32	8.17	120.7	56.26	33.09	177.01
Thr	T	33	8.20	115.5	61.92	69.90	174.67
Lys	K	34	8.39	124.0	56.62	32.96	176.44
Glu	E	35	8.39	121.7	56.01	28.85	176.43
Gly	G	36	8.45	110.2	45.23		173.94
Val	V	37	7.97	119.5	62.27	32.64	175.95
Leu	L	38	8.28	125.7	55.01	42.42	176.63
Tyr	Y	39	8.26	122.4	57.92	38.82	175.57
Val	V	40	8.08	123.4	62.16	32.82	176.13
Gly	G	41	8.05	112.2	45.16		173.97
Ser	S	42	8.25	115.6	58.25	63.78	174.88

Res		#	HN	^{15}N	CA	CB	CO
Lys	K	43	8.51	123.5	56.50	32.90	176.90
Thr	T	44	8.14	115.3	61.96	69.93	174.56
Lys	K	45	8.44	124.0	56.45	32.92	176.44
Glu	E	46	8.38	121.5	56.01	28.88	176.59
Gly	G	47	8.44	110.4	45.31		173.76
Val	V	48	7.99	119.9	62.36	32.72	176.10
Val	V	49	8.31	125.0	62.16	32.78	175.92
His	H	50	8.72	123.3	55.11	29.18	174.65
Gly	G	51	8.49	110.6	45.16		173.71
Val	V	52	8.12	119.7	62.02	32.96	175.95
Ala	A	53	8.51	128.3	52.51	19.28	177.84
Thr	T	54	8.18	114.7	61.68	69.86	174.62
Val	V	55	8.24	123.0	62.39	32.80	175.98
Ala	A	56	8.42	127.7	52.72	19.27	177.83
Glu	E	57	8.29	120.1	55.91	28.81	176.31
Lys	K	58	8.42	122.7	56.50	33.01	176.96
Thr	T	59	8.17	115.7	62.09	69.87	174.54
Lys	K	60	8.36	123.7	56.58	32.87	176.56
Glu	E	61	8.34	121.5	55.99	28.81	175.89
Gln	Q	62	8.43	122.2	55.75	29.45	175.86
Val	V	63	8.31	121.9	62.36	32.88	176.29
Thr	T	64	8.30	118.1	61.96	69.91	174.01
Asn	N	65	8.53	121.8	53.20	38.91	175.21
Val	V	66	8.25	120.7	62.58	32.65	176.81
Gly	G	67	8.56	112.7	45.34		174.63
Gly	G	68	8.24	108.9	45.11		173.71
Ala	A	69	8.17	123.8	52.35	19.31	177.63
Val	V	70	8.23	120.5	62.44	32.64	176.31
Val	V	71	8.40	125.4	62.20	32.68	176.25
Thr	T	72	8.31	118.6	61.99	69.86	174.88
Gly	G	73	8.44	111.4	45.25		174.00
Val	V	74	8.09	119.5	62.26	32.82	176.54
Thr	T	75	8.30	118.9	62.04	69.85	174.08
Ala	A	76	8.37	127.4	52.48	19.23	177.59
Val	V	77	8.14	120.0	62.20	32.88	176.03
Ala	A	78	8.41	128.1	52.72	19.09	177.68
Gln	Q	79	8.39	120.3	55.72	29.29	176.00
Lys	K	80	8.43	123.1	56.55	32.96	176.68
Thr	T	81	8.26	116.7	61.91	69.90	174.39
Val	V	82	8.30	123.2	62.18	32.76	176.07
Glu	E	83	8.51	124.6	55.88	28.74	176.48
Gly	G	84	8.50	110.8	45.07		174.00
Ala	A	85	8.31	124.1	52.88	19.15	178.50
Gly	G	86	8.51	108.3	45.29		174.31
Ser	S	87	8.15	115.7	58.35	63.83	174.69

Res		#	HN	^{15}N	CA	CB	CO
Ile	I	88	8.19	122.7	61.39	38.69	176.27
Ala	A	89	8.35	128.0	52.65	19.05	177.57
Ala	A	90	8.20	123.3	52.56	19.17	177.71
Ala	A	91	8.28	123.3	52.66	19.08	178.12
Thr	T	92	8.09	112.6	62.03	69.82	175.16
Gly	G	93	8.31	110.7	45.21		173.70
Phe	F	94	8.09	120.3	57.88	39.66	175.57
Val	V	95	8.03	123.3	62.19	32.96	175.64
Lys	K	96	8.36	126.0	56.49	32.97	176.60
Lys	K	97	8.40	122.9	56.60	33.00	176.49
Asp	D	98	8.52	119.7	53.12	37.94	175.06
Gln	Q	99	8.38	120.9	55.95	28.77	175.85
Leu	L	100	8.23	123.0	55.42	42.33	177.88
Gly	G	101	8.39	109.6	45.23		174.20
Lys	K	102	8.20	120.7	56.31	32.95	176.54
Asn	N	103	8.56	119.3	53.35	38.55	175.27
Glu	E	104	8.33	120.5	56.07	28.61	176.01
Glu	E	105	8.36	120.8	55.95	28.62	176.42
Gly	G	106	8.41	110.1	44.96		173.32
Ala	A	107	8.12	124.8	50.62	18.13	
Pro	P	108			63.20	31.73	177.05
Gln	Q	109	8.53	120.6	55.78	29.42	176.00
Glu	E	110	8.42	121.4	55.99	28.93	176.43
Gly	G	111	8.45	110.0	45.27		174.03
Ile	I	112	7.96	119.8	61.31	38.65	176.44
Leu	L	113	8.31	125.6	55.23	42.08	177.29
Glu	E	114	8.27	120.5	55.79	28.65	175.53
Asp	D	115	8.39	119.3	52.86	37.94	174.57
Met	M	116	8.18	121.7	53.21	32.18	
Pro	P	117			62.48	31.91	176.04
Val	V	118	8.28	120.5	62.18	32.67	175.68
Asp	D	119	8.60	123.2	50.84	38.03	
Pro	P	120			63.67	32.14	176.78
Asp	D	121	8.33	117.5	53.01	37.76	174.91
Asn	N	122	8.20	118.8	53.39	38.68	175.29
Glu	E	123	8.17	120.2	56.03	28.54	175.85
Ala	A	124	8.23	124.0	52.92	18.95	177.40
Tyr	Y	125	7.94	118.4	57.78	38.59	175.43
Glu	E	126	7.97	121.9	55.09	29.09	175.12
Met	M	127	8.23	122.6	53.40	32.44	
Pro	P	128			63.44	31.92	177.09
Ser	S	129	8.33	115.1	58.45	63.56	174.91
Glu	E	130	8.33	121.7	55.95	28.77	175.20
Glu	E	131	8.26	120.5	56.15	28.71	176.44
Gly	G	132	8.35	109.7	45.26		173.99

Res		#	HN	^{15}N	CA	CB	CO
Tyr	Y	133	8.02	120.1	58.14	38.64	175.87
Gln	Q	134	8.28	121.9	55.75	29.32	175.15
Asp	D	135	8.29	119.5	52.74	37.94	174.44
Tyr	Y	136	8.07	120.9	58.02	38.61	175.07
Glu	E	137	8.06	123.8	52.97	28.66	
Pro	P	138			62.91	32.12	176.70
Glu	E	139	8.40	120.4	55.77	28.87	175.65
Ala	A	140	8.45	126.8	51.62	18.91	

A.6 HSQC spectral assignment of human α-synuclein at -10 °C and pH 2.5

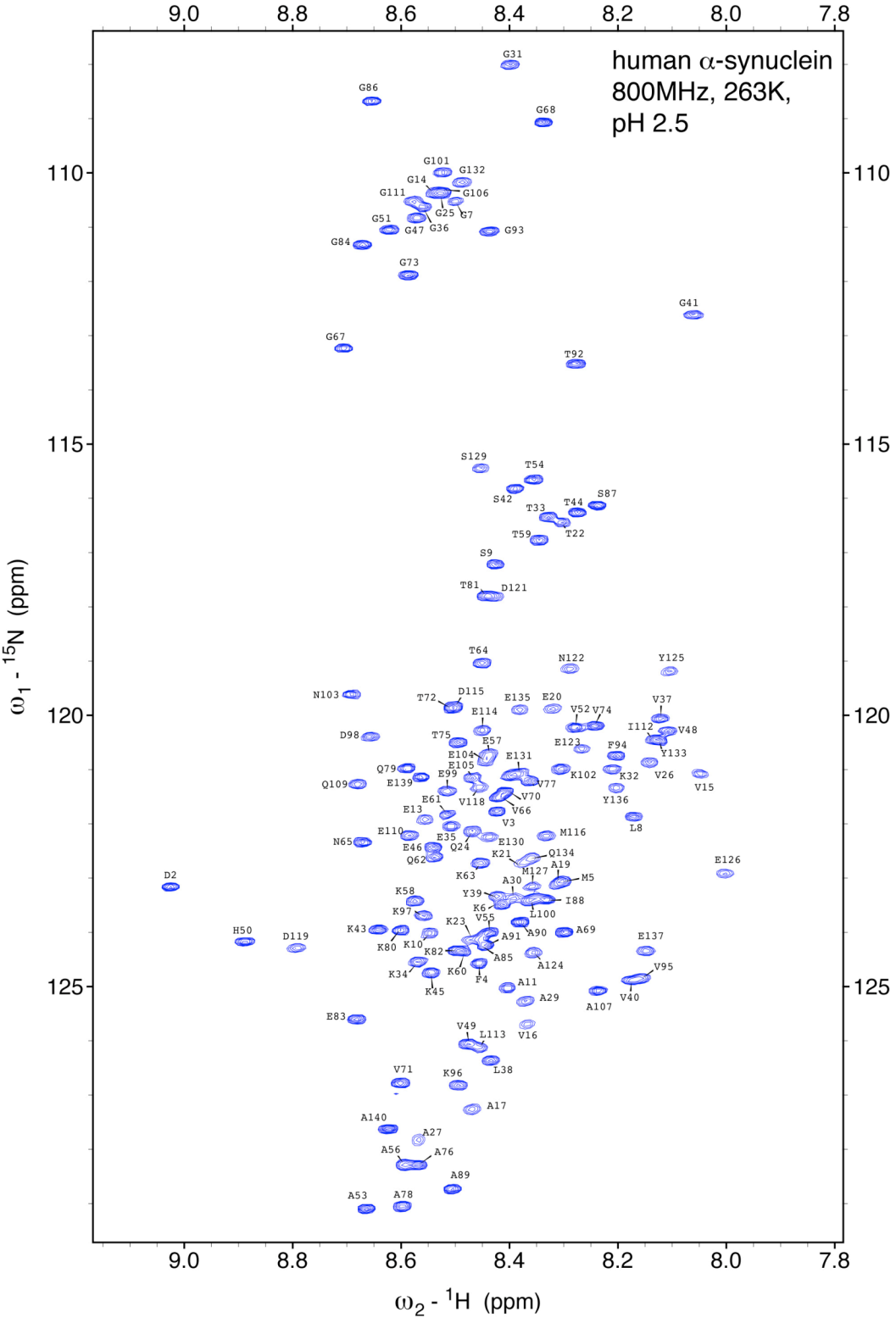

A.7 Backbone assignment of human α-synuclein in 2 M glucose at 15 °C and pH 7.4

Res		#	HN	^{15}N	CA	CB	CO
Met	M	1		119.8	59.99	34.63	
Asp	aa	2	8.65	125.2	54.44	41.58	176.35
Val	V	3	8.20	120.3	62.60	32.85	176.24
Phe	F	4	8.17	123.9	54.20	41.09	175.67
Met	M	5	8.18	121.9	55.43	32.70	
Lys	K	6	8.20	122.2	56.86		177.13
Gly	G	7	8.37	109.8	45.44	32.77	174.25
Leu	L	8	7.98	121.5	55.21	42.51	177.57
Ser	S	9	8.27	116.6	58.40	63.69	174.53
Lys	K	10	8.30	123.5	56.35	33.00	176.44
Ala	A	11	8.23	125.0	52.84	19.20	177.91
Lys	K	12	8.25	120.6	56.43	33.04	176.66
Glu	E	13	8.38	121.9	56.82	30.16	177.02
Gly	G	14	8.40	110.0	45.43		174.10
Val	V	15	7.91	120.1	62.63	32.71	176.47
Val	V	16	8.21	124.8	62.38	32.92	176.02
Ala	A	17	8.37	128.0	52.56	19.31	177.69
Ala	A	18	8.25	123.4	52.86	18.94	177.73
Ala	A	19	8.21	122.7	52.80	19.07	178.27
Glu	E	20	8.25	119.8	56.87	29.72	176.96
Lys	K	21	8.23	121.9	56.87	32.77	177.18
Thr	T	22	8.06	114.8	62.26	69.74	174.70
Lys	K	23	8.25	123.5	56.66	32.95	176.70
Gln	Q	24	8.34	121.4	56.27	29.96	176.56
Gly	G	25	8.42	110.4	45.49		174.30
Val	V	26	7.95	119.7	62.51	32.92	176.33
Ala	A	27	8.36	127.2	52.93	19.38	178.13
Glu	E	28	8.34	120.3	56.65	29.67	176.65
Ala	A	29	8.22	124.6	52.70	19.25	177.68
Ala	A	30	8.17	122.6	52.85	19.17	178.39
Gly	G	31	8.25	107.7	45.42		174.17
Lys	K	32	8.04	120.6	56.27	33.30	176.92
Thr	T	33	8.19	115.3	61.83	70.00	174.60
Lys	K	34	8.38	123.6	56.60	32.86	176.45
Glu	E	35	8.38	121.8	56.82	30.27	176.29
Gly	G	36	8.38	109.9	45.34		173.97
Val	V	37	7.83	119.5	62.16	33.00	175.76
Leu	L	38	8.23	125.7	54.92	42.64	176.51
Tyr	Y	39	8.23	122.3	57.80	38.88	177.55

Res		#	HN	^{15}N	CA	CB	CO
Val	V	40	8.06	122.8	62.15	32.87	176.12
Gly	G	41	8.04	112.1	45.31		173.96
Ser	S	42	8.21	115.6	58.36	63.86	174.66
Lys	K	43	8.42	123.3	56.45	33.07	176.80
Thr	T	44	8.13	115.2	62.05	70.06	174.66
Lys	K	45	8.43	123.7	56.50	33.14	176.41
Glu	E	46	8.25	126.2	56.91	30.88	176.30
Gly	G	47	8.38	109.9	45.19		173.85
Val	V	48	7.84	119.8	62.23	32.85	176.65
Val	V	49	8.24	124.8	62.22	34.08	175.81
His	H	50	8.54	123.7	55.47	29.11	175.11
Gly	G	51	8.40	110.4	45.19		173.72
Val	V	52	8.01	119.4	62.04	32.95	175.81
Ala	A	53	8.44	128.1	52.49	19.48	177.74
Thr	T	54	8.16	114.6	61.78	69.96	174.48
Val	V	55	8.16	122.8	62.23	32.71	175.83
Ala	A	56	8.36	127.8	52.48	19.31	177.76
Glu	E	57	8.30	120.6	56.65	30.32	176.68
Lys	K	58	8.35	122.5	56.43	33.14	176.94
Thr	T	59	8.14	115.5	61.93	69.97	174.61
Lys	K	60	8.29	123.4	56.35	32.97	176.64
Glu	E	61	8.36	121.7	56.70	30.27	176.37
Gln	Q	62	8.33	121.5	56.80	30.02	175.91
Val	V	63	8.23	121.8	62.38	32.77	176.26
Thr	T	64	8.24	117.8	61.90	70.02	174.00
Asn	N	65	8.45	121.7	53.15	38.93	
Val	V	66	8.17	120.4	62.56	32.57	176.76
Gly	G	67	8.49	112.6	45.40		174.64
Gly	G	68	8.19	108.9	45.15		173.70
Ala	A	69	8.10	123.8	52.30	19.45	177.55
Val	V	70	8.15	120.3	62.36	32.64	176.23
Val	V	71	8.32	125.2	62.18	32.86	176.17
Thr	T	72	8.24	118.3	61.86	69.86	174.84
Gly	G	73	8.38	111.2	45.27		174.02
Val	V	74	8.02	119.4	62.25	32.91	176.46
Thr	T	75	8.23	118.6	61.92	69.86	174.04
Ala	A	76	8.29	127.1	52.63	19.38	177.53
Val	V	77	8.06	119.7	62.23	32.85	175.97
Ala	A	78	8.33	127.8	53.01	19.09	178.13
Gln	Q	79	8.30	120.1	55.92	29.68	175.89
Lys	K	80	8.35	122.9	56.43	33.05	176.62
Thr	T	81	8.22	116.6	61.87	69.89	174.41

Res		#	HN	^{15}N	CA	CB	CO
Val	V	82	8.22	122.8	62.34	32.87	176.06
Glu	E	83	8.50	125.0	56.87	30.24	176.95
Gly	G	84	8.44	110.6	45.35		174.13
Ala	A	85	8.20	123.9	52.89	19.29	178.41
Gly	G	86	8.44	108.2	45.39		174.29
Ser	S	87	8.10	115.7	58.33	63.90	174.67
Ile	I	88	8.14	122.6	61.38	38.69	176.23
Ala	A	89	8.29	127.8	52.67	19.13	177.55
Ala	A	90	8.13	123.1	52.53	19.25	177.70
Ala	A	91	8.21	123.2	52.65	19.20	178.05
Thr	T	92	8.02	112.3	61.93	69.88	175.08
Gly	G	93	8.24	110.7	45.29		173.60
Phe	F	94	8.04	120.3	57.78	39.68	175.39
Val	V	95	8.01	123.5	61.92	33.15	175.34
Lys	K	96	8.33	126.3	56.39	33.14	176.44
Lys	K	97	8.41	123.6	56.58	32.98	176.35
Asp	D	98	8.35	120.9	54.43	41.05	176.16
Gln	Q	99	8.26	119.9	55.78	29.65	175.93
Leu	L	100	8.23	122.7	55.29	42.16	177.91
Gly	G	101	8.43	109.8	45.35		174.06
Lys	K	102	8.15	120.7	56.17	33.19	176.40
Asn	N	103	8.56	119.9	53.38	38.81	
Glu	E	104	8.41	121.3	56.64	30.21	176.45
Glu	E	105	8.40	121.8	56.58	30.27	176.93
Gly	G	106	8.37	110.2	45.05		173.40
Ala	A	107	8.07	124.9	50.49	18.37	175.49
Pro	P	108			63.10	32.12	
Gln	Q	109	8.51	121.1	55.81	29.70	175.89
Glu	E	110	8.45	122.3	56.58	30.54	176.75
Gly	G	111	8.42	110.2	45.27		173.74
Ile	I	112	7.94	120.1	60.90	38.71	176.16
Leu	L	113	8.35	126.9	54.98	42.39	177.03
Glu	E	114	8.37	122.1	56.45	30.47	175.80
Asp	D	115	8.30	121.2	54.18	41.13	174.89
Met	M	116	8.18	121.7	54.06	32.54	
Pro	P	117			62.76	32.19	
Val	V	118	8.21	120.6	61.89	33.01	175.64
Asp	D	119	8.45	125.6	52.09	41.12	174.58
Pro	P	120			63.28	32.30	
Asp	D	121	8.33	119.2	54.51	40.98	176.09
Asn	N	122	8.06	119.1	53.45	39.41	
Glu	E	123	8.33	121.7	56.73	29.98	175.99

Res		#	HN	^{15}N	CA	CB	CO
Ala	A	124	8.17	124.3	53.39	19.24	177.13
Tyr	Y	125	7.96	119.9	57.66	38.98	175.28
Glu	E	126	8.08	123.6	55.63	30.69	175.38
Met	M	127	8.35	123.8	53.24	32.38	
Pro	P	128			62.96	32.21	
Ser	S	129	8.42	116.7	58.18	63.90	
Glu	E	130	8.51	123.0	56.51	30.23	176.41
Glu	E	131	8.40	121.7	56.82	30.17	176.88
Gly	G	132	8.35	109.9	45.19		173.82
Tyr	Y	133	8.00	120.3	57.92	39.17	175.66
Gln	Q	134	8.20	122.6	55.83	29.17	175.91
Asp	D	135	8.21	121.6	54.19	41.09	175.39
Tyr	Y	136	7.98	120.4	57.51	39.10	174.96
Glu	E	137	8.19	125.2	53.45	30.26	173.64
Pro	P	138			62.93	32.26	
Glu	E	139	8.46	121.4	56.49	30.23	175.34
Ala	A	140	7.95	130.7	53.78	20.37	172.54

A.8 RDC values of human and mouse α-synuclein at pH 7.4 or 2.5 and at 15 °C

	Human α-synculein		Mouse α-synuclein	
residues	pH 2.5	pH 7.4	residues	pH 7.4
2	3.04		3	1.28
3	0.14	-1.27	5	-4.49
4	-5.36		8	-4.15
5		-5.29	9	-3.55
6	-2.65		11	-5.23
8	-4.52	-1.77	12	0.47
9	-2.42	-1.95	15	1.62
10	0.16		16	1.61
11	-1.73	-1.04	17	1.7
12	2.5	-2.13	18	2.12
13	-1.79		20	2.73
15	-5.93	2.37	21	2.07
16	2.77	4.02	22	1.15
17	2.69	1.35	25	1.14
18		4.29	26	0.22
19	6.76	0.85	27	2.19
20	0.4	1.15	28	4.13
21	-3.21	2.01	29	1.72
22	2.03	0.84	30	3.64
23	-2.21	1.95	31	1.46
24	-0.4	2.99	32	0.66
25		5.65	33	3.99
26	5.7	3.88	34	-0.52
27	2.63	2.19	36	1.92
28	1.41	4.01	37	2.36
29	-3.6	2.8	38	2.43
30	5.4	3.89	39	-1
31	2.29	1.34	40	3.35
32	3.84	2.99	41	1.53
33	1.49	3.29	42	2.8
34	1.76	3.21	43	4.75
35	-0.62		44	1.92
37	5.17	3.88	45	3.37
38	2.74	2.91	48	2.29
39	1.71	2.74	50	4.24
40	4.51	3.74	51	2.52
41	1.93	3.41	52	4.43
42	2.99	1.65	53	4.5
43	2.03		54	5.14

	Human α-synculein		Mouse α-synuclein	
residues	pH 2.5	pH 7.4	residues	pH 7.4
44	-1.3	2.49	55	4.42
45	2.67	1.76	56	2.62
46	3.51		57	3.01
48	1.47	3.21	58	6.44
49	1.31	6.07	59	1.45
50	5.02	4.32	60	4.07
51	7.34		61	0.9
52	2.74	7.96	62	3.33
53	4.86	5.95	63	4.64
54	5.36	6.02	64	4.41
55	5.54	3.41	65	0.2
56	7	6.81	66	3.81
57	0.79	5.17	67	1.34
58	5.03	4.79	68	0.8
59	3.64	6.56	69	2.86
60	3.33	2.42	70	4.63
61	0.61	4.13	71	3.01
62	5.93		72	3.84
63	6.41	3.94	73	3.54
64	4.85	5.65	74	3.07
65	5.62	2.74	75	5.75
66	2.26	1.59	76	4.47
67	1.35	2.85	77	4.51
68	1.09	1.33	78	4.97
69	2.79	4.26	79	5.96
70	2.37	3.28	80	5.43
71	3.39	3.22	81	3.72
72	1.95	3.52	82	4
73	3.65	3.71	83	2.17
74	2.13	5.21	84	3.09
75	8.07	4.01	85	-0.37
76	4.81	4.55	86	0.99
77	5.12	5.59	87	1.77
78	7.35	7.91	88	0.37
79	5.42		89	1.93
80	4.35	8.51	90	2.17
81	5.22	5.17	91	3.1
82	3.33	3.22	92	2.36
83	2.61	4.94	93	2.28
84	5.79	4.44	94	1.17
85	-1.18	0.54	95	3.9
86	1.29	2.01	96	2.86

	Human α-synculein		Mouse α-synuclein	
residues	pH 2.5	pH 7.4	residues	pH 7.4
87	-0.08	2.43	97	2.35
88	-1.01	3.52	98	5.88
89	1.38	2.68	99	3.55
90	0.72	2.31	100	3.34
91	-1.85	1.33	102	2.29
92	1.3	3.77	103	1.22
93	2.2	2.43	104	-1.55
94	-0.16	3.35	105	-0.43
95	1.57	2.01	106	1.55
96	1.97	3.57	107	3.41
97	2.29	2.31	109	3.75
98	1.77	2.13	110	0.32
99	0.02	2.13	111	2.44
100	3.48	0.65	112	2.7
101	0.01	3.59	113	4.78
102	-1.09	1.9	115	4.71
103	2.25	2.54	116	7.15
104	0.01	1.03	118	7.86
105	-5.09		119	6.13
106	1.88		121	-1.1
107	-1.26	4.32	122	0.51
109	-1.09	4.5	123	1.96
110	0.7	1.46	124	1.94
112	-7.96	4.07	125	6.18
113	-1.73	5.47	126	4.09
114	-0.02	5.54	127	5.29
115	-0.8	6.2	129	6.09
116	-1.27	10.21	130	5.2
118		9.05	132	2.77
119	-2.08	8.01	133	1.89
121	0.11	1.28	135	2.27
122	-0.19	1.87	136	1.52
123	-2.22	1.4	137	2.84
124	-1.3	2.37	139	0.88
125	-1.81	5.59	140	1.43
126	-1.56	5.34		
127	-1.17	11.43		
129	1.94	7.48		
130	-10.17	6.32		
131	-8.1			
132	-0.37	1.08		
133	-8.08	2.85		

	Human α-synculein	
residues	pH 2.5	pH 7.4
134	-3.11	
135	0.79	2.19
136	-8.62	2.55
137	-1.01	4.68
139	2.18	2.97
140	-2.97	1.34

A.9 Shell script of SALSA

```
#!/bin/sh
#
# a script to run SALSA analysis
# version: 0.5 2007, 10,25
#
#      Protein Sci. 2007 May;16(5):906-18.
#                A simple algorithm locates beta-strands in the amyloid fibril core of alpha-
#     synuclein, Abeta, and tau using the amino acid sequence alone.
#
#  FOR LINUX SYSTEM ONLY, so far!!!

## assign the path of a one-letter code sequence file
file_seq=/data/seq/1GB1.seq
res_length=111
max_window=20
touch _window_temp_file
output=_temp_window

echo "Your sequence file is $file_seq "
echo "You want to search the first $res_length residues"

## assign the Chou-Fasman parameters
##  order: AA Beta-sheett Alpha-helix  Beta-turn
tr 'A-Z' 'a-z' < $file_seq | tr '[:punct:]' 'b' | tr '0-9' 'b' |tr '\n' 'b'| \
sed -e 's/[o|x|z|u|j|b| ]//g' \
-e 's/a/A   0.830   1.420   0.660\n/g' \
-e 's/c/C   1.190   0.700   1.190\n/g' \
-e 's/d/D   0.540   1.010   1.460\n/g' \
-e 's/e/E   0.370   1.510   0.740\n/g' \
-e 's/f/F   1.380   1.130   0.600\n/g' \
-e 's/g/G   0.750   0.570   1.560\n/g' \
-e 's/h/H   0.870   1.000   0.950\n/g' \
-e 's/i/I   1.600   1.080   0.470\n/g' \
-e 's/k/K   0.740   1.160   1.010\n/g' \
-e 's/l/L   1.300   1.210   0.590\n/g' \
-e 's/m/M   1.050   1.450   0.600\n/g' \
-e 's/p/P   0.550   1.130   1.520\n/g' \
-e 's/r/R   0.930   0.980   0.950\n/g' \
-e 's/q/Q   1.100   1.110   0.980\n/g' \
-e 's/n/N   0.890   0.670   1.560\n/g' \
-e 's/s/S   0.750   0.770   1.430\n/g' \
-e 's/t/T   1.190   0.830   0.960\n/g' \
-e 's/w/W   1.370   1.080   0.960\n/g' \
-e 's/y/Y   1.470   0.690   1.140\n/g' \
-e 's/v/V   1.700   1.060   0.500\n/g' > $file_seq.chou

## running for n-residue window
length=4
while [ $length -lt `expr $max_window + 1` ]
do
 j=`expr $length - 1`
 i=$length
  while [ $i -lt `expr $res_length + 1` ]
   do
  mbp=`cat $file_seq.chou | head -n $i | tail -n $length |\
    tr 'A-Z' ' ' | tr '\n' ' ' | \
    awk '{beta=0; for (col=1; col <=NF; col=col+3) beta=beta+$col} \
    {sum=0;    for    (col=1;    col    <=NF;    col++)    sum=sum+$col}    {printf
"%.3f",beta/(0.5*(sum-beta))}'`
## echo the mbp values to proper residues
```

```
        x=`expr $i - $j `
        while [ $x -lt `expr $i + 1` ]
        do
           echo $mbp >> _temp.$x
           x=`expr $x + 1`
        done

   i=`expr $i + 1`
  done

 res=1
 cp _window_temp_file  _temp_window_$length

 while [ $res -lt `expr $res_length + 1` ]
 do
   cat _temp.$res |tr '\n' ' ' | \
   awk '{sum=0; for (col=1; col<=NF; col++) if ( $col >= 1.2 ) sum=sum+$col;
print sum}' \
    >>   _temp_window_$length
   res=`expr $res + 1`
 done
 rm _temp.*

 echo "$length-reisude window walking is done"
 length=`expr $length + 1`
done

paste $output* | awk '{sum=0; for (col=1; col<=NF; col++) sum=sum+$col; print
sum}' >$file_seq.salsa
paste $file_seq.chou $file_seq.salsa |awk '{print $1,$5}' |awk '{print NR,$0 }'
> $file_seq.out
```

Curriculum Vita

Kuen-Phon Wu

kpwu@eden.rutgers.edu

Education

1996.09 – 2000.06

B. S. in Life Sciences, National Tsing-Hua University, Hsinchu, Taiwan

2000.09 – 2002.06

M. S. in Life Sciences, National Tsing-Hua University, Hsinchu, Taiwan

2004.09 – 2010.01

Ph. D in Chemistry and Chemical Biology, Rutgers, the state university of New Jersey, Piscataway, NJ

Experiences

2004.09 – 2005.08

Graduate fellowship. Rutgers/UMDNJ joint Graduate Program in Molecular Biosciences, Piscataway, NJ.

2005.09 – 2007.06

Teaching assistant. Department of Chemistry and Chemical Biology, Rutgers University, Piscataway, NJ.

2007.07 – 2008.06

NIH Interdisciplinary Research Workforce Fellowship, Rutgers University, Piscataway, NJ.

2008.07 – 2010.01

Graduate research assistant, Department of Chemistry and Chemical Biology, Rutgers University, Piscataway, NJ.

Publications

1. Kuen-Phon Wu, Chih-Wei Wu, Ya-Ping Tsao, Ting-Wei Kuo, Yuan-Chou Lou, Chen-Wen Lin, Suh-Chin Wu and Jya-Wei Cheng. (2003)
   Structural basis of a Flavivirus recognized by its neutralizing antibody: Solution structure of the domain III of the Japanese Encephalitis virus envelope protein
   J. Biol.Chem. 278, 46007-46013.

2. Yun-Ru Pan, Kuen-Phon Wu, Yuan-Chou Lou, Yoa-Di Liao, and Chinpan Chen (2005)

Letter to editor: 1H, 13C and 15N assignments and secondary structure of mourine angiogenesis 4
J. Biomolecular NMR 31, 175-179

3. Iren Wang, Yuan-Chou Lou, Kuen-Phon Wu, Suh-Hsuing Wu, Wen-Chang Chang and Chinpan Chen (2005)
Novel solution structure of porcine beta-microseminoprotein
J. Mol. Biol. 346, 1071-1082

4. Daniel S. Weinstock, Anthony S. Felts, Chitra Narayanan, Michael Andrec, Ronald M. Levy, Kuen-Phon Wu and Jean Baum (2007)
Distinguishing among structural ensembles of the GB1 peptide: REMD simulations and NMR experiments
J. Am. Chem. Soc, 129, 4858-4859

5. Kuen-Phon Wu, Seho Kim, David A. Fela and Jean Baum (2008)
Characterization of conformational ensemble of natively unfolded human and mouse alpha-synuclein: implication for aggregation
J. Mol. Biol. 378, 1104-1115

6. Yu-Jen Chen, Kuen-Phon Wu, Seho Kim, Liliana Falzon, Masayori Inouye and Jean Baum (2008)
Backbone NMR assignments of DFP-inhibited mature subtilisin E
Biomolecular NMR Assignments, 2, 131-133

7. Kuen-Phon Wu, Daniel S. Weinstock, Chitra Narayanan, Ronald M Levy and Jean Baum (2009)
Structural reorganization of alpha-synuclein at low pH observed by NMR and REMD simulation
J. Mol. Biol. 391, 784-796

8. Seho Kim, Kuen-Phon Wu and Jean Baum (2009)
Deconvolution of the fast hydrogen exchange effect on ^{15}N relaxation measurement in intrinsically disordered protein.
in preparation for J. BioNMR

9. Kuen-Phon Wu and Jean Baum (2009)
Detection of transient inter-chain interactions in the intrinsically disordered alpha-synuclein using NMR paramagnetic relaxation enhancement
submitted to JACS